CO_2 SEQUESTRATION: THE RISK OF LEAKAGE

John Bleddyn Davies

Submitted in partial fulfilment of the requirements for the degree of Ph.D.

Cardiff University

December 2013

DECLARATION

This work has not been submitted in substance for any other degree or award at this or any other university or place of learning, nor is being submitted concurrently in candidature for any degree or other award.

Signed …… (candidate) Date ……

STATEMENT 1

This thesis is being submitted in partial fulfilment of the requirements for the degree of ……(insert MCh, MD, MPhil, PhD etc, as appropriate)

Signed …… (candidate) Date ……

STATEMENT 2

This thesis is the result of my own independent work/investigation, except where otherwise stated.

Other sources are acknowledged by explicit references. The views expressed are my own.

Signed …… (candidate) Date ……

STATEMENT 3

I hereby give consent for my thesis, if accepted, to be available for photocopying and for inter-library loan, and for the title and summary to be made available to outside organisations.

Signed …… (candidate) Date ……

STATEMENT 4: PREVIOUSLY APPROVED BAR ON ACCESS

I hereby give consent for my thesis, if accepted, to be available for photocopying and for inter-library loans **after expiry of a bar on access previously approved by the Academic Standards and Quality Committee.**

Signed …… (candidate) Date ……

Dedication

I dedicate this thesis to Mam and Dad. They must have thought that I'd be a student forever!! Without their patience, support and love I would not have been able to complete my work.

Diolch

Nadolig, 2013

Abstract

The Utsira Sand is a major North Sea Saline aquifer. It is currently being utilised as a CO_2 sequestration reservoir for the Sleipner project, and its large estimated storage capacity and proximity to suitable infrastructure ensures that it is an attractive prospect for further storage projects. As a forerunning CCS project it is the subject for scrutiny from environmental, industrial and governmental regulatory bodies, with the key concern being the confinement of the CO_2 within the reservoir.

Regulations are in place to ensure that operators monitor closely the migration of the CO_2 plume within storage reservoirs and that they can demonstrate that the plume is behaving as modelled. Any unexpected behaviour of the plume requires escalation of the monitoring program and leakage would involve financial penalties in addition to remediation costs. Diligent site selection and a complete and robust understanding of the reservoir, adjacent units, and the overburden is therefore critical pre-injection.

Geological features which have become apparent following CO_2 injection into the Utsira Sand would suggest that the injection site was not completely understood before injection commenced. This study has contributed to a better understanding of the storage reservoir, specifically in regards to the deformed base of the Utsira Sand, which has been shown to be the result of sand remobilisation from depth in the form of sand intrusions. These intrusions, hosted within low permeability shales, represent permeable migration pathways from the deeper subsurface to the base of the Utsira Sand. Furthermore, their post-emplacement compaction has facilitated subsidence of the overlying strata. This movement, shown to affect strata up to the top of the Utsira Sand, has formed a ring of faults which projects obliquely upwards from the base of the Utsira Sand to the top of the storage reservoir. Amplitude anomalies within the overburden suggest that these zones of increased permeability have been exploited as paleo-gas migration pathways.

Other amplitude anomalies within the succession overlying the Utsira Sand are also recognised. These include: high amplitude anomalies interpreted as gas accumulations within the Lower Seal, vertically focused ‘wipe out zones’ and zones of disrupted reflections interpreted as gas chimneys. The gas chimneys in particular, shown to extend to the seafloor, pose a significant leakage risk to sequestered CO_2. On the basis of these observations, a plumbing system, from the Mid-Miocene to the seafloor, is presented. Potential CO_2 leakage scenarios are proposed and discussed in respect to

the storage ‘site’ and storage ‘complex’. It is suggested that potential future operators within this area should be aware of the features observed and appreciate the associated risk to stored CO_2.

It is also concluded that the viability of carbon sequestration technology as a climate change mitigation option requires that it represents an attractive proposition for those that operate the technology. Therefore it is considered that the regulation of carbon sequestration requires a finely measured balance between careful regulation and appropriate penalties for poor practice and flexibility in the interpretation of a ‘storage complex’ and ‘leakage.’

Acknowledgements

I cannot thank my supervisor Joe Cartwright enough. Throughout the project he has shown immeasurable support and patience, invaluable advice, and great faith in my abilities. I consider him to be an extraordinary gentleman, an excellent supervisor and a friend.

Thank you to Fugro Robertson, Llandudno, for part funding my research and providing the data. A special mention to Chris Burgess, Mark Paton and Liam Hunt is required. My gratitude also for the support of the staff at the KESS and RACDV departments, Cardiff University.

Gwen Pettigrew has my thanks for all her technical support, especially for the rescue job on my laptop. I must also mention my fellow researchers at the 3D Lab, with a special mention to my office mate, Duarte Soares, his companionship has been greatly appreciated; to my drinking and walking partner, Peter Bird, 'this is the life'; and to the main man Olu Nwosu. Thank you also to Martino Foschi for all the geophysics help.

A thousand thanks to Mam and Dad, to whom this work is dedicated to, they have always supported me. I could not have achieved what I have without them. Mamgu Cydweli and Mamgu and Dadcu Aberaeron must also be acknowledged, for their support throughout my life. Many thanks also to Wncwl Keith for his advice and help.

I also thank my beautiful girlfriend, Rhianidd, she must have the patience of a saint to have put up with me throughout the PhD. 'Fanks x.

Contents

List of Figures

Chapter 1

Chapter 2

Chapter 3

Chapter 4

saw toothed reflection d) discordant bright spot e) concordant bright spot f) concordant high amplitude reflection

- **Fig. 4.6** An RMS map of representative examples of Lowermost Shale amplitude anomalies a and b)elongated and sub-circular c) connected by low amplitude 'saddles' d) elliptical outline of high energy and e) 'horseshoe' geometry
- **Fig. 4.7** a)A time-slice and b)RMS map an of representative examples of Lowermost Shale with 'horseshoe' geometry (1) and linear reflection (2)
- **Fig. 4.8** a) seismic profile of a pair of discordant reflections A and B b) seen on the time slice as curved (A) and linear (B) narrow, high amplitude reflections and upon the RMS map c) as sub-circular high amplitude features
- **Fig. 4.9** Seismic sections a) in Landmark colour scheme and b) in black and white colour scheme showing a concordant bright spot (B) a concordant reflection (A) and a sub-horizontal concordant bright spot (C). Sub vertical zones of disrupted reflections are projected upwards
- **Fig. 4.10** Seismic sections showing a) in Landmark colour scheme and b) in black and white discordant bright spot (A) with overlying chaotic reflection and discontinuous points of the BUH (Points B, C and D). Neither of horizons A or B can be traced across the central chaotic zone.
- **Fig.4.11** Compares two discordant high amplitude reflections from this study with an asymmetric 'V' bright penetrated by a well (from Løseth et al., 2003).
- **Fig. 4.12** a) TWT map of the Base Utsira Horizon showing the elliptical mounds forming two distinct ridges of high topography with a central low area (CA) b) A time-dip map where darker areas indicate an increase in gradient of the Base Utsira Horizon, these darker areas coincide with the edges of the elliptical mounds and denote the mound 'hinge point'.
- **Fig. 4.13** a) Seismic profile of mound 13 demonstrating how measurements of mound relief were taken. Hinge points are denoted by the increase in gradient at points A and B. The mound crest is a prominent feature at point C, although the reflection is discontinuous at the mound flanks. Reflections D and E onlap at the flanks of the mound b) TWT contour map with RMS seismic amplitude superimposed of the Lowermost Shale, with a high concentration of amplitude within the south-eastern sector c) a high amplitude reflection underlying the mound
- **Fig. 4.14** a) A time-depth map of Mound 1. This shows it is an irregular shaped feature, with three separate area of high relief (Points 1, 2 and 3) b) a W-E seismic section displaying high amplitude anomalies below the mound (points D, E and F), a slight depression along mound profile (A) and discontinuous reflection at the mound hinge points (B and C) c) a S-N section showing the chaotic nature of the reflections below the mound d) an RMS map of the Lowermost Shale with mound contour overlain demonstrating the distribution of high amplitude features.
- **Fig. 4.15** a) a contoured time-depth map Mound 2 with location of seismic section denoted by dashed line b) seismic section displayed in Landmark colour scheme and c) in black and white demonstrating that the mound is underlain by a pair of high amplitude reflections forming a wedge shape. The

reflections, of opposite dominant amplitude, are interpreted to represent the top and the base of a sand intrusion. Sub-vertical disrupted zones of reflections reaching points A and B are interpreted as the intrusion wings, while chaotic reflections, cross cutting stratified background reflections of the host unit are interpreted as sediment offshoots from the main body of the sand intrusion.

- **Fig. 4.16** a and b) seismic section demonstrating contrasting interpretations of the features underlying Mound 1 a) Mound formed by single intrusion with an irregular aperture as a result of an irregular base and top b) Mound formed by two separate intrusions, with the decrease in relief caused by the thinning towards the intrusion wing (Fig. 4.16a).
- **Fig. 4.17** a) an RMS map of the lower half of the Utsira Sand showing high amplitude areas concentrated within a depression between two mounds b) seismic section through the high amplitude feature revealing their infilling and upwards concave nature, c and d) points below the high amplitude features where the Base Utsira Horizon is discontinuous e) sub-vertical zones projected upwards from point D to discontinuous points of the Base Utsira Horizon (arrowed).
- **Fig. 4.18** a) an RMS map of the lower half of the Utsira Sand showing high amplitude areas concentrated along the boundary of an elliptical mound. b)The seismic section shows that the high amplitude feature 'infills' a depression at the mound flank and overlies a discontinuity part of the Base Utsira Horizon (arrowed) c) black and white representation of the break in Base Utsira Horizon.
- **Fig. 4.19** an example taken from by Huuse et al., (2004) indicating the possible presence of extrusive deposits.
- **Fig. 4.20** a) a mound underlain by a sand intrusion (SI) with associated sub-vertical disrupted reflections projected towards mound hinge points b) a lower section of onlapping reflections at the southern flank with overlying downlapping reflections c) onlapping reflections at northern flank (R1, R2, and R3) with overlying reflections downturned at points A and B.
- **Fig. 4.21** a) a mound with an overlying 'hanging' Top Utsira Horizon which appears to deflect downwards at point E and F b) an internal reflection which downturns at point A and downlaps onto the mound at point C c) the same pattern is mirrored at the eastern flank of the mound, the reflections downturns at point B and downlaps onto the mound at point D.
- **Fig. 4.22** a) TWT map of the Top Utsira Horizon demonstrating the subtle changes in topography
- b) an azimuth map of the same horizon showing the distinct form of two 'trenches' orientated SSW-NNE
- **Fig. 4.23** a) demonstration of how measurements for the Top Utsira depressions were taken b) time depth map of an irregular shaped mound overlain by a contour map of the Top Utsira depression c) seismic section through the mound, line location denoted by dashed black line d) time depth map of an elongated mound overlain by a contour map of the Top Utsira depression e) seismic section through the mound, line location denoted by red line
- **Fig. 4.24** a) Isopach map of the Utsira Sans demonstrating its variable thickness through the study area, and the influence of the elliptical mounds at the Base Utsira level and the elliptical depressions

at the Top Utsira level b) seismic section, location denoted by dashed line, showing the thinning of the unit due to its wedge shape and the presence of sand intrusions.

Chapter 5

- **Fig. 5.1** a) Location map of the study area. a) with respect to the UK and Norway and b) Study Area 2, large black square, in relation to study area 1 (SA1) and 3 (SA3) c) Base map of the Base Utsira Horizon with location of Fig. d and Fig. 5.2 d) seafloor reflection is the dominant negative (red) reflection, and the wavelet appears to be in minimum phase
- **Fig. 5.2** shows a representative seismic section of the two main units from which the results of the chapter are derived from; the Lowermost Shale and the Utsira Sand. The base of the Lowermost Shale is a polygonally faulted horizon. The Base of the Utsira (BU) is often displaced upwards to form local highs, while the top of the Utsira (TU) is often seen to be displaced downwards to form local lows.
- **Fig. 5.3** a) An RMS map of the Lowermost Shale with a b) time-slice intersecting six high amplitude features c) a S-N seismic section showing high amplitude feature A with a wedge shaped area of disrupted reflections (DR) and broken Base Utsira reflections (BR) d) a W-E section showing high amplitude feature A and B with associated disruption zone (DZ) and sub-vertical disrupted reflections (arrowed).
- **Fig. 5.4** a) An RMS map of the Lowermost Shale showing a group of high amplitude reflections (B,C,D and E) b) a S-N section with the high amplitude c) an arbitrary line connecting the high amplitude features to form a flat based bowl geometry.
- **Fig. 5.5** Interpretation of the high amplitude features and associated disrupted reflections see Section 5.4.1.1.
- **Fig. 5.6** a) a time-slice intersecting several high amplitude reflections and b) an RMS map of the Lowermost Shale displaying the same features (A,B,C,D and E) c) d) e)and f) seismic sections of the high amplitude reflections
- **Fig. 5.7** a) An RMS map of the Lowermost Shale with a b) time-slice intersecting the curved high amplitude reflection c) W-E section through the feature and a d) a S-N section, the reflection has a sub-vertical zone of disrupted reflections projecting from its tip to point B.
- **Fig. 5.8** a) a time-slice intersecting a pair of high amplitude reflections (arrowed) with a dominant negative (red) amplitude, considered a hard event b) a S-N seismic profile of the discordant, oppositely dipping reflections.
- **Fig. 5.9** interpretation of the semi-circle high amplitude reflection from Fig. 5.7. The north-west high amplitude segment represents the cemented sector of the sand intrusion, while the lower amplitude south-eastern segment is not cemented.

- **Fig. 5.10** examples the best representation of 'V' and' U' brights from the study area a) and b) a small scale 'V' bright c and d) asymmetric 'V' bright, preferentially developed to the north e and f) an irregular saw toothed 'V' bright
- **Fig. 5.11** a) TWT map of the Base Utsira Horizon displaying several concentrated areas of high relief, the North West Cluster Area (NWCA), North East Cluster Area (NECA) and the South West Cluster Area (SWCA) b) a time-dip map of the Base Utsira Horizon, with areas of increased gradient denoted by black lines, these areas coincide with the outlines of the mounds.
- Fig. 5.12 Individual mounds located within the North West Cluster Area
- Fig. 5.13 Individual mounds located within the South West Cluster Area.
- **Fig. 5.14** Individual mounds located to the south of the North East Cluster Area.
- **Fig. 5.15** Individual mounds located within and proximal to the North East Cluster Area.
- **Fig. 5.16** a) a W-E seismic section through the NWCA, line location denoted by dashed line b) a S-N seismic section through the NWCA, line location denoted by solid line c) an RMS map of the Lowermost Shale overlain by the NWCA contour, showing a concentration of high amplitude within the contour boundary d) a coherency slice (depth in red, Figure e) with greater coherency outside the NWCA contour.
- **Fig. 5.17** a) a seismic section through mounds 39 and 41, mound 39 is underlain by mounded reflections (MR) and a chaotic dome (CD) b) the internal geometry of the Utsira reflections, showing onlap (reflections 1 and 2) and downlap (reflections 3, 4, 5) onto the mound, reflection 6 drapes over the mound c) Mound 41 is also underlain by a chaotic dome (CD) and broken reflections (BR) project upwards from the dome to the Base Utsira Horizon
- **Fig. 5.18** a) time-depth contour of a mound is rendered over a RMS map of the Lowermost Shale b) a S-N seismic section c) a W-E seismic section d) a SE-NW seismic section display the high amplitude reflections underlying the mound
- **Fig. 5.19** interpreted sand bodies underlying a) Mounds 39 and 41 from Fig. 5.17 b) c) and d) sand body underlying mound from Fig. 5.18
- **Fig. 5.20** a) Isopach map of the Utsira Sand, showing areas of thinning which coincide with mound locations b) TWT map of the Top Utsira Sand demonstrating the subtle changes in topography in comparison with the Base Utsira (Figure 5.1).
- **Fig. 5.21** a) a S-N seismic section through Mound 3 b) contoured time-depth map of Mound 3 c) time-depth contour of the depression rendered over time-depth map of Mound 3.
- **Figure 5.22** a) a W-E seismic section through Mound 6 and 5 b) contoured time-depth map of Mounds 6 and 5 c) time-depth contour of the overlying depression rendered over time-depth map of Mounds 6 and 5.
- **Fig. 5.23** graphs of a) mound eccentricity v depression eccentricity b)mound area v depression area c)subsidence v relief

- **Fig. 5.24**, a W-E transect of Mound 12, with the vertical displacement of the Base Utsira Horizon, the Top Utsira Horizon and an internal horizon plotted along mound the profile.
- **Fig. 5.25** a S-N transect of Mound 9, with the vertical displacement of the Base Utsira Horizon, the Top Utsira Horizon and an internal horizon plotted along the mound profile
- **Fig. 5.26** a S-N transect of Mound 39, with the vertical displacement of the Base Utsira Horizon, the Top Utsira Horizon and an three internal horizons plotted along the mound profile.
- **Fig. 5.27** a) demonstrates the expected geometry of the internal reflections at the mound flank if mound subsidence was at T_2 b) demonstrates the expected geometry of the internal reflections at the mound flank if mound subsidence was at T_5
- **Fig. 5.28** a), b) and c) demonstrate the expected geometry of the reflections at the mound flanks if they are considered to be indicators of the extent of movement along the mound profile
  d) is an example of the reflection geometry which fit this hypothesis.
- **Figure 5.29** demonstrates the discussed relationship between the sand intrusion aperture, and zones of subsidence.

Chapter 6

- Fig. 6.1 a) a TWT map of the seafloor within study area 2 (Chapter 5) with study area 3 denoted by black square b) study area 3 in relationship to preceding study area.
- **Fig. 6.2** Seafloor reflection where the red (negative) reflection is the dominant amplitude, suggesting that the data is displayed in conformity to the European Convention. Wavelet appears to be in minimum phase.
- **Fig. 6.3** a S-N seismic section presenting the units and horizons discussed in this Chapter.
- **Fig. 6.4** a) an RMS map of the whole Lower Seal b) RMS map of the upper half of the Lower Seal. Both maps are co-rendered with the contour of the NWCA (Chapter 5)
- **Fig. 6.5** a) a W-E seismic section displaying three high amplitude features within the Lower Seal (A, B and C) b) location map of the W-E line c) contoured RMS map of the three high amplitude areas. The high amplitude areas have associated fingering (f), circular outliers (c.o) and irregular outliers (i.o).
- **Fig. 6.6** a) a S-N seismic section displaying two high amplitude features within the Lower Seal (D and E) b) location map of the S-N line c) contoured RMS map of the three high amplitude areas. The amplitude anomalies are concentrated within the Lower Seal High Amplitude Horizon (LSHAH).
- **Fig. 6.7** a) RMS map of the Lower Seal in comparison with the b) amplitude map of the LSHAH for more detailed analysis individual examples with the RMS contour co-rendered with the amplitude map of the LSHAH are presented c) d) and e).

- **Fig. 6.8** a) amplitude map of the LSHAH is co-rendered with the contour of the time-depth map of the LSHAH to identify conformity to structure. Only in Fig. b and c is there any indication of conformity in this example. d), e) and f) show the high amplitude features with underlying depressions (D).
- **Fig. 6.9** a) amplitude map of the LSHAH is co-rendered with the contour of the time-depth map of the LSHAH to identify conformity to structure. Greater conformity to structure is displayed by this example compared to Fig. 6.8. b) two small scale depressions underlying the high amplitude area c) 3D visualisation of the high amplitude feature.
- **Fig. 6.10** a) a time-slice shows the outline of the negative, lower, reflection of amplitude anomalies H and I, sub-circular features of black reflections are seen within their outline b) these are visible as small scale depressions along a SE-NW seismic section. The black, positive, reflection has the dominant amplitude of these features, and they are considered 'soft' events.
- **Fig. 6.11** a) TWT structure contour map of the top of the MTD unit with the protruding promontory of shallower topography (Grey area) b) a TWT structure contour map of the base of the MTD unit, showing large scour feature (S).
- **Fig. 6.12** a) NW-SE seismic section intersecting the scour feature shown in Fig. 6.11b.
- **Fig. 6.13** a) a time-slice dissecting the MTD unit, with two distinctly different areas of reflections,b) a smaller scale section of the time-slice displaying linear features c) a seismic section intersecting these linear features, interpreted as basal scours.
- **Fig. 6.14** a deeper time-slice dissecting the MTD unit, the chaotic area has progressed more to the southeast, a large area of a red reflection is located at point R
- **Fig. 6.15** an isopach map of the MTD unit with a 100m thickness contour.
- **Fig. 6.16** a) a NW-SE orientated seismic section transecting the b) area of greatest thickness. Scours at the base of the unit coincide with the black linear features evident on the time-slice which dissects the basal section of the MTD unit.
- **Fig. 6.17** the 100m contour co-rendered with the RMS map of the MTD unit. A large proportion of the high amplitude areas are located within the boundaries of the 100m contour.
- **Fig. 6.18** a) a small scale section of the RMS map with locations of seismic sections b) NW-SE section along the demonstrating the variable nature of the MTD unit within the thicker area, features include; **A** high amplitude bright spot, **B** stratified reflections ,**C** low amplitude reflections, **D** areas of low amplitude and **E** downward incisions. c) SW-NE section across the area of greatest thickness includes the following features; F chaotic area, **G and H** horizontal semi-continuous reflections, **I and J**. imbrication of the internal reflections
- **Fig. 6.19** a) location of the seismic section b) BS1 and BS2 are circular areas of high energy c) SSW-NNE seismic section showing five bright spots above a Base Utsira forced fold, discontinuous sections of the Base Utsira Horizon are arrowed, with a possible pockmark at the Top Utsira (B) d) possible polarity reverse (PR?) with a underlying discordant bright spot.

- **Fig. 6.20** a) RMS map of MTD horizon with location of seismic section b) BS6 is sub-circular feature, c and d) S-N section with BS6. The hinge point of the Base Utsira Horizon is broken (HP), and is associated with a vertical disruption zone (VZ) which extends to the Top Utsira Horizon (B), proximal to a high amplitude section of the Top Utsira Horizon (A), a secondary vertical disruption zone (VZ2) extends upwards from the MTD unit.
- **Fig. 6.21** a) RMS map of MTD horizon with location of seismic section and the group of high amplitude areas b) c) and d) S-N section with high amplitude section within the MTD unit (G). The hinge point of the Base Utsira Horizon is broken (BU), and is associated with a vertical disruption zone (VZ) which extends to the Top Utsira Horizon (TU). Sand intrusion wings are evident in the Lowermost Shale unit (W).
- **Fig. 6.22** a) a schematic diagram of extensional and compression zones associated with sand intrusion compaction. The extensional zones represent possible permeability pathways obliquely upwards from edges of the elliptical mounds b) a contour of a base Utsira mound is co-rendered with a time-slice dissecting the Utsira Sand around a 100m from the mound hinge point. An outer rim of disrupted reflections is seen to encompass the mound contour, suggesting the presence of ring faults.
- **Fig. 6.23** a time-slice dissecting the Middle Seal upper boundary horizon displays branch like system (arrows) emanating from a central area (CA).
- **Fig. 6.24** a) locations of seismic section on the time-slice of the Middle Seal upper boundary b) S-N section highlighting the features of the two western branches c) arbitrary line intersecting the two main eastern branches.
- **Fig. 6.25** a series of deepening time slices indicating the progression of the branch features from the NW to the SE.
- **Fig. 6.26** a) an RMS map of the Middle Seal with high amplitude lobe features, location of seismic section denoted by black lines b) the high amplitude lobes as concave downwards features.
- **Fig. 6.27** a) locations of seismic section on the time-slice of the Middle Seal upper boundary b) an apparent vertical chimney crosscutting the Middle Seal reflections, apparent as a discordant reflection at the Middle Seal upper boundary (DR) c) bright spots (BR) located within the chimney, also discordant reflection (DR). The chimney appears to be in connection with a high amplitude area within the LSHAH.
- **Fig. 6.28** a) a TWT and b) amplitude map of the Seafloor horizon. Small scale depressions and reversals in amplitude are present at this horizon. The labelled depressions are presented in more detail within this section.
- **Fig. 6.29** seafloor features D1 and D2 on a) amplitude map b) seafloor time slice with seismic line location c) a S-N seismic section of the seafloor features, apparent as breaks in the seismic signal, they are underlain by vertical disruption chimneys (VDC1 and VDC2) and are proximal with a mound of disrupted MTC reflections, d) and e) the VDC's include bright spots and dim or weak zones of reflections.

- **Fig. 6.30** seafloor features D3, D4 and D5 on a) amplitude map with seismic section location b) a SW-NW arbitrary seismic section of the seafloor features, apparent as breaks in the seismic signal, they are underlain by vertical disruption chimneys (VDC3, VDC4 and VDC5) and overlie an area where the Base Utsira Horizon is displaced c) VDC's include bright spots and dim or weak zones of reflections, while their deepest extent is difficult to determine.
- **Fig. 6.31** a TWT map of the seafloor co-rendered with a) 100m MTD contour and b) the Base Utsira Horizon with the NWCA labelled. The entire seafloor features lie within the 100m contour, while there is no apparent relationship with the contour of the Base Utsira Mounds.
- **Fig. 6.32** a) an example of a 'wipe out zone' (A) interpreted by Løseth et al.,(2009) as a gas chimney b) example of a 'wipe out zone' from within the MTD unit from this study area. A vertical disrupted zone of reflections emanates from the crest of the 'wipe out zone', and may be linked to pressure build up due to gas accumulating within the MTD.
- **Fig. 6.33** a schematic diagram representing the interpreted effect and increasing magnitude of the high permeability 'cone of disruption' associated with the sand intrusions.

Chapter 7

- **Fig. 7.1** a) schematic diagram demonstrating the formation of permeability pathways following post emplacement compaction of sand intrusions with representative examples from the study area b) diagram demonstrating the subsidence differential along the mound profile
- **Fig. 7.2** a) schematic diagram demonstrating the exploitation of the permeability pathways at the forced fold flank by migrating gas. Representative examples from the study area of; b) pockmark at the Top Utsira Horizon c) and d) gas accumulation within the Lower Seal High Amplitude Horizon e) sub-vertical disruption zone leading to a high amplitude area.
- **Fig. 7.3** a) schematic diagram demonstrating the presence permeability pathways from the Utsira Sand to the MTD unit. Representative examples from the study area of; b) narrow vertical zones leading to bright spots c) and d) bright spots within MTD unit e) larger area f high amplitude in MTD unit f) wider vertical zone leading to high amplitude area.
- **Fig. 7.4** a) schematic diagram demonstrating the migration from Utsira Sand to the MTD with subsequent lateral migration along MTD unit. Representative examples from the study area of; b) wider vertical zone leading to high amplitude area c) possible gas accumulation within MTD unit d) possible gas chimneys
- **Fig. 7.5** a) schematic diagram demonstrating gas chimneys from Utsira Sand through the MTD unit to seafloor. Representative examples from the study area indicating roots of chimneys b) c) chimney 1 d) and e) chimney 2.

Chapter 1

Introduction

1. Introduction

1.1. Rationale

Carbon capture and sequestration is increasingly being considered as an important and viable method of reducing the emission of anthropogenic greenhouse gases to the atmosphere (Holloway, 2006; IPCC, 2002). It has been suggested that it is 'an immediately available and technologically feasible means of reducing CO_2 emissions (Bachu, 2000, pg 87), and it is considered to have the potential to make 'significant reductions in carbon emissions from point sources' (Hosa et al., 2011). The process involves capture of CO_2 from a stationary source, its transportation by pipeline, and injection and storage within suitable geological media.

Natural accumulations of CO_2 in the Earth's subsurface are the result of biological, igneous and chemical activity, and are proof of the sub-surface's ability to store CO_2 over geological time. The injection of CO_2 into oil and gas fields is a long-established component of the enhanced oil recovery process, and is further evidence that CO_2 may be retained within geological media.

Three main types of storage options in geological formations are recognised; depleted oil and gas fields, un-mineable coal seams, and saline aquifers. Each option has advantages and disadvantages, predominantly due to storage availability, location, capacity, and geological knowledge. Each factor contributes to the economic and engineering challenges faced.

The injection and storage of CO_2 utilises technologies that have already been developed and applied by the oil and gas industry (IPCC, 2005). The engineered injection of CO_2 for EOR projects began in Texas in the 1970s, and has become a common practice in the oil and gas industry. By the late 1990's the geological storage of CO_2 in the subsurface was becoming an increasingly attractive option for oil companies producing from onshore oil fields with high natural CO_2 content (IPCC, 2005). However, the injection into suitable geological formations specifically for storage is still a relatively new process, and to fully realise the potential of this method of reducing atmospheric CO_2 emissions it must be shown to be safe, environmentally sustainable, cost-effective and capable of being broadly applied (IPCC, 2005).

To assure public safety and acceptance it must be demonstrated that the risk of leakage from proposed storage reservoirs is small. A sound and as complete as possible understanding of all aspects of storing CO_2 underground is therefore vital for the viability and success of current and

future storage projects. Careful site selection, effective regulatory oversight, an effective monitoring programme, and remediation methods to stop or control CO_2 release are required to avoid or mitigate the impact of leakage (IPCC, 2005).

The long term integrity of the sealing lithology is a major factor in determining the leakage risk during the site selection process. Sound and complete geological knowledge of potential storage sites on a case-by-case and site-specific level is therefore required. The storage reservoir and sealing lithologies must be understood and any geological features which may promote cross stratal flow identified.

The overall objectives of this research are to further understand the geology of a CCS storage reservoir, identify geological features affecting the reservoir, and to identify geological features which may pose a leakage risk to the sequestered CO_2.

1.2. Overview

The aims of this Section are to: 1) provide an overview of CCS and further describe the storage options; 2) explore the trapping mechanisms at work; 3) introduce current CCS projects, and specifically the Sleipner project.

1.2.1. Carbon capture and storage options

Carbon capture and storage involves the capture of CO_2 from major stationary sources, its transportation by pipeline, and its injection into suitable geological formations. The successful geological disposal of CO_2 has three key requirements:

- Capacity; the storage formation must offer sufficient capacity to receive and retain suitable amounts of CO_2.
- Injectivity; the ability of the reservoir to receive the CO_2 at a rate that matches that of its production.
- Containment; the injected CO_2 must be contained in the storage formation.

Both the capacity and injectivity are features of the storage reservoir and depend on relatively high porosity and permeability values. Storage capacity is provided by the pore volume of the geological

formation. The pore volume is used to calculate the mass of CO_2 which may be stored within the storage reservoir; the calculated mass is termed 'static capacity'.

Injectivity is dependent on the storage formation's permeability, the net thickness of the storage reservoir, and the viscosity of the injected fluid, and in the medium term, on the rate and magnitude of pressure build-up within the storage reservoir. CO_2 is injected through individual or multiple wells which are perforated or covered by a permeable screen. As the CO_2 is injected it causes an increase in pressure around the injection point, displacing the brine, and invading the vacated pore volume. In the case of a formation having low injectivity, the rate at CO_2 can be stored may be reduced to limit the increase of pressure within the storage formation. Generally, sedimentary rocks are the only lithologies to offer sufficient porosity and permeability for large scale, high rate CO_2 storage of the type that might be expected from a fossil fuel fired power plant or other large combustion plant.

CO_2 is likely to be stored as a supercritical fluid, sometimes described as "dense phase" CO_2, in order to achieve high storage densities. This requires reservoir conditions above the critical point (31°C, 74 bar). Under these conditions CO_2 as shares some characteristics with gas while also having the density of a fluid (600 to 800kg/m^3), this allows it to rise under the effect of buoyancy. To contain the CO_2 an impermeable rock unit is required to restrict its migration out of the storage formation. Confinement of the CO_2 is key; while storage formations with limited capacity and injectivity may still theoretically be utilised, a storage site which cannot confine the injected CO_2 to the storage formation cannot be realistically used.

The major sedimentary basins of the world host the majority of potential storage sites, their thick accumulations of sediment include porous and permeable rock formations for storing and injecting CO_2, and low porosity lithologies for its confinement. This combination of geological formations gives rise to the potential storage sites of depleted hydrocarbon fields and so-called saline aquifers (saline water-bearing reservoir rocks), which, along with deep coal seams, are the three main options for CO_2 storage. A brief overview of the main storage options is presented below.

1.2.1.1. Depleted oil and gas reservoirs

Porous and permeable rocks from which oil and gas can be produced are called reservoirs. Depleted oil and gas reservoirs have an estimated capacity of 675-900 $GtCO_2$ (IPCC, 2005), and there are four major advantage of utilising depleted oil and gas reservoirs as storage sites for captured CO_2;

- Their proven ability to hold hydrocarbons in place over geological time demonstrates their storage safety and integrity of seal.
- The exploration processes of mapping and drilling potential hydrocarbon fields ensures that the confining structures and storage reservoirs are well known.
- Modelling techniques developed and implemented by the oil and gas industries to understand each specific reservoir can be utilised to predict the behaviour of the injected CO_2.
- The infrastructure for hydrocarbon extraction is already in place and can be used to inject the CO_2.

Although exploration wells increase the geological knowledge and understanding of the trapping structures and storage reservoirs, they may also pose a leakage risk to the injected CO_2. Wells which penetrate the caprock must be considered a risk, and incorrectly capped wells may be locations of possible leakage (Wildenborg and Lokhorst, 2005).

1.2.1.2. Current oil and gas reservoirs

Current oil and gas reservoirs are also storage options. Hydrocarbon fields still in production can benefit from the infrastructure already in place and may utilise the injected CO_2 for enhanced oil or gas production (e.g Weyburn project), and thus decrease the storage costs. Storage availability is a consideration as the injection of CO_2 may cause CO_2 to be produced along with the hydrocarbons. Particularly in the case of gas production, this may adversely affect the economics of the field. Therefore, injection may need to be delayed until the field is depleted. Additionally, the majority of oil and gas field are a significant distance from major sources of CO_2, increasing cost and engineering problems (Wildenborg and Lokhorst, 2005).

1.2.1.3. Un-mineable coal seams

Sequestration of CO_2 in coal seams involves a different confinement mechanism to that at work in saline aquifers and hydrocarbon reservoirs. Coal seams can physically adsorb gas molecules and the use of CO_2 for Enhanced Coal-Bed Methane Recovery (ECBM) has highlighted the possibility of storing CO_2 as a byproduct of this process. Injected CO_2 flows through fractures within the coal seams and is adsorbed onto the surfaces of the coal micropores. When using this method to release the coal-bed methane, a CO_2:CH_4 adsorption ratio of between 1:1 and 1:10 is possible depending on

the maturity of the coal, and injection into bituminous coal seams can theoretically result in a highly efficient storage mechanism (Shi and Durucan, 2005).

Storage through ECBM is an attractive option due to the large volume of coal in the world's sedimentary basins and the common proximity of coal fields to sources of CO_2. Storage costs may also supplemented by the revenue from the methane produced.

A major limiting factor is the permeability of the coal seams. ECBM relies on the fractures within the seams to allow the CO_2 to permeate through the storage formation, and they are generally considered to be of low permeability. Most un-mineable coal seams are at a significant depth, and coal seam permeability generally decreases with depth due to the effect of increasing effective stress closing the fractures. The swelling (Shi and Durucan, 2005) and plasticisation (Larsen, 2003) of the coal following adsorption are other factors which effectively reduce permeability. Due to the permeability issues, capacity estimates for un-mineable coal seams are uncertain and wide ranging, with estimates ranging between 3 Gt and 200 Gt CO_2 (IPCC, 2005). European potential storage capacity is estimated at 6 Gt (IEA GHG, 2005).

1.2.1.4. Deep Saline Aquifers

Deep saline aquifers are defined as: "aquifers whose groundwater salinity makes them unfit for human consumption" (Bachu and McEwen, 2011), and due to their depth and high salinity the water cannot be economically exploited. Deep saline aquifers are considered a promising storage option due to their great potential storage volume and geographical spread (IPCC, 2005, Michael, 2010). They total an estimated 90% of the storage resource in most regions (Hosa et al., 2011). While shallower aquifers are preferable for smaller injection costs, sufficient storage depth is requires to contain the injected CO_2 within the supercritical state (generally greater than 800m) (Hosa et al., 2011).

Bentham and Kirby (2005) divide the storage of CO_2 in aquifers to 'confined' and 'unconfined'. Storage in confined aquifers is via stratigraphic or structural means, similar in manner to the confinement of hydrocarbons in reservoirs. When CO_2 is injected into an aquifer without large scale stratigraphic or structural closure it is considered unconfined. In this case the CO_2 migrates upwards from the injection point until it reaches an impermeable barrier, at this point it begins to spread laterally infilling any minor structural closures it encounters. CO_2 stored in unconfined aquifers is

therefore generally distributed over a larger area than in confined aquifers (Bentham and Kirby (2005). The storage volume within an unconfined aquifer is dependent on the 'roughness' (traps per unit area) of the upper sealing surface.

Worldwide capacity for saline aquifers is estimated at a minimum of 1000 Gt CO_2 storage capacity, and may be several orders of magnitude larger (IPCC, 2005). Aquifer storage is generally readily available and does not require the depletion of hydrocarbon fields; however conflict may exist between CO_2 storage and natural gas storage or geothermal operations in saline aquifers (Bentham and Kirby, 2005).

A major disadvantage of saline aquifers as storage formations is the increase in geological uncertainty. While oil and gas reservoirs have been proven to trap hydrocarbons the cap rock integrity of saline aquifers is less assured, and significant investigation would be required to confirm seal effectiveness (Bentham and Kirby, 2005). Hydrocarbon reservoirs are also extensively drilled and are therefore better understood, their structures and the physical properties of the reservoirs are well characterised and the migration of the CO_2 within them can be modelled generally with greater confidence than would be the case for saline aquifer storage sites. Reservoir heterogeneities of saline aquifers are not so well understood, as highlighted at the Sleipner project where monitoring of plume development has revealed geological features that have only become apparent post injection (Eiken et al., 2011).

1.2.1.5. Other storage options

Storage options which may offer local and 'niche' opportunities for CO_2 sequestration are:

- **Basalts**. The possible reaction of CO_2 with silicates within the basalts to form carbonate minerals, may offer a form of mineral trapping. This would require the low permeability, low porosity, basalts to be fractured to allow the CO_2 to permeate through them, and a suitable seal to stop leakage (McGrail et al., 2006). Basalts occur globally in large volumes, but are currently considered an impractical storage option (IPCC, 2005).

- **Oil or gas rich shale** adsorbs CO_2 onto organic material in the same way as coal. This method has also the advantage of reduced storage costs (as with EOR and ECBM) if associated with the

production of shale gas. There are no current storage estimates, but the large volumes of shale gas suggest that there may be substantial potential storage volume available. Shallow depths of shale beds and their low permeability may be disadvantages to this option.

- **Salt caverns and abandoned mines** have potential storage structures but offer limited storage capacity for CO_2. Storage security is questionable and may require costly engineering solutions.

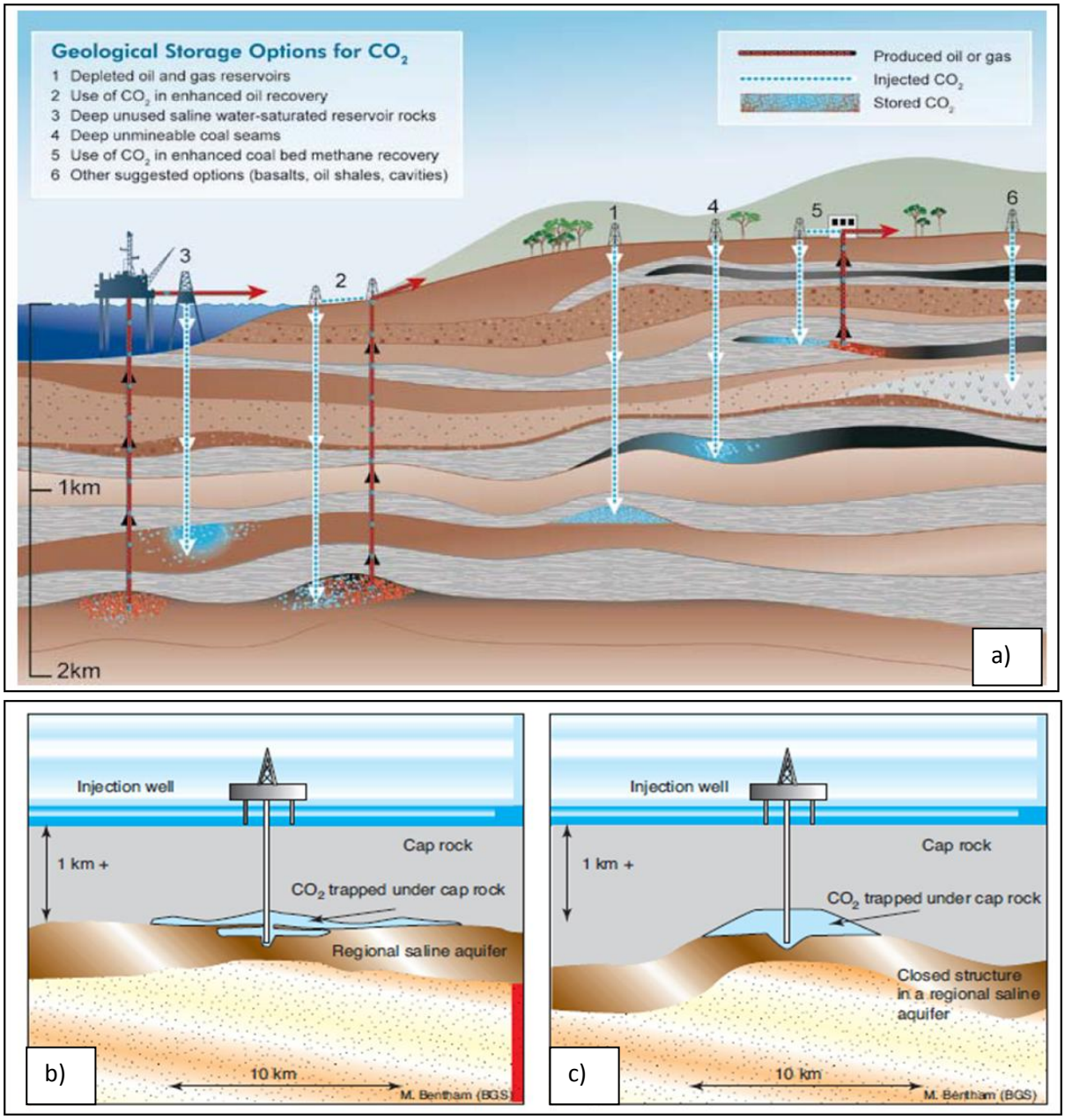

Fig. 1.1a) Summary of the storage options for CO2 sequestration (taken from the IPCC, 2005). Conceptual diagram of storage in an b) initially unconfined "migration-assisted" storage and c) confined, structurally trapped storage

1.2.2. Trapping mechanisms and storage security

The sequestration of CO_2 in the subsurface is possible by several different physical and geochemical trapping mechanisms. These mechanisms can be sub-divided into four classes; structural and stratigraphic trapping, residual trapping, dissolution/solubility trapping and mineral trapping (IPPC, 2005).

Structural and stratigraphic trapping and residual trapping are forms of physical trapping, while both solubility and mineral trapping are geochemical trapping mechanisms. Physical trapping allows the CO_2 to retain its chemical composition, while geochemical trapping promotes change in its chemical composition (Bachu and McEwen, 2011).

Storage security increases with time as the CO_2 becomes less mobile under the increasing influence of multiple trapping mechanisms. The influence of each class of trapping mechanism varies with time, and when their contribution to the confinement of CO_2 with time is compared to the duration of the injection period it allows their classification into primary or secondary trapping mechanisms (Bachu and McEwen, 2011). Those with comparable timescales to injection are classified as primary mechanisms and consist of structural and stratigraphic, and hydrodynamic trapping. Secondary trapping mechanisms consist of residual, dissolution, and mineral trapping and they result from the movement and interaction of the CO_2 with the surrounding formation water. They are reliant on effective primary trapping, operate on longer time scales than primary trapping, and are most effective following the cessation of injection (Bachu and McEwen, 2011). As secondary trapping involves the decrease of free-phase mobile CO_2 it is associated with increasing storage security and decreasing risk of leakage (Bachu, 2008).

We can therefore conclude that during the period from the commencement of injection to its cessation, CO_2 confinement is mostly reliant on physical and primary trapping mechanisms. The risk of leakage is at its highest, and this can be considered a critical period for the success of sequestration projects.

1.2.2.1. Structural and stratigraphic trapping

Structural and stratigraphic trapping are both primary and physical trapping mechanisms. They are initially the dominant trapping methods and involve the physical trapping of CO_2 by a sealing lithology in a similar manner to the way in which hydrocarbons are trapped below a cap rock. Structural and stratigraphic traps consist of a permeable lithology which is overlain by a low permeability seal. The seal acts as a barrier to the upward movement of the buoyant CO_2 back towards the atmosphere. An effective seal requires the capillary pressure it produces to be equal to or greater than the buoyancy forces driving the medium that is being trapped. Capillary pressure is a function of the interfacial tension, wettability, and the pore throat radii of the seal (Berg, 1975):

$$\text{Capillary pressure} = \frac{2\gamma cos\theta}{R}$$

Where γ is the interfacial tension between the hydrocarbon/CO_2 and brine, θ is the wettability, expressed as a contact angle of the hydrocarbon/CO_2-water interface, and R is the radius of the pore throat. Most rock surfaces are considered 'water wet' and θ may be taken as zero, and the equation can be simplified to:

$$\text{Capillary pressure} = \frac{2\gamma}{R}$$

The sealing capacity of a rock therefore decreases with decreasing interfacial tension, and increases with decreasing pore throat radii. The main difference between the sealing mechanism of a hydrocarbon system and CO_2 storage is that the interfacial tension between CO_2 and brine is less than that between hydrocarbons and water. As a result, a specific seal is slightly less efficient at containing CO_2 than it is for hydrocarbons, although still sufficiently effective to contain CO_2. A seal is only as efficient as its largest connected series of pore throats, and even quality class seals of homogeneous, low permeability lithologies may fail to contain hydrocarbons (Nordgård Bolås et al., 2005) if they are cut by geological features which breach the seal and compromise its capacity as an efficient barrier to migrating hydrocarbons and sequestered CO_2. Such features will be discussed in section 1.2.4.1

1.2.2.2. Residual trapping

As the CO_2 migrates within the storage reservoir, residual trapping becomes a significant trapping mechanism (Benson, 2005), which becomes increasingly influential with time. Residual trapping also enhances storage security as it does not directly depend on an intact seal (Suekane et al., 2008). As with structural and stratigraphic trapping it is considered a physical trapping method and involves the trapping of CO_2 as immobile residual droplets left behind within pore spaces as the CO_2 plume migrates.

As the supercritical CO_2 is injected into the formation it moves upwards and displaces fluid from the pore spaces in the reservoir. As the majority of the CO_2 plume continues to migrate upwards the displaced fluid once again refills the pore spaces. However, not all the CO_2 remains in contact with the plume, and residual 'bubbles' of CO_2 which are too big to pass through the pore throat are left behind, and are trapped by capillary pressure at a pore scale. This mechanism has been termed 'capillary snap-off' (Bachu and McEwen, 2011). These CO_2 'bubbles' remain as residual droplets within in the pore space under a trapping mechanism referred to as residual gas or capillary trapping (Suekane, 2008; Bachu and McEwen,2011).

It is considered that a significant amount of CO_2 can be trapped in this manner (Juanes et al. 2006; Ide et al.2007). Residual trapping contributes to the physical trapping of the CO_2 immediately, although at a lesser initial amount than structural and stratigraphic trapping.

1.2.2.3. Dissolution/solubility trapping

Classified as a geochemical trapping mechanism, dissolution trapping further increases the storage security of the injected CO_2 (IPCC, 2004). It is effective immediately post injection and its contribution increases with time. CO_2 dissolves where in contact with water at both the interface of the CO_2 plume and the surrounding brine and when residually trapped in the pores (Gunter et al. 1997). When in solution the CO_2 loses its free phase buoyancy and flows with the brine (Bachu and McEwen, 2011).

Dissolution trapping has a twofold effect on storage security. Firstly, as CO_2 dissolves into the reservoir brine it is stored in solution. Secondly, as this solution is denser than the surrounding brine, it begins to sink towards the base of the storage reservoir, and thus increases the storage security

further. The movement of the heavier CO_2-saturated brine creates convection cells and the solution is replaced by CO_2-unsaturated brine at the plume-brine interface, this effectively accelerates the dissolution process (Ennis-King and Paterson, 2007).

1.2.2.4. Mineral trapping

The final and most secure trapping phase, mineral trapping, becomes active between 10 and 100 years post injection, although it is most effective on the millennia time scale (IPCC, 2004). This form of geochemical trapping involves the reaction between weak carbonic acid and the mineralogy of the storage reservoir. It is a mechanism which increases storage security further, and results in the long term immobilisation of CO_2 as it promotes the precipitation of CO_2 as solid carbonate minerals within the storage reservoir.

The carbonic acid is formed as a by product of dissolution trapping and mineral trapping is therefore dependent on that process. This reliance is reflected by the initial lack of mineral trapping contribution. It is also a relatively slow process; its rate is determined by the amount of formation brine and rock which is available for reaction (Bachu, 2008), and generally requires centuries to millennia for carbonates to precipitate (Xu et al., 2003).

1.2.2.5. Hydrodynamic trapping

If the CO_2 is injected into a saline aquifer with a large storage volume and at a sufficient depth but without structural or stratigraphic traps it may still be confined due to hydrodynamic trapping. This method of confinement is considered to be a primary trapping mechanism which is a combination of residual, dissolution and mineral trapping (Bachu, et al.,1994). It is therefore both a physical and geochemical trapping mechanism, and has been also termed as Migration Assisted Storage.

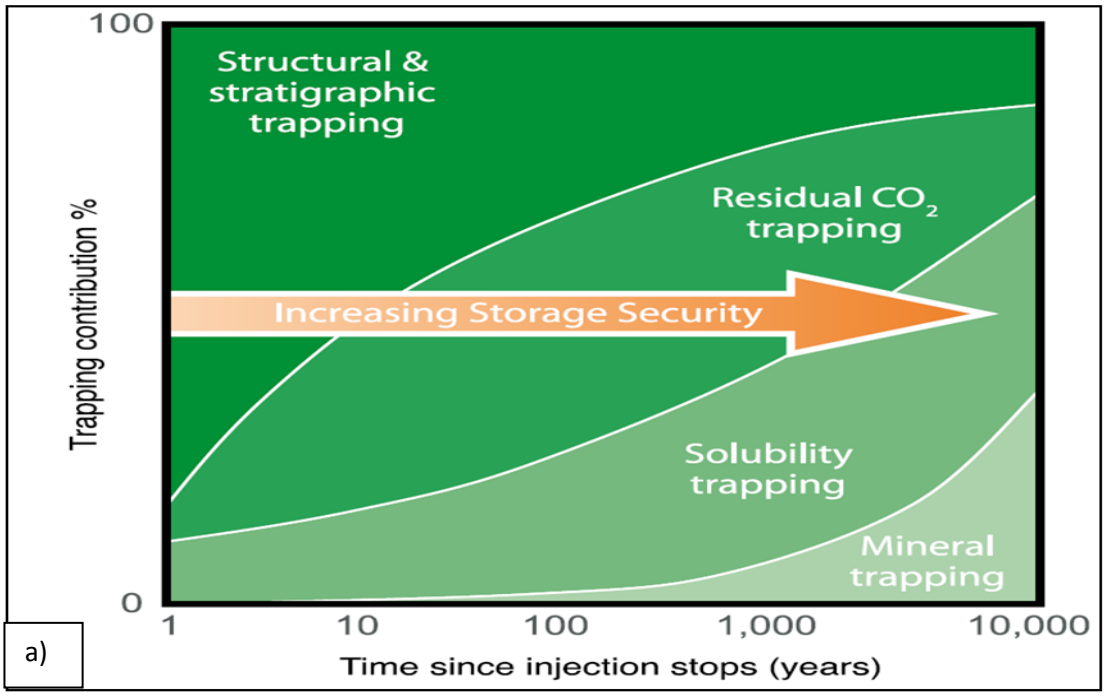

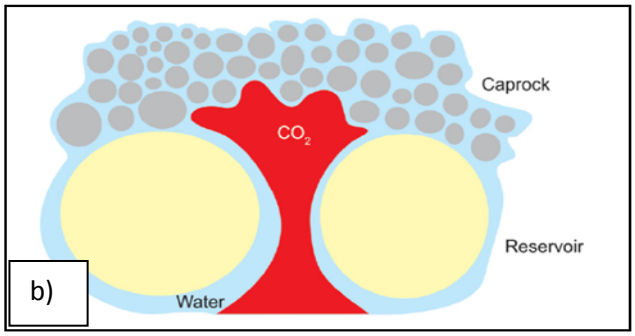

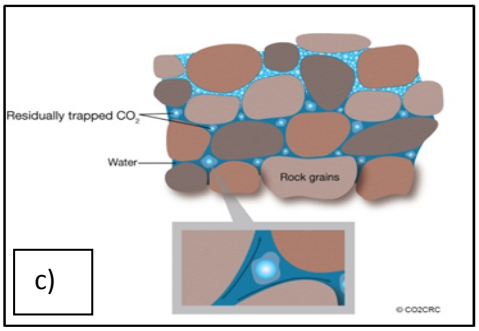

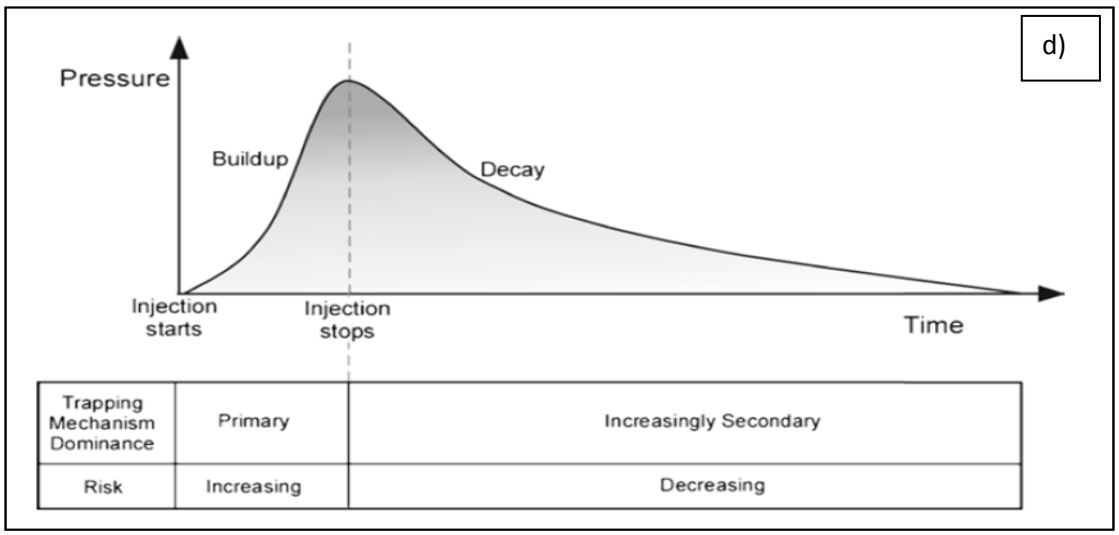

Fig. 1.2a) diagram demonstrating the changing influence of trapping mechanisms over time (taken from IPCC, 2005) b) trapping of CO2 via pore throat radii at caprock interface (taken from the CO2 Capture Project, 2009) c) a representation of residual trapping (taken from CO2CRC) d) changing levels of risk with trapping mechanisms (taken from Bachu, 2008).

1.2.3. Leakage

The leakage of CO_2 from a storage site back to the atmosphere is considered unavoidable but acceptable if the amount is small enough (Humez et al., 2011). Determining acceptable leakage rates and amounts has been an ongoing discussion within the scientific community (Bøe et al., 2005). If the sole purpose of injecting CO_2 into geological media is to prevent its emission into the atmosphere as a climate change mitigation option, a minimum performance requirement is that any leakage from a storage site should not have a worse effect on climate change than its direct venting to the atmosphere (Bøe et al., 2005). More specifically it is suggested that storage time should exceed 1000 years (Lindeberg, 2003), while the rate of leakage should not exceed 0.01% of the total injected CO_2 over the project life time (Hepple and Benson, 2002).

While the obvious effect of CO_2 leakage would be to compromise CO_2 storage as an effective climate change mitigation option, the consequences of leakage can be classified as; environmental, economical, and health and safety, and can be assessed on their effects in both the short and long term. A short term health and safety consequence is the acute danger to human and animal life through asphyxiation, although this does require exposure to high concentrations, and is highly unlikely especially when considering CCS involving offshore saline aquifers. Long term effects of leakage are relevant to the environment and specifically ecosystems. Onshore consequences would result in the death of or damage to vegetation and animals, while offshore, coral reefs would be affected. The degradation of potable groundwater is also possible, where carbonic acid may alter the pH of the water, mobilizing heavy metals, sulphate and chloride (Wang and Jaffe, 2004). Economic consequences include the degradation of hydrocarbon and mineral resources (IPCC, 2005).

Major leakage risks associated with storing CO_2 underground include leaking injection wells, leakage through abandoned wells, and leakage due to geological factors such as faults and fractures (Celia et al., 2009). Mechanical failure of the seal can be generally discounted as regulations limit the bottom hole pressure of the injection wells (Bachu and McEwen, 2011).

The presence of a low permeability cap rock as a sealing lithology can only physically contain the injected CO_2 if it is not broken or interrupted by potential fluid conduits which by pass its sealing capacity (Daniel, R. F., and Kaldi, J. G., 2008). This study will attempt to identify and present examples of such features, and discuss their leakage implications for sequestered CO_2.

1.2.4. CCS projects and site selection

Carbon storage projects can be generally sub-divided into three separate classes; commercial, demonstration, and pilot projects. They can be defined by their purpose, injection rate and life span (Michael et al. 2010);

Commercial projects purpose are to reduce greenhouse gas emissions from stationary industrial sources, they have an injection rate of over 1 Mt/yr and a life span of over 10years.

Demonstration projects are for research and verification of technology and safety at commercial injection rates. They have a life span of a year or more.

Pilot projects research and test injection, they also monitor technology at smaller injection rates and have a short project life (10 kt/year, for a period of a few weeks to a few years).

Some current commercial projects are associated with gas production from fields with a gas stream of high CO_2 content, examples of which include; Sleipner in the North Sea, Snohvit in the Barents Sea, and In-Salah, onshore in Algeria. The Sleipner Project is the first commercial scale project with the sole purpose of disposing of CO_2 from natural gas production (Michael et al., 2010), it will be described in more detail in section 1.2.5. A major forthcoming commercial project, expected to commence in 2014, is the Gorgon project in Australia. It plans to utilise an offshore saline aquifer and store a total of a 129 Mt, dwarfing the current maximum storage total by over a 100 Mt.

Other commercial projects are associated with the enhanced oil recovery (EOR) method, and although not originally intended or directly designed as storage operations, they are being used as further testing grounds for CO_2 storage and monitoring technology. The Weyburn CO_2-enhanced oil recovery project utilises CO_2 produced as a by-product of a coal gasification plant to enhance the oil recovery from the Weyburn Field in south east Saskatchewan, Canada. Injection commenced in 2000 and is planned to continue for 20 years, with a total estimated stored volume of 20Mt. The storage formation is a fractured carbonate which is overlain locally by an anhydrite seal, while a flat lying shale is considered to be an effective regional seal. An extensive monitoring programme is in place, including high resolution time-lapse seismic. Surface monitoring indicates to date that there has been no leakage to surface (White, 2009).

CO_2 driven Enhanced Coal Bed Methane (CO2-ECBM) projects are generally still at the demonstration or pilot stages (IPCC, 2005) and is considered an immature technology (Bachu,

2008). The majority of pilot projects have been based in the USA; however, the REPOCOL project in Poland is the first CO_2-ECBM outside of this area (Lokhorst and Wildenborg, 2005).

1.2.4.1. Site selection

All three of the main suitable options for geological storage of CO_2 are located within the sedimentary basins of the world. Site selection may be performed at several scales, from basin scale suitability, to regional scale suitability, and finally site specific suitability. With each stage of decreasing scale the potential storage volume also decreases.

Basin scale suitability assessment requires consideration of 'geological, geothermal, hydrodynamic, hydrocarbon potential, basin maturity, and economic and societal criteria' (Bachu, 2000; Bachu, 2003, pg 89). These criteria are sub-divided into hard and soft classes, with geology, geothermal and hydrodynamic considered 'hard' as they do not change on a human time scale (Bachu, 2003). Basins with relatively simple geological histories which are mature, cold, and tectonically stable are preferential (IPCC, 2005), as they are generally better understood, allow the storage of CO_2 as a dense state at shallower depths, and are unlikely to be affected by seismic activity.

On a site specific scale a site suitable for CO_2 sequestration needs to satisfy 2 general requirements; adequate capacity and injectivity, and a satisfactory sealing lithology, (IPCC, 2005). Both the capacity and injectivity are features of the storage reservoir and are dependent on relatively high porosity and permeability values. A detailed CO_2 site characterisation is required to prove practical CO_2 storage capacity on a case by case basis (Eiken et al., 2011). Specific examples of porosity and permeability values for saline aquifer projects are presented by Michael et al., (2010); porosity values are shown to range between 5-35%, with the majority of projects utilising siliciclastic reservoirs and a few injecting into carbonates. High injection rates are associated with high aquifer permeability; however, these injection rates can be matched in low permeability reservoirs by increasing the number of injection wells (Michael et al., 2010).

Confinement is dependent on a satisfactory sealing lithology, and as with capacity and injectivity, a site characterisation for the immediate and ultimate potential for leakage on a case by case basis is required (Bachu, 2002). The immediate safety concerns the potential for the upward migration of the CO2 during or shortly after injection. This could be facilitated by faults and natural or manmade fractures (Bachu, 2002). Lateral migration is of concern when evaluating ultimate safety, with the possibility of cross formational flow or migration past the spill point to overlying strata a risk.

1.2.5. The Sleipner Project

Statoil began CO_2 injection at Sleipner in 1996. It was the world's first industrial scale CO_2 storage operation undertaken entirely to reduce CO_2 emissions. The Sleipner Project is located within the Norwegian sector of the North Sea, and the operation involves the stripping of CO_2 from natural gas produced from the Sleipner Vest gas field (3500m bsl) and its injection it into the Utsira Sand storage reservoir. CO_2 removal takes place at the Sleipner T platform and the CO_2 is injected via a deviated well at a depth of 1000m, around 200m below the reservoir top. Injection rate is 1Mt a year, with an initial projected final storage target of 20Mt (Arts et al., 2004). The natural gas produced from the Sleipner Vest field has a high CO_2 content (9%). This has to be reduced to meet the quality standards of the Zeepipe export pipeline and to avoid Norway's offshore CO_2 emission tax. Therefore, the decision to sequester the CO_2 in the Utsira Sand was made (Kongsjorden et al., 1998).

The Utsira Sand is an elongated sand body, more than 400km north to south and between 50 and 100km east to west, covering a total area of 26,100km^2 (Torp and Gale, 2004). It is has two main depocentres, a northern one which is 200m thick, and a southern one, where injection takes place, which is 300m in thickness (Chadwick et al., 2010). Depth to top of reservoir ranges between 550-1500m, but is generally between 700 to 1000m. The Utsira Sand consists largely of uncemented fine-grained sand, with occasional medium and coarse grains, with porosity values between 35% and 42.5% (Arts et al., 2004).

1.2.5.1. Monitoring and modelling programme

Recognised as a pioneering CO_2 sequestration project, Sleipner is the subject of intense scrutiny and interest from political, industrial and environmental parties. The success of projects such as Sleipner could act as a catalyst for an escalation of storage projects worldwide, and with this in mind the saline aquifer CO_2 storage (SACS) and CO_2STORE projects were initiated (Torp and Gale, 2004). The aim of these multi-institutional research projects was to monitor and attempt to predict the development of the CO_2 plume through the use of 3D time lapse seismic surveys, reservoir simulations and modelling.

A set of 7 repeat 3D surveys over a period of 14 years have been acquired to monitor the plume at Sleipner (Eiken et al., 2011). Time lapse, or 4D, seismic is considered to be a successful monitoring

and verification method (Michael et al., 2010). The aims of the seismic monitoring programme are to track plume migration, demonstrate CO_2 containment within the storage reservoir and to provide quantitative information to better understand the detailed flow processes which control plume development (Chadwick et al., 2010). The simulation packages have been calibrated against the time lapse seismic surveys and have been shown to be capable of replicating the position of the CO_2 within the storage reservoir (Torp and Gale, 2004).

The greater seismic impedance contrast between the shale and sandstone when CO_2 is present, affects the reflectivity of the seismic data (Chadwick et al., 2004) and results in significant, measureable and observable changes in seismic signal (Torp and Gale, 2004). The CO_2 creates a stronger negative amplitude, and is seen as 'bright spots' on the seismic data (Arts et al., 2004), and the plume is imaged as several sub-horizontal bright reflections (Chadwick et al., 2010). A further effect of the plume is the 'push down effect' due to the seismic waves travelling more slowly through the CO_2-saturated rock than the surrounding 100% brine-saturated pore space (Chadwick et al., 2009).

Due to the costs of seismic monitoring other monitoring options have been explored by the SACS project, and the potential of using pressure monitoring and observation wells, used to monitor conventional gas storage projects, has been evaluated but considered impractical at Sleipner (Torp and Gale, 2004). Due to the high permeability and large pore volume in comparison to the volume of injected CO_2, and the broad and shallow domal trapping structures the pressure increase resulting from CO2 injection is expected to be below what is observable. Despite this, Chadwich et al., (2012) report a small (0.1MPa) increase in pressure at distances 500 and 4000m from the injection point. Time-lapse seabed gravimetry has been used to verify changes in the subsurface mass during injection, and has the potential to estimate the amount of CO_2 going into solution, and to provide an 'early warning system' to detect CO_2 accumulating in traps within the sealing layers (Chadwick et al., 2006).

1.2.5.2. Plume migration and development

The effect of the CO_2 on the seismic signal is significant (Eiken et al. $_2$000) and the time lapse seismic data shows that the injected CO_2 has risen, under the effects of buoyancy, upward from the injection

point (Torp and Gale, 2002). By 1999 the CO_2 had reached the top of the reservoir and begun to spread laterally and accumulate underneath the overlying cap rock (Arts et al., 2004).

The reservoir properties of the UtsiraSand allow CO2 to flow through the reservoir relatively easily (Eiken et al., 2011). However, in the short term, vertical migration of the CO_2 is dependent on reservoir heterogeneities (Zweigel et al., 2000), and following injection the presence of thin intra reservoir barriers became apparent as the result of the appearance of several sub-horizontal layers of high reflectivity which are thought to represent CO_2 accumulating below, what are inferred to be, thin shale layers within the otherwise clean sand (Chadwick et al., 2004). Although they had been previously noted on well data, they were not noticeable in pre-injection seismic surveys due to their insufficient impact on the seismic signal as a result of their thickness being thinner than the vertical resolution limit (Eiken et al. 2000). The shale layers have 'radically affected the distribution of the CO_2 within the reservoir (Torp and Gale, 2004), and as a result of which, by 2009, only a third of the injected CO_2 had reached the top of the reservoir (Hermanrud et al., 2009). The influence of the shale layers, local mini traps, capillary flow resistance and hydrodynamic drive have been cited as reasons for this delay (Hermanrud et al., 2009). Although the CO_2 has been shown to have spread laterally below these layers (Chadwick et al., 2010), vertical migration of the plume is also occurring due to fractures and/or holes within the layers, caused by differential subsidence and erosion (Zweigel et al., 2000). This vertical migration has increased steadily with time and it is thought that the pathways are becoming more transmissive or more numerous (Chadwick et al., 2009).

Medium term migration and plume development is reliant on the topography of the cap rock. The Top Utsira has an irregular topography, consisting of several linked domal and anticlinal structures, which are considered to be the result of subsidence anomalies affecting the underlying strata (Zweigel et al., 2000). It is estimated that there is sufficient structural closure at the top of the Utsira Sand to contain the CO_2 within 12km of the injection site (Torp and Gale, 2004). The plume is 200m in height and is imaged as ellipse-shaped in plan view with a NNE-trending long axis 3.6km in length (Chadwick et al., 2009).

A model for the long term fate of the CO_2 plume at Sleipner has been based on the assumption of a fine grained sealing lithology restricting the upwards migration of CO_2, but allowing for molecular diffusion of CO_2 through the overlying sealing units (Torp and Gale, 2004).The results of this model suggest, just like the medium term migration, that the long term migration of the CO_2 will be controlled by the topography of the seal. Following the cessation of injection the CO_2 is expected to form a single “bubble” or continuous mass saturating the pore space, spread laterally below the seal,

and begin to dissolve into the formation brine. The bubble is expected to reach its greatest size 300 years after injection, following which it will begin to shrink and dissolve, disappearing after 4000 years (Torp and Gale, 2004). The upward migration of CO_2 to the seafloor due to diffusion through the water-saturated sealing layers is expected to take in excess of several hundred thousands of years (Torp and Gale, 2004).

1.2.5.3. Storage capacity and security

Total pore volume of the Utsira has been estimated at $6x10^{11}$ m^3, however only around 0.3% of this pore volume consist of structural or stratigraphic traps. Chadwick et al. (2004) suggest that the likelihood of the CO_2 entering all of these trapping structures is around 0.11%, therefore an effective storage capacity of $6.6x10^8 m^3$ is proposed. Intra reservoir trapping, evident from the accumulations of CO_2 below the shale layers, may significantly increase the storage volume, acting as 'speed bumps' to the migrating plume, and increasing the rate of dissolution trapping. From regional well data measurements, the natural reservoir pressure and temperature at the injection point are 10 MPa and 36C respectively (Arts et al., 2004) and under current reservoir conditions the CO_2 is stored in a super-critical state and is dissolving in the brine (Gaus et al., 2005).

Capillary leakage is considered unlikely (Chadwick et al., 2004; Torp and Gale, 2004), and diffusion of CO_2 into the caprock is expected to trigger geochemical reactions between the mineralogy of the sealing unit and the CO_2, these reactions will further decrease the porosity of the cap rock , and increase the effectiveness of the seal (Gaus et al.,2005).

Geochemical experiments and modelling studies suggest there is a limited reaction between the mineralogy of the Utsira Sand and the CO_2, and that mineral trapping is not a significant influence on the storage security (Pearce et al., 2001). However, CO_2 solubility under the pressure and temperature conditions at Sleipner is around 53kg/m3, and therefore dissolution trapping is considered a potentially significant influence on storage security (Torp and Gale, 2004).

The significant response of even thin layers of CO_2 on the seismic signal and the current lack of seismic response within the overburden suggests that the CO_2 is being contained within the reservoir (Chadwick et al., 2009).

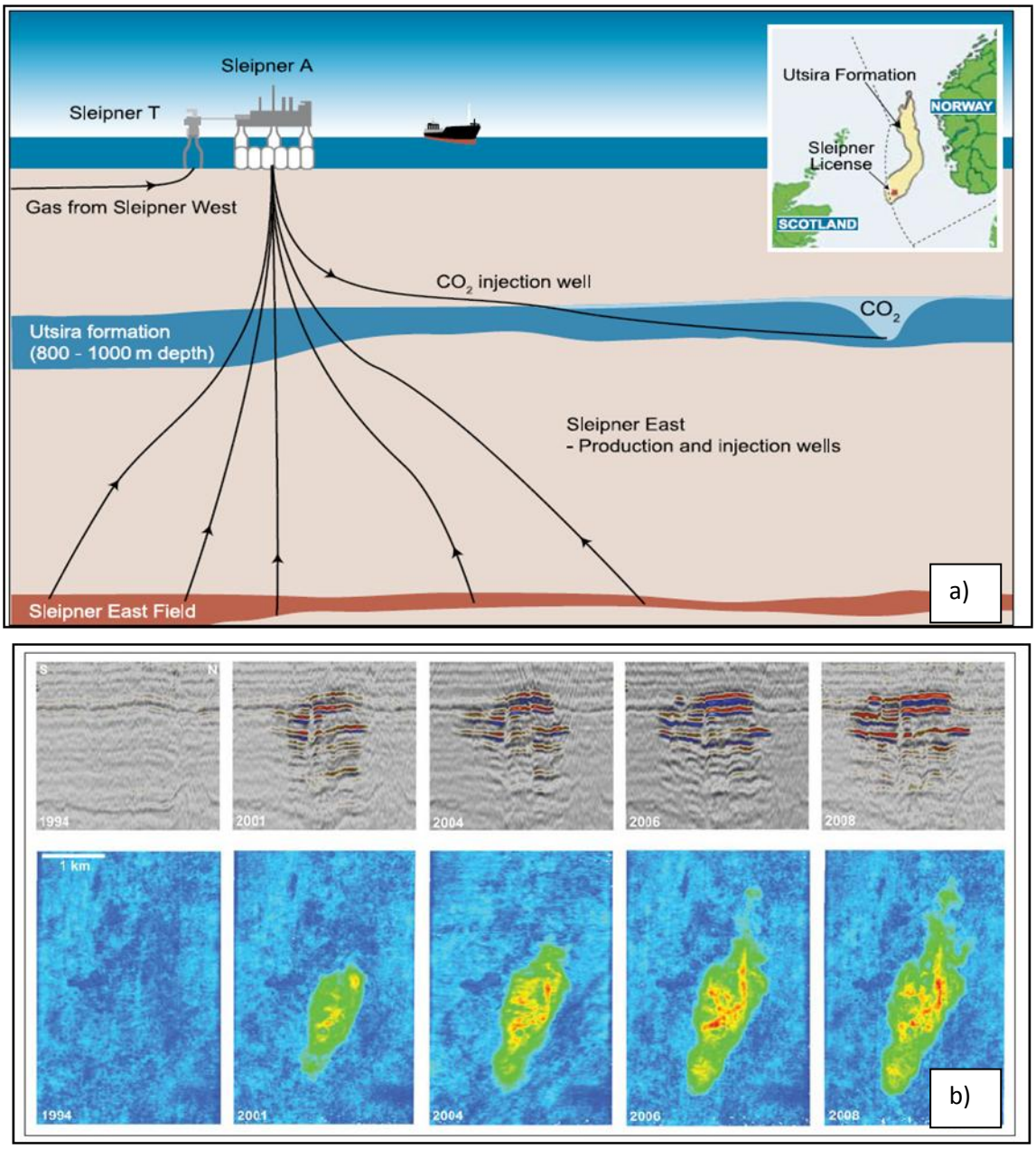

Fig. 1.3 a) demonstration of the Sleipner Project (taken from IPCC,2005) b) time-lapse seismic imaging of the CO2 plume growth (taken from Chadwick et al., 2009).

1.3. Aims of study

This study aims to;

1. Better understand the structures and geological features affecting, and associated with, the Utsira Sand, a current carbon sequestration reservoir
2. Identify geological features which control the short to medium term CO_2 plume migration
3. Identify any indicators of previous cross stratal fluid flow through the sealing lithology

1.4. Layout of thesis

Chapter 1 has been an introduction into the concept Carbon Capture and Storage and the Sleipner project. **Chapter 2** gives a brief description of the regional geology of the study area. **Chapter 3** is an introduction to 3D seismic reflection data and the interpretation methods used. **Chapters 4, 5 and 6** present the results derived from three different study areas within the 3D seismic volume. Although the data volume presented in Chapter 4 was received following that presented in 5 and 6, it was considered a more natural progression to present the findings from this smaller area first, then expanding the findings, and demonstrating the geographic distribution of these findings, into the larger, adjacent study area.

Chapter 4 investigates amplitude anomalies in the stratigraphic unit directly below the Utsira Sand. Their effect on the host unit, the base of the Utsira Sand, and the internal reflections of the Utsira Sand are presented. **Chapter 5** expands the findings of Chapter 4 into a larger adjacent study area. Controls on the topography and structures at the top of the Utsira Sand are investigated, and the geometry of the internal reflections is discussed further. **Chapter 6** investigates amplitude anomalies in the strata overlying the Utsira Sand, in an attempt to identify seismic expressions of leakage, fluid flow and permeable pathways which would allow cross stratal migration of sequestered CO_2.

Chapter 7 summarises the major finding and presents a conceptual plumbing system based on the observations made. Potential CO_2 leakage scenarios are also described. The main conclusions of the thesis are presented in **Chapter 8**.

Chapter 2

Geological Setting

2. Geological Setting

The aim of this chapter is to briefly outline the geological context of the study area used to derive the results presented in Chapters 4, 5 and 6. The study area is located within the southern part of the Viking Graben, which is a major structural feature located within the northern area of the North Sea Basin (Fig. 2.1). This chapter aims to firstly describe the North Sea Basin, and then more specifically, in respect of the scope of the project, the Cenozoic succession and the Utsira Sand itself.

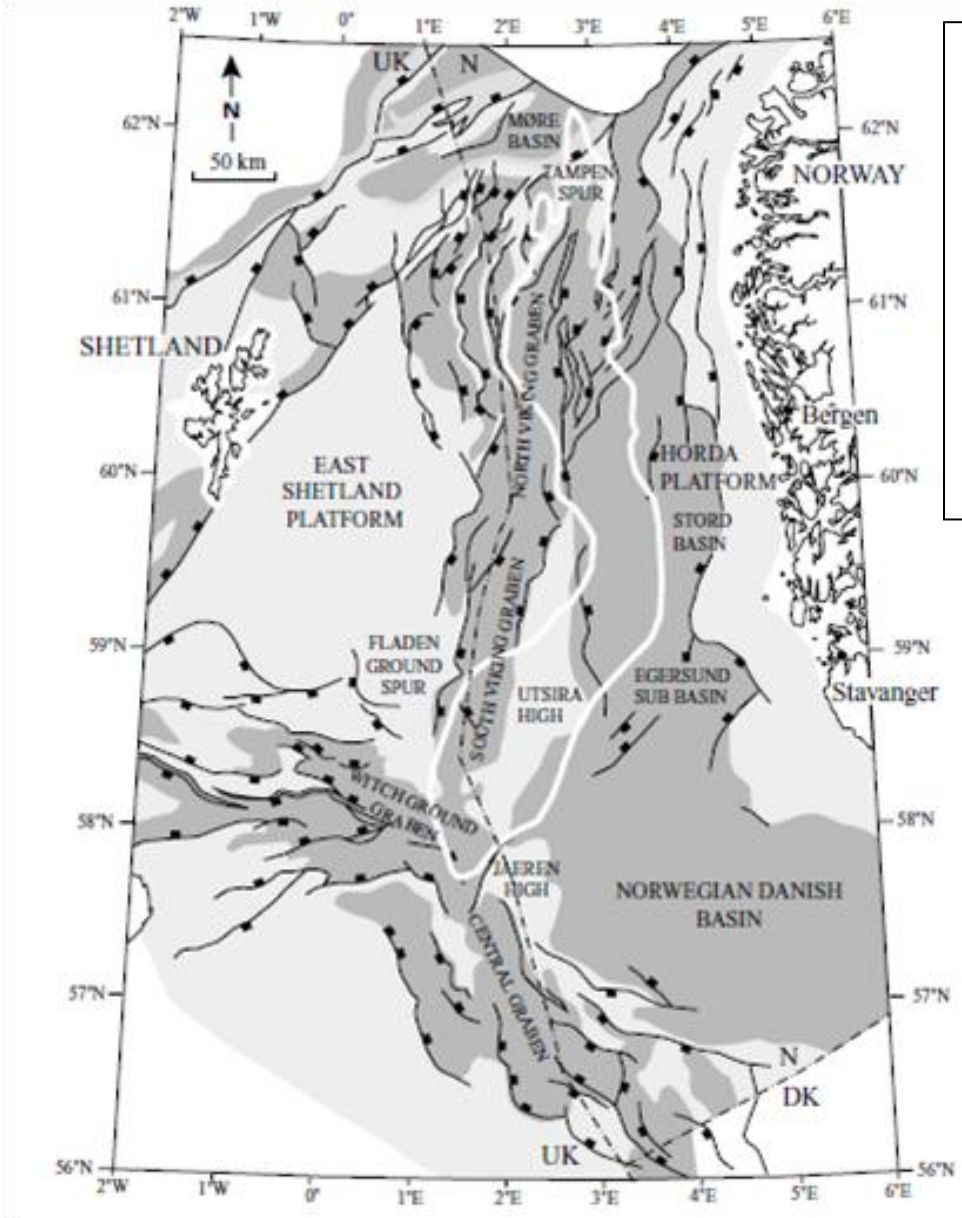

Fig. 2.1 The main structural features of the North Sea. The South Viking Graben forms the northern branch of triplet of North Sea rift systems. Outline of Utsira Sand in white (From Gregersen and Johannessen, 2007).

2.1. North Sea Basin

The epicontinental basin of the North Sea is bounded by the Scandinavian and British landmasses and connected to the Norwegian-Greenland Sea to the North (Ziegler, 1990). Three stages of North Sea tectonic evolution are recognised by Coward et al. (2003); a Paleozoic continental collision and plate accretion period, a Mesozoic continental rift period, and a Late Mesozoic to Cenozoic period of thermal subsidence and basin fill.

2.1.1. Paleozoic continental collision

The period of Paleozoic continental collision consists of three main convergent episodes; the Grampian Orogeny (460 to 450 Ma), the Acadian Orogeny (400 Ma) and the Variscan Orogeny (400 to 330 Ma) (McKerrow et al., 2000). These episodes are grouped into two separate accretionary events, the Caledonian (Grampian and Acadian) and the Variscan (Coward et al., 2003).

As a result of the Caledonian Orogeny the North American plate (Laurentian Shield) and the Northwest European plate (Fenno-Scandinavian Shield) collided (Ziegler, 1975), and thus the ancient continents of Laurentia, Baltica and Avalonia became conjoined. The Caledonian phase in its entirety lasted from 510Ma to approximately 390Ma and includes the whole of the Ordovician and Silurian, and the Early Devonian (Ziegler, 1975). Tectonic activity during this period is described as episodic (Coward et al., 2003), and the Grampian Orogeny phase is recognised as the most well developed.

Strike slip tectonics dominated the basin during the Devonian, forming a pull-apart basin in the vicinity of what would later develop into the Viking Graben. The Variscian Phase occurred over a period lasting from the Late Devonian to the Late Permian (380Ma to 250Ma), and fold structures in the North Sea and Scotland are indicators of inversion during this period (Zanella and Coward, 2003). The end of the Permian saw the onset of basin subsidence due to extension and thermal cooling; however, the main period of extension was to follow during the Mesozoic.

2.1.2. Mesozoic continental rift period

The second stage of the North Sea tectonic evolution saw the transition from a compressive tectonic setting to a period of extensional tectonics throughout the Mesozoic (Ziegler, 1975). During initial Triassic east-west extension, several horst and graben structures began to develop; of which, the Viking Graben structure dominates the south-central part of the basin (Gregersen, 1997). The most significant period of extension commenced during the Late Jurassic. During this phase, which lasted until the Cretaceous, the proto-Viking Graben, initially formed during the Devonian, developed

further to form the northern branch of a triplet of North Sea rifts (Coward et al., 2003). At its southern extent the Viking Graben is connected to the Witch Ground Graben, orientated E-W, and the Central Graben, which is NW-SE striking.

2.1.3. Late Mesozoic to Cenozoic

The third stage of tectonic evolution saw the cessation of this extension, possibly by the Late Jurassic or Early Cretaceous (Gregersen, 1997) and the basin began its current day conFig.uration as a post rift, regionally subsiding basin. The abatement in extensional tectonism coincides with the observations Martinsen et al., (1999) of a 'transition between block-and-basin topography to ramp type basin margins', and sediments began to accumulate within the 'saucer shaped' sag basin (Ziegler and Von Hoorn, 1989).

By the end of the Cretaceous the majority of the rift topography had been filled (Jordt, 1995), and the following Cenozoic depositional system was controlled by regional basin subsidence, with sediment supply from topographic highs, and episodic marginal uplift. Changes in sediment distribution reflect the complex pattern of uplift along the continental margins (Jordt, 1995).

2.2. Cenozoic

Regional basin subsidence and episodic uplift of basin margins controlled the depositional system of the Cenozoic North Sea (Gregersen and Johannessen, 2007). Over 2km of siliclastic sediments were supplied to the central axis of the basin during this period (Huuse, 2004), 1.5km of which are accounted for by Miocene to Recent deposition (Gregersen and Johannessen, 2007). Uplift of the basin margins related to igneous activity and break-up of the North Atlantic created an abundant supply of coarse clastic sediment from areas such as the Shetland Platform and southern Norway (Huuse and Mickelson, 2004). As a result large sand rich fans and channel lobe systems were deposited during the late Paleocene and earliest Eocene (Ziegler, 1990). During this period the provenance areas for sediment supply fluctuated, causing the 'amalgamation and isolation of sandbodies in the centre of the basin' (Huuse and Mickelson, 2004; Den Hartog Jager et al., 1993; Jones et al., 2003). These isolated sandbodies are generally well sorted, with very high net:gross ratio (proportion of the gross rock volume formed by the reservoir rock), and are hosted by low permeability, smectite-rich mudstones. Despite their enclosure by the low permeability mudstones, they are generally close to normal pressure (Huuse and Mickelson, 2004).

As a result of plate reorganisation in the mid-Cenozoic the North Sea became better connected with the Arctic to the north-east. Rundberg (1989) suggests that the changes in lithostratigraphy, mineralogy and biostratigraphy at this Eocene-Oligocene boundary were controlled by the global temperature drop identified by Zachos (2001). Rundberg and Eidvin (2005) also identify the affects of increased ocean circulation as a factor, as was the changing of the North Sea physiography due to the uplift of the Tampen Spur in the northern North Sea. They also attribute each phase of clastic input into the basin as a response to uplift of NW Europe.

The Early Miocene was dominated by slow, argillaceous sedimentation, which was followed by a hiatus during the early to mid-Miocene which was accompanied by the erosion of Oligocene and Miocene deposits (Gregersen and Johannessen, 2007). Tilting of the Horda Platform and further uplift during the mid-Miocene resulted in an extensive unconformity (Gregersen and Johannessen, 2007). Erosion of the uplifted margins, and transportation by the outbuilding deltas of the East Shetland Platform and Norwegian basin margin resulted in the deposition of the Utsira Sand within the basin centre. A period of agrillaceous deposition followed, resulting in the deposition of a thick blanket of continuous mudstone, colloquially referred to as the Shale Drape on top of the Utsira Sand. This deposition has been associated with a rise in relative sea-level which was possibly caused by an increase in basin subsidence rates (Faleide et al., 2002).

Gregersen and Johannessen (2007) suggest that global cooling and icecap growth led to an increase in O18 isotopic composition of seawater during the Pliocene (Buchardt, 1978). This may have resulted in glacio-eustatic sea-level lowering, which along with ice sheet movement, promoted Pliocene progradation (Henriksen and Vorren, 1996). Further uplift of the basin margins resulted in erosion and an increased sediment supply which also contributed to the prograding system (Gregersen and Johannessen, 2007). The upper part of these prograding Pliocene deposits was removed by Pleistocene glaciations, resulting in unconformities.

2.2.1. Lithostratigraphy

Early work by Deegan and Scull (1977) divided the post-Eocene to recent into the Hordaland and Nordland groups, and they defined a solitary formation, the Utsira Formation, at the base of the Nordland Group. The Hordaland Group and Nordland Group are separated by the Mid Miocene unconformity, caused by the uplift of the northern North Sea Basin, which has been linked to structural doming on the mid-Norwegian margin (Rundberg and Eidvin, 2005).

Work by Isaksen and Tonstad (1989) identified further regionally important sand bodies; the Late Oligocene Skade Formation, an unnamed Early Oligocene sand, both attributed to the Hordaland Group. Galloway (1993) also recognises three periods of clastic, basin centred deposition within the Viking Graben during the Oligocene and Miocene. Rundberg and Eidvin (2005, 2007) revised the earlier lithostratigraphic subdivision, and assigned the Skade Formation to the Early Miocene and not the Oligocene. Each period of clastic deposition has been linked to the uplift and erosion of the basin margins (Rundberg and Eidvin, 2005)

The inclusion, by Isaksen and Tonstad (1989,) of Lower Miocene and Middle Miocene strata in the Utsira Formation in type well 16/1-1 causes an overlap with their own definition of the Lower Miocene strata within the Skade Formation in type well 24/12-1. Eidvin and Rundberg (2005) identify this error in defining the UtsiraFormation in the type well as a possible reason for inconsistency in definition between the Skade and Utsirain previous work by Gregersen (1997).

2.2.2. Seismic stratigraphy

One of the original and most cited divisions of the Cenozoic sequence stratigraphy is presented by Jordt et al. (1995). They divide the Cenozoic into ten main Cenozoic Seismic Sequences (CSS-1 to CSS-10). Units CSS-2 to CSS-6 belong to the Hordaland Group, while CSS-7 to CSS-10 represent the Nordaland Group.

Within the study area, CSS-5 and CSS-6 are not present due to erosion, and subsequently the CSS-4 (Oligocene) directly underlies CSS-7, which is designated to the Utsira Formation. These are separated by the Mid-Miocene unconformity which also correlates with the lithostratigraphic boundary between the Hordaland and Nordaland Group. The Utsira Formation is overlain by three seismic sequences; the Pliocene CSS-8, the Lower Quaternary CSS-9 and Upper Quaternary CSS-10.

Rundberg and Eidvin (2005) concentrate on the Oligocene-Miocene succession, dividing it into two megasequences, an Upper Hordaland and a Lower Nordland. Lower Nordland Unit 1 (LN-1) consists of a Middle Miocene mudstone, which is overlain by the thick, blocky sands of the Utsira formation (LN-2). An Upper Pliocene-Pleistocene section, 900m in thickness, completes the Nordaland Group (Eidvin and Rundberg, 2007).

In work specific to the Sleipner area, the overlying strata are divided into three separate units. The first of these, directly above the Utsira Sand, is termed the Lower Seal, while the second and third units are the Middle Seal and Upper Seal respectively. The Lower Seal (Gregersen, 2001), or shale drape (Gregersen and Johannessen, 2007), equates to the Jordt et al. (1995) Pliocene CSS-8, while the Lower Quaternary CSS-9 and Upper Quaternary CSS-10 correspond with the Late Pliocene/Pleistocene Middle Seal and the Pleistocene Upper Seal. The Utsira Sand is underlain by a mid-Miocene Lowermost Shale unit, which would equate to Rundberg and Eidvin's (2005) Lower Nordaland Unit 1, and they define the base of this unit as the Mid Miocene Onlap Surface (Gregersen et al., 2000; Chadwick et al., 2000).

A more recent synthesis of Cenozoic sedimentation is presented by Anell et al., (2012). Their division of the Cenozoic consist of seven units; comprising of three Paleogene units (PAL 1 to 3) and four Neogene units (NEO 1 to 4). NEO 1 incorporates CSS-5 and CCS-6 of Jordt's (1995) subdivision, while NEO-2 represents CSS-7 (the Utsira Formation). NEO 3 combines the Pliocene of CSS 8 and the Lower Quaternary of CSS 9, and NEO 4 equates to CSS-10.

Based on observations from the data -set, the units mapped within the study area are based, in part, on the Cenozoic sub-division by Jordt et al., (1995), Rundberg and Eidvin (2005) and the Sleipner

specific division of the overburden by Gregersen and Johannessen ((2007) Fig. 2.2 and2.3)). The upper and lower boundaries of the units are mapped to the closest mappable horizon to those presented by Gregersen and Johannessen ((2007) Fig 2.4)).

2.2.2.1. Unit Description

2.2.2.1.1. Lowermost Shale

Lowermost Shale unit is Middle Miocene in age (Gregersen and Johannessen, 2007). Its base is defined by a composite set of high amplitude reflections, which has been termed the Mid Miocene Onlap Surface (Gregersen et al., 2000; Chadwick et al., 2000), and ties into a high gamma ray log marker of Rundberg and Eidvin (2005). It is a basin infilling sequence and onlaps the underlying unit to the west and the east (Rundberg and Eidvin, 2005), and consists mainly of mudstone (Rundberg and Eidvin, 2005) or shale (Gregersen, 2000), with sparse, thin sands reported in some wells (Rundberg and Eidvin, 2005).

The unit is characterised by low amplitude, sub-parallel, semi-continuous reflections, and although generally between 200m to 250m in thickness, local areas of greater thickness do occur. Locally high amplitude reflections are present, and the unit reflections are seen to be disrupted and chaotic in the vicinity of these high amplitude reflections.

2.2.2.1.2. Utsira Sand

The Utsira Sand is clearly distinguishable from surrounding units within the study area, and consists of a basin restricted unit with internal, stacked mounds (Gregersen, 2001). It is considered to be Late Miocene to earliest Late Pliocene in age (Eidvin et al., 2000; Eidvin and Rundberg, 2001, Piasecki et al., 2002), and was a shallow marine sand with interbedded mud during the Miocene to late Pliocene (Head et al., 2004).

The lower boundary of the Utsira Sand is marked by a velocity increase (a peak, if displayed in SEG normal polarity), and consists of a high amplitude reflection, while its upper limit is defined by a velocity decrease (trough) and a medium to high amplitude reflection (Gregersen, 2001). The unit itself is characterised by low gamma ray-values (Eidvin et al., 2000) and the basal reflection coincides with an abrupt gamma ray increase, which reflects the change from the sand rich Utsira Sand to the

shale rich Lowermost Shale (Fig. 2.5). The upper boundary has an abrupt upwards gamma ray increase (examples of logs in Appendix A).

Its base is highly deformed and irregular, and areas of domed mounds are easily distinguished from the sections of undeformed base. The unit itself consists of a sandy deposit which exceeds 300m at its maximum thickness within the study area, although when affected by mounds, the unit thins considerably. The unit pinches out to the south and west of the study area.

The internal reflections of the Utsira Sand onlap the Lowermost Shale to the west of the study area. The lower reflections of the unit also onlap at the flanks of the mounds; while the upper section of reflections can be seen to consist of stacked mounds (Gregersen, 2001; Chadwick 2000.).

The Utsira Sand is overlain by the Nordland Group Mudstones, whose age spans from the Pleistocene to the Holocene. They are considered to represent a deep water transitional environment (Head et al., 2004). Gregersen and Johannessen (2007) divide the overburden into three separate units; however, this study recognises four, and sub-divides the Middle Seal into two units based on observations from the study area.

2.2.2.1.3. Lower Seal

The Lower Seal (Gregersen and Johannessen, 2007) has also been termed the Shale Drape (Chadwick et al., 2004). It constitutes the lower part of the regional seal. Its upper boundary has been mapped to the closest mappable horizon to that of the Pliocene Lower Seal as defined by Gregersen and Johannessen (2007). However, it incorporates much of the lower part of the Middle Seal and therefore is significantly thicker, especially at the western extent of the study area where the Utsira pinches out.

The unit reflections are horizontal to sub-horizontal and generally low to medium amplitude, and drape onto and follow the undulating nature of its lower boundary. To the west of the study area the unit consists of east to south westward prograding clinoforms. High amplitude bright reflections are locally present, and are concentrated within the lower half of the unit.

The unit is easily distinguishable from the overlying Lower Middle Seal which is more chaotic in nature and has brighter internal reflections.

Based on marine palynomorphs and foraminifera from well 15/9-A11, Head et al., (2004) date this unit to ~1.8-2.5 Ma (Gelasian) and consider it to represent a maximum flooding surface.

2.2.2.1.4. Mass Transit Unit

This unit is an additional unit to the sub-division by Gregersen, (2007). It is seismically distinct from both the underlying Lower Seal and overlying Middle Seal, with strong reflections at its basal and upper limit. The internal reflections of the unit vary greatly, and can consist of high to low amplitude, horizontal to sub-horizontal reflections, discordant high amplitude reflections, and chaotic zones of low to high amplitude. The greatest unit thickness coincides with the areas of chaotic reflections, and is concentrated along a north-east to south-west orientated axis through the centre of the study area. The thinner section of the unit corresponds with the low amplitude sub-horizontal reflections. Towards the north-west and south-east the unit thins and 'pinches-out'.

This unit is interpreted here as a mass transit deposit (MTD) by analogy with the interpretation and descriptions of similar seismic units elsewhere (Gamboa, 2011; Bull et al., 2009; Frey-Martinez et al., 2004; Frey-Martinez et al., 2010).

2.2.2.1.5. Middle Seal

The middle seal consists of the greatest thickness (500m) of the sealing overburden. Within the central study area its base coincides with the top of the MTD unit, while in the north-west of the study area it directly overlies and onlaps onto the Lower Seal. The unit generally consists of low amplitude reflections which are parallel, sub-horizontal to inclined, with low angle progradational clinoforms. Its upper limit is a strong, continuous reflection which coincides with the Pleistocene unconformity (Gregersen and Johannessen, 2007).

Limited variation in thickness and angle of reflections suggests a period of high sediment supply with a steady relative sea level fall (Gregersen and Johannessen, 2007), and the eastward prograding direction suggests a provenance area located to the west. High amplitude reflections within the unit are correlated with sand intervals in wells to the north of the study area and possibly represent shallow gas accumulations.

2.2.2.1.6. Upper Seal

The Upper Seal is a Pleistocene flat lying, tabular, unit around 200m in thickness. Its base is defined by the Base Pleistocene Unconformity and its upper limit coincides with the seafloor. It consists of glacio-marine clays deposited under shallow marine and arctic conditions. Glacial tills are also present.

Scattered high amplitude seismic anomalies suggest locally sandy lithologies (Gregersen, 2007), while grounding ice sheet are considered responsible for internal troughs and incised valleys which occasionally affect the Pleistocene unconformity (Huuse et al., 2000; Praeg, 2003; Jorgensen and Sandersen 2006; Jorgensen and Sandersen 2008; Lonergan; 2006).

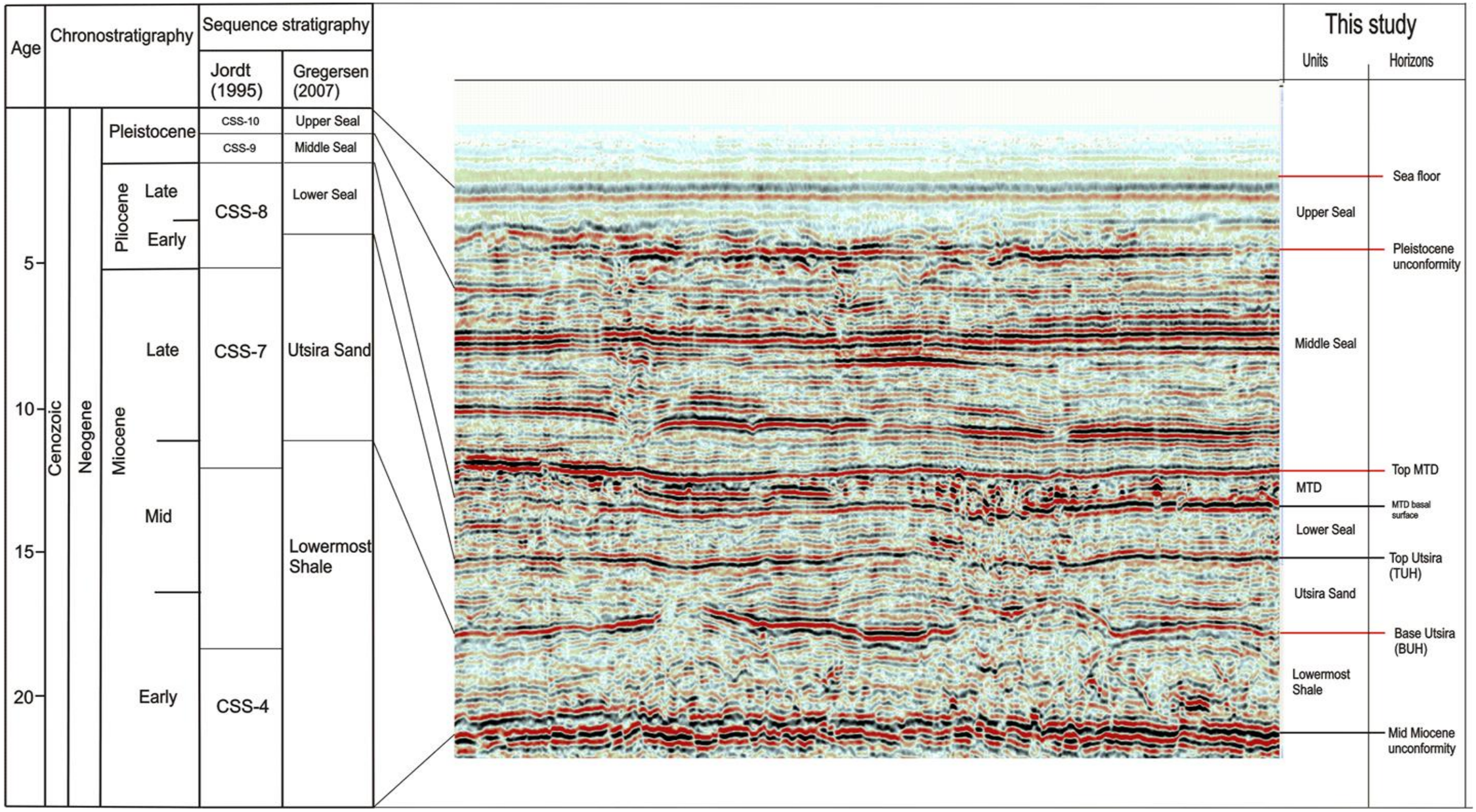

Fig. 2.2 a comparison of the sequence stratigraphy of Jordt et al., (1995) and Gregersen and Johannessen (2007) with the units mapped in this study.

2.2.3. Biostratigraphy

A biostratigraphic framework developed by Eidvin et al. (2000) suggests that the Utsira Sand contains both Early Pliocene and Upper Miocene benthic assemblages.

Eidvin and Rundberg (2005) recognise diagnostic Mid Miocene planktonic microfossils within the unit underlying the Utsira Sand. The presence of the Mid Miocene *Bolboforma badenensis* and *B.reticulta* assemblages within this underlying unit, dated by Strontium isotope analysis at 15.5Ma, suggests an oldest possible age of early Late Miocene for the Utsira.

Piaseki et al. (2002) identified Early Pliocene dinoflagellate cysts within Utsira core samples from Well 15/9-A23. They distinguish between reworked dinoflagellate cysts and in-situ cysts, and state that the in-situ flora is dominated by Late Miocene to Pliocene species. The presence of the Early Pliocene species *Hystrichokolpoma rigaudie* and *Reticulatosphaera actinocoronata* suggests a minimum age of Early Pliocene for the Utsira Formation.

A comprehensive correlation of biostratigraphy and chronostratigraphy by Eidvin and Rundberg (2007) analysed benthic and planktonic foraminifera from six wells. They identified a close correspondence between the Utsira Sand and a sediment column dated Late Miocene to Early Pliocene: the benthic foraminifera *Uvigerina venusta saxonica* (Upper Miocene/Early Pliocene), and planktonic foraminifera *Globorotalia puncticulata* (Upper Miocene/Early Pliocene) are present in all six wells. Their work concurs with Eidvin and Rundberg's (2005) maximum, and the Piaseki et al., (2002) minimum age for the Utsira Sand.

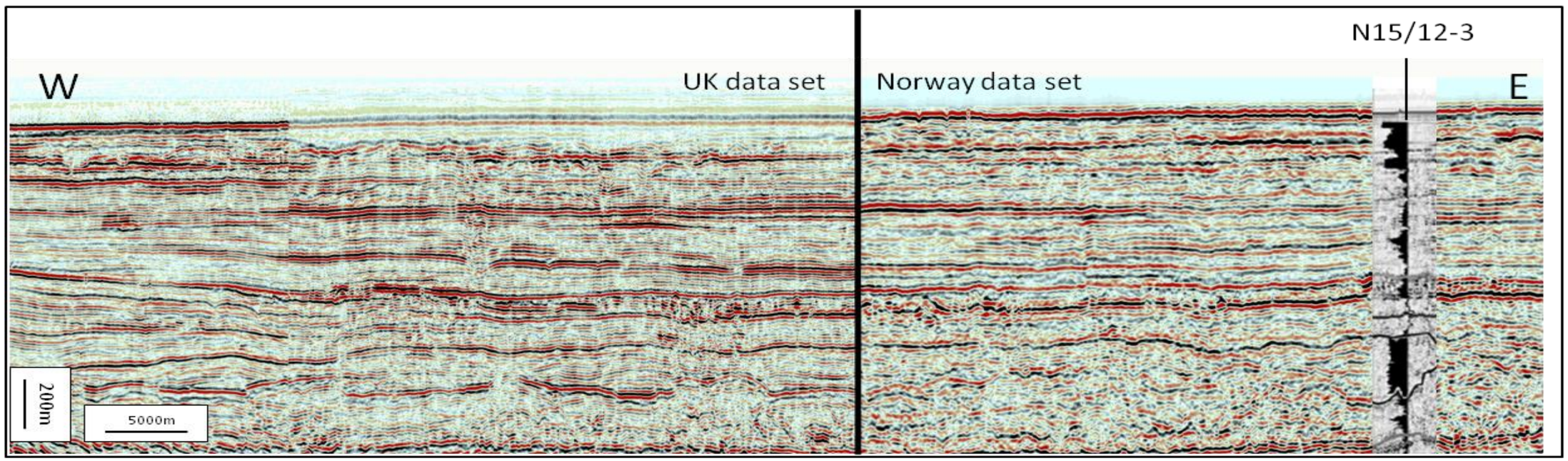

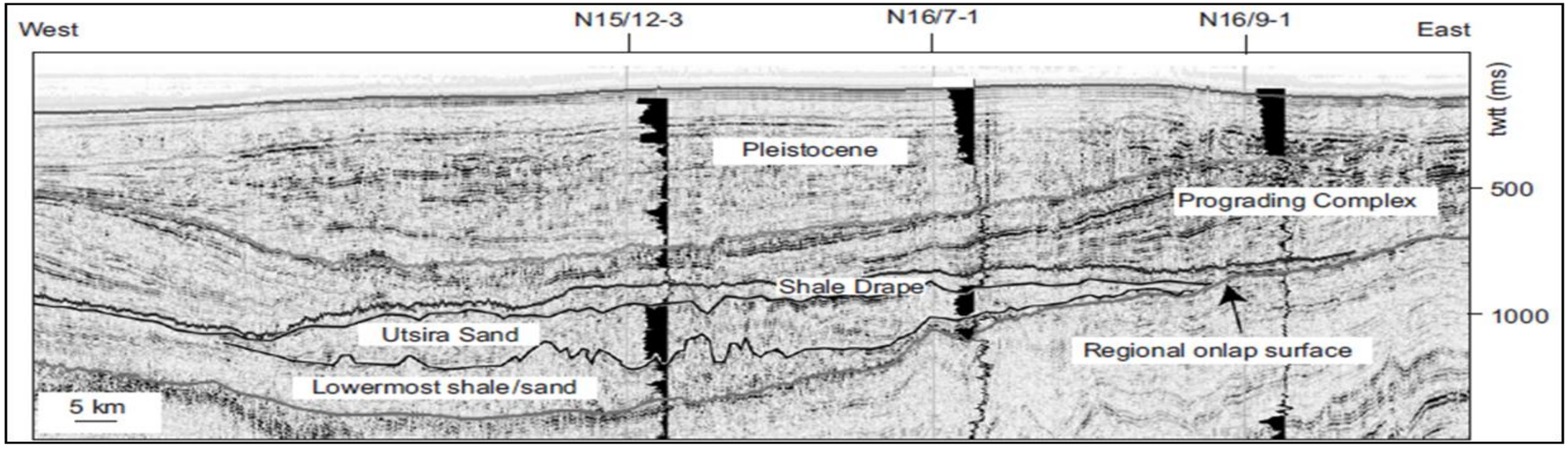

Fig. 2.3 a) an amalgamated seismic line across both study areas, and encompassing the western extend of the Utsira Sand, co-rendered with a gamma ray log from Gregersen and Johannessen (2007), used to aid interpretation b) Seismic section of the whole extent of the Utsira Sand displaying the seismic stratigraphy after Gregersen and Johannessen (2007).

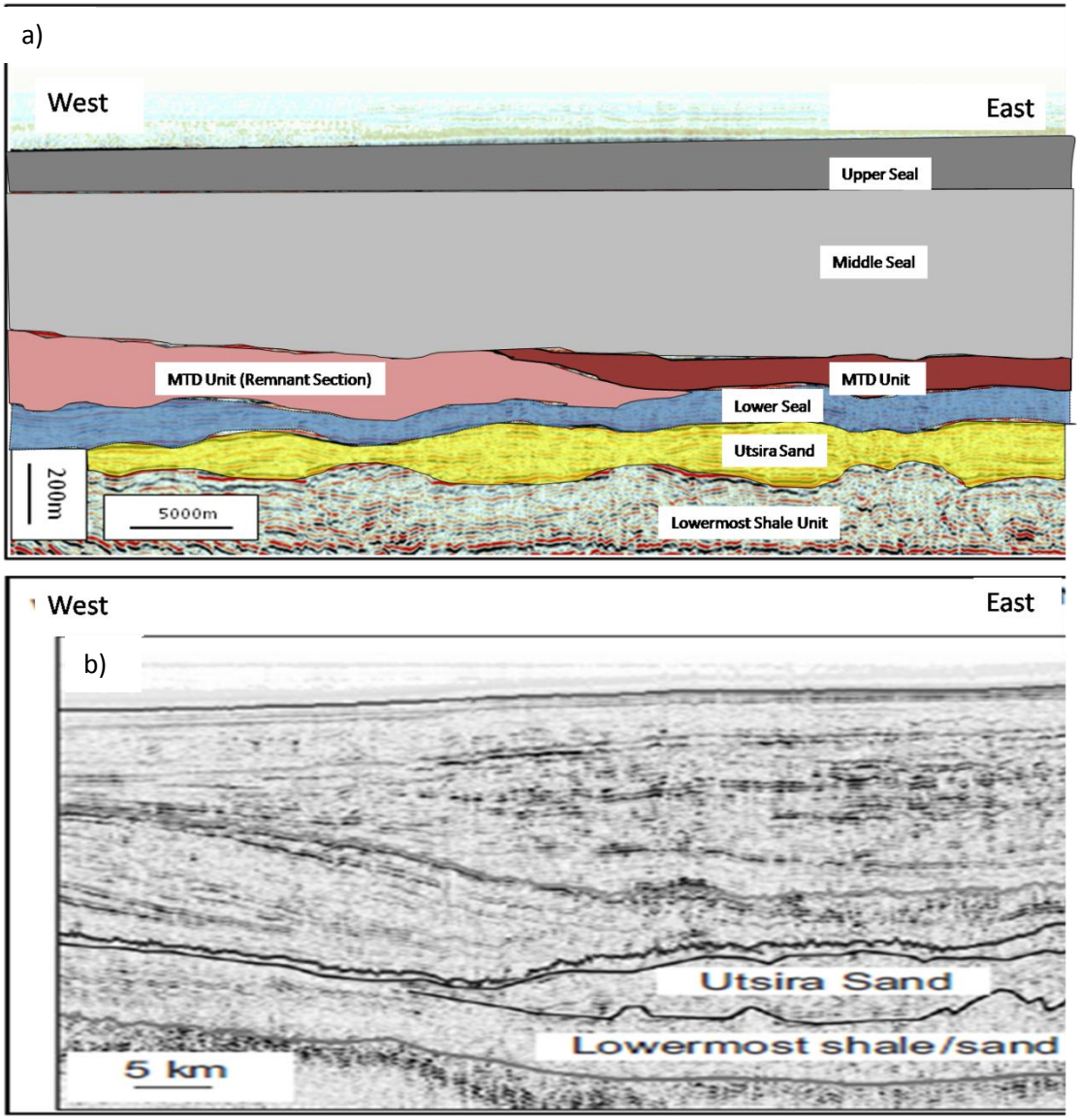

Fig. 2.4 a) The units as interpreted within this study in comparison to b) those proposed after Gregersen and Johannessen (2007).

2.3. Utsira Sand

A major North Sea aquifer (Lindeberg et al., 2009), the Utsira Formation 'constitutes the basal part of the Upper Cenozoic Nordland Group' (Gregersen, 1997). Its sandy, quartzose, basin restricted member has been termed and mapped as the Utsira Sand by Gregersen (1997) and Chadwick et al., (2000). Eidvin and Rundberg (2007) subdivide the Utsira Formation into three units of similar age; a South Utsira Sand Member, a Central Utsira Sand Member and a North Utsira Sand Member. Their division is based on lithological differences, the South Utsira Sand Member can be considered analogous with the Utsira Sand unit of Gregersen ((1997) Fig. 2.6)) and Chadwick (2000), and is considered to be Late Miocene to earliest Late Pliocene in age (Eidvin et al., 2000); Eidvin and Rundberg, 2001, Piasecki et al., 2002).

Located within the South Viking Graben, the Utsira Sand as a whole covers an area extending some 450 km in a north-south direction and between 70-130 km in an east-west direction, see Fig. 2.4 (Gregersen, 1997). Two main depocentres are recognised (Fig. 2.7), achieving a thickness of 300m at the southern depocentre, and 200m to the north. Gregersen (1997) suggests a third depocentre, an Utsira East unit, located to the east of the northern depocentre, also achieving 200m in thickness. The South Utsira Sand Member, as defined by Eidvin and Rundberg (2007), coincides with the southern depocentre, while the North Utsira Sand Member is analogous with the northern depocentre. The Central Utsira Sand Member consists of a thin, shallow saddle connecting both depocentres. Greater thickness within the southern area is attributed to a longer period of deposition (Gregersen, 1997) and erosion in the north (Eidvin et al, 2000).

Depths to the top of the Utsira Formation range between 550-1100m, but are generally within 700-1000m at the southern depocentre and over 800m at the injection point of the Sleipner CCS project (Chadwick, 2001). The base of the Utsira Sand attains depths of between 600-1300m but is mainly constrained to between 700-1100m.

The Hutton Sand, which is in part time equivalent to the Utsira Sand, and may be in hydraulic connection with, the Utsira Sand (Gregersen, 2007). Deposited throughout most of the Cenozoic, it is also suggested as a possible source for the Utsira Sand by Galloway (2003) and Gregersen (2007).

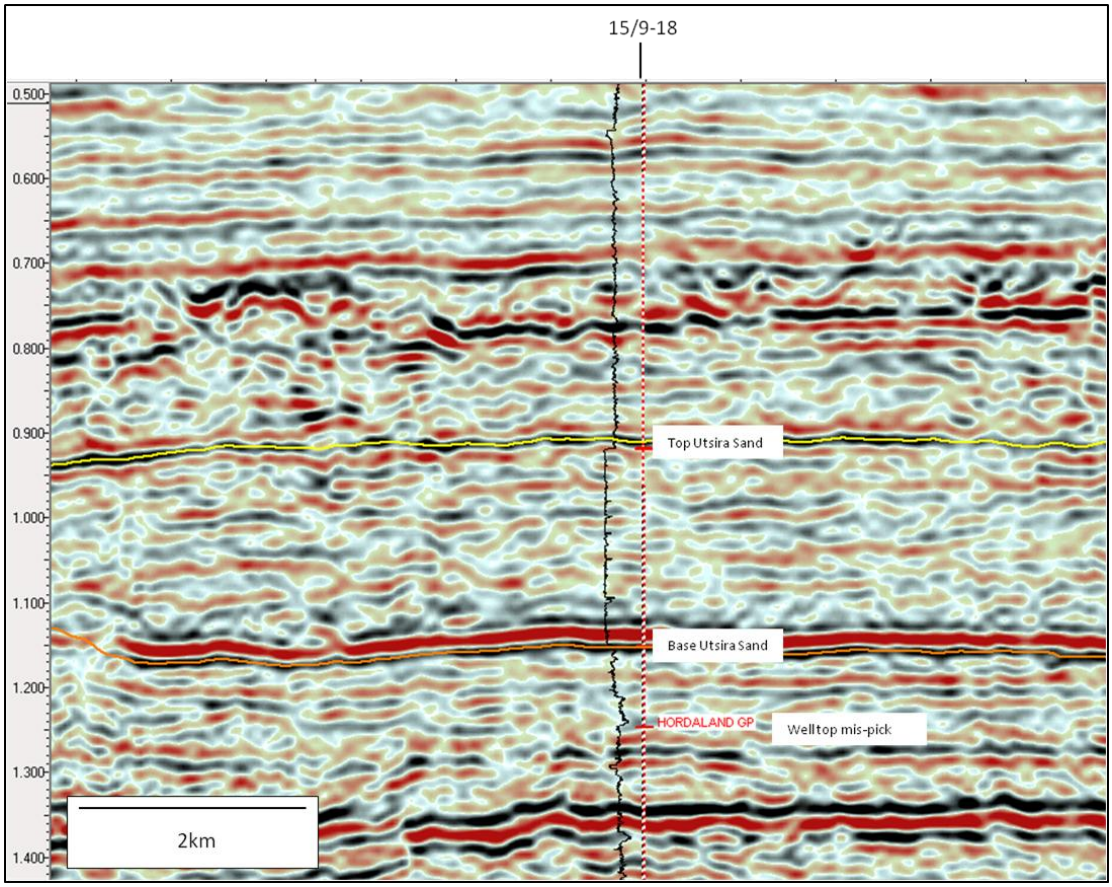

Fig. 2.5 Screenshot of well top tie from well 15/9-18, with gamma ray log (with permission from Fugro Roberston).

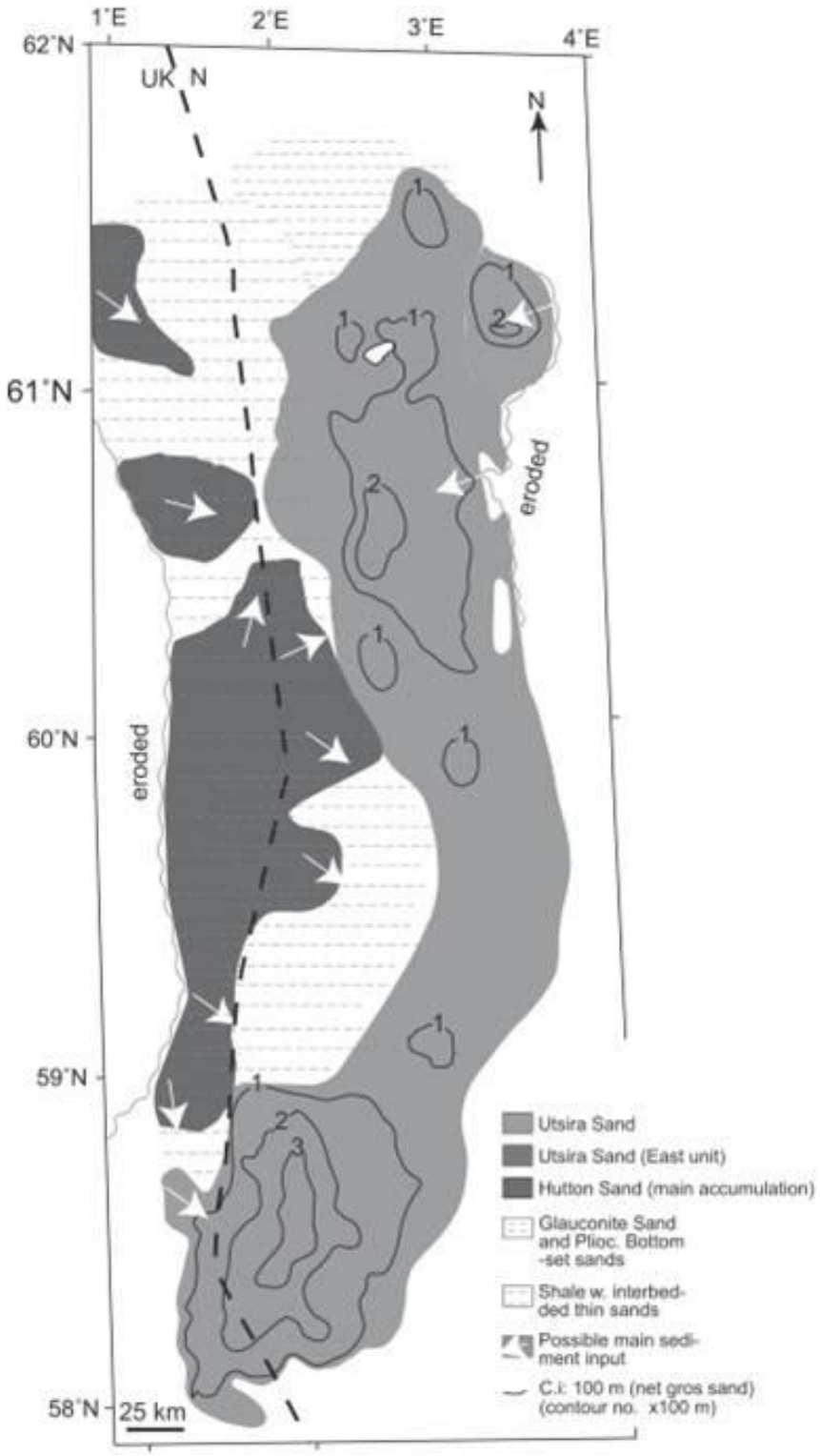

Fig. 2.6) The sub-division of the Utsira Sand as suggested by Gregersen and Johannessen (2007).

2.3.1. Caprock

Up to 800m in thickness, the overburden above the Utsira Sand has been subdivided into a Lower Seal, Middle Seal, and an Upper Seal (Chadwick et al., 2004; Gregersen et al., 2007). The Lower Seal consists of a 50-100m shale drape. It is a tabular, basin-restricted unit, and overlaps the Utsira to the west and east. Where the Utsira is not present it downlaps onto the Mid-Miocene mudstone. The Middle Seal comprises a Pliocene prograding wedge (Chadwick, 2001). The glacio-marine clays and glacial tills of the Quaternary make up the Upper Seal. Arts et al (2004) suggest that the lack of any potential CO_2 seismic response in the overburden indicates that the shale drape is an effective seal.

2.3.2. Lithology

The Utsira Sand consists of unconsolidated, fine to medium grained sand composed mainly of angular to sub-angular quartz. Minor feldspar, sheet silicates, glauconite, shell fragments and lignite are also described from well core (Pearce et al., 2000). Chadwick et al. (2000) describe the physical properties of the Utsira Sand from microscopic and macroscopic analysis of core and cuttings samples. It consists of angular to sub-angular, fine, occasionally medium to coarse grained quartz. Glauconite is most common within the central and northern areas, while rare within the southern depocentre (Gregersen, 2007). Estimates of average porosity range from 27 to 31% with some samples exceeding 40%. Laboratory experiments have yielded porosity values of 35 to 42.5%. These are comparable with regional porosity estimates based on geophysical logs of between 35-40% (Chadwick et al, 2004)

2.3.3. Depositional environment

Although considered a depositional sand body, the exact depositional model for the Utsira Sand is a topic of long standing debate. Rundberg (1989) interpreted that the sands of the Utsira were deposited under high energy conditions, suggesting a model where strong shallow marine currents reworked sediments to form North-South trending sand mounds. Galloway (1993) expands upon this model, identifying the Scandinavian Platform as a source for the clastic influx. Conversely, Galloway (2002) identifies the eastward prograding Shetland Platform as a sediment source (Fig. 2.7), with a

high level of sediment reworking within an elongated seaway creating elongated mounds parallel to the basin margins.

Gregersen (1997 and 2003) suggests a turbiditic origin for the sands; however, this interpretation may have been hampered by the erroneous inclusion of the Skade sands within the Utsira Formation (Eidvin and Rundberg, 2005). This model would also seem unlikely considering the water depths of 100-200m suggested by biostratigraphical work by Piaseki et al., (2002). The location of the Utsira Sand at the centre of the basin, with no clear indication of progradation suggests that it is a basin floor fan. It is also worth considering that the North Sea has been classified a large sandstone intrusion province (Cartwright, 2010), and therefore the influence of sand injectites should not be overlooked. Wild and Briedis (2010) have reinterpreted the nearby Hermod and Balder sands as remobilised sands, emplaced by sand injection rather than depositional units. Loseth et al,. (2012) has interpreted a large body of sand, at a similar stratigraphic level as the Utsira, as an extrudite deposit. It is therefore possible that the Utsira Sand is not wholly depositional, and that in part it consists of extrudite deposits.

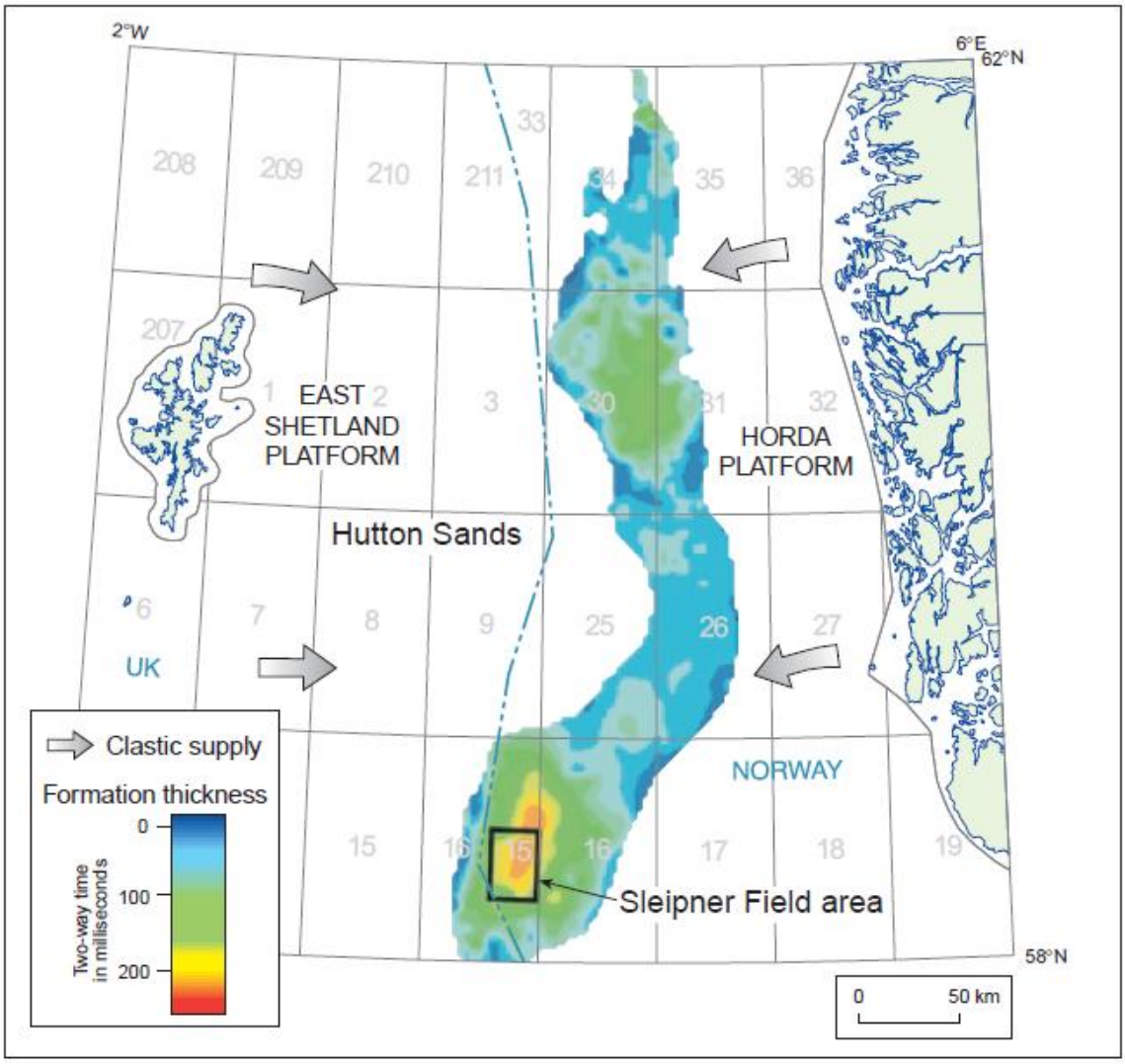

Fig. 2.7 Map of the distribution and TWT thickness of the Utsira Sand, showing clastic sediment provenance areas of the Utsira Sand (taken from Gregersen and Johannessen, 2007).

Chapter 3

Methods

3. Methods

The results presented in this thesis are derived from the interpretation of 3D seismic reflection data volumes. The aims of this chapter are 1) to give a brief overview of 3D seismic data; 2) to outline the datasets used in this thesis; and 3) to introduce the main interpretation methods used to derive the results presented in Chapters 4, 5 and 6.

3.1. 3D Seismic Data

In its most rudimentary form 3D seismic reflection surveying involves recording the time for a seismic wavelet to travel from source, reflect from a sub-surface interface, and return to a surface detector (Kearney et al., 2002; Sheriff and Geldart, 1995). In comparison to 2D seismic data, 3D seismic allows a more accurate imaging and interpretation of the subsurface due to closely spaced sampling distances and the collection of data in both horizontal and vertical directions in map view (Bacon et al., 2003). Typically with marine 3D seismic, data is acquired using a near surface seismic energy source and a series of hydrophones which detect the reflected energy of compressive (P) waves from subsurface physical boundaries. The strength of the reflected energy is the result of the acoustic impedance between two different lithologies. Acoustic impedance (z) is the function of the rock density (p) and the p-wave velocity (v).

$$Z = V\rho \qquad \text{(equ. 1)}$$

(Brown, 2004; Kearney et al., 2002). Acoustic impedance, and therefore the reflected energy, is greater between a high density rock and a low density rock than the impedance between two rocks of similar density.

The time from the seismic source to an acoustic impedance boundary and back to the geophone detectors is termed the two way travel time (TWT), it is often given as the vertical scale in a seismic section and may also be converted to a vertical distance with knowledge of wave velocity (Brown, 2004).

$$t = 2\frac{d}{V} \qquad \text{(equ. 2)}$$

Generally, seismic wave velocity increases with depth as the wave advances through more compacted sediment and rock (Brown, 2004; Kearney et al., 2002). However, other properties of the

subsurface can control the velocity of the seismic wave, these include; lithological composition, porosity, density, material texture, elastic modulus and fluid content.

Two other key properties of a seismic data volume are the wavelength and frequency of the wavelet. Wavelength is the distance from wave peak to peak, while frequency is a measure of how many peaks pass through a point per second. Both are related to wave velocity where wavelength (λ) is the quotient of the velocity (v) of the wave and the frequency (f), and if assuming a constant velocity, wavelength is inversely proportional to frequency i.e. higher frequencies form shorter wavelengths.

$$\lambda = \frac{v}{f} \qquad \text{(equ 3.)}$$

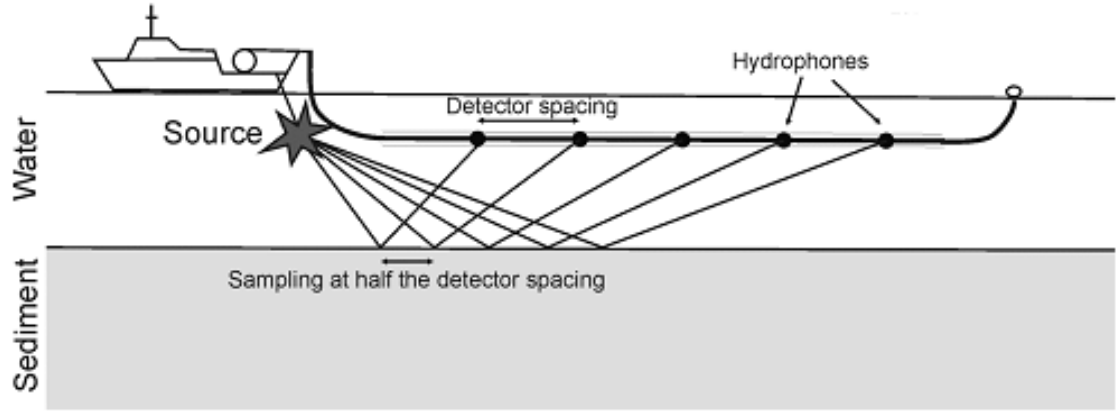

Fig. 3.1 Schematic representation of how 3D seismic survey is acquired (from Bacon et al., 2003).

3.1.1. Polarity and Phase

When seismic data is displayed so that an increase in acoustic impedance corresponds with a peak in the seismic wavelet it is considered to be in accord with the Society of Exploration Geophysicist normal polarity (SEG normal polarity) (Brown, 2004). A decrease in acoustic impedance would therefore be represented by a 'trough'. A clear example of an increase in impedance would be where the seismic wavelet passes from water to the seafloor.

Data may be in zero-phase, maximum, or minimum phase, but zero phase has become the preferred type for seismic interpretation. The zero-phase data means that the wavelet is symmetrical and the majority of energy is coincident with its peak (Yilmaz, 1987; Brown, 2004), which has a great advantage on seismic stratigraphic interpretations as the centre of the wavelet is coincident with the geological interface causing the reflection.

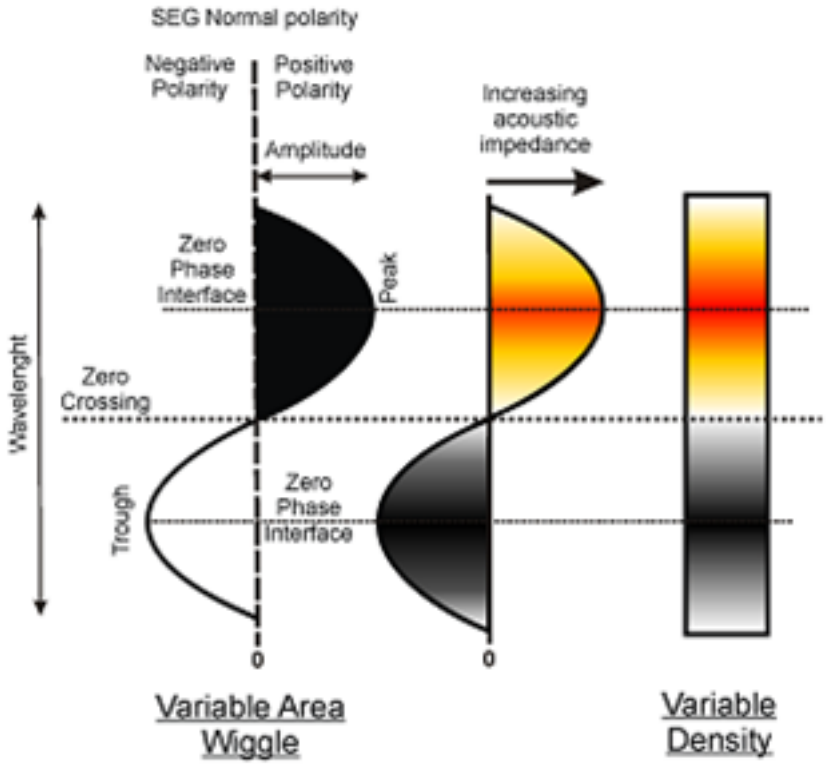

Fig. 3.2 This plot represent a 90 degree European wavelet (full cycle) and the relative graphical outputs (variable area and density) as observed on the workstation during the interpretation (from Hart, 1999).

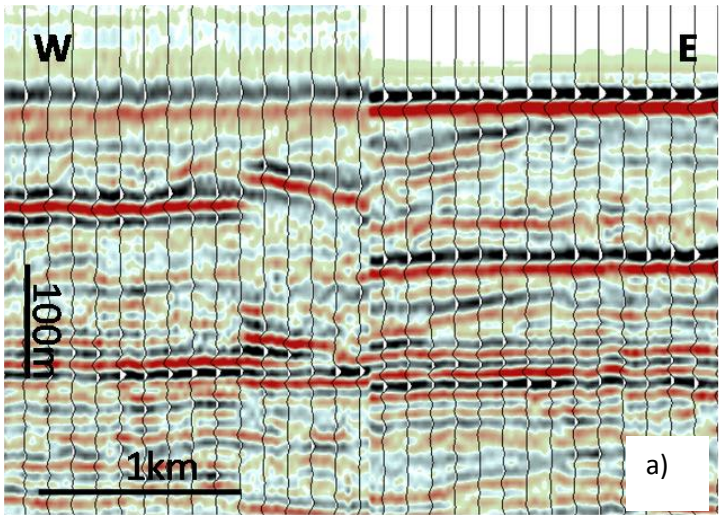

Fig. 3.3 a) seismic line from study area SA2 across a survey boundary. The dominant amplitude of the seabed reflection is the red, negative reflection b) the wavelet is therefore considered to be in European Convention, and in minimum phase.

The acquisition and processing history of the data used in this study are unknown. Observation of the seabed surface (the surface separating the water and the sediments) indicates that the data is consistent with the European convention (negative reflection for an increasing acoustic impedance with depth) and phase rotated to 90 degree (Fig 3.3a and b).

3.1.2. Resolution

Seismic resolution is defined as the ability to distinguish between separate features; the minimum distance between two features so that the two can be defined separately rather than as one (Yilmaz, 1987). The resolution of seismic data varies both vertically and horizontally, and in both cases the wavelength is a factor.

3.1.2.1. Vertical resolution

Vertical resolution is the ability to differentiate between closely spaced layers, it is also called the limit of separability (Brown, 2004), and is usually around a ¼ of the dominant wavelength. It generally decreases with depth as the sub-surface behaves as a filter which preferentially removes, or absorbs, higher frequencies. As the frequency decreases, the wavelength increases, and therefore the resolution decreases (ref to equation 3).

A ¼ of the wavelength is termed the 'tuning thickness', below this thickness events become undistinguishable from each other. The tuning effect is constructive when bed thickness is below the tuning thickness; in this instance two separate reflections constructively interfere with each other to create a singular reflection of higher amplitude (Sheriff and Geldart, 1995).

The tuning thickness is especially relevant when monitoring and imaging the migration and containment of a CO2 plume. Increasingly brightening internal layers within the Utsira Sand have been observed and interpreted as thin accumulations of CO2 underneath intra reservoir shale layers (Arts et al., 2004). These accumulations are below the tuning thickness (considered to be 8m), and are therefore interfering constructively with the shale layers to create a 'brightening' effect (Fig. 3. 3),

3.1.2.2. Horizontal resolution

Horizontal resolution is the minimum horizontal distance between two features so that the two can be defined separately. It is a function of the hydrophone spacing and the width of the Fresnel Zone (Kearney et al., 2002). The Fresnel Zone is defined as 'the portion of the reflector from which the reflected energy can reach the receiver within the first half cycle (1/2 a wavelength) of the reflection' (Brown, 2004). If the reflected energy returns within this zone, and is in phase, they

interfere constructively to give the reflected signal. 3D Seismic data is usually migrated to improve the horizontal resolution. This is achieved by correcting the spatial location of the reflections and creating a narrower Fresnel Zone by focusing the spread of energy (Bacon et al., 2003). Ideally, with accurate migration the Fresnel Zone should be reduced to the width of a ¼ wavelength; however, ½ wavelength is the usual result (Brown, 2004).

Closer hydrophone spacing leads to a smaller sampling distance, resulting in more reference points for depth estimates, which in turn gives a more accurate reconstruction, and better coverage of the subsurface. Generally, the horizontal sampling distance for a horizontal reflection is equal to half the hydrophone spacing (Kearney et al., 2002).

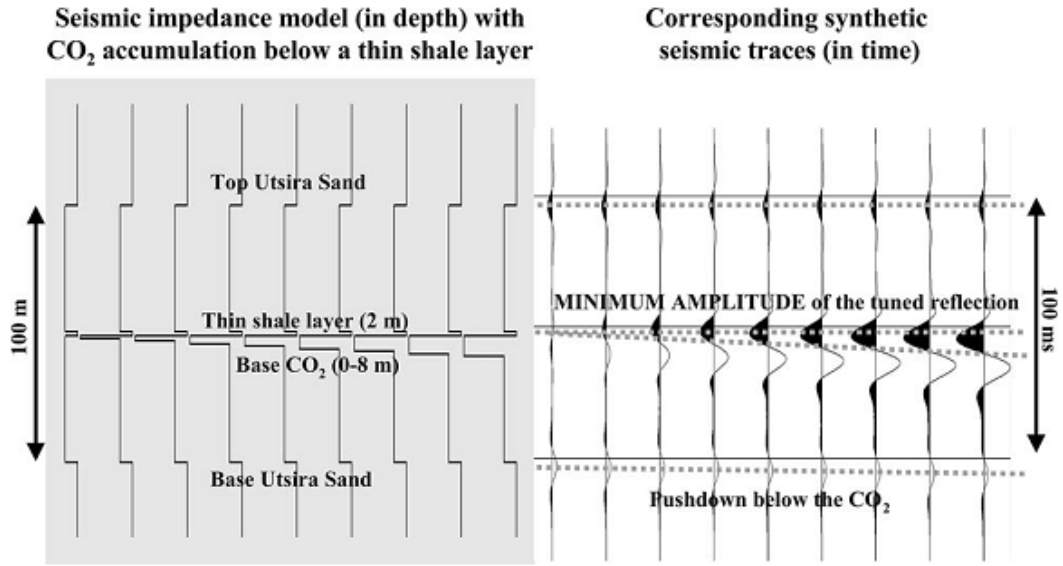

Fig. 3.4 Diagram represents how the thin layers of shale constructively interfere with the accumulations of CO_2 to cause a 'brightening' effect (from Chadwick et al., 2005).

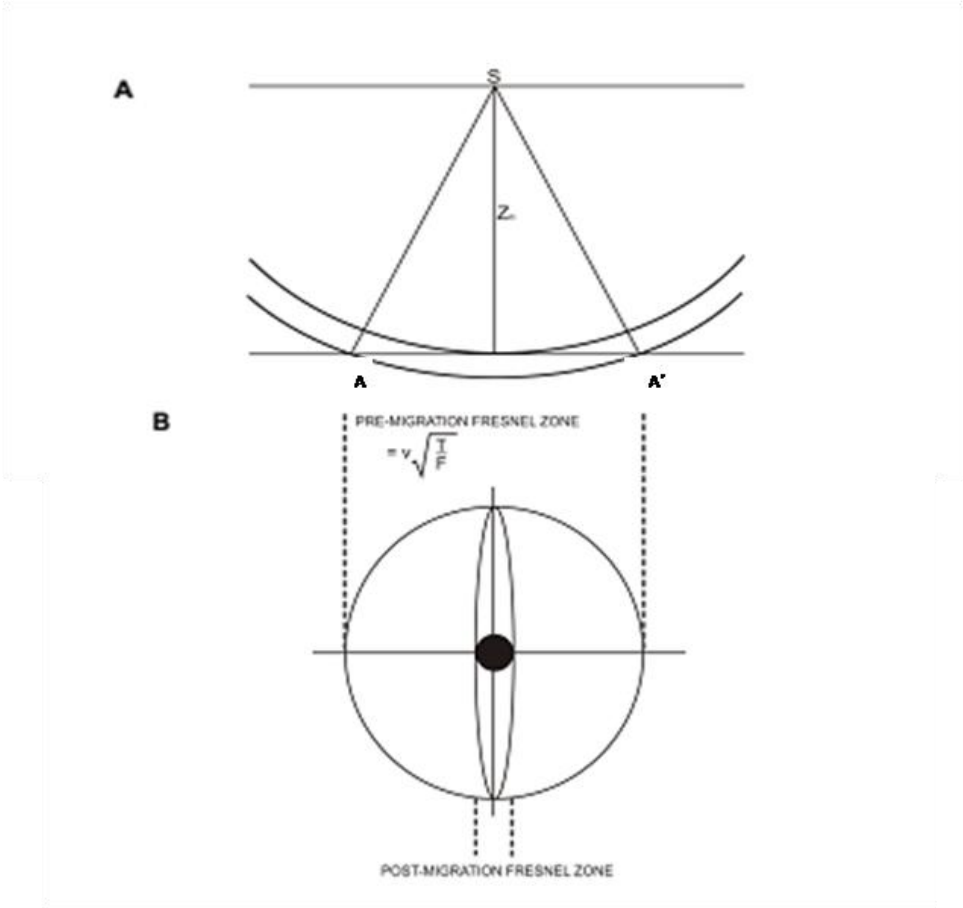

Fig. 3.5 a) the Fresnel Zone for a reflected wave from a sub-surface interface reflection at depth Z is represented by A-A', wavelets reflected from within the zone interfere constructively with each other, and cannot be separated from each other b) the principle of migration is to reduce the width of this zone

3.2. Interpretation of 3D seismic data

The results presented in this thesis are derived from mapping 3D seismic data volumes using IHS Kingdom Software. Seismic interpretation and mapping is the method of: "picking and tracking laterally consistent seismic reflectors for the purpose of mapping geological structures, stratigraphy and reservoir architecture," (Avseth et al. 2005). From this method of "picking and tracking" maps of the sub-surface are created, and in turn these surfaces can be used to create attribute maps which further aid the identification of other geological features.

Horizons of interest can be tracked manually through the study area over a series of lines orientated perpendicular to each other, termed in-lines and cross-lines. Within the data volumes used for this study, in-lines are orientated north to south, while cross-lines are west to east. These lines are mapped to form a grid pattern, with the spacing between lines initially at a similar scale to the geological features of interest. More detailed mapping, or mapping of complex features and areas can be achieved by decreasing the spacing between mapped lines or creating arbitrary lines.

3.2.1. Autotracking

Lines picked manually form the basis of 'seed points' which are used by the automated tracking algorithms which interpolate the data in the unmapped areas. Various parameter can be restricted or changed to control the autotracking process in order to ensure the accuracy of the final map, or in some cases to limit the geographic or stratigraphic extent of the map;

- Confidence: confidence of automated picking can be set between 0 and a 100%. The higher the value gives the autotracking process less freedom to try and 'interpret' the horizon itself i.e. If autotracking in complex areas with a high confidence set the autotracking will not pick the horizon. Closer spaced seed points allow improved autotracking at higher confidence levels.
- Amplitude: mapping a horizon of specific amplitude is possible by setting an amplitude range. This is especially useful when attempting to map amplitude anomalies.
- Time window: a time window can be set to block the autotracked horizon from 'jumping' up or down to other reflections.

- Polygon search: autotracking can be limited to a specific area by delineating a polygon to interpolate within.

Two way time maps, as presented in this study, are a 2D reconstruction of the subsurface. They represent the travel time of a wavelet from source to a subsurface boundary or horizon and back to source again. Seismic sections are 2D vertical 'slices' of the 3D data cube, where the subsurface boundaries are represented by reflections of opposite polarity and varying amplitude. Reflections can be traced and mapped along seismic sections to produce Two way time maps. Once a map of sufficient and satisfactory accuracy and detail has been created it can be used to derive attribute maps which further highlight geological features, and can be used to calculate contoured, isopach and isochron maps. The seismic attributes used within this thesis are described below:

3.2.2. Attributes

- Amplitude: variations of amplitude along a mapped horizon may be viewed in map form in addition to seismic sections. Lateral variations in amplitude are the result of changes in the acoustic impedance, which may be the result of changes in density and/or acoustic wave velocity. These changes can generally be attributed to changes in lithology or fluid content. (e.g. Fig. 6.8).
- Coherency/Semblance: Is calculated by comparing adjacent waveforms and producing a value based on their similarity. Coherency slices can highlight chaotic areas or discontinuous features, and are free of interpretation bias. (e.g. Fig. 5.12).
- Time-Dip: dip maps outline areas of a horizon where the gradient changes. They can be used to identify topographic features and variations in slope. They are especially useful when delineating the outlines of folds and mounds (e.g. Fig. 4.12).
- RMS amplitude: Root mean square amplitude volumes square the amplitude values within a specific depth range and then average the results. Higher amplitudes, both positive and negative, are accentuated by this process, and are therefore more noticeable on maps. The depth range can be delineated by time windows or by mapped horizons. (e.g Fig. 6.4).

3.3. Data set

The research presented in Chapters 5 and 6 is based on a collection of local and regional 3D Seismic surveys from the Norwegian Petroleum Directorate Diskos database. Individual surveys have been matched and merged as best as possible by Robertson GeoSpec on behalf of CGG Data Services AG. The results in Chapter 4 (Fig.3.5a) are based on a study area within a 2,327km^2 section of survey from the UK sector of the Central North Sea, cut at a depth of 2 seconds. Chapters 5 and 6 (Fig 3.5a) are derived from a larger portion of data with an aerial coverage of 11,554km^2 to a depth of 3 seconds. Data quality is variable through the volume due to the difference in the acquisition parameters of individual surveys before they were merged. The merged dataset has a sample interval of 4ms and an output bin size of 25m. The dominant frequency in the area of higher quality presented in Chapter 6 is 24-30Hz. Using a phase velocity of 1800m/s for the Cenozoic interval, a vertical stratigraphic resolution of c. 16-19 m was calculated.

3.3.1. Limitations of data

Digital well data for loading to the workstation was not available. Screen shots of well tops, and correlation from published and online Norwegian Petroleum Directorate wells was used to aid horizon interpretation. Appendix A includes examples of these. Only one diagram of a coherency cube is used within this study, due to limitations with the SMT Kingdom License.

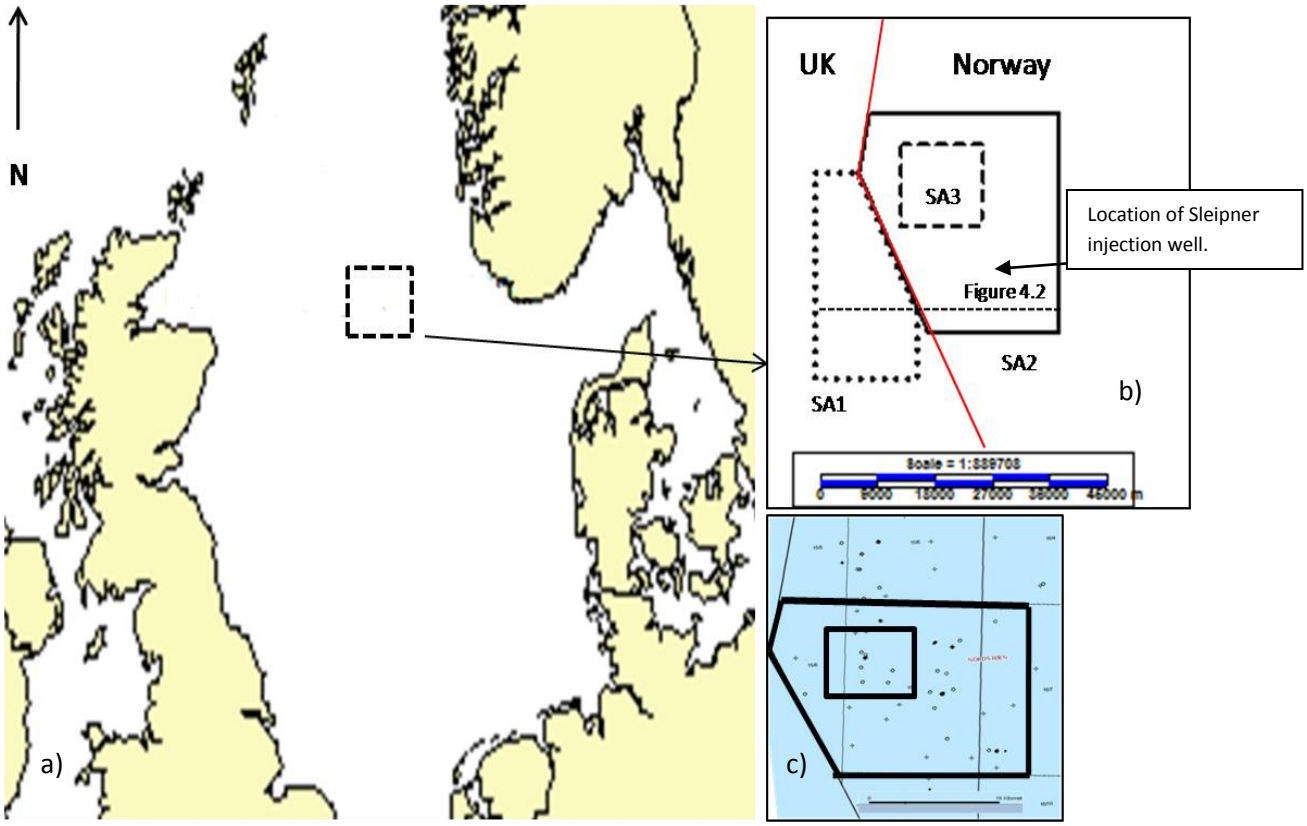

Fig. 3.6a) Location of study area in respect of the UK and Norwegian coasts b) a map the three study areas in respect of each other and the UK-Norwegian boundary line

CHAPTER 4

A description of sandstone intrusion indicators and the interpretation of forced folding of the basal horizon of the Utsira Sand by hydraulic 'jack up.'

4. Chapter 4

4.1. Introduction

The aim of this chapter is to describe and better understand high amplitude reflections which are associated with, and may be indicators of, sand intrusions which underlie the UK section of the Utsira Sand. The Utsira Sand is a large North Sea saline aquifer exceeding 25,000 km^2 in area. Located around a 100km off the west coast of Norway, it is described as the 'sandy, quartzose' part of the Utsira Formation. It consists of fine grained sand, with occasional medium to coarse grains, and includes shell fragments and glauconitic beds.. A small area of the southern depo-centre, the Main Utsira Sand (Eidvin and Rundberg, 2005), is currently being utilised for carbon dioxide sequestration.

The base of the Utsira Sand has been described as structurally complex, and is characterised by circular or elliptical mounds (Chadwick et al., 2004). These mounds have been interpreted as the result of mud volcanoes (Heggland, 1998, Arts et al, 2000,) channels (Kirby et al, 2001), shale deformation (Gregersen, 2007), and mud diapirs (Galloway, 2002; Chadwick et al., 2004). However, Loseth et al., (2003) and Huuse (2010) suggest a relationship between a number of these mounds and underlying seismically imaged 'V' bright reflections and present wells with sandy intervals correlate with the high amplitude features.

These discordant, 'V' shaped high amplitude reflections are characteristic of sand intrusions. Sand intrusions have been described as an 'enigmatic' class of soft sediment deformation (Shoulders and Cartwright (2010) and are considered members of the intrusion related seal bypass family (Cartwright et al, 2007) and a result of subsurface sediment remobilisation (andresen, 2012).

Reservoir scale sandstone intrusions are common in the North Sea Basin, prompting the classification of this area as a large sandstone intrusion province (LSIP) (Cartwright, 2010). Shallow intrusions are known to cause domal forced folding of the paleo-seafloor as a result of hydraulic 'jack up', and a causative relationship between the sand intrusions and sea floor mounds has been suggested for the intrusion network in the Faeroe-Shetland Basin by Shoulders and Cartwright (2007) and in the North Sea by Cartwright (2010). The presence of sand intrusions below the Utsira Sand may therefore account for the structural complexity observed at its base.

In Chapter 5, the study is extended to an adjacent larger dataset within the Norwegian sector of the North Sea, in an attempt to determine the geographic spread of the sandstone intrusions.

4.2. Dataset

The results presented in this Section are derived from a 2,300km^2 3D seismic volume from the UK section of the Central North Sea. The study area itself covers an area around 400km^2 within the larger volume (Fig. 4.1).

The processing history of the data is unknown; however, observation of the seafloor suggests that this horizon corresponds with a negative amplitude, red reflection, and that the data is displayed in reverse polarity, following the European Convention (Fig. 4.2a). The data volume is an amalgamation of local and regional 3D seismic surveys, hence the high variability in data quality. The dominant frequency in the areas of better quality is around 40 to 45Hz, and using velocity value of between 2000m/s and 1800m/s from NPD synthetic seismograms (http://factpages.npd.no/factpages/default.aspx), the vertical resolution is calculated between 11 and 12.5 m Digital well data was not available to aid interpretation, and it was not possible to create coherency cubes due to licensing limitations associated with the IHS Kingdom software. Depth conversion was not carried out for the data, and the depths reported within this study are based on the velocity values from NPD synthetic seismograms.

The geological setting of this study area is presented in Chapter 3 of this volume; a brief description of the main units mapped for this chapter is presented in section 4.3.1.

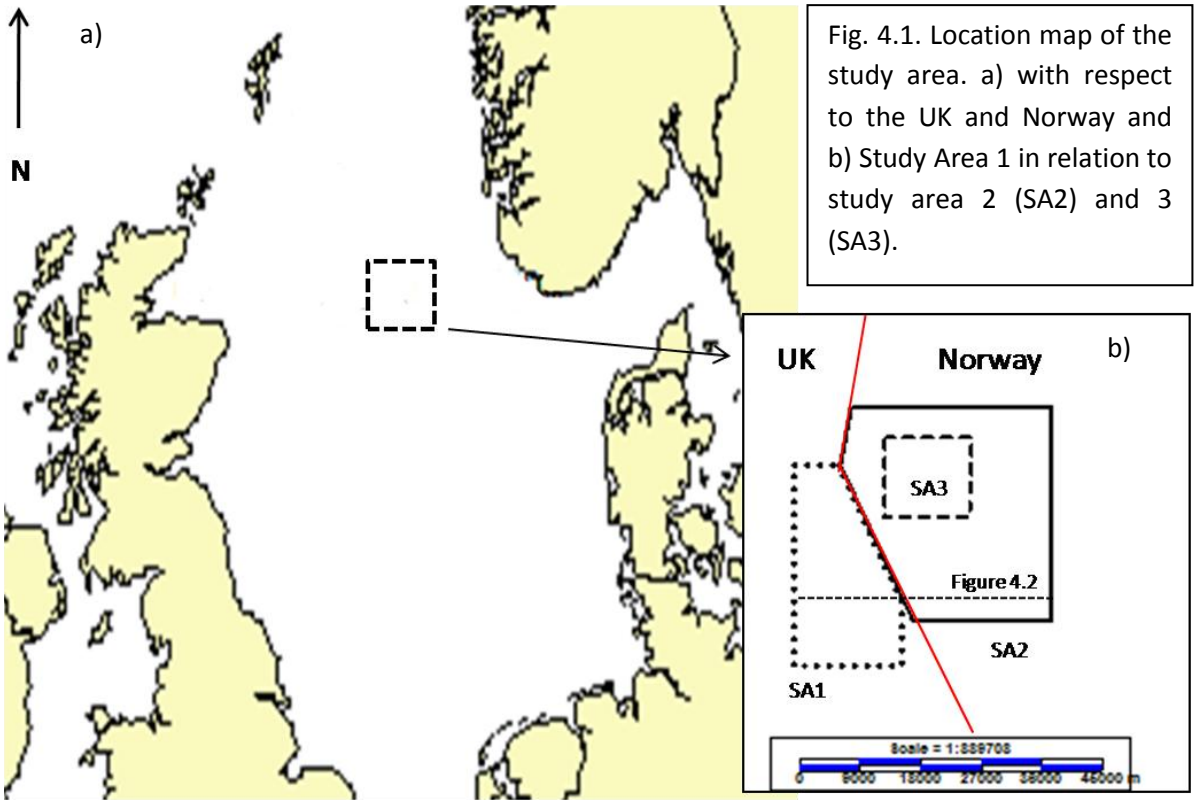

Fig. 4.1. Location map of the study area. a) with respect to the UK and Norway and b) Study Area 1 in relation to study area 2 (SA2) and 3 (SA3).

4.3. Results and Observations

4.3.1. Main units mapped

The units described in this chapter have previously been described in section 2.2.2.1. They consist of a Lower Miocene Shale unit (Hordaland Shale) and the Upper Miocene to Lower Pliocene Utsira Sand (Fig. 4.2b).

4.3.1.1. Hordaland Shale

The lower boundary of this unit is a discontinuous and faulted high amplitude couplet, while the upper boundary is a semi-continuous horizon of medium amplitude. At its deepest, in the south of the study area, it achieves a depth of 1.4 km. The unit is relatively flat lying within the southern and central areas; it shallows towards the north-west with an increasing gradient, reaching a depth of around a kilometre (Fig. 4.3a). The unit is at its thinnest at the western edge of the study area where

it is around 100m thick. It thickens towards the centre, and is generally 170m to 240m thick in the rest of the study area. Localised areas of greater thickness are present where its upper boundary horizon is deformed and pushed upwards.

A dip map of the basal horizon highlights its discontinuous nature. In map view this horizon consists of a polygonal network of interconnected features which are hundreds of metres in width (Fig. 4.3b). This network is similar to the irregular, well connected polygonal fault pattern of Lonergan et al., (1997), and consists of a mixture of linear and curved fault traces, which are indicators of a well matured fault network. These faults generally have a small throw of around 25m, and are preferentially orientated, dipping towards the west in the west area of the data set. They become sub-horizontal towards the centre section with occasional westwards dipping faults in the east (Fig. 4.3c).

The internal reflections of the unit are generally of a low amplitude, and are semi-continuous, concordant and parallel. Locally high amplitude reflections are present, these are generally discordant and cross cut the internal reflections of the unit. High amplitude concordant reflections and 'bright spots' are also present.

4.3.1.2. Utsira Sand

The Utsira Sand extends around 50km north to south, 30km east to west, and covers an area of over 1000km^2 within the study area. A continuous high amplitude reflection, the Base Utsira Horizon (BUH) defines its base. Irregular elliptical areas of high relief are evident from a time depth map of this horizon (Fig. 4.4a). These features are present as two prominent ridges of high topography which crudely follow a linear trend.

The upper horizon of the unit is a medium to high amplitude undulating reflection. Its depth in the central area is around 1000m. Areas of low relief depressions are revealed by a time depth map of this horizon (Fig. 4.4c). The undulating nature of the upper horizon is expressed in several broad, low relief antiforms flanked by slightly narrower synforms. Contrastingly, the mounds at the basal horizon are narrower but of greater relief.

At the western edge of the study area, near the UK/Norway boundary, the Utsira Sand achieves its maximum thickness of 230m. It thins and pinches out to the west, south and north, and the pattern of thinning in these directions is irregular. Areas of fluctuating thickness are present throughout the study area, with several sections of reduced thickness saddled between thicker portions. These

thinner areas correspond with the locations of ellipsoid mounds at the base of the unit, and elliptical depressions at the upper horizon (Fig. 4.4b). In some cases the basal and upper horizons are close to being in contact and the Utsira almost pinches out. This effect, especially at the western extremities of the study area where the unit is at its thinnest, has the result of creating thin 'slivers' of sand which may be separate from the main Utsira Sand body.

The internal reflections of the Utsira Sand can be sub-divided into two sections, a lower section which onlaps onto the mounds and an upper section which mirrors the undulating nature of the upper horizon. Occasional bright reflections are present within the lower section, often at the flanks of the mounds. In places the onlapping reflections of the lower section display a slight downlapping profile, while the upper section of the unit follows the undulating geometry of the upper boundary.

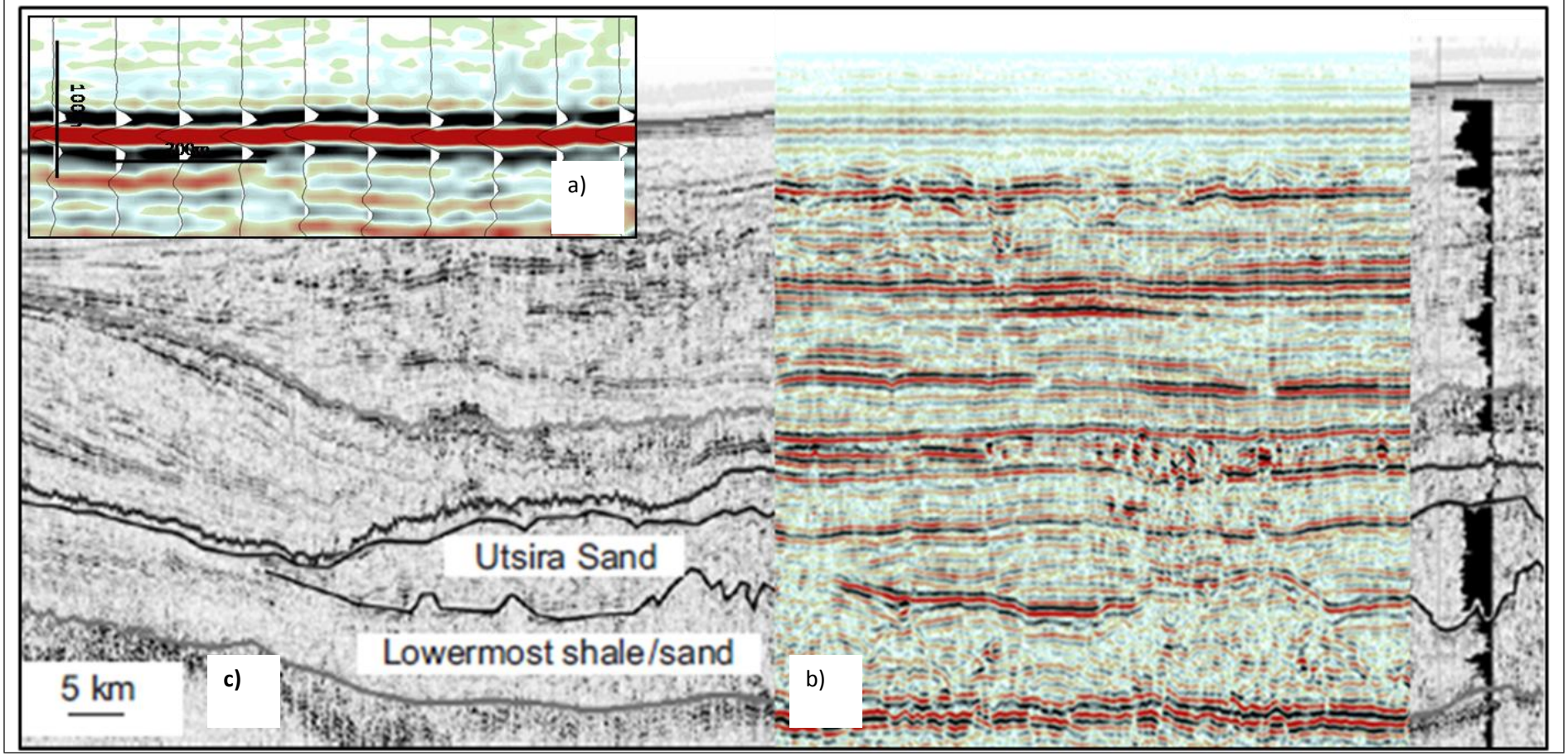

Fig. 4.2 a) Seabed reflection with wiggle overlay, negative (red) reflection is the dominant amplitude, data is considered to be in accord with the European Convention. b) Seismic section from this study area (in colour) in conjunction to c) that presented by Gregersen (2007)

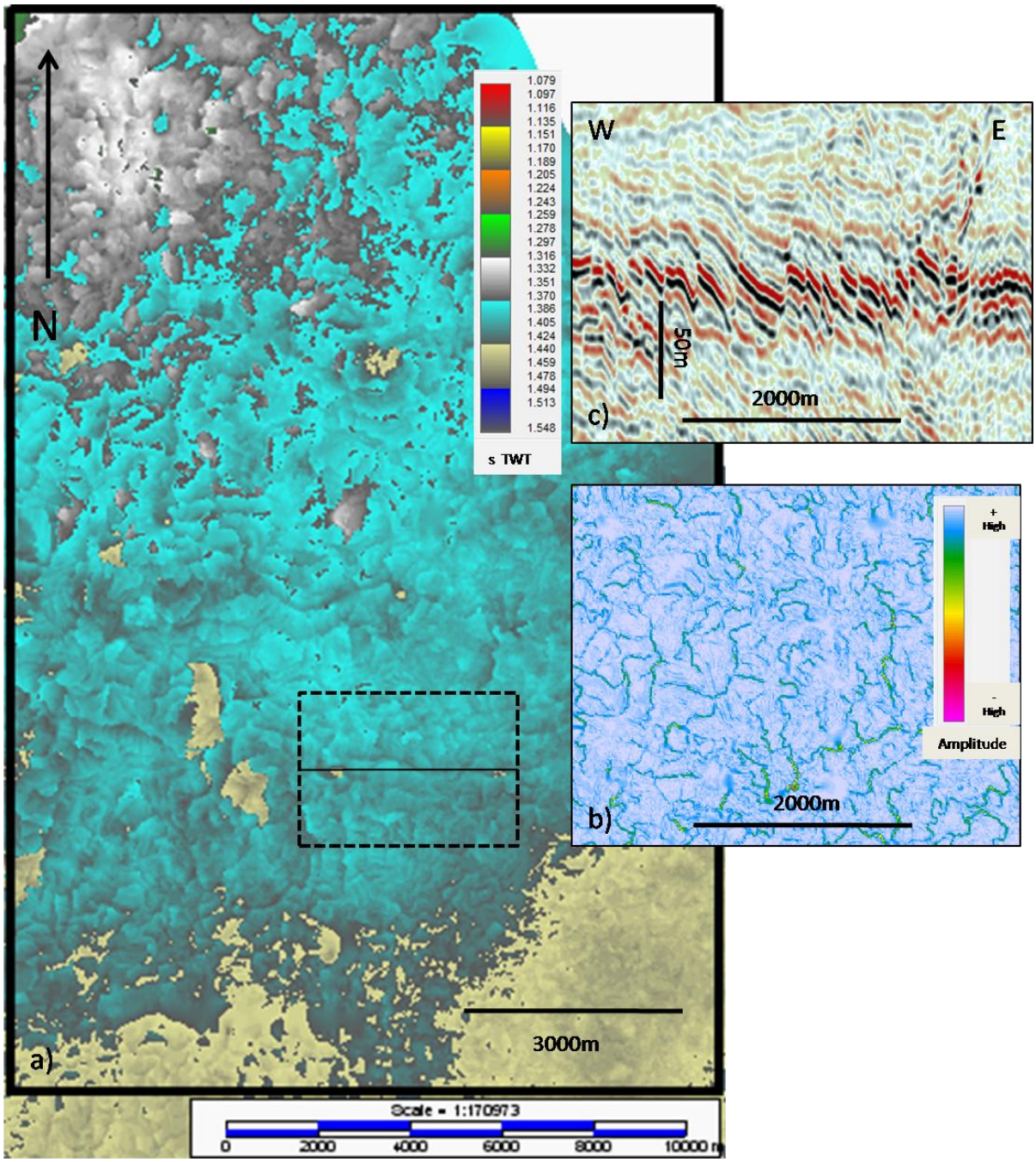

Fig. 4.3a) TWT map of the basal horizon of the Lowermost Shale. b) time-slice of the area within dashed box, consisting of a mixture of linear and curved fault traces, which are indicators of a well matured fault network. c) Seismic section showing the polygonally faulted basal horizon of the Lowermost Shale

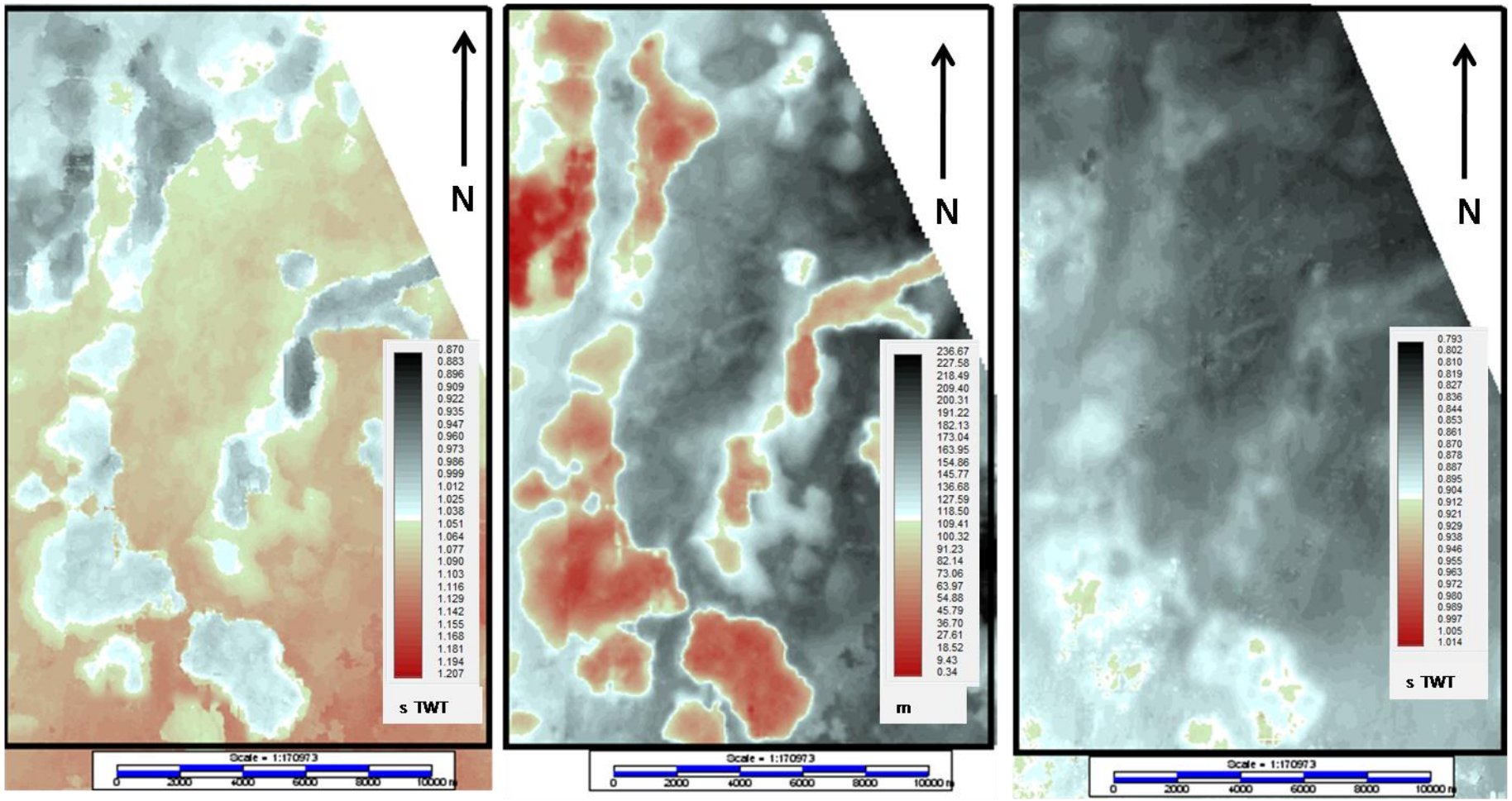

Fig. 4.4a) TWT map of the Base Utsira Horizon reveals the presence of elliptical mounds b) Isochron map of Utsira Sand suggests the significant influence of the mounds on unit thickness c) time depth map of the Top Utsira Horizon shows more subtle features at this level which appear to mirror those at the Base Utsira Horizon.

4.4. 3D seismic detailed description of the Utsira Sand and adjoining intervals

4.4.1. Miocene Mudstone amplitude anomalies

Despite the general low to moderate amplitude reflections of the unit there are several incidences of high amplitude within the unit. The form, geometry and dimensions of these amplitude anomalies vary in their manifestation on RMS maps, time slices and in seismic sections.

Seismic cross sections of these high amplitude packages reveal both stratal-discordant and concordant reflections. The stratal-discordant reflections can be seen to diagonally cross cut the host unit reflections and be observed to be either one or a combination of several forms; singular and linear discordant reflections, linear discordant reflections emanating from a bright spot, sub-vertical bright spots (<300m in length), or a combination of concordant and discordant reflections which result in irregular 'saw toothed' features. Horizontal reflections which do not cross cut the host unit reflections are visible as either concordant reflections which exceed 300m in lateral extent, or as horizontal bright spots (<300m).

Reflections from the host unit are observed to terminate against the high amplitude discordant reflections. Discordant reflections can cross cut up to 100m vertically of the host unit and exceed 300m from their base to tip (Fig. 4.5a), and they are often seen to be in connection with concordant or discordant bright spots (Fig. 4.5b). Discordant bright spots are less than 300m in length and cross cut less than 50m of the host unit (Fig. 4.5d). Concordant bright spots are horizontal to sub-horizontal reflections which lie comfortably with the host unit reflections, their lateral extent does not exceed 300m (Fig. 4.5e), and they can be seen in conjunction with discordant reflections and bright spots to form saw toothed reflections (Fig. 4.5c). Concordant high amplitude reflections are horizontal to sub-horizontal reflections which exceed 300m in lateral extent (Fig. 4.5f).

RMS maps reveal these high reflectivity reflections to be circular to sub-circular and elongated features of high amplitude (Fig. 4.6a,b,c). They can be isolated, but are generally in close proximity to other high reflectivity features, and are often connected by lower reflectivity 'saddles' (Fig.4.6c,

point S). Grouped high reflectivity features can be occasionally seen to form indistinct outlines of larger elongated sub-circular or horseshoe geometries (Fig. 4.6e and d).

The high reflectivity features seen on the RMS map are often replicated in their geometry upon time slice maps which intersect the features. Circular to sub circular and elongated features are commonly observed (Fig. 4.7a and b, feature A). In addition to these, linear or curved high amplitude features are also apparent, and can comprise a single polarity high amplitude reflection (Fig. 4.7a, Point 1), or pairs and triplets of contrasting polarity (Fig. 4.7a, Point 2), although these differ in their appearance on the RMS map (Fig. 4.7b). When intersected at specific depths along their profile they display a sharp boundary and are seen as prominent and noticeable features in comparison with the background reflections.

RMS maps give the best indicator of the areal extent of the amplitude anomalies, while seismic sections and time slices give a more detailed view of their vertical and horizontal cross sectional geometry respectively. A combination of all three gives the most complete and accurate interpretation of the high amplitude features seen.

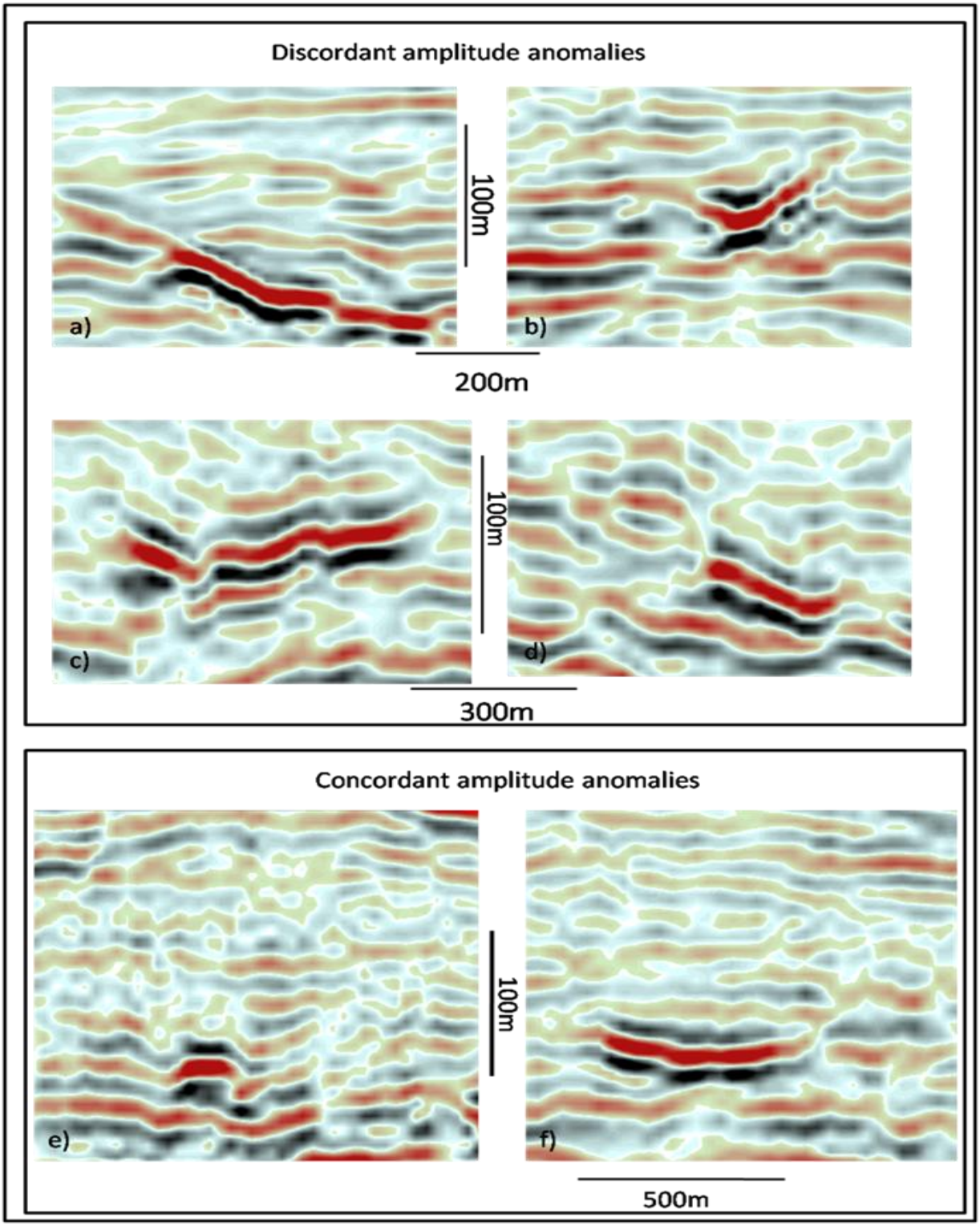

Fig. 4.5 Seismic profiles of representative examples of high amplitude features within the Lowermost Shale a) discordant high amplitude reflection b) discordant reflection with connected bright spot c) saw toothed reflection d) discordant bright spot e) concordant bright spot f) concordant high amplitude reflection

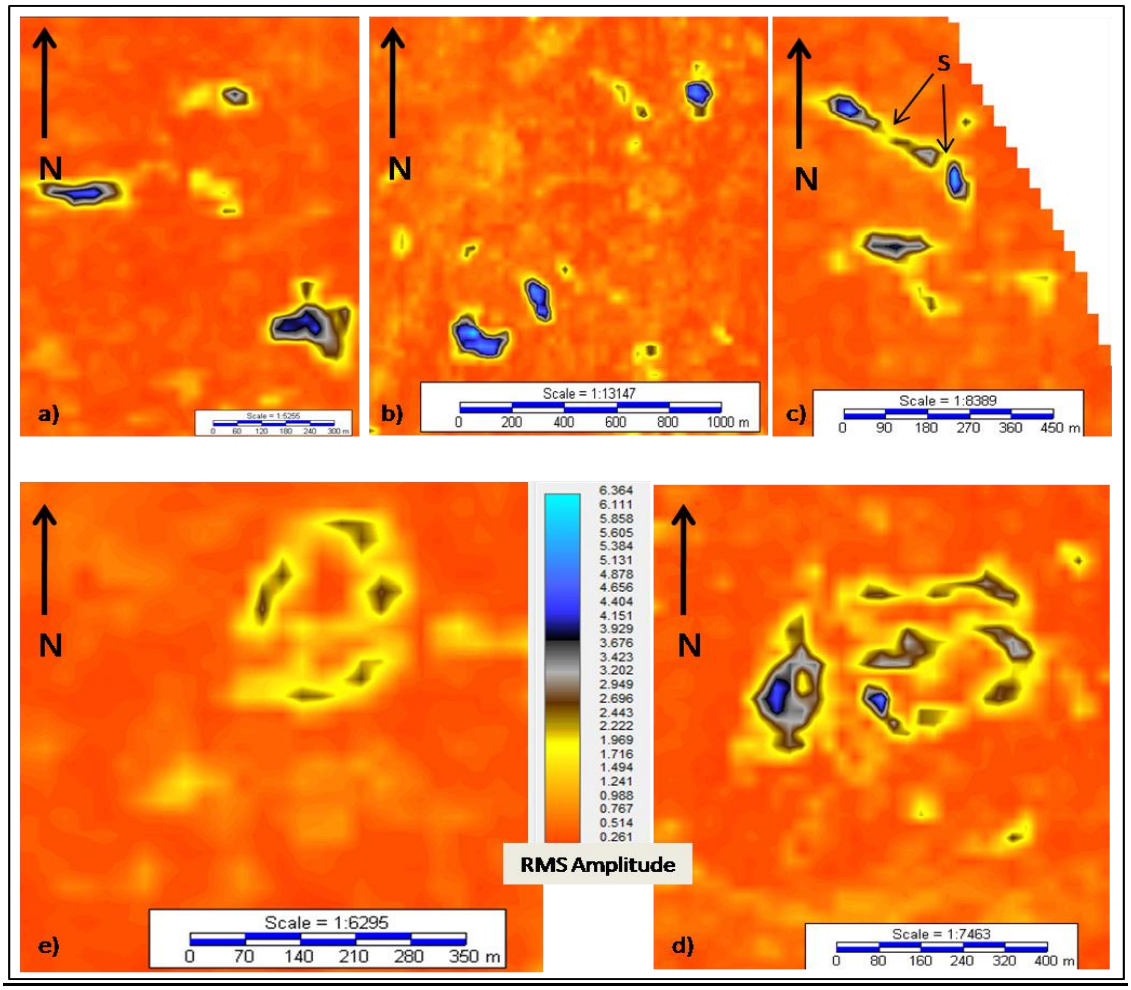

Fig. 4.6 An RMS map of representative examples of Lowermost Shale amplitude anomalies a and b)elongated and sub-circular c) connected by low amplitude 'saddles' d) elliptical outline of high energy and e) 'horseshoe' geometry

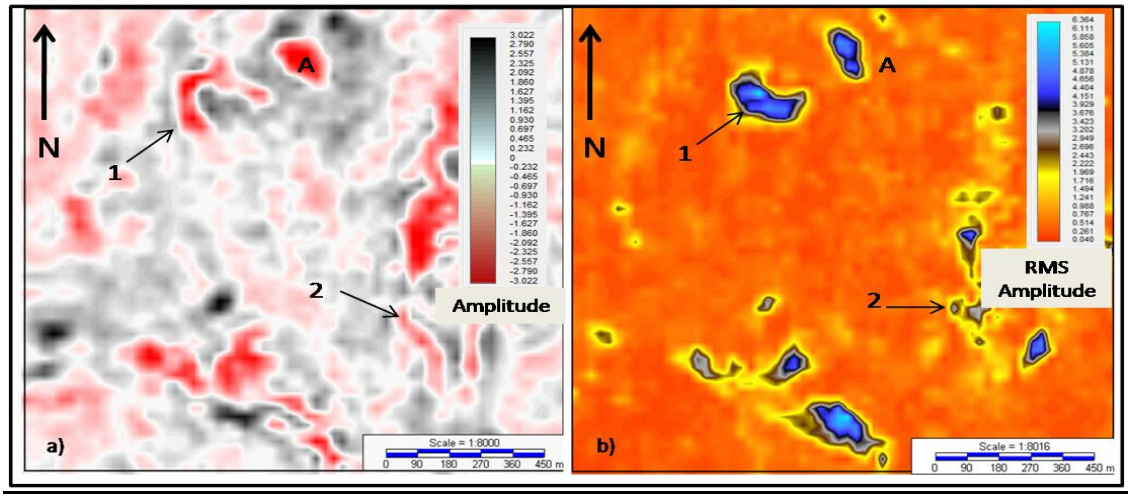

Fig. 4.7 a)A time-slice and b)RMS map an of representative examples of Lowermost Shale with 'horseshoe' geometry (1) and linear reflection (2)

4.4.1.1. Pair of discordant reflections

A pair of high amplitude features are located along the north to south seismic section are shown in Fig. 4.8a. Both features are apparent on the time slice as bright red reflections (Fig. 4.8b, points A and B). The southern reflection (A) is slightly curved with a sharp boundary against the surrounding black background reflections, while the northern reflection (B) is broader and less curved. Reflection A is part of a group of high reflectivity features which form a roughly elliptical shaped area of high reflectivity on the RMS map (Fig. 4.8c, A), while reflection B is a circular feature in close proximity to several other high reflectivity areas.

In seismic section the high amplitude features are seen as a pair of discordant reflections, of opposite dip direction. They are separated by a section of low amplitude around 800m in length. The southern discordant reflection (A) crosscuts a section of bedding by around 80m in vertical height and around 600m in length from its base to its tip. Its tip appears to terminate abruptly while its base it is connected to a horizontal bright spot (Fig. 4.8a, BS) which dims towards the north. The second discordant reflection is located 800m to the north (B), it is smaller, around 300m, and cross cuts around 50m of the host unit. It dims at both its southern base and its northern tip. The dominant amplitude of both features is negative (red reflection), and they can be considered as a 'hard' events (i.e. an increase in acoustic impedance). The reflections of the host unit can be seen to terminate against the underside of both the discordant reflections (Points T), and the central area in between the pair consists of disrupted and chaotic reflections. The overlying Base Utsira Horizon (BUH) is domed upwards, heavily disrupted, and is difficult to trace.

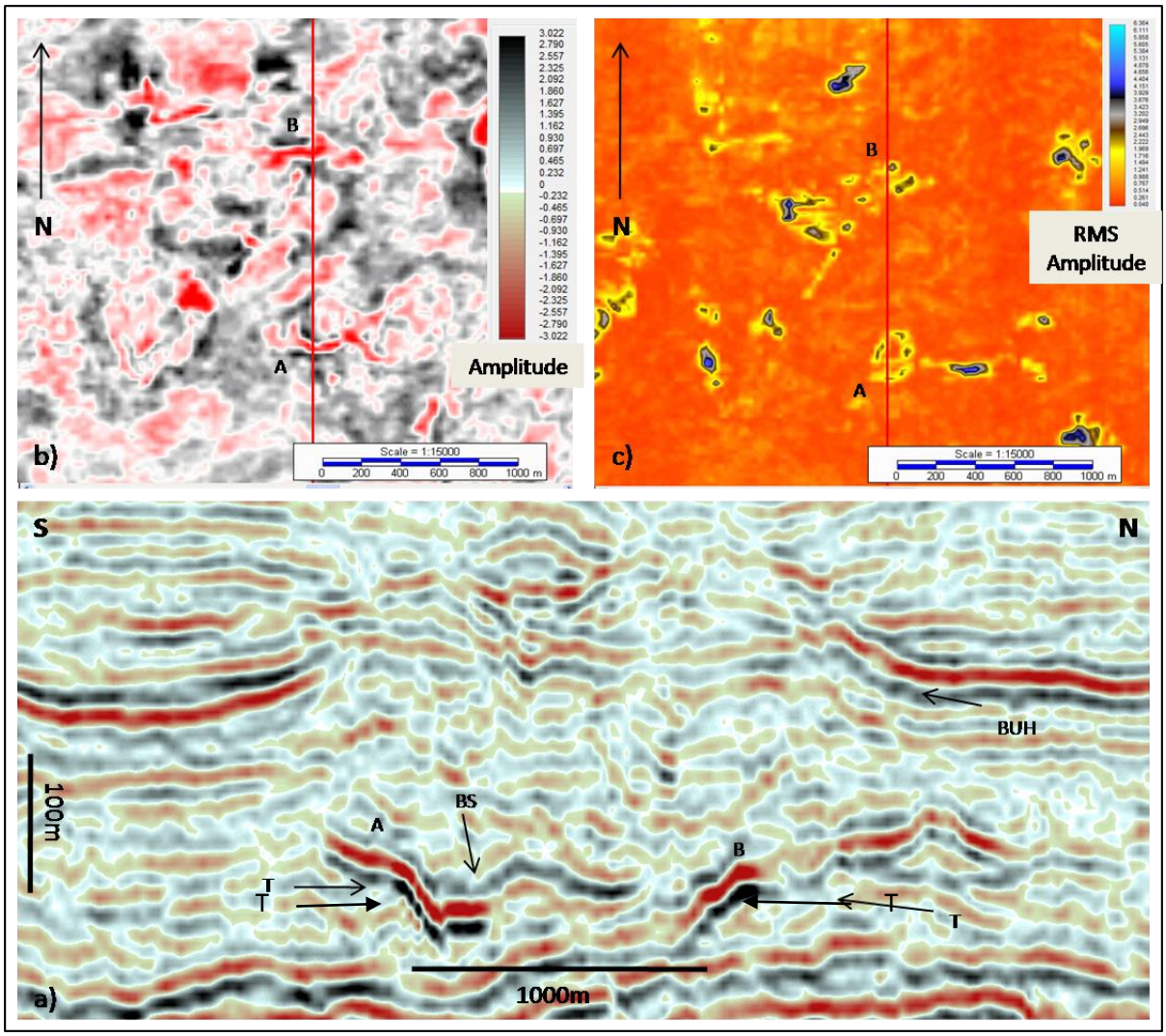

Fig. 4.8 a) seismic profile of a pair of discordant reflections A and B b) seen on the time slice as curved (A) and linear (B) narrow, high amplitude reflections and upon the RMS map c) as sub-circular high amplitude features

4.4.1.2. Effect on host unit

The presence of the high amplitude reflections effectively changes the nature of the background unit and coincides with areas where the overlying reflections become chaotic and disrupted and the BUH is deformed and domed upwards (Fig.s 4.9 and 4.10). Where undisturbed, the host unit reflections are generally semi-continuous, sub-parallel, are generally concordant, and the unit thickness varies only slightly. However, the presence of high amplitude reflections are often accompanied by broken and displaced reflections and zones of chaotic reflections within the host unit. The doming of the overlying reflections, and of the Base Utsira horizon, causes local thickening of the unit. Examples of this effect are presented below.

Example 1

Several high amplitude reflections are located along a north-south seismic profile (Fig. 4.9a and b). These consist of a concordant high amplitude reflection (Point A), a horizontal bright spot (Point B) and a sub-horizontal bright spot (point C). Points A and B have a dominant negative amplitude (red reflection), considered to be hard events within this data set, while point C has a dominant negative amplitude (black reflection), and is a soft event.

A sub-vertical zone of broken reflections can be seen emanating from point B towards the BUH at point D. The reflections of the host unit are visible to the left of point B and consist of horizontal to sub-horizontal reflections displaying stratification; they terminate against the sub-vertical zone which connects point B to point D. The central area (between points B and C and overlying point A), consists of broken, disrupted and chaotic reflections. A less prominent sub-vertical zone of broken reflections may be seen to overlie point C and project upwards to point E. The BUH is upturned and discontinuous at point D, and is upturned and displaced at point E. Between these two points the Base Utsira Horizon is not prominent. A medium amplitude bright spot, of negative amplitude, lies 80m directly above point A.

Example 2

The effect on the host unit can also be demonstrated by attempting to trace specific horizons across the affected areas. A negative high amplitude, discordant, bright spot is visible along a north to south seismic section (Fig. 4.10, point A). The overlying BUH is prominent to the south and to the north of the section, although in the area directly above the bright spot it is seen to be displaced and broken in places (Points B, C and D). Two horizons within the Hordaland Shale (Fig. 4.10, Horizon A, Horizon B) are annotated and are present to the north and to the south of the bright spot. However, they cannot be traced through the central zone overlying the bright spot. The Hordaland Shale is seen to thicken from around 200m where unaffected to over 250m where the BUH is displaced.

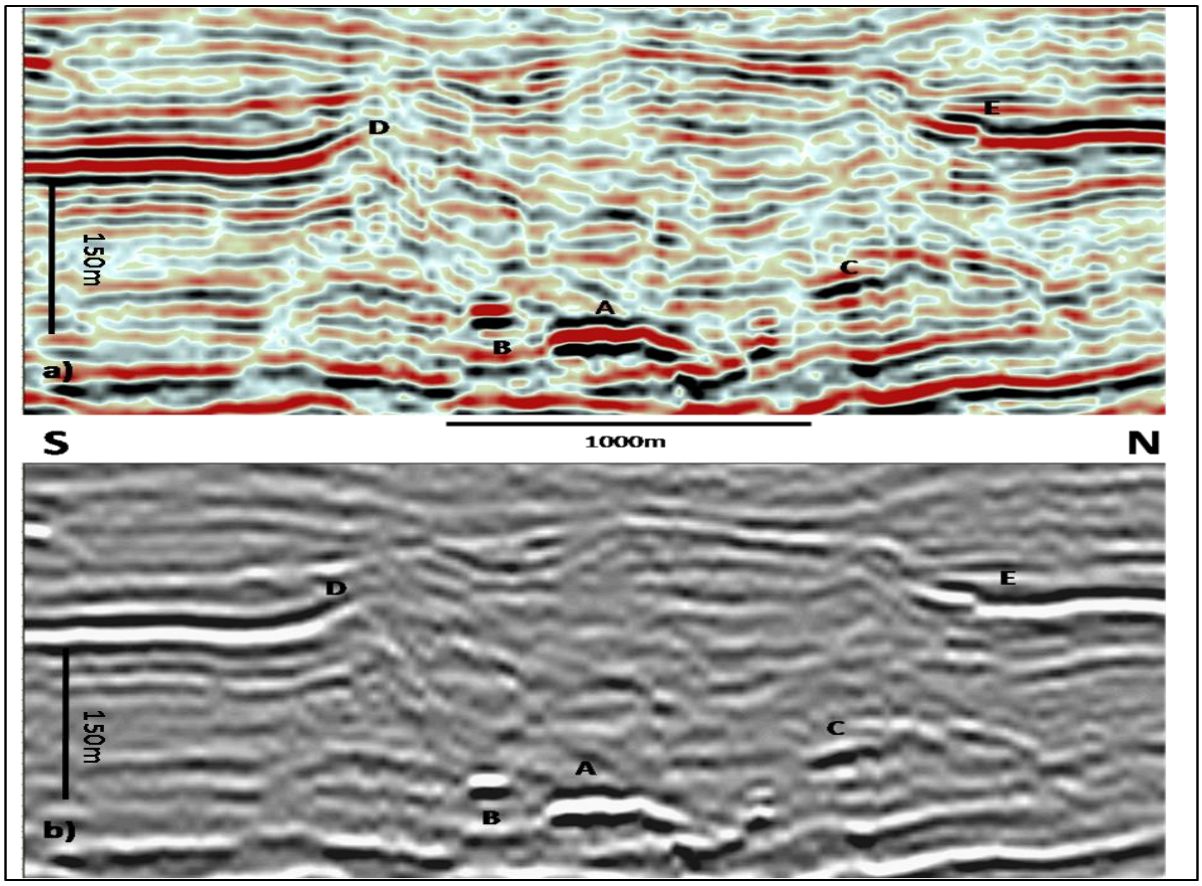

Fig. 4.9 Seismic sections a) in Landmark colour scheme and b) in black and white colour scheme showing a concordant bright spot (B) a concordant reflection (A) and a sub-horizontal concordant bright spot (C). Sub vertical zones of disrupted reflections are projected upwards

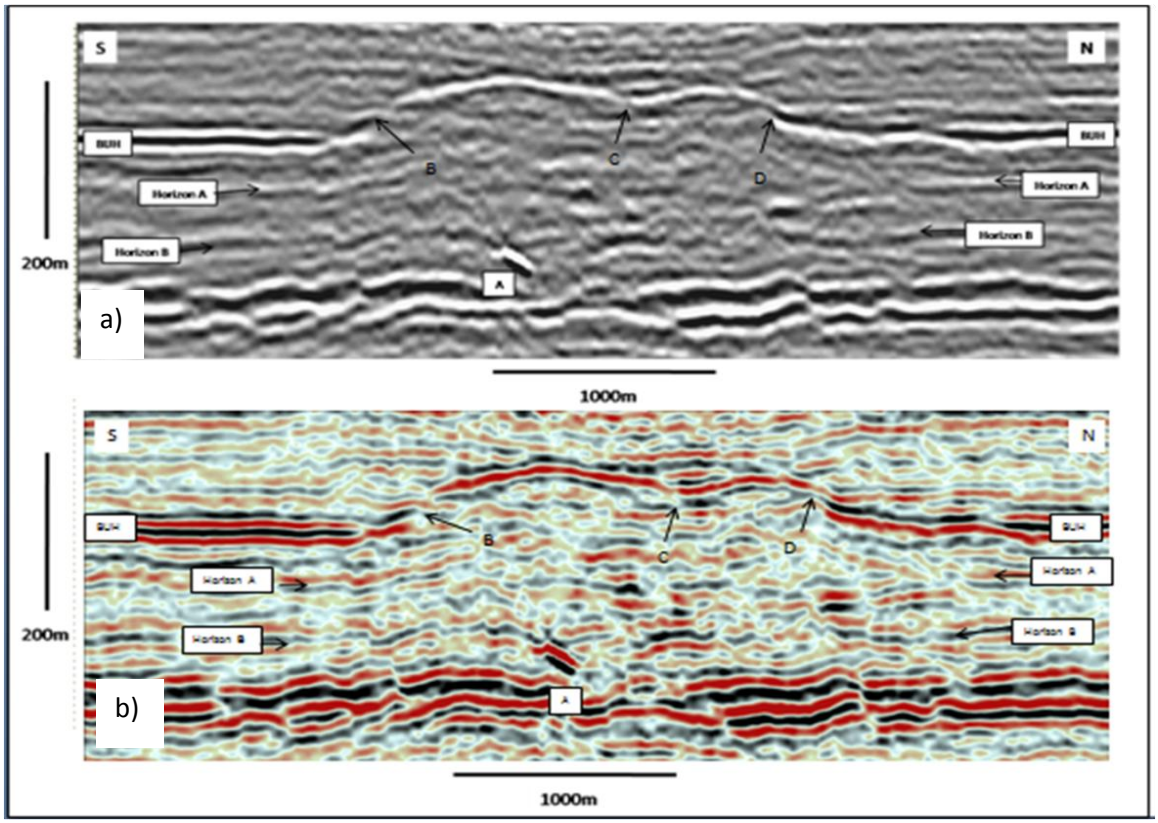

Fig. 4.10 Seismic sections showing a) in Landmark colour scheme and b) in black and white discordant bright spot (A) with overlying chaotic reflection and discontinuous points of the BUH (Points B, C and D). Neither of horizons A or B can be traced across the central chaotic zone.

4.4.1.3. Interpretation and discussion

4.4.1.3.1. High amplitude reflections

Based on their appearance, effect on the background host unit reflections, and their location within the North Sea Sand Intrusion Province, the amplitude anomalies seen within this data set are interpreted as sandstone intrusions.

Seismic expressions of similar amplitude anomalies have been observed throughout the North Sea. When fully imaged they are often seen to be V shaped in cross section, while U and W shaped anomalies are also seen (Huuse and Mickelson, 2004). Examples from the North Viking Graben and the Tampen Spur are presented by Loseth et al., (2003) and Huuse and Mickelson (2004). Loseth et al., (2003) and Huuse et al., (2004) also present examples from the South Viking Graben, while examples from the Outer Moray Firth are well documented (Lonegran et al., 2000; Huuse et al.,

2005; Molyneux et al., 2002). Zigzagged outlined bases and tops are also characteristic of intrusive sand in seismic data (Shoulders et al., 2007).

Wells which penetrate these features (Molyneux, 2001; Gras and Cartwright, 2002; Molyneux et al., 2002; Loseth et al., 2003; Huuse and Mickelson, 2004 and Huuse et al., 2004), have shown that then correlated to sandstones tens of metres in thickness. Loseth et al., (2003) show that Norwegian well 24/12-1 penetrates one V-bright, which correlates with a sandy interval which was partially carbonate cemented (Fig. 7.11a). These sandy intervals have over double the velocity (4500m/s) of the background sand and clay (2200m/s), and appear as 'spikes' on the sonic log. The amplitude anomaly in this case can be considered a hard response. Both soft and hard responses are associated with these discordant amplitude anomalies (Loseth et al., 2003), however the majority presented are hard events (Molyneux, 2001; Gras and Cartwright, 2002; Molyneux et al., 2002; Loseth et al., 2003; Huuse and Mickelson, 2004 and Huuse et al., 2004; Cartwright et al., 2008).

Huuse and Mickelson (2004) present two exploration wells (34/7-4 and 34/7-9) which penetrate two separate discordant anomalies. These wells are located within quadrant 34 in the Norwegian North Sea, and are 400km to the north of this study area. In their examples the amplitude anomalies have a black peak at their top, which represents a positive amplitude, or hard, reflection. Both sandstones are water wet and partially cemented. They also observe a negative reflection loop underlying the positive loop, and interpret this as a representation of the top and the bottom of the sand body, suggesting that the sandstones must be greater than 20m thick (i.e. greater than vertical resolution).

In the examples presented by Huuse and Mickelson (2004), the wells either penetrate the anomalies through the discordant wings (34/7-9), or at the margin (34/7-9) of the concordant high amplitude reflection. The thicknesses of the penetrated sands are given as 65m and 50m respectively. Considering the location of the intercepted intervals it is worth taking into account that the greatest sand thickness (aperture) of a sand intrusion has been shown to be its centre of the intrusions, and that this would suggest that the maximum thickness of both penetrated intrusions is greater than penetrated by the wells.

Two geometrical end members for sand intrusions ; flat-based bowls and apical cones, are described and presented by Cartwright et al. (2008). Both end members are represented at their flanks by strata-discordant wings, while the flat -based bowl end members have a central concordant tabular body, the apical cones have a sharp apex where the discordant wings meet, and lack the concordant central component. While fully imaged intrusions of both end members are rarely present within

this data set, partially imaged intrusions with geometries ranging between these two end members are commonly seen. The lack of fully imaged intrusions in other work (e.g. Loseth et al., 2003) has been previously attributed to a lack of cementation throughout the intrusion, preferential sand development in a specific direction, or imaging problems.

It is suggested here that the range in form of the high amplitude reflection reflect different cemented sections of the intrusions. Where discordant reflections correspond with cemented wings, bright spots correspond with intrusion apexes, and concordant reflections are the cemented bases of flat-based bowls.

4.4.1.3.2. Sub-vertical disrupted zones

In several cases, these high amplitude anomalies are present as isolated bright reflections which are connected to zones of lower amplitude and discontinuous reflections. Generally these zones of disrupted reflections are sub-vertical and appear to be projected from the high amplitude reflections towards the paleo-seafloor. These lower amplitude zones are interpreted as un-cemented intrusion wings. In a similar observation, Huuse and Mickelson (2004) describe a discordant wing penetrated by well 34/7-4 as being connected to a concordant high amplitude reflection by 'a zone of scattered amplitudes'.

There is a lack of imaged wings (discordant amplitude anomalies) which reach the paleo-seafloor within this study area. This may be due to the thinning of the wings towards their tips, resulting in their thickness being below the vertical resolution of the seismic data. Lack of cementation within the wings may also be a factor. However, there are indications that do suggest that the wing tips reach, and possibly penetrate the Base Utsira Horizon. The zones of broken reflections, often continuing along the angle of the discordant amplitude anomalies suggest that there are sub-vertical features connecting the intrusion wings to the paleo-seafloor. These zones of broken reflections are often seen to intersect the B.U.H in close proximity to the hinge points of the ellipsoid mounds, and in these cases the B.U.H is often broken and displaced (Fig. 4.9 points D and E).

4.4.1.3.3. Chaotic zones

The high amplitude reflections seen in vertical seismic sections are interpreted as the cemented bases of sand intrusions. The bright spots or high amplitude reflections are often seen to be

accompanied by overlying zones of chaotic reflections, and this phenomenon has been previously noted by Hurst et al., (2003) to be associated with sand intrusions. Chaotic zones in conjunction with bright reflections have also been correlated to sandstone interval in wells by Huuse and Mickelson (2004). We suggest that these overlying packages of chaotic reflections represent the main body of intruded sand.

An upper defining reflection above these chaotic zones is rarely seen within this dataset. It is possible that this may be caused by a lack of cementation at the upper limit of the sand body, due to the presence of parasitic sand offshoots from the main body of the intrusion, or due to post-emplacement fluid expulsion disrupting the upper surface of the sand.

Due to this lack of a clearly imaged and robustly calibrated top reflection, it is difficult to quantify the thickness of the sand bodies. However, the thickness of the chaotic packages overlying the interpreted cemented base of the intrusions makes it possible to estimate intrusion thickness, and it is proposed that the upper limit of these chaotic zones corresponds with the upper boundary of the intruded sand body. As described above, the bedding parallel background reflections of the unit are displaced upwards by the presence of the intrusions, and replaced by chaotic packages. Assuming that the stratal-discordant reflections are the cemented base of the intrusions and that the upper limit of the chaotic packages are the top of the intrusion, then intrusion thickness can be tentatively estimated (Fig. 4. 9). It is proposed that the high amplitude anomalies present can be used to infer the base of the intrusion (Fig. 4.9, points A,B and C), while the sub-vertical zones of disrupted reflections represent the intrusion wings. A shallower bright spot, 80m above point A and of opposite polarity, is interpreted as the upper boundary of the intrusion, which suggests an intrusion aperture of around 80m at this point.

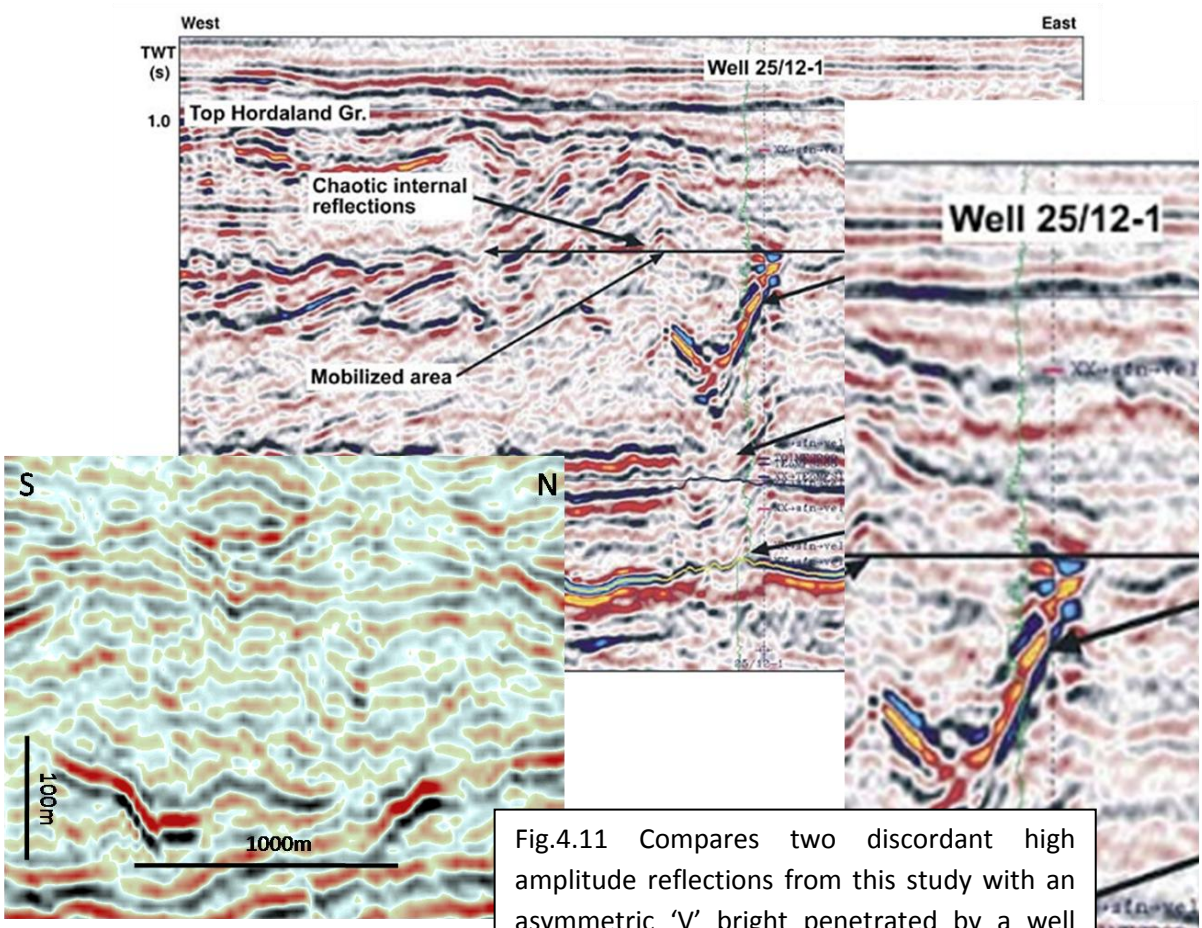

Fig.4.11 Compares two discordant high amplitude reflections from this study with an asymmetric 'V' bright penetrated by a well (from Løseth et al., 2003).

4.4.2. Base Utsira Mounds

A TWT (two-way-time) map of the Base Utsira shows that there are several prominent features of high topography located within the study area (Fig. 4.12a). A total of eighteen individual high relief features, roughly ellipsoid in map view, have been mapped, and their area and relief measured. The majority of the mounds are located within two roughly parallel ridges which trend NNE-SSW (Fig. 4.12b, Ridge 1 and 2). Two larger mounds, located at the south west termination of these ridges, and individual, outlying mounds are also present. A central area, (around 40 km^2) bounded to the south, east, north and west by the ellipsoidal mounds, is unaffected (Fig. 4.4, CA). The north east limit of this area is not included within the data set.

The areal extent of these mounds can be clearly seen on a dip map of the Base UtsiraHorizon (BUH). Using a black and white colour bar, where the black areas indicate an increase in dip, it is possible to delineate the points where the sub-horizontal BUH is inflected upwards and increases in gradient. These points, denoted on the map by the black outlines, are termed the 'hinge points' of the mounds

and therefore represent their boundary (Fig. 4.12b). These mounds have an average area of 7.66 km^2, with the largest exceeding 16 km^2.

Seismic sections through these mounds display their topographic relief. The relief can be measured by creating a line connecting two hinge points across the mound profile and measuring the maximum vertical distance, perpendicular to the line, upwards to the displaced BUH (Fig. 4.13a). The measured relief of the mounds within this study area ranges between 40 m and a 100 m.

4.4.2.1. Small mound.

The smallest mound in the study area, Mound 13, measures just over 1km^2 in area, and exhibits a structural relief of around 65 m (Fig. 4.13a). Along the fold profile, the BUH is difficult to follow but can be delineated by the points where the Base Utsira Horizon bends upward (point A and B), by the medium to high amplitude fold crest set in a low amplitude background (point C), and by the presence of onlapping reflections which terminate at either side of the fold (reflections D and E). The BUH reflection is seen to be displaced and disconnected from the rest of the reflection just after the hinge points (A and B).

When overlain by a contour map of mound 13 the RMS map of the Hordaland Shale reveals that a large area of high amplitude lies directly beneath the south eastern corner of the mound (Fig. 4.13b). This high reflectivity area is apparent as a sub-horizontal, negative high amplitude reflection which underlies the eastern extent of the mound when viewed on an west to east seismic section (Fig. 4.13c).

4.4.2.2. Irregular mound

Mound 1 consists of three separate areas of high relief which combine to create a total mound area of 3.9km^2 (Fig. 4.14a, points 1, 2 and 3). The south western and south eastern areas are roughly elliptical in geometry while the northern section is sub-circular. The mound achieves a maximum topographic relief of close to 90m in both the south western and south eastern areas. These southern sections of the mound can be seen to be separated by a depression located halfway along the mound profile (Fig. 4.14b, point A). The BUH reflection is upturned, displaced, and broken at both hinge points (Fig. 4.14b, points B and C), and the mound is underlain by high amplitude reflections within the Hordaland Shale (Fig. 4.14b, points D, E, F). A lower section of Utsira Sand

reflections can be seen to onlap the mound flanks. High amplitude reflections are shown to underlie the mound on both the north to south and east to west seismic sections (Fig. 4.14b and c). A contour map of the mound underlain by the Hordaland Shale RMS map reveals several areas of high reflectivity which are contained within the mound boundary (Fig. 4.14d).

4.4.2.3. Large Mound

Mound 2 is a large, ellipse-shaped mound which exceeds 11 km^2 in area. It has a maximum topographic relief of over 100 m, which is located in the north-west corner of the mound (Fig. 4.15a). A west to east seismic section through this area of greatest relief show the BUH to be broken and displaced at the hinge points (Fig. 4.15b, points A and B) and the Utsira Sand reflections onlap the mound flanks at points C and D.

Below the mound is a pair of overlying, semi-continuous, high amplitude reflections of opposite polarity (Fig. 4.15b, arrowed). The upper reflection has a dominant negative amplitude ('hard' event) while the lower reflection is a positive amplitude ('soft' reflection). This pattern of reflections is consistent with that of a 'hard' upper boundary of a cemented sand intrusion underlain by the basal 'soft' boundary.

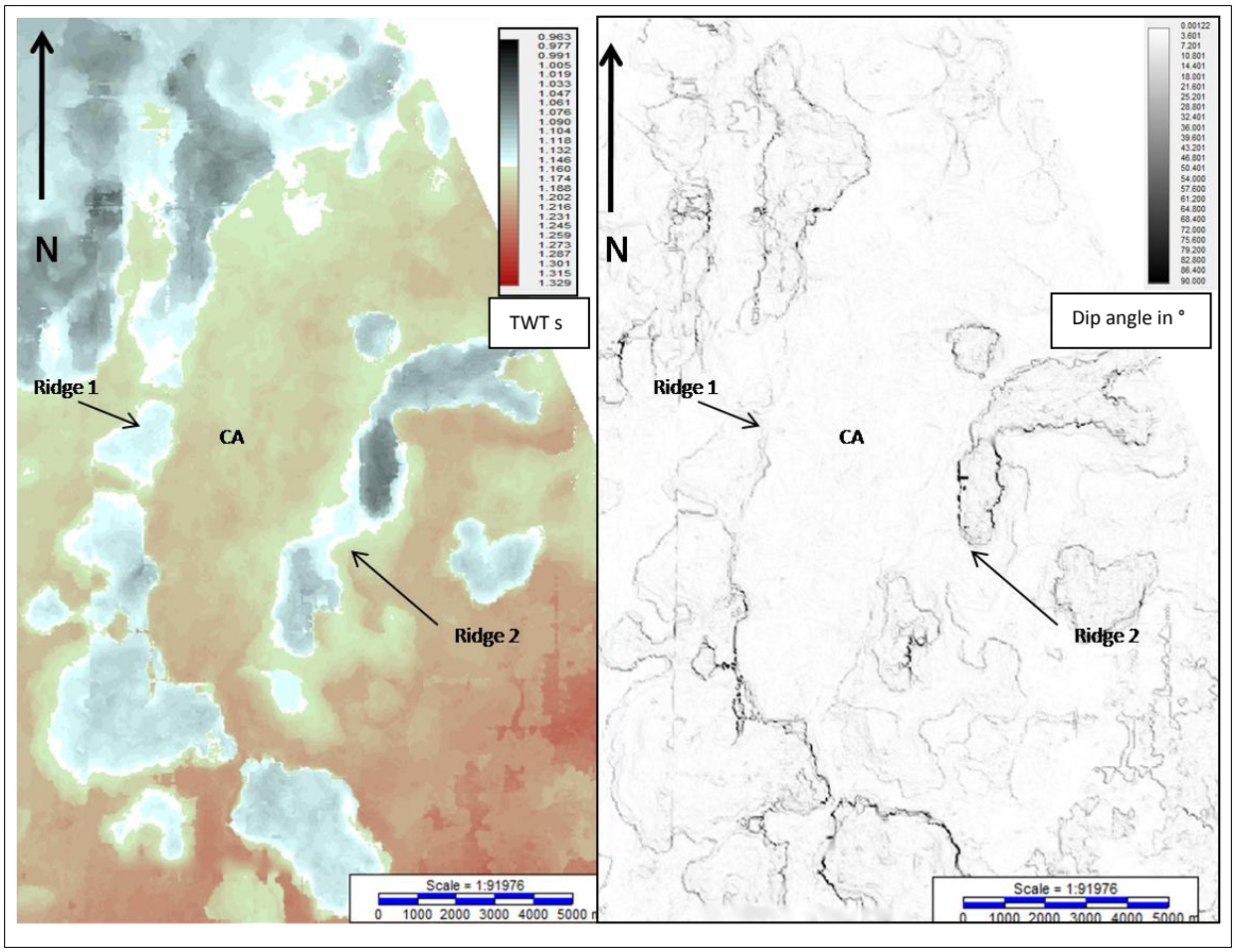

Fig. 4.12 a) TWT map of the Base Utsira Horizon showing the elliptical mounds forming two distinct ridges of high topography with a central low area (CA) b) A time-dip map where darker areas indicate an increase in gradient of the Base Utsira Horizon, these darker areas coincide with the edges of the elliptical mounds and denote the mound 'hinge point'.

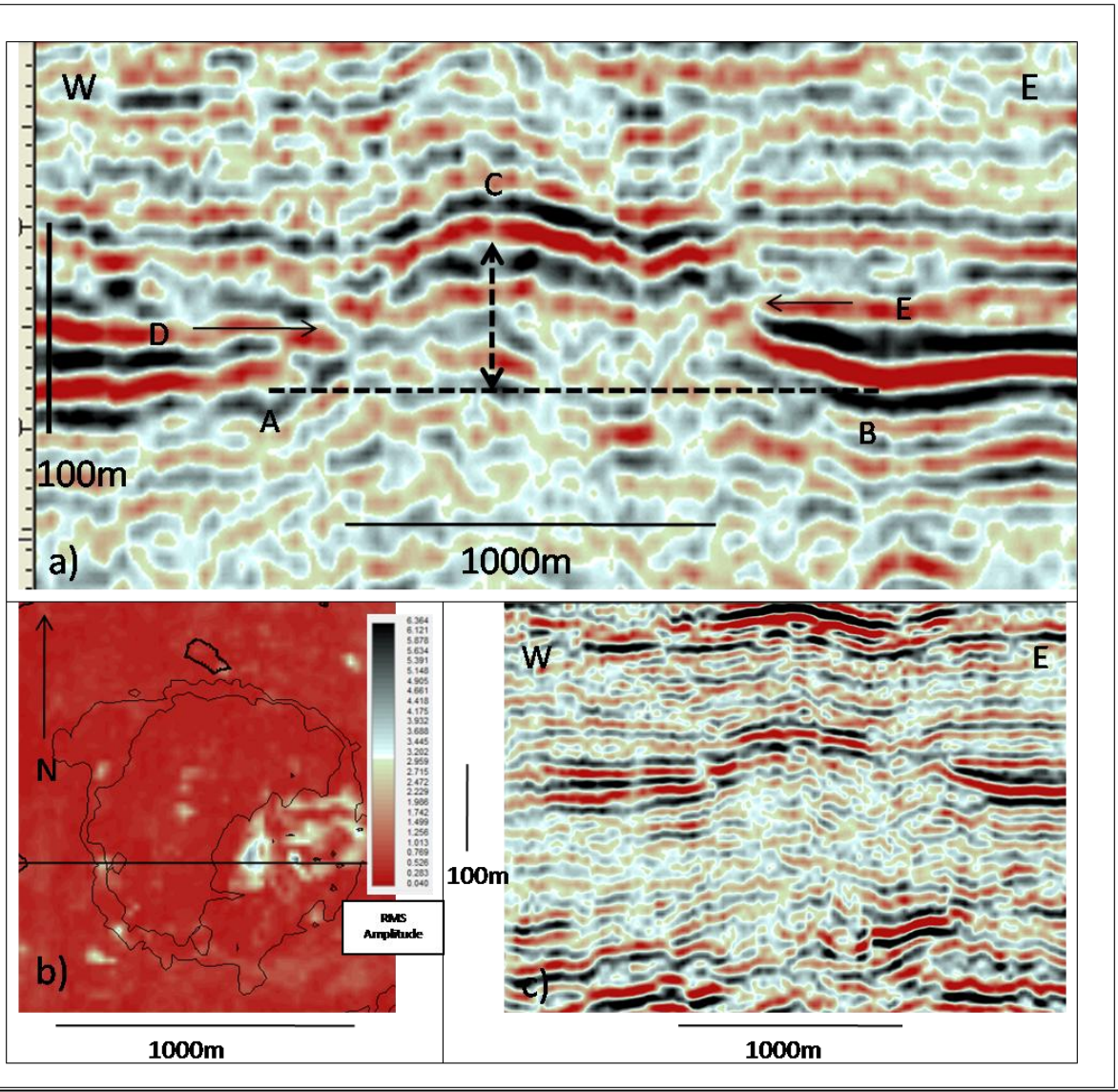

Fig. 4.13 a) Seismic profile of mound 13 demonstrating how measurements of mound relief were taken. Hinge points are denoted by the increase in gradient at points A and B. The mound crest is a prominent feature at point C, although the reflection is discontinuous at the mound flanks. Reflections D and E onlap at the flanks of the mound b) TWT contour map with RMS seismic amplitude superimposed of the Lowermost Shale, with a high concentration of amplitude within the south-eastern sector c) a high amplitude reflection underlying the mound

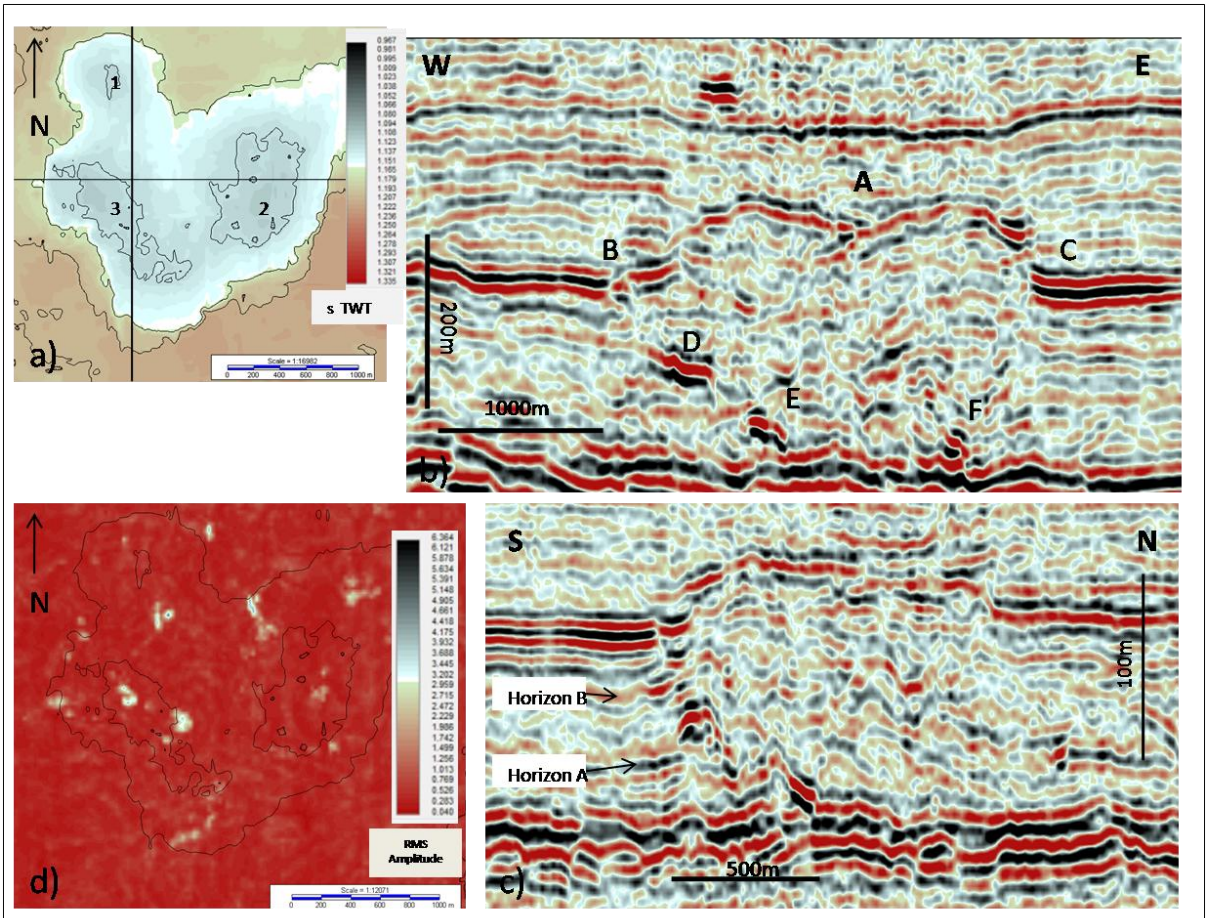

Fig. 4.14 a) A time-depth map of Mound 1. This shows it is an irregular shaped feature, with three separate area of high relief (Points 1, 2 and 3) b) a W-E seismic section displaying high amplitude anomalies below the mound (points D, E and F), a slight depression along mound profile (A) and discontinuous reflection at the mound hinge points (B and C) c) a S-N section showing the chaotic nature of the reflections below the mound d) an RMS map of the Lowermost Shale with mound contour overlain demonstrating the distribution of high amplitude features.

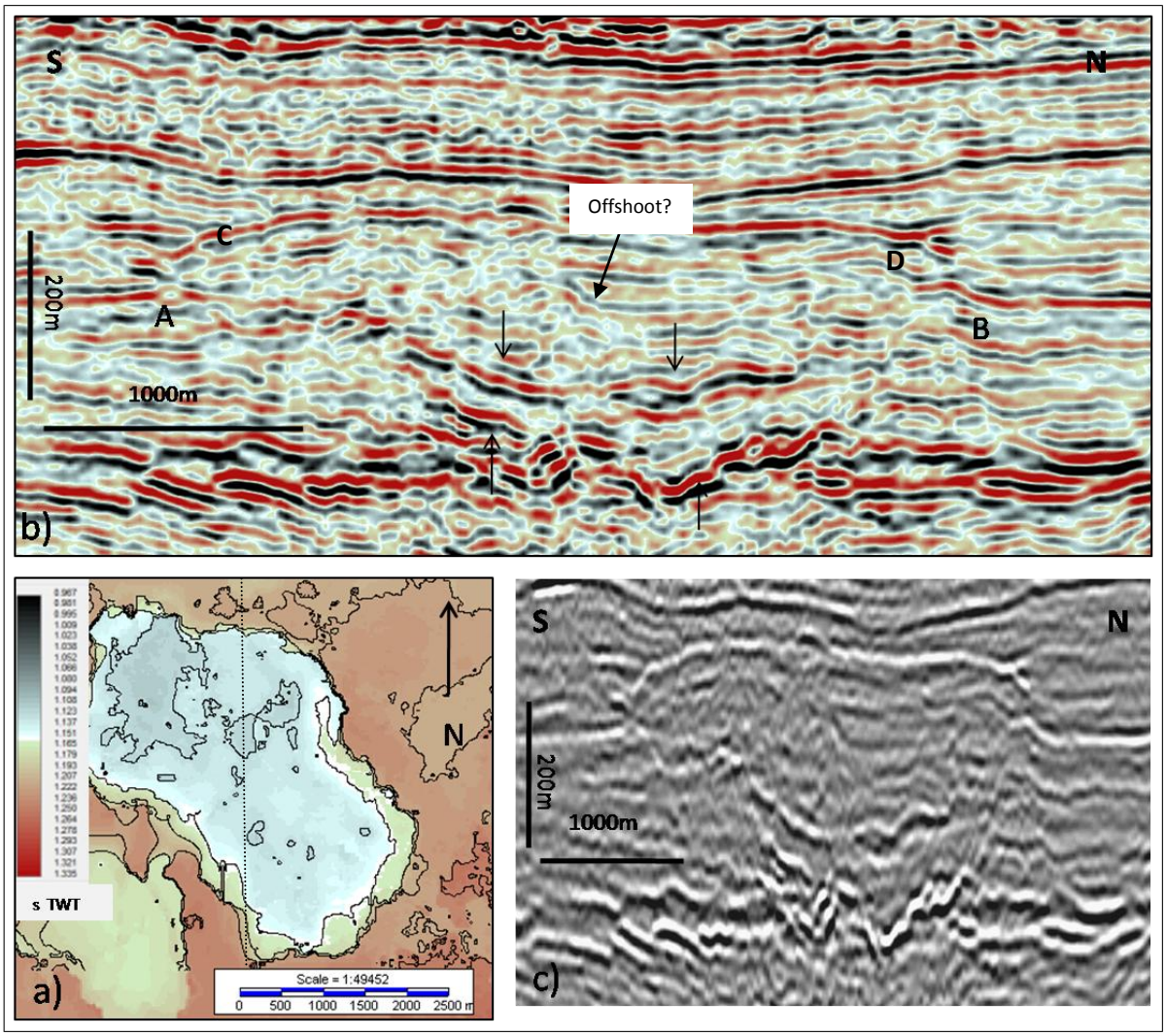

Fig. 4.15 a) a contoured time-depth map Mound 2 with location of seismic section denoted by dashed line b) seismic section displayed in Landmark colour scheme and c) in black and white demonstrating that the mound is underlain by a pair of high amplitude reflections forming a wedge shape. The reflections, of opposite dominant amplitude, are interpreted to represent the top and the base of a sand intrusion. Sub-vertical disrupted zones of reflections reaching points A and B are interpreted as the intrusion wings, while chaotic reflections, cross cutting stratified background reflections of the host unit are interpreted as sediment offshoots from the main body of the sand intrusion.

4.4.2.4. Interpretation and discussion

A strong spatial relationship exists between the amplitude anomalies within the Hordaland Shale and the elliptical shaped areas of high relief affecting the overlying B.U.H. This relationship is best presented when superimposing the outline of the mounds over RMS extraction maps of the unit. The anomalies have already been interpreted as sections of partially cemented sand intrusion (section 4.3.2.1.1), and the mounds themselves are therefore interpreted as the result of these sand intrusions, and more specifically the result of forced folding associated with the hydraulic 'jack up' of the overburden which occurs during sandstone intrusion emplacement. This 'jack up' effect is identified as a diagnostic feature of clastic intrusions (Cartwright et al., 2008), and a 'key' criterion in differentiating between injected sand bodies and those of depositional origin (Szarawarska et al., 2010). Onlapping reflections at the edges of the mounds do not share the mounded geometry and must therefore post-date mound formation.

A similar relationship between mounds and an underlying sand intrusion is presented by Shoulders and Cartwright (2004), where they describe a forced fold which is underlain by a sand intrusion in the Faroe-Shetland Basin. In the example given, they highlight this spatial relationship between the high amplitude reflections and the fold affecting the intra-Neogene unconformity by superimposing the outline of the domal forced fold above RMS maps of the underlying sandstone intrusion. They suggest that this 'direct spatial correspondence' 'implies a causative relationship'. The relief of the fold presented is 25 to 30m, which they describe as comparable to that of the intruded sand body below, and is similar to the measured relief of some of the smaller folds found in this dataset

Mounds, or forced folds, are commonly seen to overlie sandstone intrusion indicators within the area termed by Cartwright (2010) as the North Sea Intrusion Province as well as in laboratory experiments involving intrusive bodies (Rodriguez, 2009). Loseth et al., (2012) also describe mounds, with similar dimensions to the ones described within this dataset, resulting from force folding by intrusions. Forced folds are defined as 'folds in which the final overall shape and trend are dominated by the shape of some forcing member below,' (Stearns, 1978).

By way of comparison with the forced folds interpreted here, the 'jack up' effect of emplacement of intrusive igneous bodies on its host strata has previously been described in detail (Trude at al., 2003; Hansen and Cartwright, 2006). The spatial coincidence between saucer-shaped igneous sills and folds affecting an overlying horizon is noted and described as a 'remarkable observation' by Hansen and Cartwright (2006). They highlight the similarities between the underlying intrusions, geometry

and thickness with that of the overlying folds. They interpret these folds as forced folds whose development is directly linked to the mechanical emplacement of the underlying igneous sills.

In a similar vein to Hansen and Cartwright (2006), Cartwright et al. (2008) investigated the relationship between the aperture of clastic sand intrusion and forced fold relief. They suggest a 'roughly proportional' relationship between intrusion aperture and the relief of the overlying mound. The greatest mound relief should therefore be located above the thicker, central, flat lying concordant sand body, while the steeply dipping mound flanks should overlie the intrusions wings, where the sand thickness tapers towards the wing tips.

Hansen and Cartwright (2006) describe the crestal faulting located at the top of their forced folds, and, by analogy, this may be considered a factor in the discontinuous, dimmed and broken nature of the Base Utsira horizon which is observed across the fold profiles in several examples described in section 4.3.2.2

4.4.2.4.1. Mound profiles and differentiating between single and multiple intrusions

It worth considering that in observing forced folds, their 'final overall shape and trend are dominated by the shape of some forcing member below,' (Stearns, 1978). Taking into account the inferred causative relationship between the sand intrusions and the mounds (cf. Shoulders and Cartwright, 2004), the similarities between the geometry and thickness of the intrusions and the mounds (Hansen and Cartwright, 2008), and the roughly proportional relationship between intrusion aperture and mound relief (Cartwright et al. (2008), it may be possible to infer sand intrusion thickness and geometry from observations made of the mound and mound profile.

If it is considered that the greatest intrusion aperture is located within its central section , and that this aperture tapers off towards the intrusion wing tips, then the area of greatest mound relief should be located above the centre of the intrusion and the mound flanks should coincide with the intrusion wings. An idealised 'V' shaped intrusion would therefore be overlain by an inverted V shaped mound, with greatest intrusion aperture overlain by greatest mound relief within the apex of both the 'V's'. A gradual and constant decrease in thickness towards the left and right tips of the intrusions should form symmetrical mounds which overlie symmetrical intrusions. However, asymmetrical mound profiles are most commonly observed, which would suggest that the underlying intrusion is also asymmetric. Depressions and variations in relief along the mound profile may also be resultant of irregular intrusion aperture.

Another possibility is that mounds mapped as singular mounds may be in fact two adjacent mounds, caused by two adjacent intrusions, which due to their close proximity are conjoined and appear as a single area of raised topography. Spatial clustering of sand intrusions is described as 'not uncommon' by Cartwright (2008) and is also noted by Huuse and Michelsen (2004). A causative relationship between intrusions and mounds would tend to suggest that mound clusters or closely conjoined mounds would be the result of intrusion clusters or pairs. In this case, mound asymmetry may be explained by the difference in aperture between two separate intrusions, and any loss of relief along mound profile would overlie the wing tips of the intrusions.

Mound 1, mapped as a singular ellipsoid mound, is underlain by several separate and incomplete intrusion indicators (Fig. 4.14). The mound consists of three separate areas of high relief, which suggests that the mound may be the result of several intrusions. A slight depression along the east to west profile separated the areas of maximum relief (Fig. 4.16, point D). This loss of relief may be interpreted in two ways;

- Mound formed by two separate intrusions, with the decrease in relief caused by the thinning towards the intrusion wing (Fig. 4.16a).

- Mound formed by single intrusion with an irregular aperture as a result of an irregular base and top, thus creating an irregular mound profle (Fig. 4.16b).

The quality of the imaging of the intrusions limits the ability to make a definitive interpretation of the cause of the mound profile in this case.

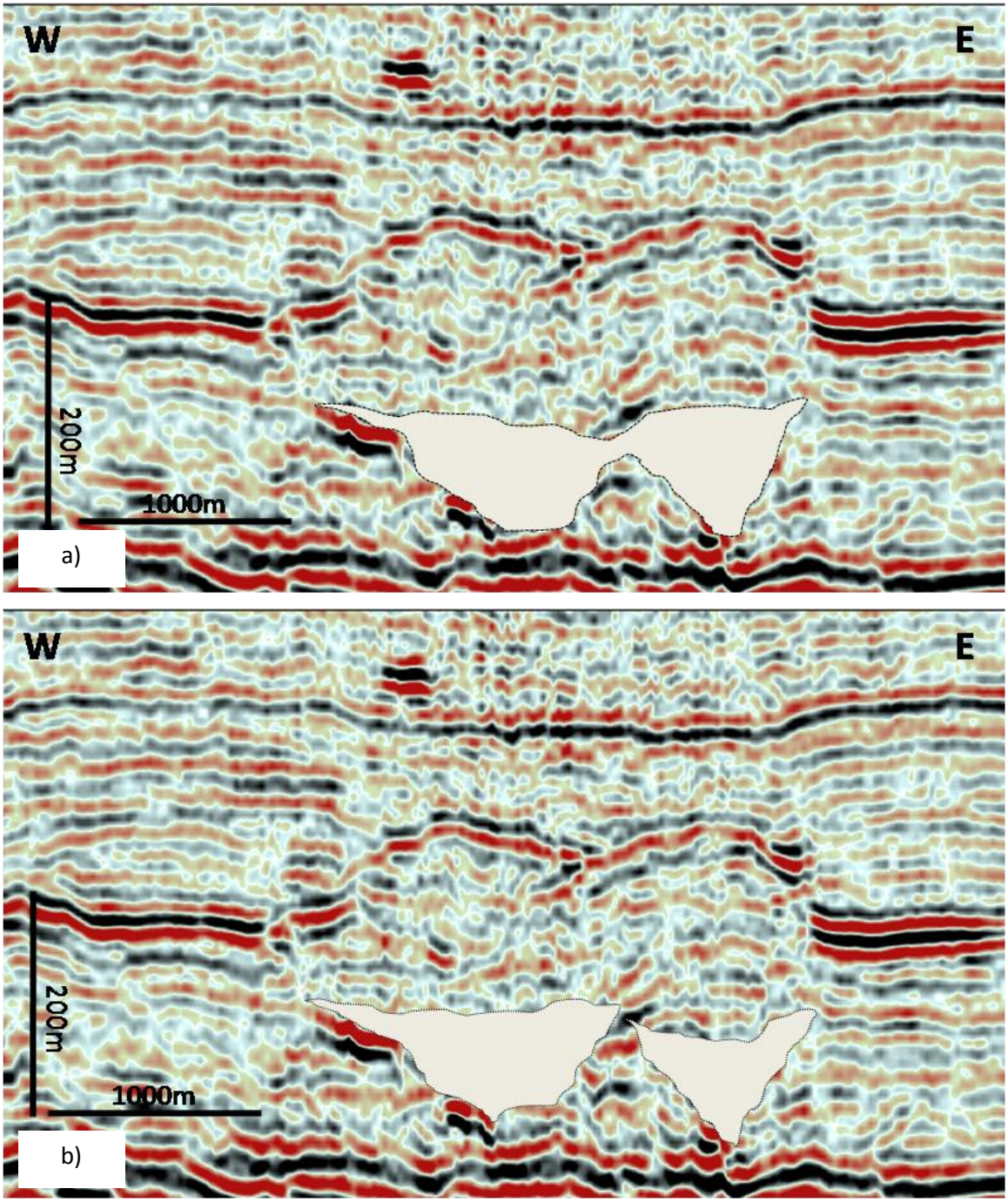

Fig. 4.16 a and b) seismic section demonstrating contrasting interpretations of the features underlying Mound 1 a) Mound formed by single intrusion with an irregular aperture as a result of an irregular base and top b) Mound formed by two separate intrusions, with the decrease in relief caused by the thinning towards the intrusion wing (Fig. 4.16a).

4.4.3. Internal Utsira bright reflections

An RMS amplitude map of the lower section of the Utsira Sand (lower 50m of unit), overlain by contour maps of the mounds, reveals several areas of high amplitude that are concentrated at the flanks of the mounds and in close proximity to their hinge points. These packages are concentrated around the outlined boundaries of the area affected by the mounds. The high reflectivity features are generally between 20 m^2 and 50 m^2 in area, generally circular to sub-circular in geometry, and connected to other high reflectivity features by lower reflectivity areas. Representative examples of these features are presented below.

Example 1

An RMS map of the Utsira Sand reveals two areas of high reflectivity which are located between Mounds 5 and 6 (Fig. 4.17a). The southern area of high reflectivity (Fig. 4.17a, Area 1) is located at the boundary of Mound 5, while the northern area is located at the boundary of Mound 6 (Fig. 4.17a, Area 2). Both areas of high amplitude follow the outline of the mound boundaries. In seismic section across these areas they can be seen to take the form of a concave upwards reflection which effectively forms a bridge between the flanks of the mounds (Fig. 4.17b, Bridge 1). This reflection extends for 700 m between the areas of raised BUH, and is brighter at the flanks and dims towards the middle of the 'bridge'. A second concave upwards reflection is located to the south, forming a bridge between Mound 5 and Mound 4 (Fig. 4.17b, Bridge 2). Both bridges consist of positive amplitude reflections, and considered to be are ‘soft’ events. The BUH is broken at points underlying the bridges (Fig. 4.17c, Point A, and Fig. 4.17d, Points B, C), and sub-vertical zones of disrupted reflections can be seen emanating from a bright spot (Fig. 4.17e, point D) within the Hordaland Shale upwards to the points where the BUH is broken.

Example 2

High reflectivity areas within the Utsira Sand are also seen to follow the boundary of Mound 10 (Fig. 4.18a). Along a west to east section this area can be seen as a bright reflection which infills a depression at the eastern flank of Mound 10 (Fig. 4.18b), and consists of a negative amplitude (hard event). A discontinuous point of the BUH underlies the high amplitude reflection (Fig. 4.18c, arrowed).

4.4.3.1. Interpretation and Discussion

4.4.3.1.1. Extrudite deposits

High reflectivity areas are concentrated at the flanks of the ellipsoid mounds which have been created by the forcible emplacement of intruded sand bodies. When viewed in seismic section they can be seen as concave upwards reflections which infill depressions sandwiched between the high relief mounds. High amplitude reflections, located below these mounds, have already been interpreted as sand intrusions, and sub-vertical zones of disrupted reflections, emanating from these sand intrusions, have been interpreted as intrusion wings. These wings are suggested to retain a high level of permeability (Cartwright el al., 2008) and the hydraulic pumping and expulsion of sand slurry through these highly permeable wings may be responsible for feeding sand to the paleo seafloor. We therefore interpret these concordant amplitude anomalies as extrudite deposits.

A high amplitude, concordant, reflection located at the paleo-seafloor and associated with an underlying sand intrusion is presented and interpreted as a possible extrudite deposit by Huuse et al., (2004) (Fig. 4.19).

The possible upward movement of sand, in large volumes, through subsurface fractures and fissures until eruption at the seafloor or surface has long been considered possible (Gill and Kuren, 1957; Gallo and Woods, 2004; Hurst et al., 2006). Such extrusive sand accumulations at the seafloor or at the surface are termed extrudite deposits (Hurst et al., 2006) and they are connected to their source sand body via hydraulic fractures. The sand remains within these fractures, and can become cemented, but still retain a high level of porosity and permeability in comparison to their host strata, and they are considered to increase 'the cross formational permeability by orders of magnitude (Hurst et al., 2003). This, along with the fact that the intrusion wing tips can be interpreted as culminating close to or beyond the paleo-seafloor, raises the possibility of extrudite deposits within this study area.

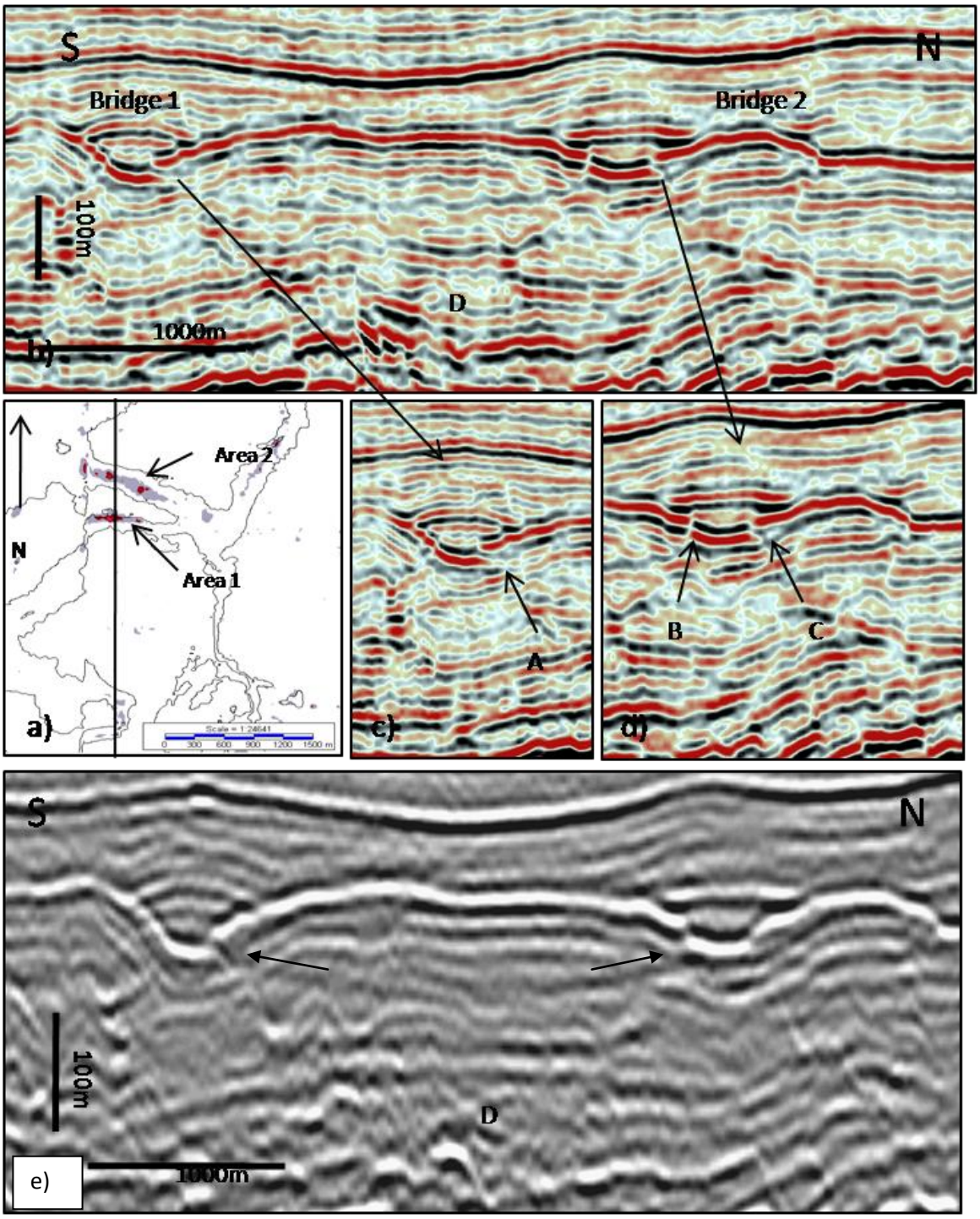

Fig. 4.17 a) an RMS map of the lower half of the Utsira Sand showing high amplitude areas concentrated within a depression between two mounds b) seismic section through the high amplitude feature revealing their infilling and upwards concave nature, c and d) points below the high amplitude features where the Base Utsira Horizon is discontinuous e) sub-vertical zones projected upwards from point D to discontinuous points of the Base Utsira Horizon (arrowed).

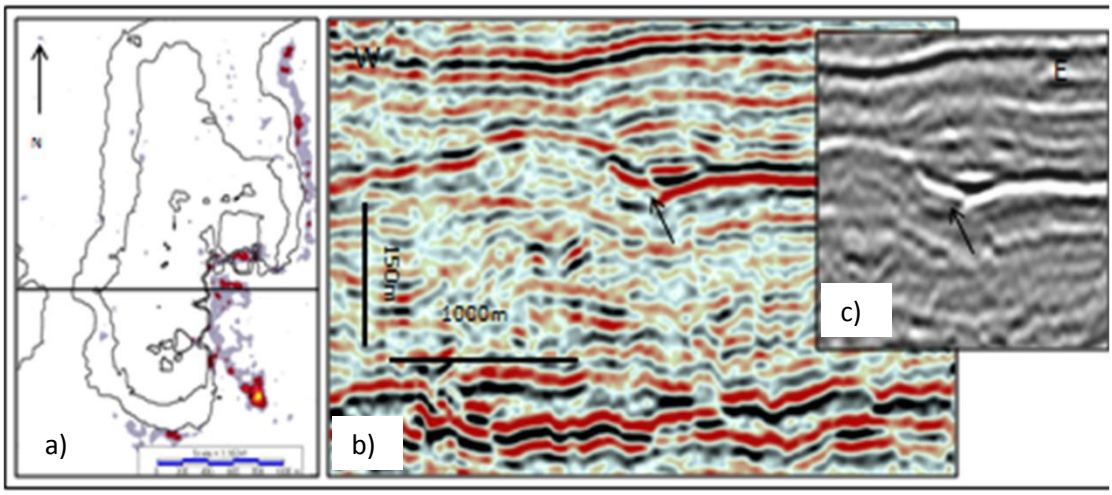

Fig. 4.18 a) an RMS map of the lower half of the Utsira Sand showing high amplitude areas concentrated along the boundary of an elliptical mound. b)The seismic section shows that the high amplitude feature 'infills' a depression at the mound flank and overlies a discontinuity part of the Base Utsira Horizon (arrowed) c) black and white representation of the break in Base Utsira Horizon.

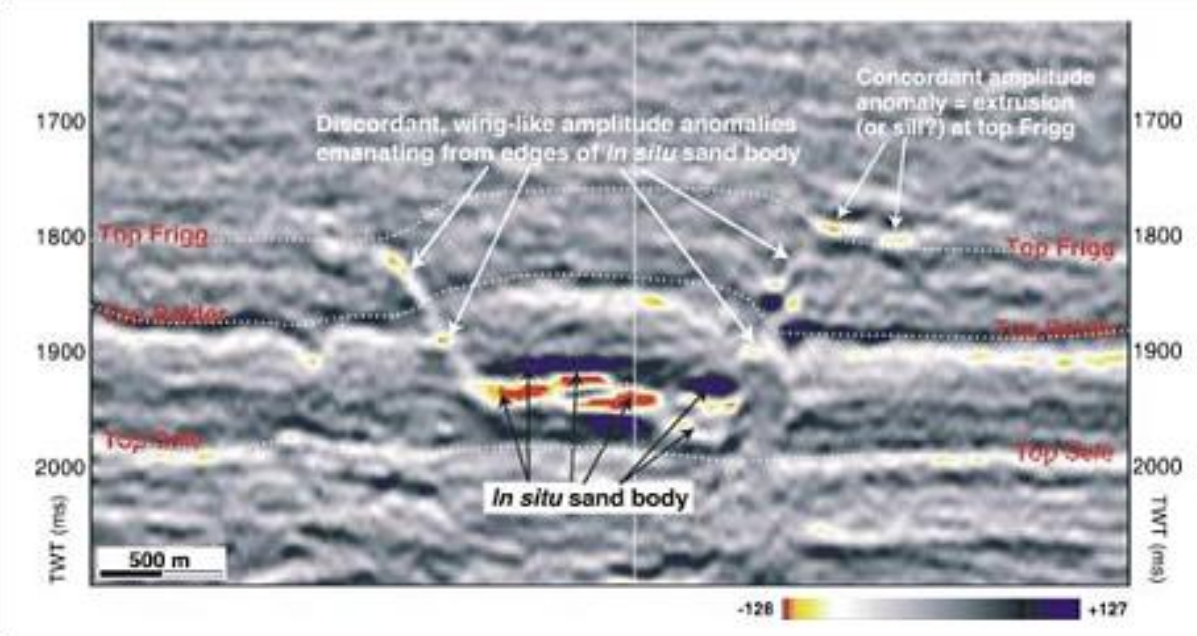

Fig. 4.19 an example taken from by Huuse et al., (2004) indicating the possible presence of extrusive deposits.

4.4.4. Lower Utsira internal reflections

When in close proximity to the elliptical mound the geometry of the lower section of the internal reflections of the Utsira Sand is markedly different to that of the overlying section. Generally, the first two reflections are horizontal, parallel, and onlap the mounds flanks, while the middle section are horizontal and parallel up to a point and then downturn and downlap onto the mounds. Two representative examples of this are presented below.

Example 1

An inline through an elliptical mound shows the displaced and domed upwards BUH (Fig. 4.20a). The mound is underlain by a high amplitude reflection which consists of both discordant and concordant sections, and is hosted by the Hordaland Shale. At the northern flank of the mound the first two reflections above the BUH can be clearly seen to be horizontal, and onlap the north extent of the mound, while a third reflection also appears to onlap, but is broken and discontinuous (Fig. 4.20b, reflections 1, 2, 3). This lower, onlapping section is approximately 70m in thickness. A fourth reflection is horizontal up until point A, at which point it turns downwards and converges with the crest of the mound. The next prominent overlying reflection is the Top Utsira Horizon, and this reflection is also seen to downturn at point B.

This pattern is also replicated at the southern flank of the mound (Fig. 4.20c). While the BUH is initially horizontal, it is displaced and pushed upwards due to the effect of the underlying intrusion, whose presence is indicated by a high amplitude reflection (Fig. 4.20a, SI). The lower section (around 70m) consists of semi-continuous reflections which can be seen to onlap the mound flanks. The overlying section of reflections downturn and appear to downlap onto the mound flank.

Example 2

This example also consists of a lower section, around 70m in thickness, of reflections which are poorly imaged (Fig. 4.21a). The most continuous and prominent horizon overlying this lower section is clearly seen to turn down at points A and B either side of the mound, and downlap onto the mound flanks at points C and D (Fig. 4.21b and c). The TUH (Top Utsira Reflection) replicates this draping geometry and its points of downturn, the hinge points, are located at E and F respectively.

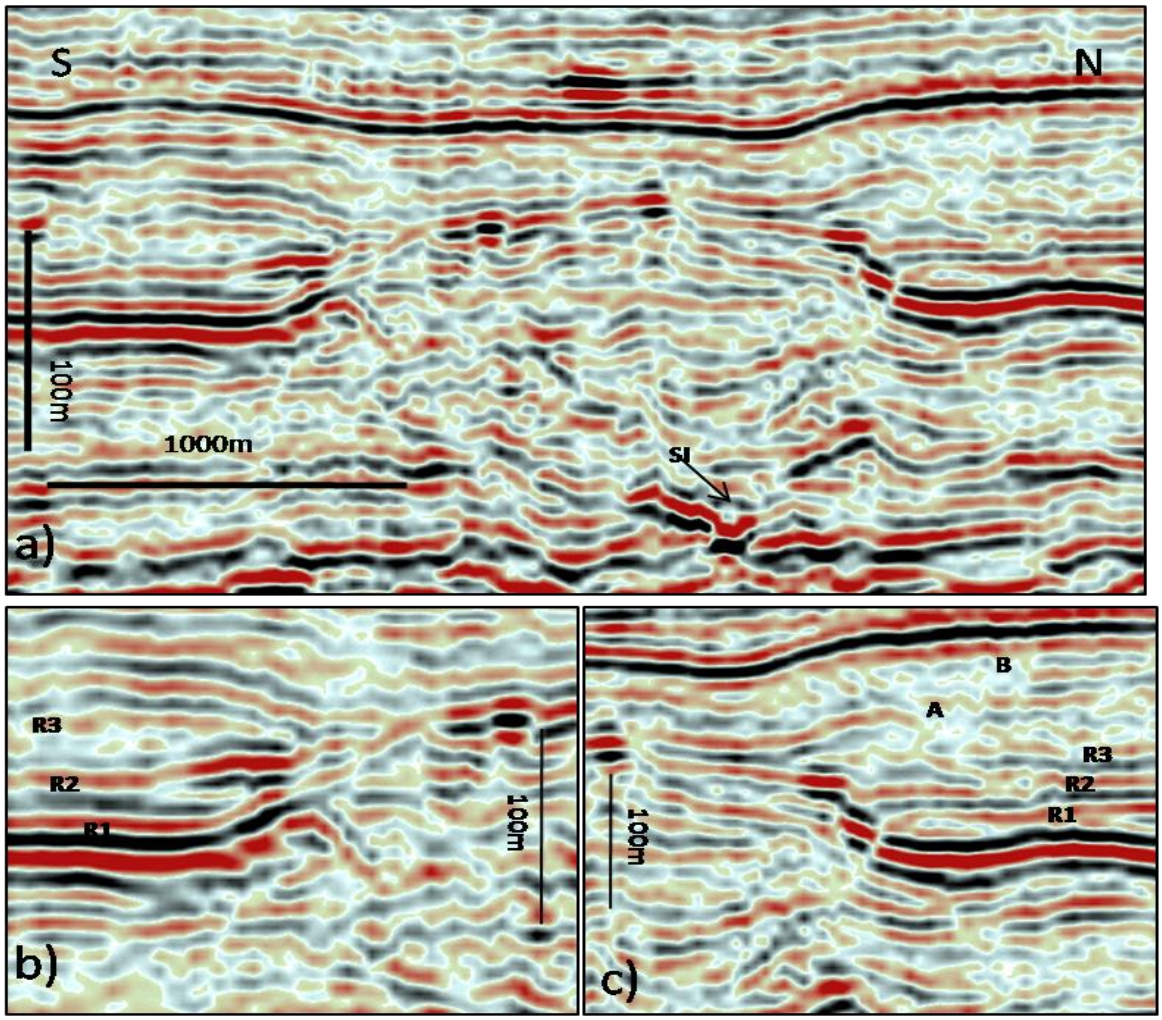

Fig. 4.20 a) a mound underlain by a sand intrusion (SI) with associated sub-vertical disrupted reflections projected towards mound hinge points b) a lower section of onlapping reflections at the southern flank with overlying downlapping reflections c) onlapping reflections at northern flank (R1, R2, and R3) with overlying reflections downturned at points A and B.

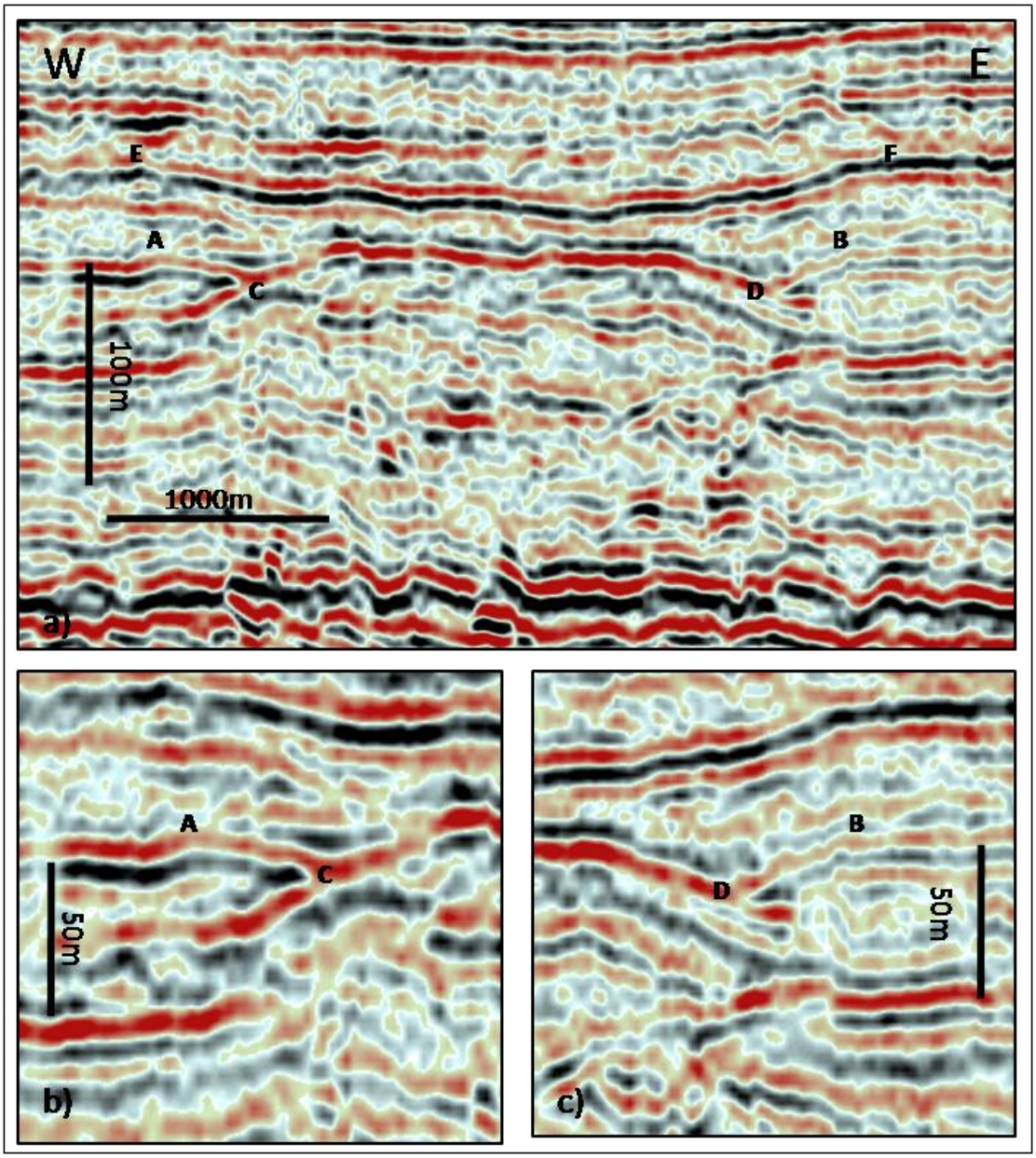

Fig. 4.21 a) a mound with an overlying 'hanging' Top Utsira Horizon which appears to deflect downwards at point E and F b) an internal reflection which downturns at point A and downlaps onto the mound at point C c) the same pattern is mirrored at the eastern flank of the mound, the reflections downturns at point B and downlaps onto the mound at point D.

4.4.4.1. Interpretation and discussion

4.4.4.1.1. Mound timing

The presence of onlapping reflections at the flanks of elliptical mounds have previously been described by Shoulders and Cartwright (2004), and used as a method of indirectly dating the formation of the mounds. The mounds must post-date the Base Utsira Horizon, as the horizon is clearly affected by the mounds, and must pre-date the onlapping lower reflections of the Utsira Sand. The Utsira Sand has been dated as Upper Miocene to Lower Pliocene (EIdvin and Rundberg, 2005), mound formation and sand intrusion emplacement can be limited to post-date the Upper Miocene and pre-date the reflections which onlap the mound flanks.

4.4.4.1.2. Sign of downward movement

We interpret the downward trajectory of the middle section of reflections as an indicator of movement which has affected the ellipsoid mounds. These curved reflections are not present at every mound, and occasionally are only located at one flank. This suggests that the movement has affected one side only, or has been of a greater magnitude at the flank with the associated down turned reflection. The presence of onlapping reflections have been used by Shoulders and Cartwright (2004) as an indirect method of dating the formation of the mounds, it is suggested that the presence of downlapping reflectors can be used as indicators of movement.

The pressure which induced the fractures to accommodate the emplacement of the sand intrusions must decline with time due to depletion of pressure within the source formation, and although sand intrusions do retain a high level of permeability and porosity, there must follow a period of settlement with accompanying sagging of the mounds. Loading of the mounds would be minimal at this time (40-60 ms of deposits), with only onlapping reflectors present, therefore compaction and sand grain reorganisation would be minimal.

While displaying similar dimensions in map view, the relief of the mounds within this data set are significantly smaller than the relief of the mounds above igneous intrusions described by Hansen and Cartwright (2006). Although this may be purely a result of greater volume of igneous material being intruded, it does raise the possibility that some form of post emplacement decrease in relief has occurred.

Intrusions are known to experience loss of height and aperture thickness following emplacement (Cartwright et al, 2008). Depending on composition of the remobilised sand 'slurry' a variation of up to a half between the emplacement aperture and final aperture is suggested by Cartwright et al (2008). It is suggested here that the aperture loss is a result of loading which results in sand grain compaction, water expulsion and a loss of porosity.

4.4.5. Top Utsira depressions

A TWT map of the top Utsira Horizon (TUH) shows several areas of low relief (Fig. 4.22a). However, due to their more subtle nature, the depressions are more difficult to identify on a TWT map than the underlying elliptical mounds. Nevertheless, the presence of two topographic linear 'trenches', roughly orientated SSW-NNE, is suggested by the azimuth map of the TUH (Fig.. 4.22b, Trench 1 and 2). These appear to correspond with the locations of the Base Utsira topographic high 'ridges' identified in Fig. 4.12a. The relationship between mounds and depressions is best demonstrated by overlaying a contour map of the TUH over a TWT map of the BUH (Fig. 4.23, a and b).

The negative relief of the depressions is measured in a similar manner to the positive relief of the mounds. The hinge points are defined as the point where the top Utsira reflection dips downward, while the maximum negative relief equates to the perpendicular distance between an arbitrary line connecting the hinge points, and the lowermost depth of the hanging TUH (Fig. 4.23a).

Generally, individual depressions cover a greater area but display a smaller vertical relief than their corresponding mound. The average area of the depressions exceeds 10 km^2, and their negative relief ranges between 15 and 50 m, with an average relief of 24 m.

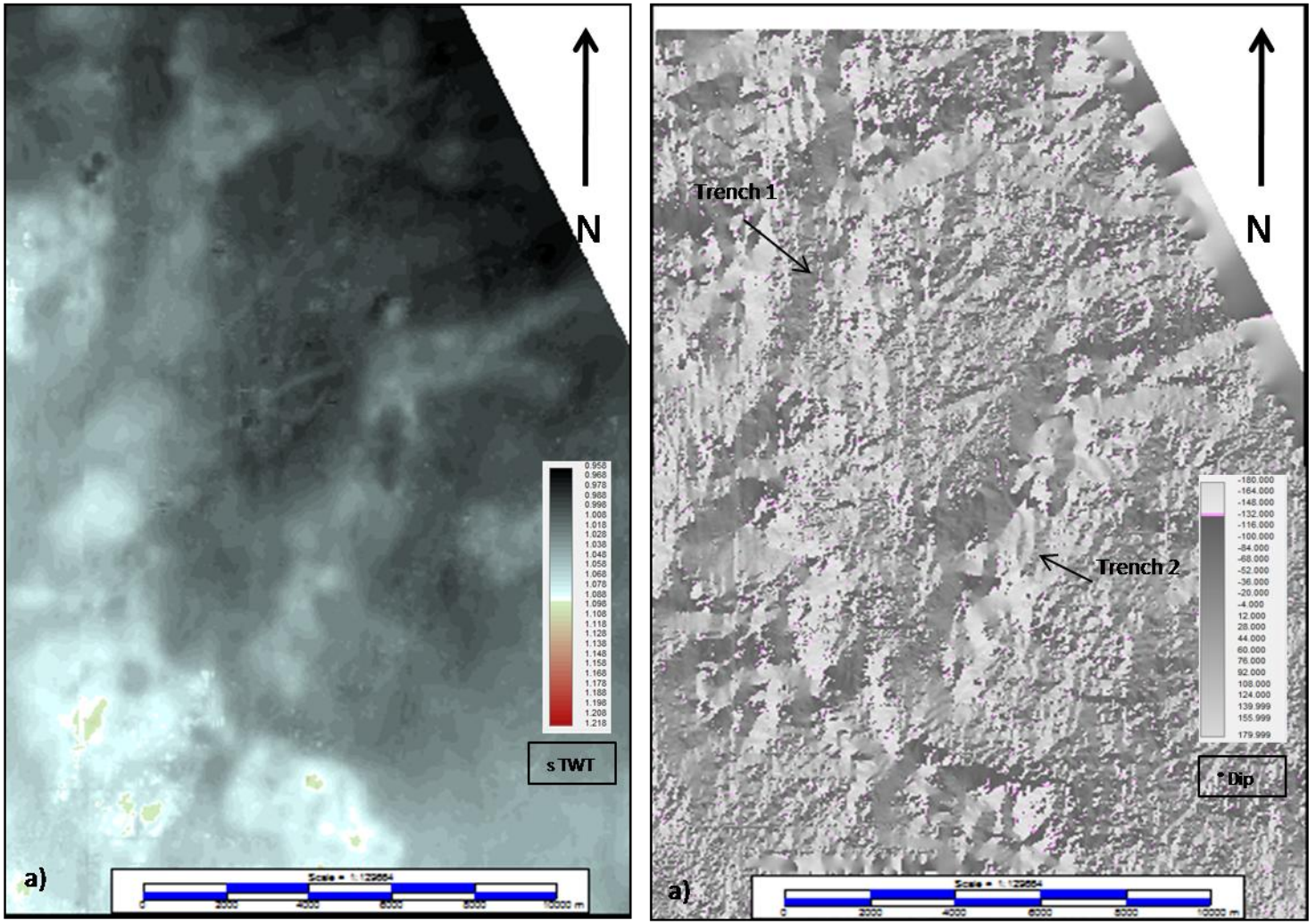

Fig. 4.22 a) TWT map of the Top Utsira Horizon demonstrating the subtle changes in topography

b) an azimuth map of the same horizon showing the distinct form of two 'trenches' orientated SSW-NNE

4.4.5.1. Comparison of depressions with mounds

Mound 1

Mound 1, as described in section 4.3.2.2, is an irregular shaped section of raised BUH which totals 3.9 km^2 (Fig. 4.23b). A time depth map of the mound is overlain by the contour of the overlying depression, and it can be seen that the bold black contour line which denotes the extent of the depression exceeds the dimensions of the underlying mound in every extent except the north-west corner of the area (Fig. 4.23b). The depression is 4.4 km^2 and its outline roughly conforms to the geometry of the underlying mound.

The TUH hangs by around 30 m within the depressed area while the mound displays a maximum positive relief of 90 m (Fig. 4.23b). Two areas of maximum relief can be seen along the mound profile, these are separated by a low section of the BUH. Although the data quality is fair, it appears that the depression mirrors this geometry, and consists of two low areas separated by a slightly raised middle section which directly overlies the low section of the mound

Elongated Mound

An elongated mound, close to the western extent of the Utsira Sand, can also be seen to be smaller in area than the overlying depression (Fig. 4.23d). The outline contour of the depression roughly follows the geometry of the mound. The mound has a positive relief of 90m while the depression hangs by 35 m, and the TUH and BUH are in contact in this example (Fig. 4.23e). A high amplitude, discordant reflection is apparent below the mound, and the BUH is broken in close proximity to the hinge points, while the TUH is intact across the whole profile of the depression. The sudden decrease in thickness of the Utsira Sand where affected by the mound and depression is in contrast with the gradual thinning of the unit towards the west.

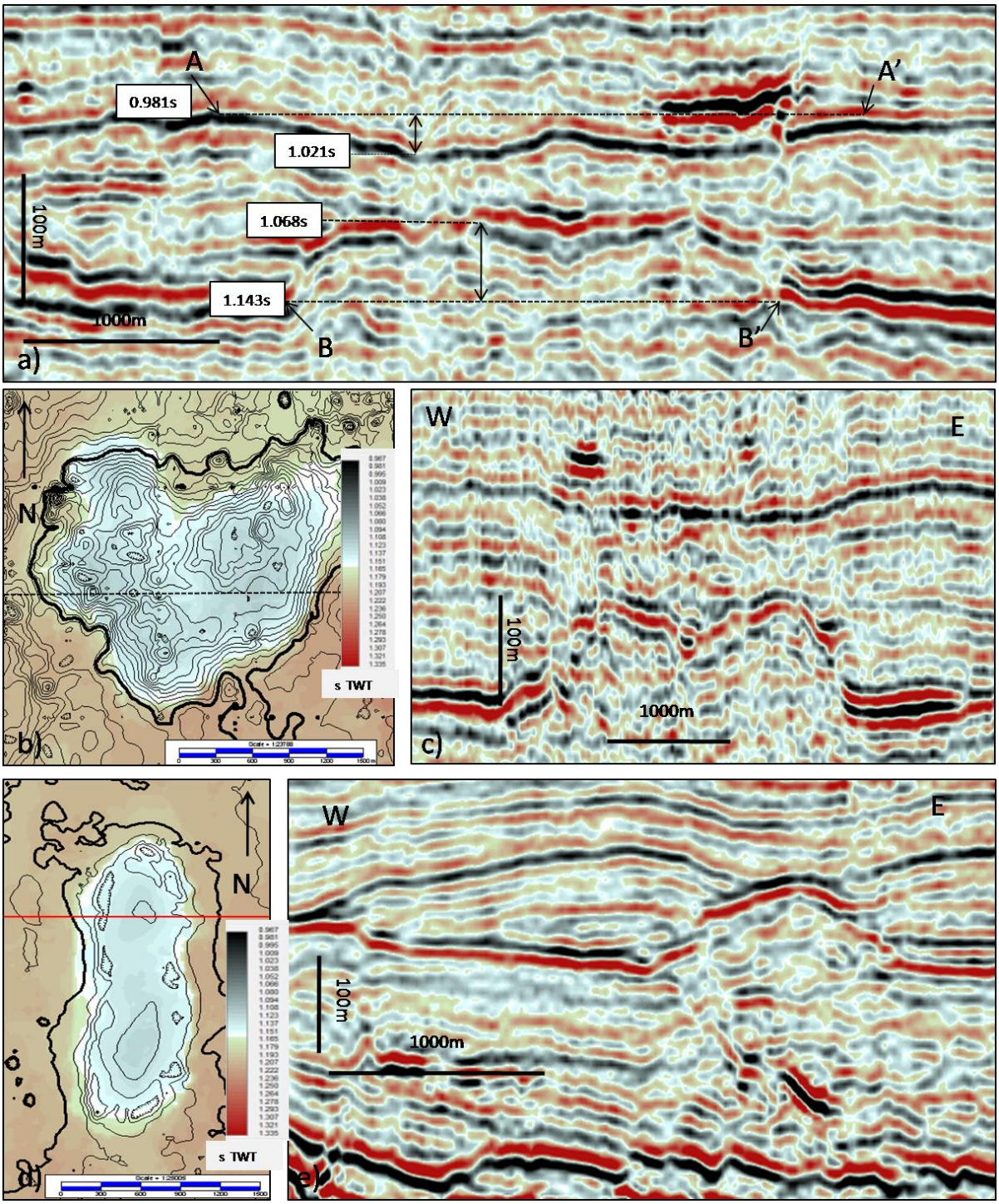

Fig. 4.23 a) demonstration of how measurements for the Top Utsira depressions were taken b) time depth map of an irregular shaped mound overlain by a contour map of the Top Utsira depression c) seismic section through the mound, line location denoted by dashed black line d) time depth map of an elongated mound overlain by a contour map of the Top Utsira depression e) seismic section through the mound, line location denoted by red line

The spatial coincidence and similarity in geometry between the Base Utsira mounds and Top Utsira depressions suggests that there is a relationship between the features. Downturned and downlapping reflections at the flanks of the mounds have already been interpreted as indicators of downward movement affecting the mounds, caused by post emplacement aperture loss of the sand intrusions. It is therefore suggested that the depressions are a further manifestation of this downward movement, and are also caused by the sand intrusion aperture loss.

While the basal reflection often appears broken and detached at the hinge points of the Base Utsira, the Top Utsira reflection does not display this feature; this may be attributed to the smaller vertical movement. The Top Utsira reflection can also be followed across the whole of the profile of the depressions, unlike the basal reflection which dims, is displaced, broken and hard to follow across the fold profile. The irregular topography of the Utsira Sand has previously been noted by Zweigel et al., (2000), and has been described as consisting of several linked domal and anticlinal structures which are considered to be the result of uneven subsidence of the underlying strata.

Depressions which overlie mounds formed by the forced folding of the overburden during sand intrusion emplacement have previously been noted by Loseth et al., (2012). These depressions are interpreted as further evidence of an amount of settlement or downward movement affecting the mounds and overlying strata. As suggested in section 4.3.4.1. the presence of downturned and downlapping reflections onto the mound crests and flanks is evidence of downward movement which has affected the elliptical mounds. The downward curve of the reflections is interpreted to be the result of aperture loss within the underlying sand intrusions. This aperture loss is considered to be the result of mound settlement following grain reorganisation and post-emplacement abatement of the ‘jack up’ pressure within the intrusions following dewatering and sediment expulsion at the paleo-seafloor.

4.4.6. Isopach patterns and thickness relationship of the Utsira Sand

A combined effect of the BUH 'push up' and the associated downward movement of the TUH is to form areas of localised thinning of the Utsira Sand. Regionally the unit thins and pinches out to the south and west, however, an isopach map reveals several localised areas of thinner sections within in the central zone (Fig. 4.24a). These areas coincide with the locations of the Base Utsira mounds and the Top Utsira depressions, and the geometry of these thinner areas mirrors that of the underlying mounds.

This effect is evident from an east-west seismic profile across the study area (Fig. 4.24b). Where undisturbed, the Utsira Sand is in excess of 200m in thickness, while the double effect of the BUH push up and the TUH drop down decreases the thickness to less than 30m (Fig. 4.24b), and in places it appears that the TUH and BUH are in contact. To the west of the mound, the Utsira Sand achieves a thickness of around a 160m, and thins gradually to the west.

4.4.6.1. Interpretation

The Utsira sand is described as a 'basin restricted' sand body. Its geometry is typical of a sand body that has in-filled accommodation space at the centre of the basin, and it is consequently wedge shaped. The study area is located within the UK sector of the North Sea, at the western extremity of the Utsira Sand body, and therefore the general thinning towards the western area of the study area is due to the wedge shaped geometry of the sand body. However, the pattern of thinning is irregular along the east to west profile, and at the extremities of the sand body it displays localised thinning to such an extent that the basal and top Utsira horizons are in contact. This effectively results in the creation of individual sand 'cells'.

The thinning effect due to the wedge shaped geometry of the Utsira Sand would be negligible within the central section of the study area; it is more likely to be the effect of the jack up of the Base Utsira and the hanging of the Top Utsira which combine to create the thinning irregular profile. These localised areas of thinning are coincident with the sand intrusion indicators hosted within the Hordaland Shale.

The Utsira, within its thicker portion, can be as much as 300m thick. The push up effect of the intrusions on the BUH has been shown to exceed 100m in many cases. This push up is accompanied by a lowering of the Top Utsira horizon, and this combination of push up and drop down can decrease the Utsira thickness by as much as half in certain examples.

The effect is more pronounced towards the western extremity of the Utsira Sand causing the Base Utsira and Top Utsira to apparently come in to contact. This pattern of thinning and pinch out away from a central zone of greater thickness has been previously noted by Loseth et al., (2012), where the areas of thinning are associated with underlying mounds.

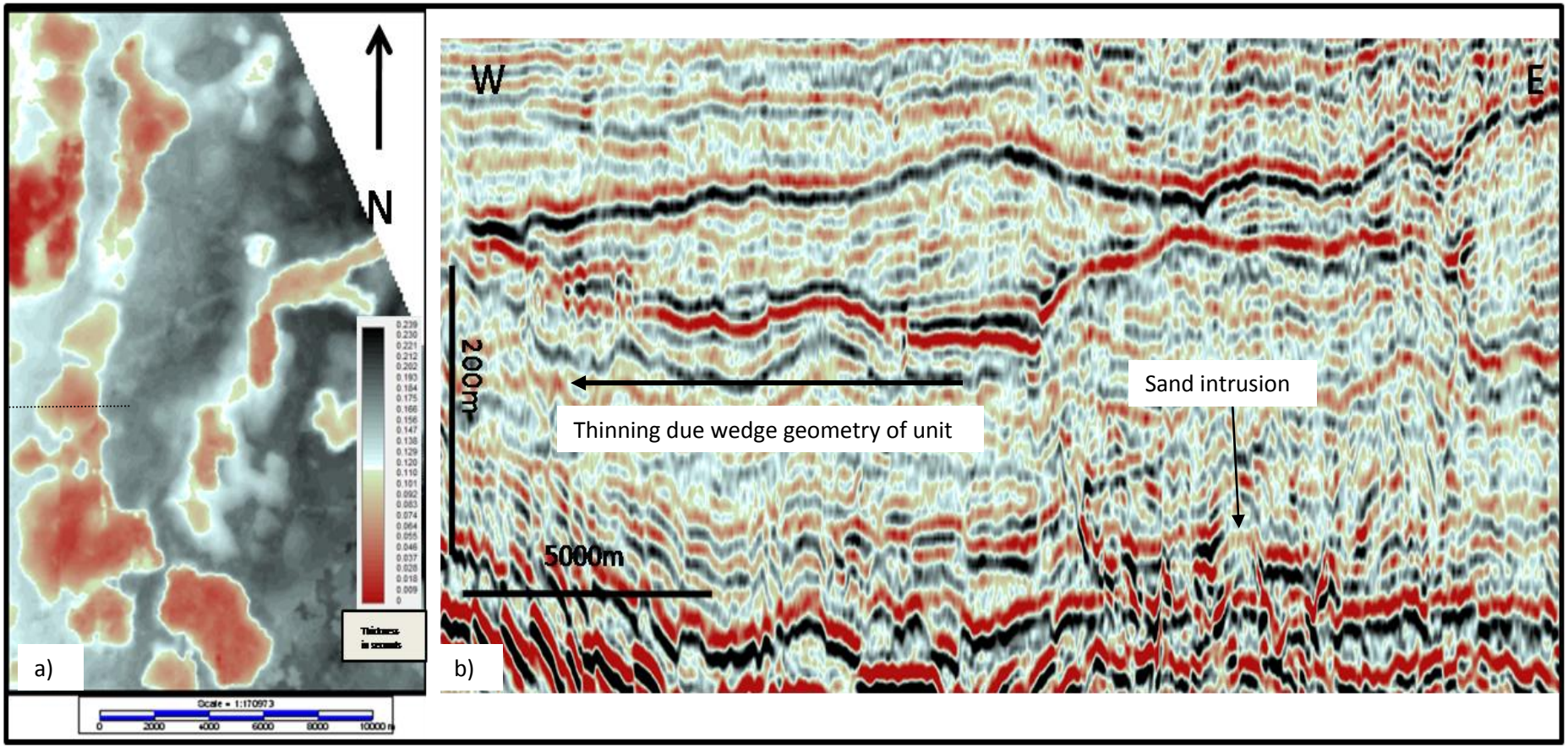

Fig. 4.24 a) Isopach map of the Utsira Sans demonstrating its variable thickness through the study area, and the influence of the elliptical mounds at the Base Utsira level and the elliptical depressions at the Top Utsira level b) seismic section, location denoted by dashed line, showing the thinning of the unit due to its wedge shape and the presence of sand intrusions.

4.5. Summary of discussions

The south-western extent of the Utsira Sand has been mapped from a larger area of varying quality 3D seismic data. Key observations and interpretations are summarised below:

Stratal discordant reflections

- High amplitude reflections within the Lowermost Shale unit are interpret as partially imaged sand intrusions
- The high amplitude reflections can be both concordant or discordant and represent the partially cemented bases or wings of the intrusions respectively
- Areas of chaotic reflections which overlie the cemented bases of the intrusions represent the main body of the sand intrusions
- Sub-vertical zones of broken and disrupted reflections which emanated upwards from the intrusions to the base Utsira Sand are indicators of the un-cemented, but highly permeable wings of the intrusions, and represent highly permeable fluid pathways

Mounds

- Elliptical mounds at the base of the Utsira Sand are the result of force folding of the overburden during the emplacement of the intrusions
- Concave upward reflections which infill areas between the mounds represent extrudite deposits of sand which have been fed to the paleo-seafloor through the highly permeable intrusion wings
- Discontinuous areas along the mound hinge points are the result of penetration by the intrusion wings
- The profile of the forced folds mirrors the geometry and thickness of underlying intrusions.
- A lower section of onlapping Utsira Sand reflections at the flanks of the mounds are indicators that the mounds pre-date the deposition of the Utsira Sand.
- Downturned and downlapping reflections of the Upper Utsira section are interpreted as indicators of a decrease in mound relief
- Decrease in mound relief is linked to the loss of sand intrusion aperture, possibly due to fluid/sand slurry expulsion, sand grain reorganisation and porosity loss

Depressions

- The topography and thickness of the Utsira Sand has been modified by the emplacement, and post emplacement compaction, of the sand intrusions

4.6. Conclusion

The medium term migration and plume development of injected CO_2 is reliant on the topography of the cap rock. The topography is also a major influence on the long term migration and storage security at Sleipner (Torp and Gale, 2004). The irregular topography of the top Utsira Sand has previously been noted (Zweigel et al., 2000)., and described as consisting of several linked domal and anticlinal structures. These features had previously been considered as the result of differential compaction. This study identifies that these structures are the result of post-emplacement aperture loss within the sand intrusions hosted by the underlying Lowermost Shale. The presence of sand intrusions, therefore, has an influence on the migration pathways of the CO_2 plume, and may also responsible for the creation of trapping structures at the top Utsira Sand.

Further Work

In the next chapter aims to;

1) Describe further the sand intrusion indicators located within the Lowermost Shale unit

2) Demonstrate the geographic distribution of the sand intrusions

3) Identify the effect of the sand intrusions on the overlying strata

3) Attempt to quantify the relationship between the intrusions and the effect on the overlying strata.

Chapter 5

Norway results. Description of Mid Miocene amplitude anomalies with associated elliptical mounds and depressions.

5. Chapter 5

5.1. Introduction

The study area for this Chapter is located within the North Sea Intrusion Province, as defined by Cartwright (2010), where it is estimated over 1000 reservoir scale intrusions are located within an area 40,000km^2. Sand intrusions are rapidly becoming recognisable geological features, helped in part by the advent of 3D seismic data. They are commonly seen as V or U shaped high amplitude reflections in seismic cross sections or as elliptical or horseshoe shaped reflections in time-slices (Cartwright, 2008). In Chapter 4, the observed sand intrusion indicators are sub-divided into three groups; (1) high amplitude reflections (both concordant and discordant), (2) bright spots, and (3) a combination of both.

Work by Molyneux et al., (2002) and Huuse and Mickelson (2004) describe a number of possible alternative origins for these amplitude anomalies (channel bodies, pockmarks, incised valleys). However, they conclude, along with Shoulders and Cartwright (2004) that most likely explanation is clastic intrusions. Igneous origins for such features within this study area are discounted on the basis that there are no known drilled igneous intrusions at the depths included in the dataset.

5.1.1. Sand intrusion emplacement

Emplacement of sand intrusions involves the remobilisation of a sand body allied to hydraulic fractures propagating within its overburden as a result of high pore fluid overpressure within the sand layer. The three key criteria for remobilisation are a suitable source, priming conditions and a trigger mechanism. Sand intrusions require a parent body of highly porous and unconsolidated sand (Cartwright et al.,2008) that has been enclosed rapidly by low permeability sediments which restrict the escape of inter-granular water. Priming conditions facilitate the build up of pressure within a parent sand body to a state of overpressure, this is followed by hydraulic fracturing of the overburden, and the liquefaction and flow of the sand ‘slurry’ (Jolly and Lonergan, 2002).

Overpressure is not sufficient by itself to remobilise the sand, a trigger mechanism is required and is described as a ‘critical factor’ by Cartwright (2010). Lateral pressure transfer and seismic triggering are cited as the most plausible (Cartwright, 2010; Jonk 2010), however several other mechanism have been proposed; thermal pressurisation (Ujiie et al., 2007), impact craters (Strukell and Ormo, 1997) and igneous intrusions (Curtis and Riley, 2003). Hydrocarbon migration is suggested by Davies et al. (2006), but is considered as a primer rather than a trigger by Cartwright (2010).

Intrusion complexes have been seen to emanate at specific points from possible parent sand bodies (Cartwright et al, 2008; Cartwright, 2010), and are considered to have broken through the fine grained sealing unit at these locations. Seismic evidence suggests that an intrusion complex can penetrate over hundred of meters of lithology upward from the sand source (Shoulders and Cartwright, 2004; Shoulders, 2007; Cartwright et al., 2008; Rodrigues et al., 2009), and are often seen to terminate at a horizon in close proximity to the paleo-seafloor (Molyneux et al., 2002; Huuse and Mickelson, 2004). The proximity of some intrusions to the seabed suggests that sand may be extruded onto the seafloor (Molyneux, 2001; Huuse et al., 2004, 2005; Shoulders and Cartwright, 2004; Hurst et al., 2005, Loseth, 2012).

Intrusion emplacement is accompanied by the forced folding or the hydraulic 'jack up' of overlying strata. This hydraulic ‘jack up’ process promotes the creation of stacked, mounded, concave upward reflections which directly overlie the intrusions, and the formation of mounded relief at the paleo-seafloor. A spatial relationship between force fold mounds and underlying sand intrusion indicators has been identified by Shoulders and Cartwright (2004) and a causative relationship suggested. Cartwright et al., (2008) suggest that this forced fold relationship is a diagnostic aid for intrusive bodies.

A singular emplaced intrusion typically consists of a horizontal, concordant, main body of sand at its centre, with low angle, discordant, wings protruding at either side. The greater thickness and volume of remobilised sand lies within the central component of the intrusion (Cartwright, 2008), and it is here that the hydraulic ‘jack up’ effect is greatest i.e. where the greatest volume of intruded sand needs to be accommodated. The aperture vs. distance profiles presented by Cartwright et al (2008) suggests that forced fold relief is proportional to the intrusion aperture (thickness), it therefore follows that the greatest relief of the forced fold should be located above the central area of the sand intrusion. Force fold relief is considered to be no less than half of the intrusion aperture and close to unity in some cases (Cartwright et al., 2008).

5.1.2. Intrusion distribution

The majority of intrusions within the North Sea Intrusion Province studied to date are hosted within the Eocene. However, large sand intrusions are not uncommon within the Oligocene and Miocene succession (Molyneux, 2001; Loseth et al., 2003; Huuse, 2008).

The intrusion indicators studied within this study area have already been identified by Huuse (2004) and their effect on the Base Utsira noted. These intrusions are hosted by the hemipelagic smectite-rich mudstone of the Hordaland Group, and are limited to a horizon between the Base Utsira reflection (BUH) and a laterally extensive, bright reflection which is considered to be the mid-Miocene unconformity and has been termed the Mid-Miocene Onlap surface. A strong possibility exists that this high amplitude, polygonally faulted reflection is the Opal A to Opal CT conversion boundary identified by Davies et al. (2006) and Davies and Cartwright (2002 and 2007). At several points high amplitude discordant reflections emanate from this horizon and may be the 'breakthrough' points for the intruded sands. The proximity of this possible diagenetic boundary to the base of the intrusions also supports Davies et al. (2006) suggestion that the dehydration reactions which take place during the conversion from Opal A to Opal CT may in fact act as a priming mechanism for sand intrusion, or that the diagenetic boundary might have acted as an important mechanical contrast.

Intrusions are commonly located within areas affected by polygonal faults, especially within the Lower-Middle Eocene of the North Sea (Cartwright, 1994; Huuse et al., 2004; Lonergran and Cartwright, 1999; Molyneux et al., 2002), and are often seen to cross cut or exploit polygonal faults (Shoulders and Cartwright, 2004), especially so when the faults are favourably orientated (Huuse and Mickelson, 2004). Spatial clustering of sand intrusions is described as 'not uncommon' by Cartwright (2008); it is also noted by Huuse and Michelsen (2004).

5.1.3. Intrusion timing

Shoulders and Cartwright (2004) describe a method for constraining the timing of intrusions by the onlapping reflections at the forced fold flanks, and Huuse (2008) has previously identified the onlapping of the Utsira Sand at the flanks of the force folds by the lower reflections of the Utsira Sand, and argued for a mid-late Miocene timing for intrusions at this level. The maximum age of the emplacement can be constrained by the age of the host sediment (Shoulders and Cartwright, 2004).

5.1.4. Intrusion Compaction

Intrusions are known to experience loss of height and aperture thickness following emplacement (Cartwright et al, 2008). Depending on composition of the remobilised sand 'slurry', a variation of up to a half between the initial emplacement aperture and final aperture is suggested by Cartwright et al (2008).

The mounds in Chapter 4 are accompanied by depressions at the top Utsira level; and these were considered to be the result of subsidence associated with intrusion aperture loss (see Chapter 4, Section 4.3.2.5). Fluid expulsion, grain rearrangement, and porosity loss under loading are possible causes for this decrease in intrusion aperture.

5.1.5. Implications for sequestered CO_2

Sand intrusions are included in the Cartwright et al., (2010) intrusive family of seal-by-pass systems (SBS's), they are known to breach sealing lithologies and increase cross-stratal permeability. The intrusions in Chapter 4 are located below the storage reservoir, however, the identification of possible SBS's associated with the formation of mounds, sand intrusion emplacement, and the subsequent subsidence of the overlying strata is paramount to the safety of the injected CO_2 plume and crucial in selecting further storage structures within the Utsira Sand.

Sand intrusions are shown to lose ~15% porosity under burial, and their final aperture (thickness) is less than the initial aperture of the intruded body (Cartwright et al, 2008). Differential compaction and subsidence of the strata overlying the intrusions is therefore a strong possibility, and the resulting movement and juxtaposition of strata may in turn create possible leakage conduits. The rate of movement of this effect and the amount of vertical movement affecting the top of the storage reservoir is of interest; a relatively sudden collapse would facilitate faulting and fracturing at the flanks of the depressions, and subsequently create possible leakage pathways, while a slower subsiding movement would be less of a risk, and may in fact create possible trapping geometries and storage structures which would confine and control the migration of the CO_2 plume.

5.2. Data set and Geology

The results presented in this chapter are derived from a 2,300 km^2 3D seismic volume from the UK section of the Central North Sea, the study area itself covers an area around 400 km^2 within the larger volume (Fig. 5.1a).

The processing history of the data is unknown; however, observation of the seafloor suggests that this horizon corresponds with a negative amplitude, red reflection, and that the data is displayed in reverse polarity, following the European Convention (Fig. 5.1d). The data volume is an amalgamation of local and regional 3D seismic surveys, hence the high variability in data quality.

The dominant frequency in the areas of better quality is around 40 to 45 Hz, and using velocity value of 1800 m/s from NPD synthetic seismogram http://factpages.npd.no/factpages/default.aspx, a vertical resolution of between 10 and 11.5 m is calculated. Digital well data was not available to aid interpretation, and it was not possible to create coherency cubes due to licensing limitations associated with the IHS Kingdom software.

The geological setting of this study area is presented in Chapter 3 of this volume; a brief description of the main units mapped for this chapter is presented in section 5.4.1.

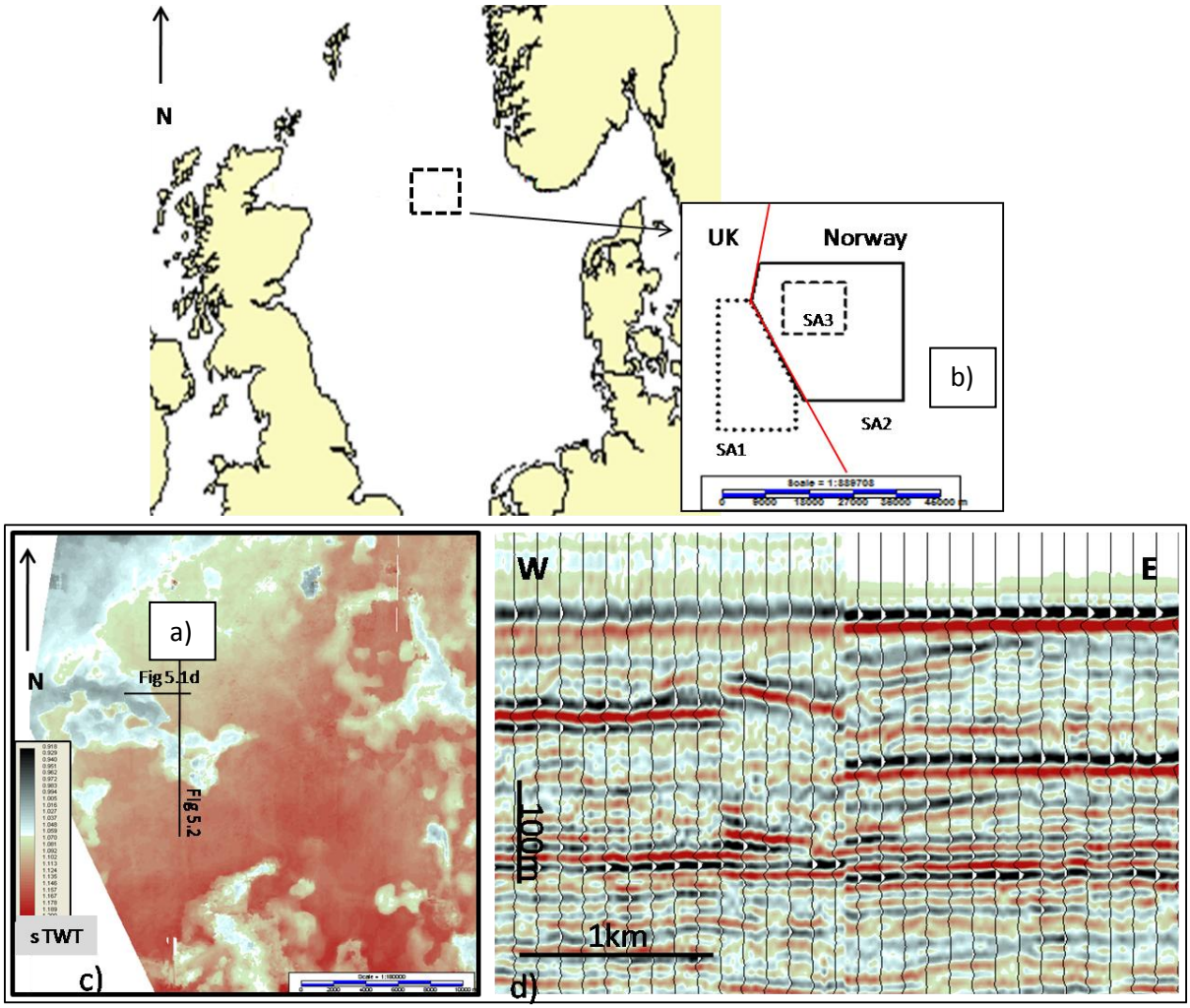

Fig. 5.1 a) Location map of the study area. a) with respect to the UK and Norway and b) Study Area 2, large black square, in relation to study area 1 (SA1) and 3 (SA3) c) Base map of the Base Utsira Horizon with location of Fig. d and Fig. 5.2 d) seafloor reflection is the dominant negative (red) reflection, and the wavelet appears to be in minimum phase

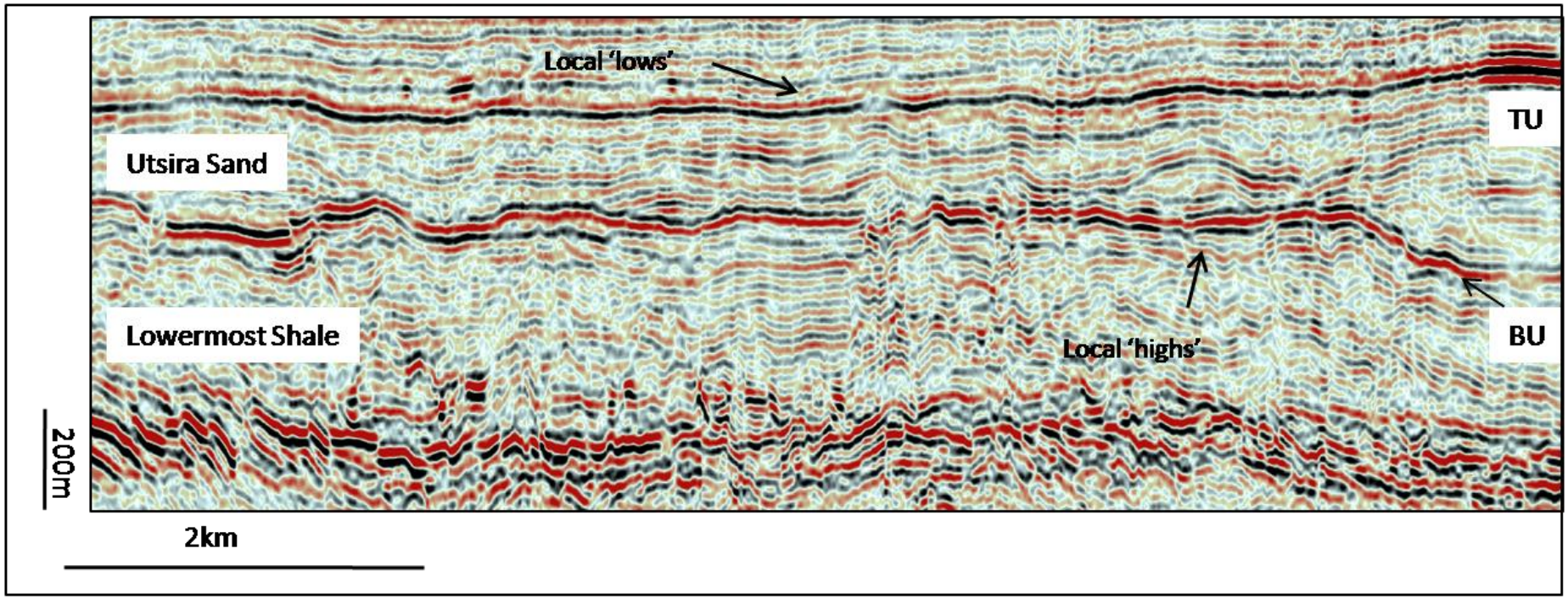

Fig. 5.2 shows a representative seismic section of the two main units from which the results of the chapter are derived; the Lowermost Shale and the Utsira Sand. The base of the Lowermost Shale is a polygonally faulted horizon. The Base of the Utsira (BU) is often displaced upwards to form local highs, while the top of the Utsira (TU) is often seen to be displaced downwards to form local lows.

5.3. Results

General description of main units mapped

The units discussed in this Chapter are the Lowermost Shale and the Utsira Sand, they have been previously been described in section 2.2.2.1 and 4.3.1, and they are the focus of the observations in Chapter 4. A brief overview of their character in this study area is presented below.

5.3.1. Lowermost Shale

The Lowermost Shale consists of low to medium amplitude, continuous to semi-continuous, parallel to sub-parallel reflections. Local areas of chaotic and disrupted reflections are present. Its upper boundary is a high amplitude continuous reflection, and its basal boundary is a high amplitude polygonally faulted horizon (Fig. 5.2), termed the Mid Miocene Onlap surface and also considered to be the mid-Miocene unconformity. Within this study area unit thickness is generally between 200 and 250m, and is at its thickest within the central area. Depth to base varies between 1.3km and 1.5km, with the areas of greatest depth located in the centre of the study area.

Despite the general low amplitude characteristic of the unit, an RMS map allows identification of several areas of high reflectivity which are generally circular to sub-circular in plan form. Time slices through these high reflectivity packages reveal a range of geometries, from circular to sub-circular high amplitude reflections to linear or curved reflections of opposite polarity. They are present as singular features, but more often as groups of high amplitude features.

In seismic section these anomalies are typically expressed as one of three seismic expressions; bright spots, discordant or concordant high amplitude reflections, or a combined to create asymmetrical or symmetrical U or V shaped high amplitude reflections. The various forms of these amplitude anomalies and high amplitude reflections are described in section 5.4.2.

5.3.2. Utsira Sand

Directly overlying the Lowermost Shale is the Utsira Sand. Its base is clearly defined by a strong and continuous reflection (top of Lowermost Shale), which is considered to be the paleo-seafloor at the time of Utsira Sand deposition. The upper boundary is denoted by a medium to strong, continuous reflection. Both upper and lower boundaries show local vertical displacement (Fig. 5.2).

Unit thickness varies considerably, with areas of considerable localised thinning within the study area. These areas are apparent on an isopach map of the unit, and roughly correspond with the areas where the basal and top horizons are deformed (Fig. 5.3). The greatest deformation affects the basal boundary and a map of this horizon reveals several areas of raised topography (Fig. 5.3). These high relief areas are present as either individual or mound clusters. The clusters are located within the north-west, north- east, south-west and south-east corners of the study area (Fig. 5.3), and within these areas the basal reflection is often seen to be displaced upwards as much as 100m (0.1s TWT) higher than its average depth (1100m) within the study area (Fig. 5.2).Individual areas of raised topography are also present within the study area, they are seen to be crudely elliptical in plan view with a long and short axis, and are termed elliptical mounds for the purpose of this study. The basal reflection is often broken at the flanks of these mounds.

At locations where the lower boundary of the Utsira Sand is elevated the upper boundary is seen to form a low point (Fig. 5.2). The negative vertical movement affecting the upper boundary is less than the corresponding positive vertical movement affecting the base. However, the areas of the depressions exceed that of the corresponding underlying mounds. As a result of this, the deformation affecting the basal boundary appears as a sudden and dramatic change in depth while the upper boundary has a gentle, undulating appearance (Fig. 5.2).

There is a notable difference between the geometry of the reflections within the upper and lower parts of the unit when in close proximity to the deformed base. The lower section generally consists of around 80m of mostly concordant, horizontal, and parallel reflections which onlap the flanks of the mounds. The reflections of the upper section are inflected downwards and drape over the mounds and mirror the undulating nature of the upper boundary (Fig. 5.2). They display a degree of convergence, and downlap onto the reflections of the lower section, and onto the flanks and crest of the elliptical mounds.

5.3.3. Lowermost shale amplitude anomalies

The amplitude anomalies hosted by the Lowermost Shale unit are revealed by an RMS map. While high amplitude areas are present throughout the area, they are best presented in detailed small scale RMS maps of unit. In chapter 4 it was proposed that the high amplitude features within the Lowermost Shale can be broadly divided into three different classes based on their appearance on seismic section; 1) bright spots, 2) high amplitude reflections; and 3) a combination of both. Examples of each class are described and interpreted in the sections below.

5.3.3.1. Bright spots

'Bright spots' are defined as areas of high amplitude which do not exceed 300 m in diameter or long axial length. This length is proposed as an arbitrary cut-off determined from the spectrum of examples from Chapter 4. Features exceeding this length are termed high amplitude reflections. Bright spots are circular to sub-circular in plan view on RMS maps and time slices, and appear as either concordant or discordant to bedding in seismic section. They are the most commonly seen sand intrusion indicators within this data set.

5.3.3.1.1. Bright spot cluster

An RMS map and time slice (1.269 ms) of five representative examples of high amplitude reflections are presented in Fig. 5.3.

Bright spot A (BsA) appears as a single isolated package located 400 m west of a cluster of high amplitude features (Fig. 5.3a, A). It consist of a central, circular, zone of high amplitude which is roughly 40 m in diameter, contained within a medium amplitude sub-circular and elongated outer 'halo' which is an additional 100 m in diameter. In cross section (Fig. 5.3c) it appears as a high amplitude bright-spot roughly 140 m in length, and located around 30m above the polygonally faulted basal horizon of the unit. The reflection continues, but dims, to the south, and is broken and slightly upturned to the north. A time slice (at 1.269 ms depth) shows its geometry to be slighty elongated and sub-circular with a long axis of 140 m (this corresponds with its combined long axis on the RMS map).

The bright spot lies beneath a raised section of the Base Utsira Horizon (BUH). The BUH horizon is broken (Fig. 5.3c, points BR) and sub-vertical zones of discontinuous reflections appear to connect the bright spot and the BUH (DR). Either side of these disrupted zones, the background reflections of the host unit appear concordant, semi continuous, and parallel. Directly above, and obliquely upwards from the bright spot, the reflections are broken and chaotic. This area of chaotic reflections is roughly wedge shaped; thicker in the central zone overlying the bright spot and thinning towards the edges. The vertical distance from the base of the bright spot to the top of the chaotic wedge is roughly 90 m. The semi-continuous and horizontal reflections of the host unit are present above and to the side of the wedge.

Bright spot B (BsB) is roughly circular with a diameter of around 100 m. In seismic cross section (Fig. 5.3d, crossline 10955), BsB is visible as 3 stacked bright spots comprising an uppermost bright black (soft) reflection underlain by a bright red (hard) and a secondary bright black reflection. The dominant amplitude of the triplet is the negative red reflection, and this can be considered a 'hard' event (from the seafloor reflection). Along this transect BsA is observed to be a discordant bright spot and is connected to BsB by a continuous, horizontal, flat based reflection low of amplitude. BsA is tilted and discordant to the surrounding reflections, while BsB is slightly raised and concordant. A sub-vertical zone of broken and disrupted reflections can be seen to project obliquely upwards from the BsB towards the BUH (Fig. 5.3d, arrowed). A similar disrupted zone to that seen above BsA in Figure 5.c overlies the horizontal low amplitude reflection (DZ).

The area in between and above the bright spots consists of a zone of chaotic reflections, which is again wedge shaped with a thicker central area which thins to the edges. The western and eastern edges of the chaotic wedge is delineated by sub-vertical disrupted reflections which propagate upwards from the bright spots to the BUH, discordant, low amplitude reflections are also present. To the west and the east of the wedge, the reflections of the host unit are apparent as parallel, horizontal to sub-horizontal, low amplitude reflections. From the base of the flat lying reflection to the top of the chaotic wedge is around 120 m in thickness, and the horizontal reflections of the host unit directly overlie the wedge.

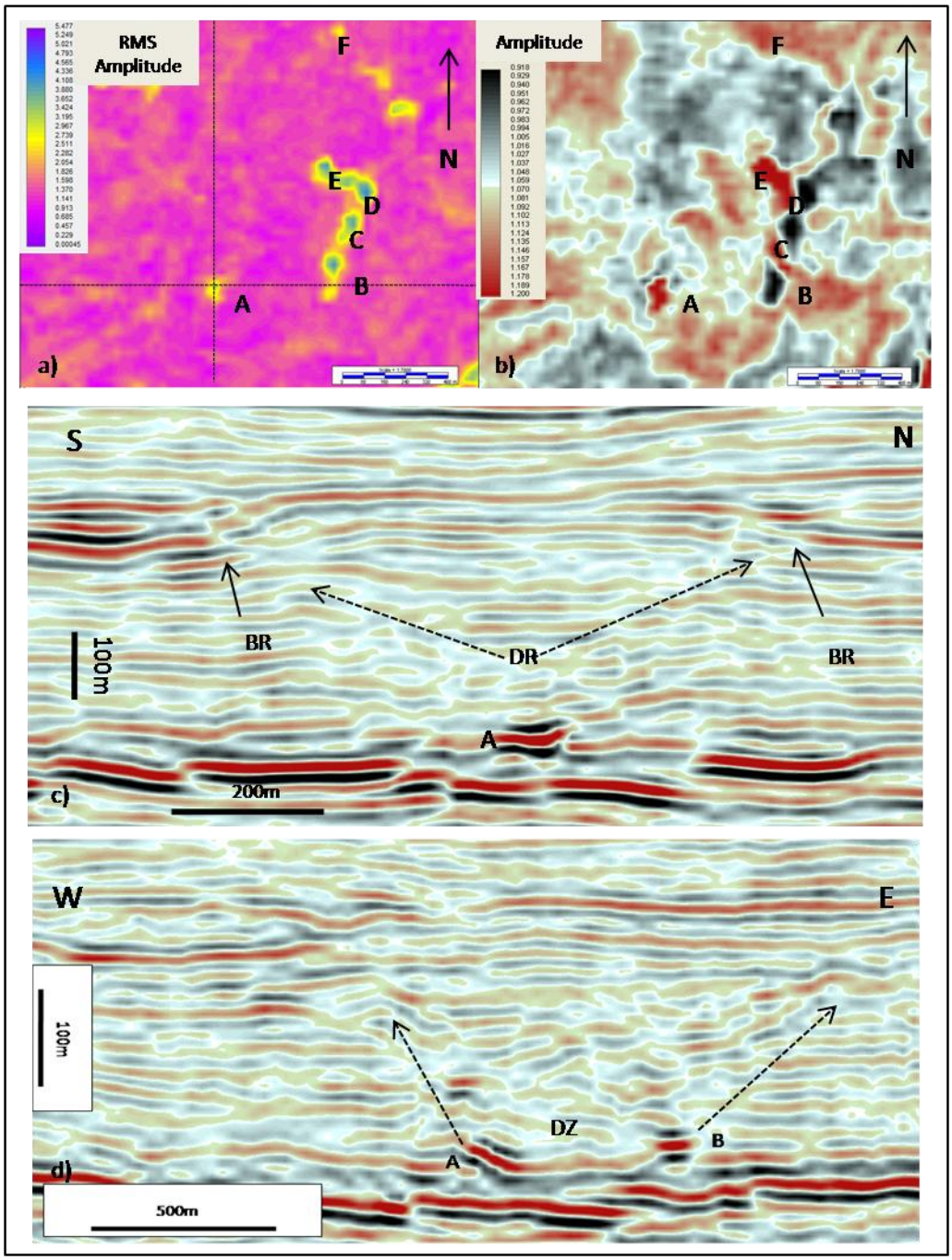

Figure 5.3 a) An RMS map of the Lowermost Shale with a b) time-slice intersecting six high amplitude features c) a S-N seismic section showing high amplitude feature A with a wedge shaped area of disrupted reflections (DR) and broken Base Utsira reflections (BR) d) a W-E section showing high amplitude feature A and B with associated disruption zone (DZ) and sub-vertical disrupted reflections (arrowed).

5.3.3.1.2. Grouped bright spots

In plan form BsC is sub-circular with a slight elongation at its south western edge (Fig. 5.4a), this 'finger' of high amplitude extends the long axis of the bright spot to around 100 m. The sub-circular BsD and BsE are 80 m and 60 m in diameter respectively and are connected by a lower reflectivity 'saddle' some 100 m in length. Bright spots B, C and E are all intercepted by Inline 10600 (Fig. 5.4b). Along this profile the seismic section shows BsB and BsC to be conjoined, while to the north the reflection dims, is slightly displaced, and is connected to BsD. Further along the section, to the north, BsF is visible.

The RMS map shows the four main bright spots and their connecting areas as a series of high reflectivity features connected by lower reflectivity outlines. This can be visualised further by forming an arbitrary line which intercepts all four bright spots (Fig. 5.4c). The southwest to northwest seismic section shows all four bright spots to be connected. The reflection is an upward convex, concordant, and continuous reflection with no visible dimming of the amplitude, which is dominantly negative (hard), along its length.

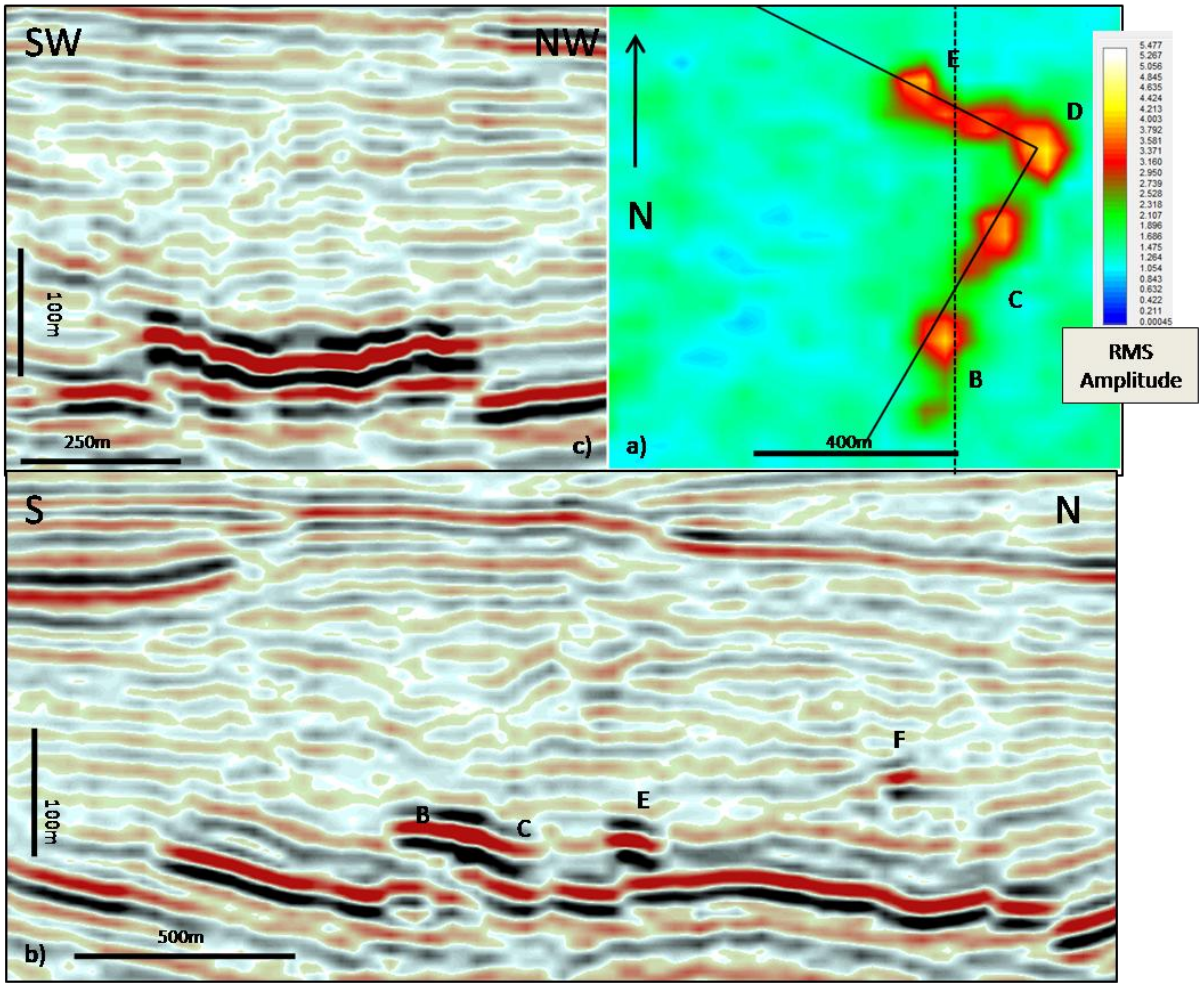

Figure 5.4 a) An RMS map of the Lowermost Shale showing a group of high amplitude reflections (B,C,D and E) b) a S-N section with the high amplitude c) an arbitrary line connecting the high amplitude features to form a flat based bowl geometry.

5.3.3.2. Interpretation

The bright spots observed are both concordant and discordant to the host units internal reflections. They are circular, sub-circular or elongated in plan form, and do not exceed 200 m in diameter or long axis length. As with those described in section 4.3.2.1.1 the concordant bright-spots are interpreted to represent the partially imaged, flat lying, central bases of sand intrusions, while the discordant bright spots are interpreted as examples of partially imaged intrusion wings.

These bright spots are often accompanied by overlying chaotic reflections, and this phenomenon has been previously noted by Hurst et al. (2003) to be associated with sand intrusions. While the mounding and displacement of the host unit reflections is a commonly noted feature associated

with sand intrusion emplacement (Shoulders, 2007), and is described as a diagnostic feature by Cartwright et al., (2008).

Chaotic reflections, which accompany and overlie the bright spots, are interpreted as the main sand body of the sand intrusions (Fig. 5.5a,b and e, MB), while the 'hard' bright spot represents the partially cemented bases of wings of the sand intrusions. In the examples given the thicknesses of these zones have been measured and are 90m (Fig. 5.5a) and 120m (Fig. 5.5a), respectively. These values are comparable to those measured in Chapter 4, section 4.3.2.1, and are consistent with the displacement of the overlying BUH.

Sub-vertical zones of broken and discordant reflections denote the boundaries of the chaotic wedges (Fig. 5.5), these are interpreted these as intrusion wings (W) . It is considered here that they are not imaged as hard reflections due to a lack of cementation, or possibly due to the fact that the intrusions thin towards their wing tips and are below the vertical resolution of this survey. These 'wings' are often seen to terminate in close proximity to the paleo-seafloor (BUH), and may penetrate the BUH where it is displaced and broken (Fig. 5.5d).

Bright spot A (Fig. 5.5a) is interpreted as the partially cemented apex of an intrusion. Its southern extent is horizontal and it is inflected upwards towards its northern end. This upward trajectory is considered to represent the beginning of an intrusion wing, and coincides with a sub-vertical zone of disrupted reflections (Fig. 5.5b, arrowed W), which is interpreted as the continuation of the wing. These sub-vertical zones appear to reach the BUH. The 'chaotic wedge' which overlies BsA is thicker directly above the bright spot and underlies the centre of the Base Utsira mound, while the thinner 'wings' underlie the flanks of the overlying mound.

The horizontal reflection which connects bright spot A and B is interpreted as the flat base of the central section of the intrusion (Fig. 5.5d). The upwards inflection at both the southern and northern end of the reflection represent the beginnings of the intrusion wings. The associated sub-vertical zones again represent the continuation of the wings, which are either un-cemented or below the vertical resolution of the data (Fig. 5.5d). The sub-vertical zones contrast with the horizontal, semi-continuous reflections of the host unit, which terminate against the wings, and represent the boundary between the intruded sand and the host. The relief of the mound does not decrease with the decrease in intrusion aperture (towards the wings) in this example; possibly due to the presence of an adjacent intrusion (Fig. 5.5c, point I2).

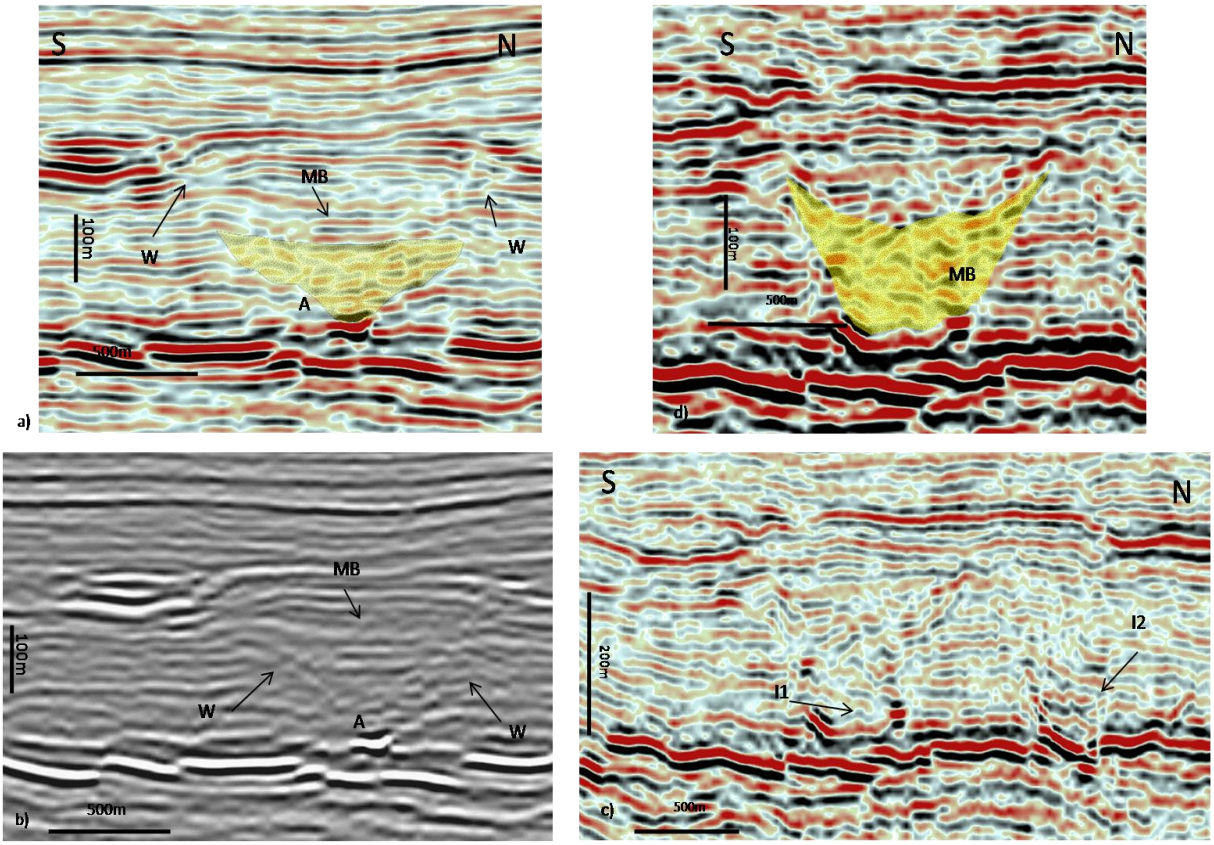

Fig. 5.5 Interpretation of the high amplitude features and associated disrupted reflections see Section 5.4.1.1.

5.3.3.3. High amplitude reflections

High amplitude reflections (HAR's), in some cases, display similar geometries to bright spots when viewed on an RMS map. However, they usually have greater dimensions and areal extent, and can also take the form of large irregular polygons of high amplitude. In seismic section they can be concordant (CHAR) or discordant (DHAR) to the host unit reflections. They exceed 300m in length, and can cross cut up to and above of 100m of the host unit stratigraphy. They are generally present as isolated high amplitude reflections or in close proximity to bright spots and other HAR's.

The appearance of DHAR on time slices differs from that of bright spots and HAR's (High amplitude reflections). This difference in appearance their main defining feature. While time slices of bright spots generally replicate their geometries as seen on RMS maps and are circular to sub-circular features, DHAR's, when intercepted by a time slice, appear as a single high amplitude reflection, or

as a couple of concordant high amplitude reflections of opposite polarity which can be either linear or curved. Amplitude is not always consistent along the reflection length. CHAR have a greater areal extent but are generally similar in appearance to bright spots on RMS maps and time slices.

5.3.3.3.1. DHAR with associated bright spot

An RMS map and time- slice of an area are presented in Fig. Fig. 5.6. Five separate areas of high amplitude are shown on the RMS map (Fig. 5.6b, points A,B,C,D,E). With the exception of high reflectivity area E, these high amplitude areas can be contained within an elliptical shaped area around 500m^2.

The time slice (Fig. 5.6a, depth 1.272TWTs) reveals 2 pairs of bright reflections of opposite polarity (Fig. 5.6a, points A and B). The southernmost pair (Fig. 5.6c, Point A) is around 250m in length and have a combined thickness of a 110m. They are orientated north to south and dim at their northern extent. The northern pair (Point B) consists of a prominent red (hard) reflection and a thinner black (soft) reflection. They are also around 250m in length and are also orientated roughly north to south. They can be seen on the RMS map as sub-circular areas of similar area (Fig. 5.6, points A and B).

Due east of the northern pair, on the time slice, is a single red reflection of similar length and orientation (Fig. 5.6, point C). It is much dimmer in amplitude and is only visible as a bright spot on the RMS map where it brightens at its northern extent, above point C (Fig. 5.6). A sub-circular bright spot is located at point D (Fig. 5.6). The difference in geometry upon the time slice between the bright spot and the DHAR's is a defining feature in this study's sub-division of bright spots and DHAR's. When viewed upon the RMS map the bright spot and the DHAR's are not so easily distinguished, however they are expressed in noticeably different forms on time slices.

The southern pair of bright reflections is best displayed on a seismic section perpendicular to their orientation (Fig. 5.6c, point A). They appear on the seismic section as three stacked discordant reflections of varying amplitude. A middle red reflection (negative, hard) is the dominant amplitude, it is underlain by a high amplitude black reflection which dims along its length. The upper black reflection is not so prominent on either the time-slice or the RMS map due to its lower amplitude. The base of the middle reflection is in close proximity to the polygonally faulted horizon. Its base to tip is around 430m in length and it cross cuts some 80m of the background unit reflections. Parallel

and continuous reflections to the west of the DHAR terminate against it (arrow). The area to the east of the DHAR consists of several bright spots (BS) and a zone of chaotic reflections (CZ).

Crossline 10817 intercepts the northern pair of bright reflections (Fig. 5.6d). The discordant reflection is semi-continuous, and can be seen to be broken (point 1). It is around 250m from base to tip and cross cuts 80m of the background reflections. The central red reflection has the greatest consistency in amplitude along its length, while the underlying black reflection is also high amplitudet but dims in places. At the uppermost extent of the red reflection it appears to dim and become concordant to bedding (point 2). A small dimple located on the basal horizon of the unit appears to lie along the same plane as the discordant reflection (Fig. 5.6d, point 3), and may be the 'breakthrough' point of the intrusion.

Points C and D are both present on inline 10648 (Fig. 5.6e). Point C is a concordant bright spot consisting of three stacked bright reflections (soft, hard, soft), of which the hard red reflection is the dominant amplitude. It is sub-circular in plan view and has a diameter of 90m. Point D is also a concordant bright spot greater than 250m in length. A sub-vertical plane of broken reflections can be projected from its tip upwards towards the BUH.

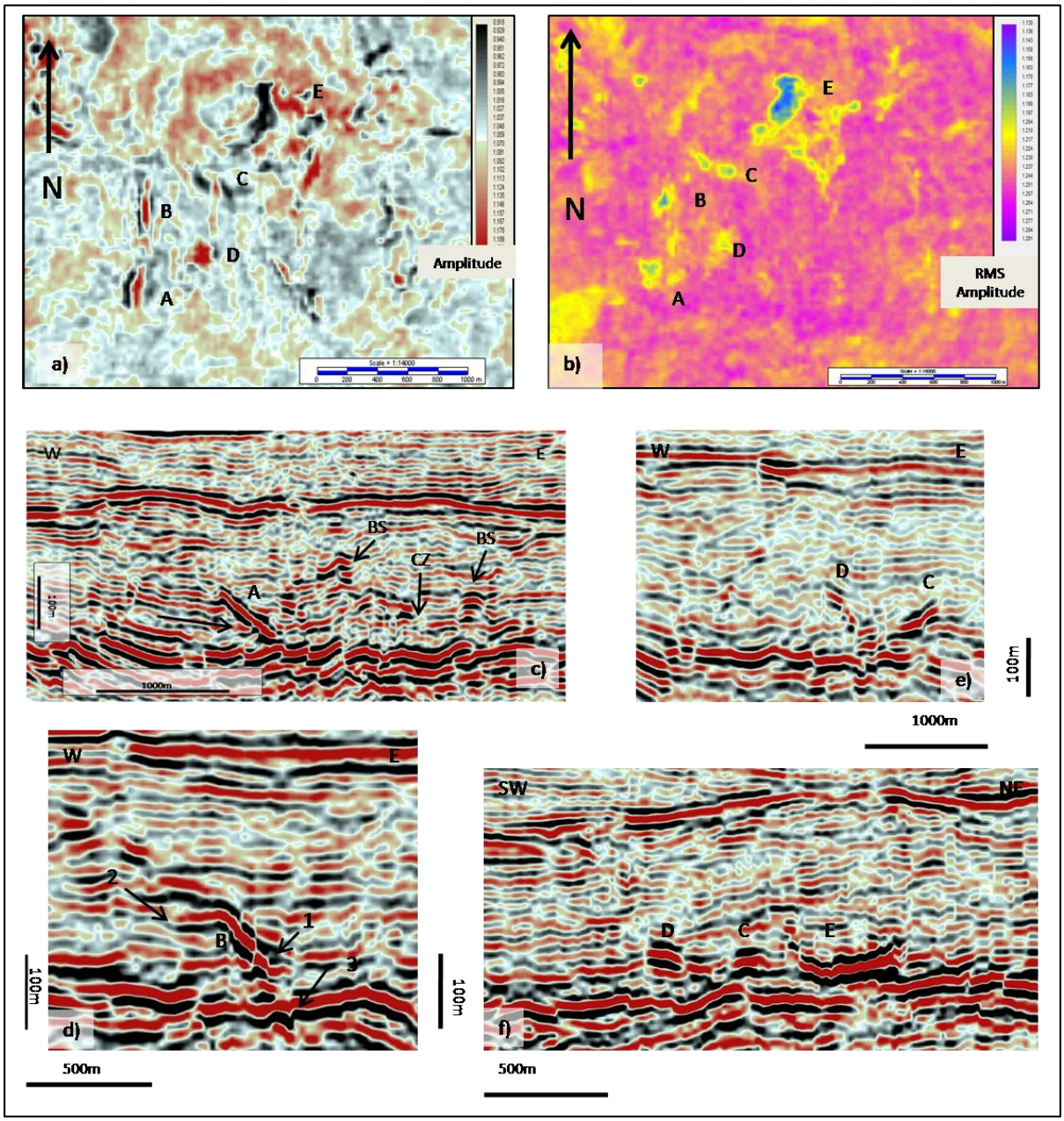

Fig. 5.6 a) a time-slice intersecting several high amplitude reflections and b) an RMS map of the Lowermost Shale displaying the same features (A,B,C,D and E) c) d) e)and f) seismic sections of the high amplitude reflections

5.3.3.3.2. Isolated DHAR

An isolated DHAR can be seen on an RMS map as two separate areas of high amplitude contained within a roughly semi-circular area of medium amplitude (Fig. 5.7a, points 1 and 2). Upon a time slice it is viewed as a semi continuous, curved, red reflection with high amplitude areas which dim along its length (Fig. 5.7c). Either side of the red reflection are areas of high amplitude black reflections. The combined areas of high amplitude have a semi-circular geometry.

Along its east-west profile (Fig. 5.7c, crossline 10916) this DHAR is 380m along its length and cross cuts around 50m of the host unit reflections). At point A it is slightly displaced and dims. Directly above, and to the east, the DHAR is overlain by a zone chaotic reflections. A north-south profile Fig. 5.7d, inline 10554) reveals that the DHAR is connected to a concordant bright reflection (Fig. 5.7). In total the discordant and concordant sections are 500m in combined length. Northwards from the discordant reflection a sub-vertical zone of broken reflection can be seen to project from the tip of the DHAR towards the BUH (Point B).

5.3.3.3.3. Pair of DHAR's

A pair of DHAR's are shown along inline 10920 (Fig. 5.8b), and a time slice at depth 1.264s (Fig. 5.8a). The southern DHAR (DHAR1) is dipping towards the north while the northern DHAR (DHAR2) dips to the south. They are approximately 800m apart and appear to be connected at their bases by a lower amplitude concordant reflection.

DHAR1 is around 450m in length and cross cuts 50m of the background reflections. It dims to the north and is slightly displaced at its base. DHAR2 is 500m from it base to tip and crosscuts over 90m of the background reflections. It also seems broken at its base. The semi-continuous and semi-parallel reflections of the background unit are displaced within the area in between the DHAR's by 50m, as is the BUH horizon. Sub-vertical zones of broken and disrupted reflections can be seen to project from the tips of the DHAR's towards points where the BUH horizon is displaced and broken.

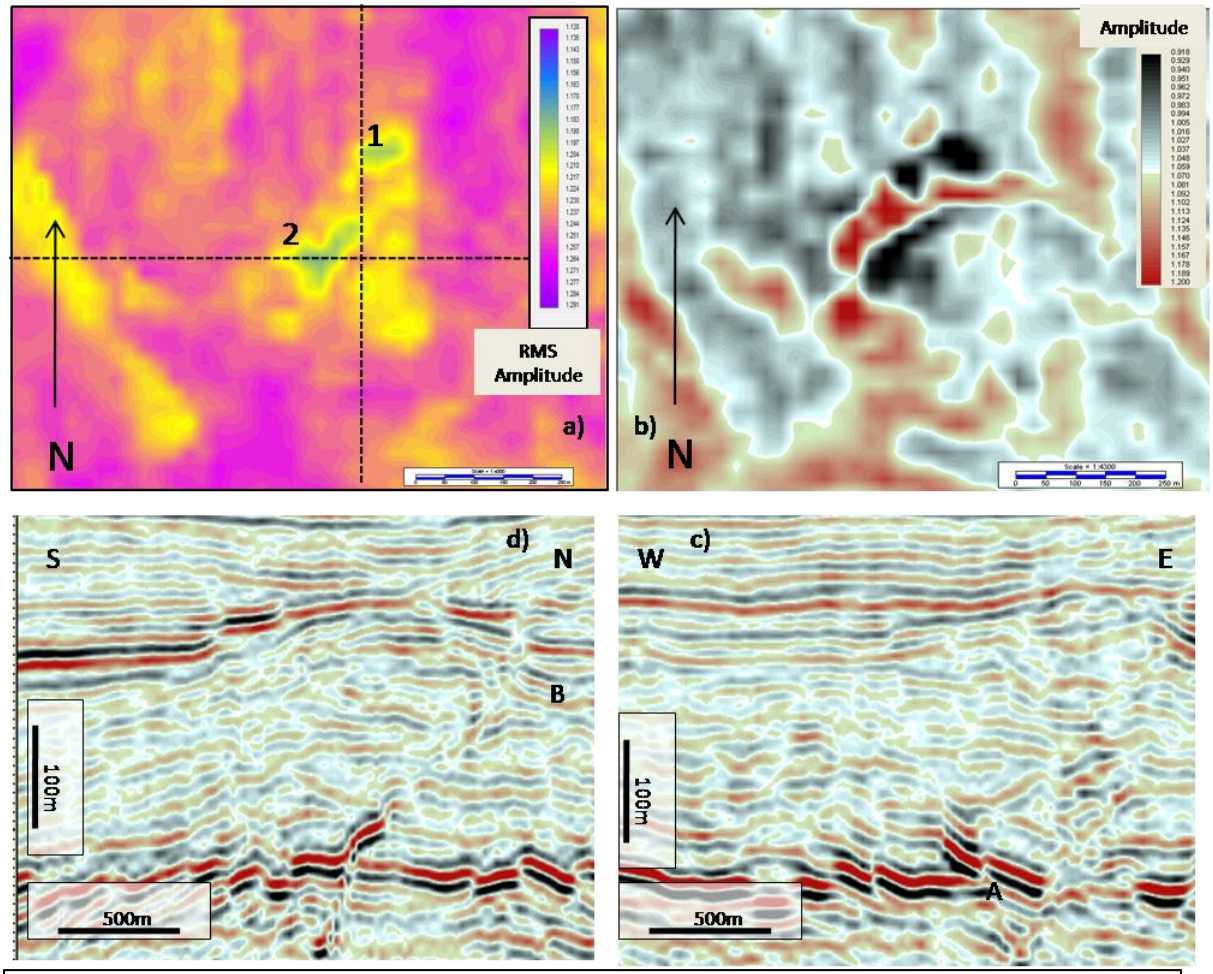

Fig. 5.7 a) An RMS map of the Lowermost Shale with a b) time-slice intersecting the curved high amplitude reflection c) W-E section through the feature and a d) a S-N section, the reflection has a sub-vertical zone of disrupted reflections projecting from its tip to point B.

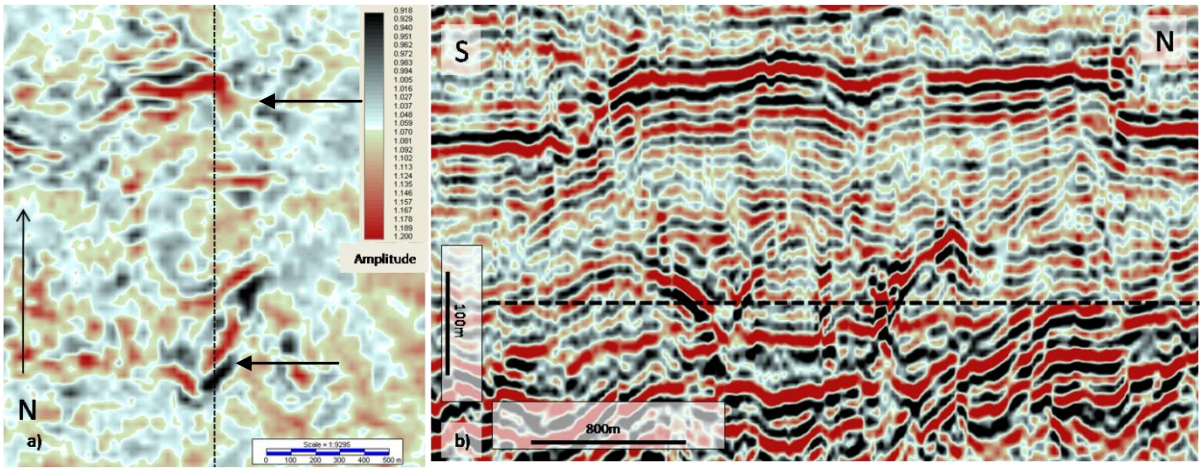

Fig. 5.8 a) a time-slice intersecting a pair of high amplitude reflections (arrowed) with a dominant negative (red) amplitude, considered a hard event b) a S-N seismic profile of the discordant, oppositely dipping reflections.

5.3.3.4. Interpretation

HAR's are the second most commonly seen type of sand intrusion indicators within the study area. They can be distinguished from bright spots on time slices as a concordant pair or single, curved or linear, parallel reflections of opposite polarity. In seismic section they are observed as a couplet or triplet of high amplitude discordant reflections which cross cut the reflections of the host unit. The dominant amplitude of all the DHAR's in the examples is the positive (red) reflection, which is a hard event in this survey, and represents an increase in acoustic impedance. In some cases the discordant reflections are attached to a bright spot, which can be either concordant or discordant reflections. As with the bright spots of section 5.3.2.3 and the amplitude anomalies described in section 4.3.2.1.1 these DHARs are interpreted as partially cemented sand intrusions, and specifically the sand intrusion wings. CHAR are generally flat lying reflections which lie comfortably with the unit reflections; these are interpreted to consist of the flat base of the central section of the intrusion.

5.3.3.5. DHAR with associated bright spot

Several representative examples of high amplitude reflections are presented in Fig. 5.6. High amplitude features A and B are present on parallel cross sections which are 300m apart, they can be observed as discordant high amplitude reflections which dip to the east. Both these examples are interpreted to be sections of the same western wing of an intrusion. High amplitude feature C is also a discordant high amplitude reflection, in this case dipping to the west, and is interpreted to represent the opposite, eastern, wing of the intrusion. Feature C, along with feature D, is present on an arbitrary line (roughly S to NE), the high amplitude refection of feature D turns upwards to the south, while C is turns upwards to the north. These inflections are interpreted to represent the boundary between the horizontal base of the intrusion and the upwards trajectory of the wings. Feature E is present to the north-east as a concave upwards reflection, these are interpreted as the main body of a separate intrusion. The outline of the high amplitude areas on the RMS map crudely follow an elliptical shaped feature which is suggested to represent the outline of a partially imaged, flat based bowl intrusion (Fig. 5.6), with a similar geometry to examples presented by Cartwright et al., (2008).

5.3.3.5.1. Isolated DHAR

This DHAR (Discordant High Amplitude Reflection) appears as a southwest- northeast orientated semi-circle on the time-slice (Fig. 5.7b), and is apparent as an eastward dipping DHAR on a west-east section, and a south dipping DHAR on a north to south section. This asymmetrical feature is interpreted as an intrusion which has either only developed a wing in its north western segment, or which has been partially cemented in this area only (Fig. 5.9).

5.3.3.5.2. Pair of DHAR's

The pair of opposite dipping DHAR's in Figure 5.8b are simply interpreted as two opposite wings of a flat based bowl. The central areas is interpreted as the main sand body, and its thickness mirrors that of the overlying relief of the raised BUH, except at its northern extent, where the intrusion thickness decreases, but the mound retains its relief.

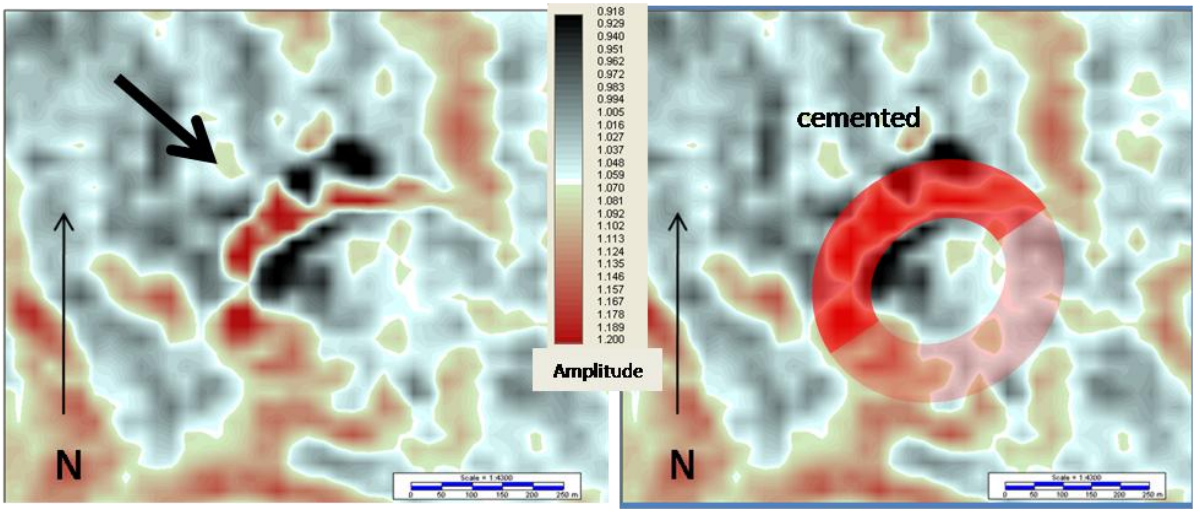

Figure 5.9 interpretation of the semi-circle high amplitude reflection from Figure 5.7. The north-west high amplitude segment represents the cemented sector of the sand intrusion, while the lower amplitude south-eastern segment is not cemented.

5.3.3.6. 'V and U brights'

Bright spots and high amplitude reflections can form composite high amplitude features which take the form of symmetrical or asymmetrical V or U high amplitude reflections - terms that were first defined by Loseth et al., (2003). Examples of various forms of these combinations are presented below.

5.3.3.6.1. Small V bright

This V bright is located within the south east cluster area, it is visible on inline 11006 (Fig. 5.10a) and on a time slice at a depth of 1.344 s (Fig. 5.10b). On the time slice it is imaged as a central elongated area of negative high amplitude surrounded by a circular ring of positive high amplitude. Along a north-south seismic profile its brightest sections can be seen as two v shaped reflections of contrasting polarity, with a red, positive, reflection overlying the black, negative, reflection. The distance from tip to tip along the seismic section is equal to the diameter of the outer circle on the time slice (330 m).

5.3.3.6.2. Asymmetrical V bright

Located within the north east cluster area, an asymmetrical V bright is located along inline 11595 (Fig. 5.10c). A seismic section along its north-south profile reveals a high amplitude northern limb and a low amplitude southern limb. The well developed, brighter, limb consists of an upper and lower high amplitude positive reflection, with a middle negative reflection. The middle, negative, reflection is the dominant amplitude in this case. The bright section of the limb is 765 m in length from base to tip, it vertically cross cuts 60 m of the host reflections, and its dip decreases towards its base. The dimmed section is around 500 m in length, and the distance from tip to tip exceeds 1.3 km. The whole reflection is overlain by a zone chaotic reflections, and the BUH is broken and displaced. To the north of the V bright the host unit reflections are semi-continuous and semi-parallel.

5.3.3.6.3. V bright

An example of an irregular V bright is shown on a west to east seismic section (Fig. 5.10e). In seismic section it has a distinct zigzagged outline, with a roughly V shaped geometry, and consists of two

irregular 'wings' which meet at a sharp, central apex. Flank tips are 920 m apart, and the distance from the base of the apex to the top of the tips is around 100m. The V shape is slightly asymmetrical, with the eastern flank longer (600 m) than its western counterpart (433 m). The base of the apex seems to be embedded in the lower boundary of the unit, and may be considered the intrusion 'breakthrough' point. A slight upwards displacement (25 m) of the semi-continuous, semi-parallel host unit reflections can be seen, they are present above the V bright, and the BUH is displaced by a similar amount. Three areas of bright red reflections can be seen on the time slice (Fig. 5.10f), they form a roughly elliptical outline of high amplitude features connected by lower amplitude areas.

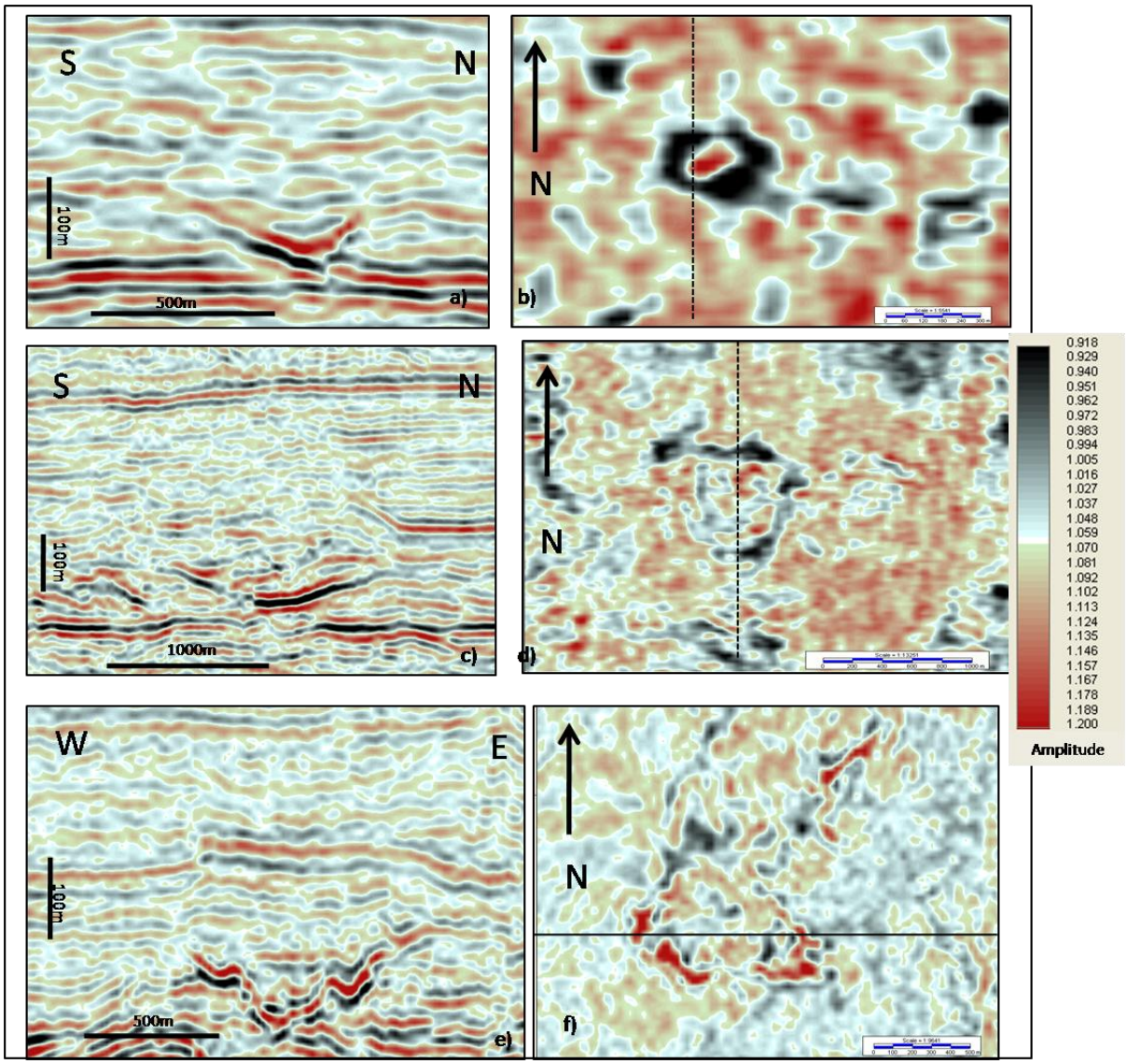

Figure 5.10 examples the best representation of 'V' and' U' brights from the study area a) and b) a small scale 'V' bright c and d) asymmetric 'V' bright, preferentially developed to the north e and f) an irregular saw toothed 'V' bright

5.3.3.7. Interpretation

V or U brights are the atypical seismic expression of sand intrusions in the area studies, though they were originally described in areas proximal to the study area (Molyneux et al., 2002; Hurst et al., 2002; Shoulders et al., 2007; Cartwright, 2010; Szarawarska et al., 2010; Løseth et al., 2012). They represent fully imaged flat based bowls and the conical cone end members of the sand intrusions suite (Cartwright et al., 2008). They are the least common form of amplitude anomalies within this data set, and where present they are often only partially imaged. The examples presented are the closest to fully imaged intrusions within the data set, their identification is often retrospective, as they are only fully appreciated as intrusions in conjunction with the overlying mounds of the BUH.

5.3.4. Base Utsira Horizon

A time depth map of the Base Utsira Horizon (BUH) clearly shows areas of topographic relief. For the purpose of this study these areas have been sub-divided into the North-West Cluster Area (NWCA), the North-East Cluster Area (NECA), the South-West Cluster Area (SWCA) (Fig. 5.11a). Within the clustered areas it is occasionally difficult to distinguish between mounds due to their proximity to each other. Several mounds which appear as single large mounds may be separated into individuals. The use of contouring is therefore advantageous in identifying individual mound boundaries. Areas of topographic relief are not exclusive to these cluster areas, with smaller outlying raised areas, generally elliptical in plan view, also present.

The large cluster areas can be seen to consist of smaller, individual ellipse shaped areas of topographic highs. The areal extent of each ellipse is defined by the point at where the dip of horizontal BUH changes (Fig. 5.11b). These points are termed 'hinge points' and may be imaged on a dip map of the BUH, where the darker outlines represent increase in horizon dip. The maximum relief of a mound is measured by creating an arbitrary line connecting the 'hinge points' and measuring upwards to the displaced reflection. Forty nine individual mounds have been mapped within the study area (Fig. 5.12, 5.13, 5.14 5.15).

Representative examples of a mound cluster area and an individual mound are described below.

5.3.4.1. North-West Cluster Area (NWCA)

The NWCA consists of 16 individual mappable mounds covering an area of 45 km^2. North-south and east-west seismic sections across the area show the raised section of the BUH to extend 5 km and 12 km respectively (Fig. 5.16a and b). The depth of the undisturbed area to the east is 1100 m (1.1s TWT) and 1075 m (1.075s TWT) to the north, and sections of the raised BUH can be seen to exceed 90m of topographic relief above the unaffected depths.

Along both transects, examples of amplitude anomalies are commonly seen to underlie the raised BUH, they are not present within the undisturbed section. This is also apparent by overlaying a contour map of the NWCA over an RMS extraction map of the area (Fig. 5.16c). The majority of the high amplitude features are located within the boundary of the NWCA. Examples of these high amplitude areas have been presented in section 5.4.2 and they have been interpreted as sand intrusions.

A coherency slice at a horizon below the mounds is shown in Figure 5.16c. It demonstrates that there is a decrease in coherency (white areas) of the reflections at this level below the mounds. The decrease in coherency corresponds well with the contour of the mounds (Fig. 5.16c). The darker areas denote greater coherency of reflections, and correspond with the areas surrounding the mound cluster.

Mounds 39 and 41, located within the NWCA, are presented in Fig. 5.17a. They are separated by a low area which is around 440m across. At 90m high, Mound 41 has the greatest relief of all the mounds in the NWCA, while Mound 39 has the second largest at 85m. Both are similar in area, Mound 39 is 3.84km^2 in extent and Mound 41 is 3.90km^2.

The internal reflections of both the underlying Lowermost Shale and the Utsira Sand change considerably in close proximity to the mounds. The reflections of the Lowermost Shale below the mounds consist of an upper section of mounded, semi-continuous, semi-parallel reflections (Point MR), and a lower, domed shape section (Fig. 5.17c, Point CD), which is chaotic in nature. Sub-vertical zones of broken reflections propagate upwards from the chaotic area to the base of the mounds (Point BR).

At the southern flank of mound 39 the internal reflections of the Utsira Sand can be sub-divided into three sections (Fig. 5.17b). The first 2 reflections are horizontal and onlap the flank of the mound. The next 3 reflections downlap onto the mound, while the upper reflections of the unit mirrors the undulating upper boundary, and drape over the mound. The low area between the mounds is also infilled by onlapping reflections. The raised sections of the mounds coincide areas with sections where the TUH hangs, this relationship will be further described in section 5.4.4.

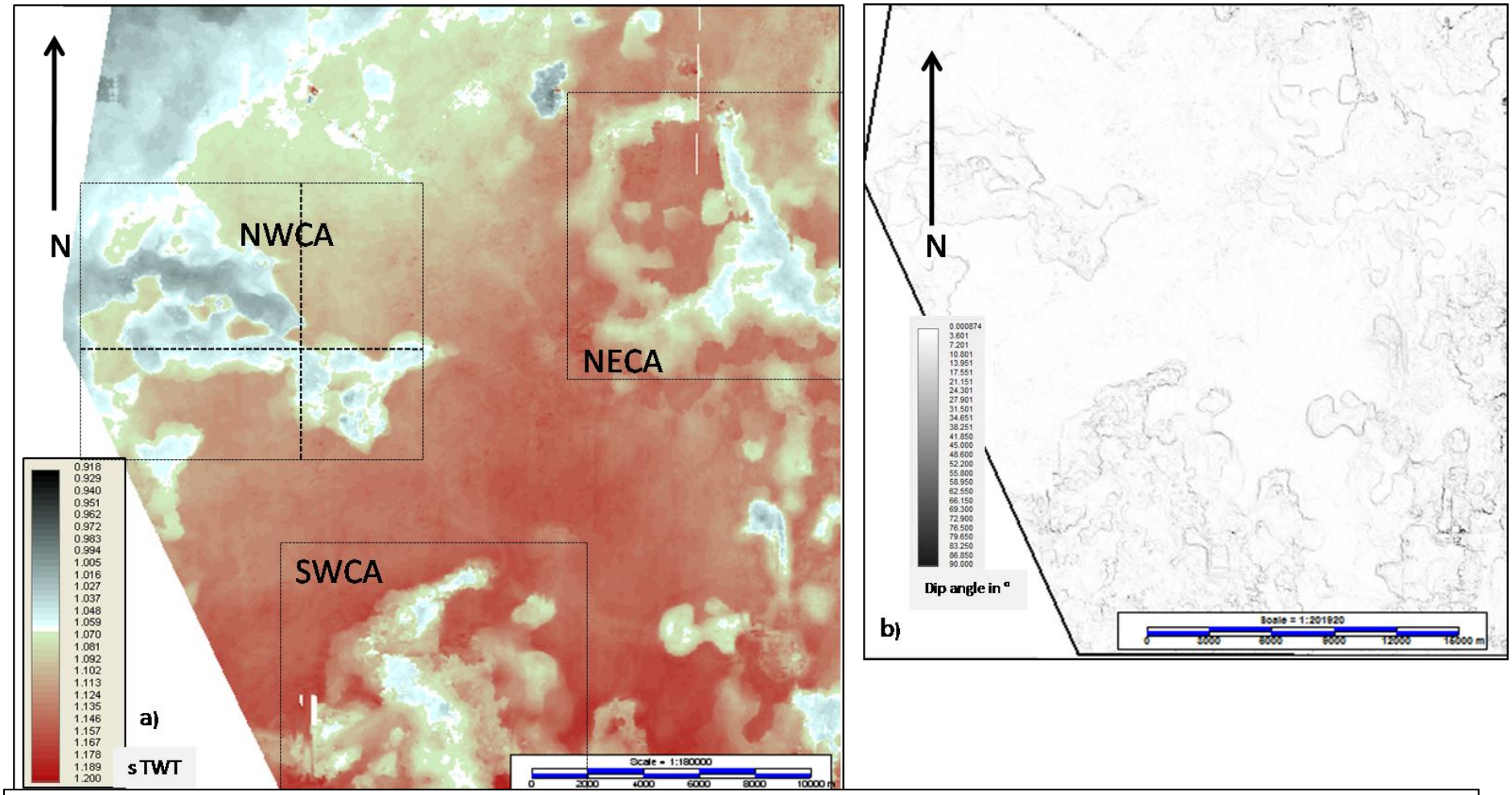

Figure 5.11 a) TWT map of the Base Utsira Horizon displaying several concentrated areas of high relief, the North West Cluster Area (NWCA), North East Cluster Area (NECA) and the South West Cluster Area (SWCA) b) a time-dip map of the Base Utsira Horizon, with areas of increased gradient denoted by black lines, these areas coincide with the outlines of the mounds.

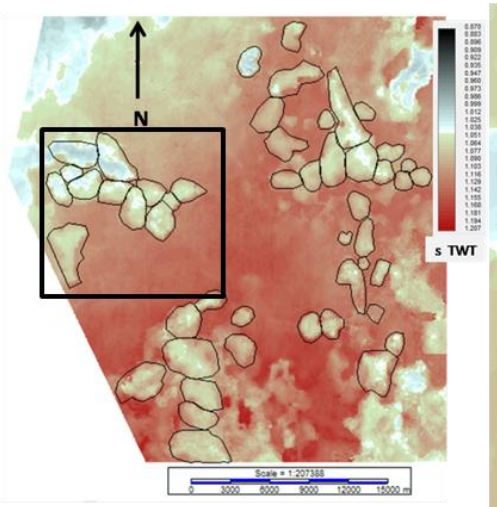

Fig. 5.12 Individual mounds located within the North West Cluster Area

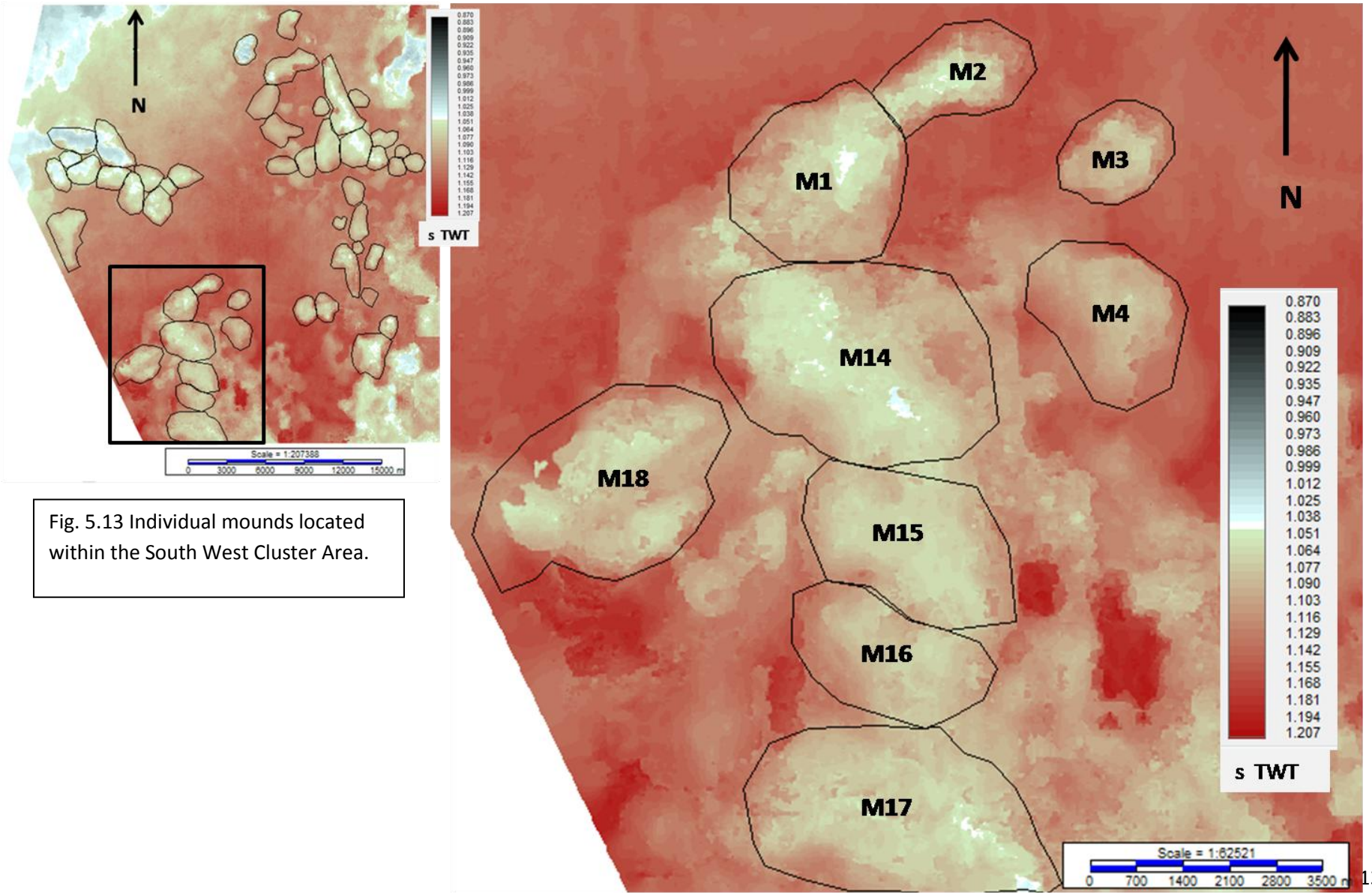

Fig. 5.13 Individual mounds located within the South West Cluster Area.

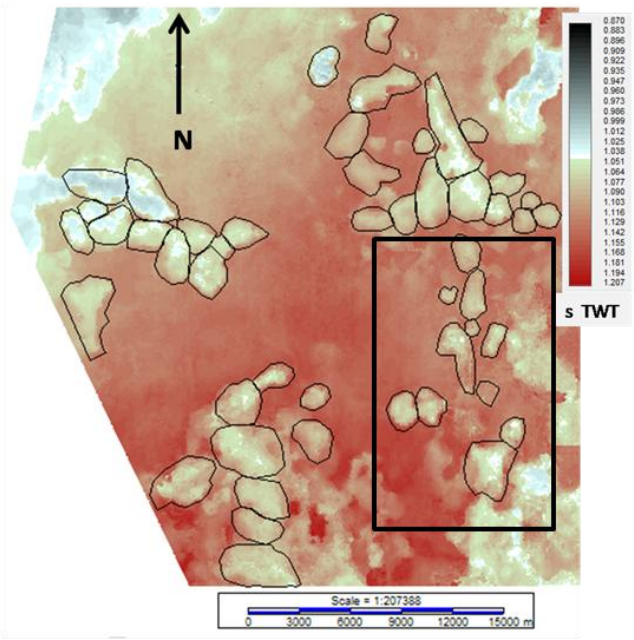

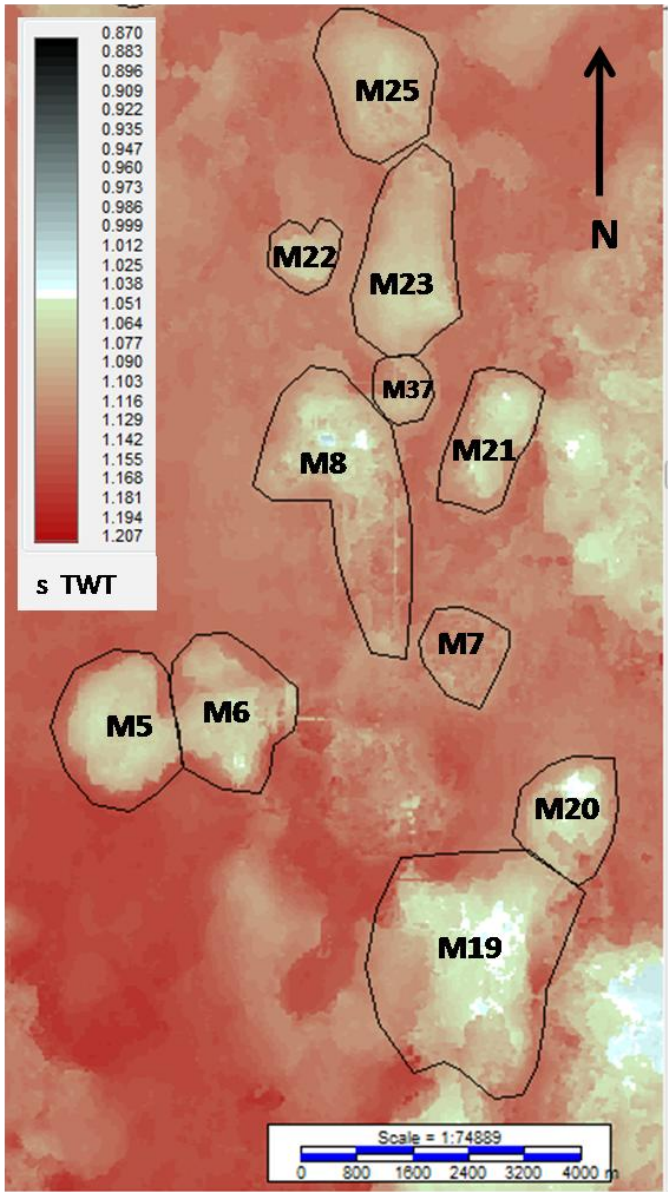

Fig. 5.14 Individual mounds located to the south of the North East Cluster Area.

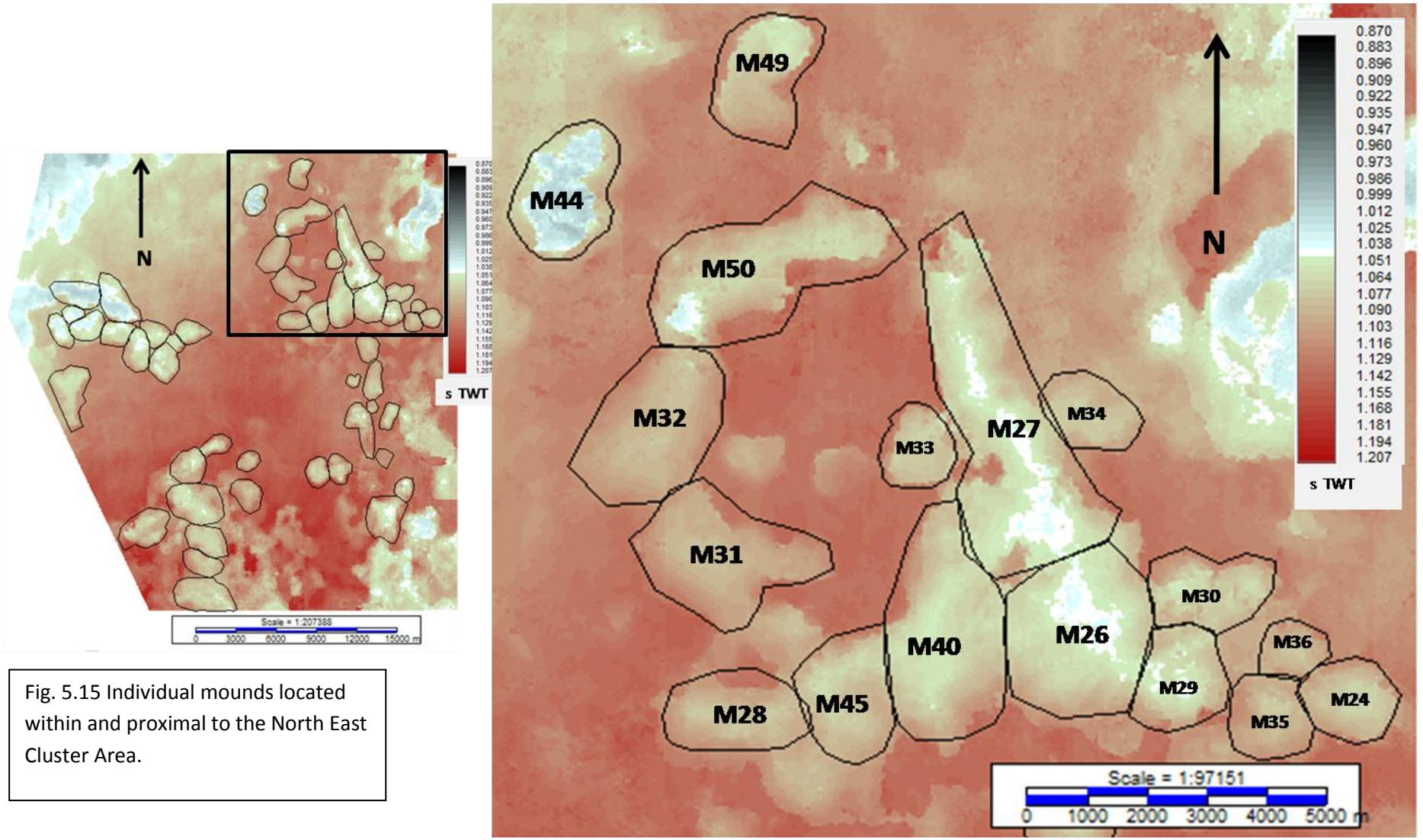

Fig. 5.15 Individual mounds located within and proximal to the North East Cluster Area.

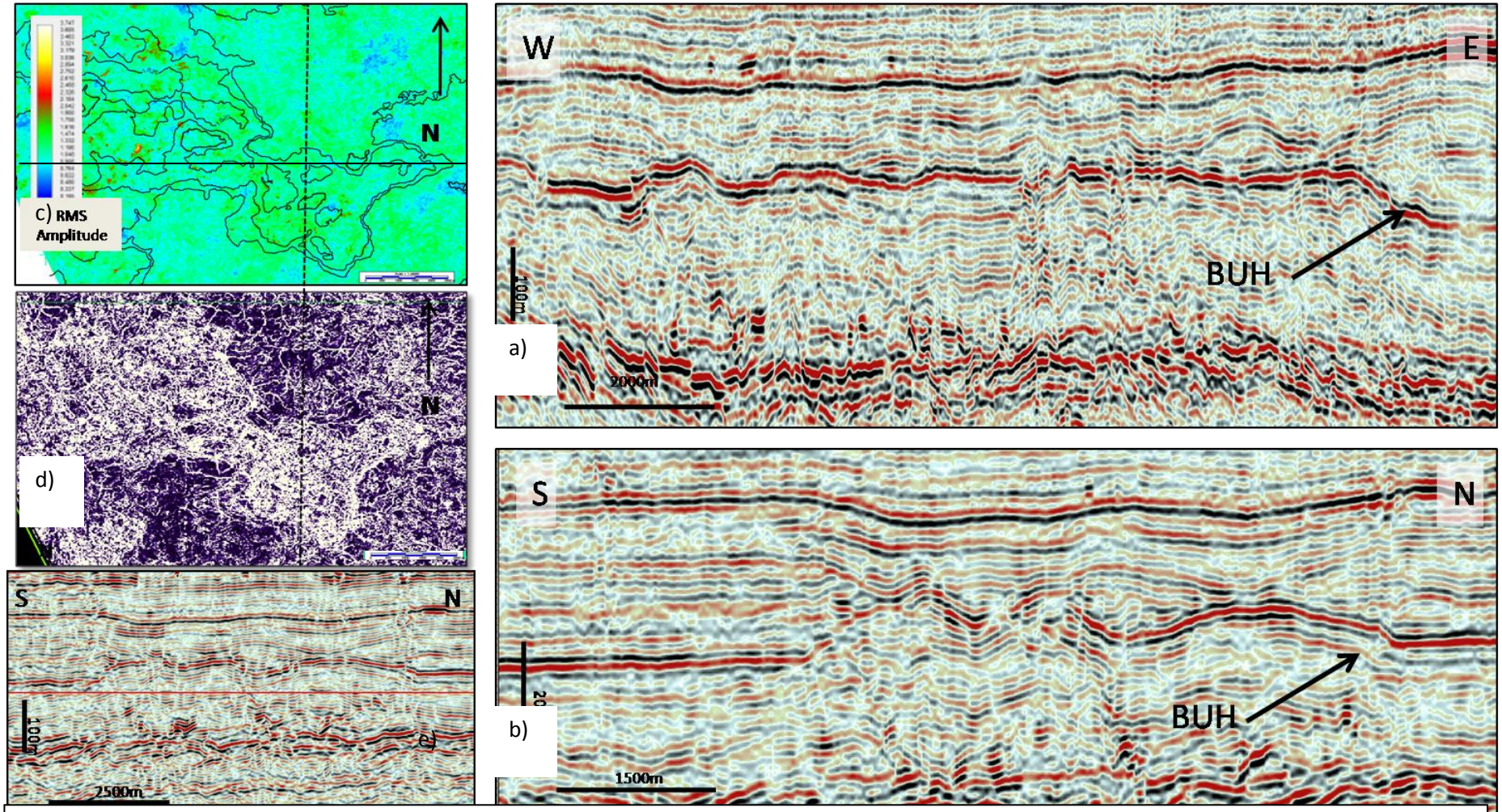

Figure 5.16 a) a W-E seismic section through the NWCA, line location denoted by dashed line b) a S-N seismic section through the NWCA, line location denoted by solid line c) an RMS map of the Lowermost Shale overlain by the NWCA contour, showing a concentration of high amplitude within the contour boundary d) a coherency slice (depth in red, Figure e) with greater coherency outside the NWCA contour.

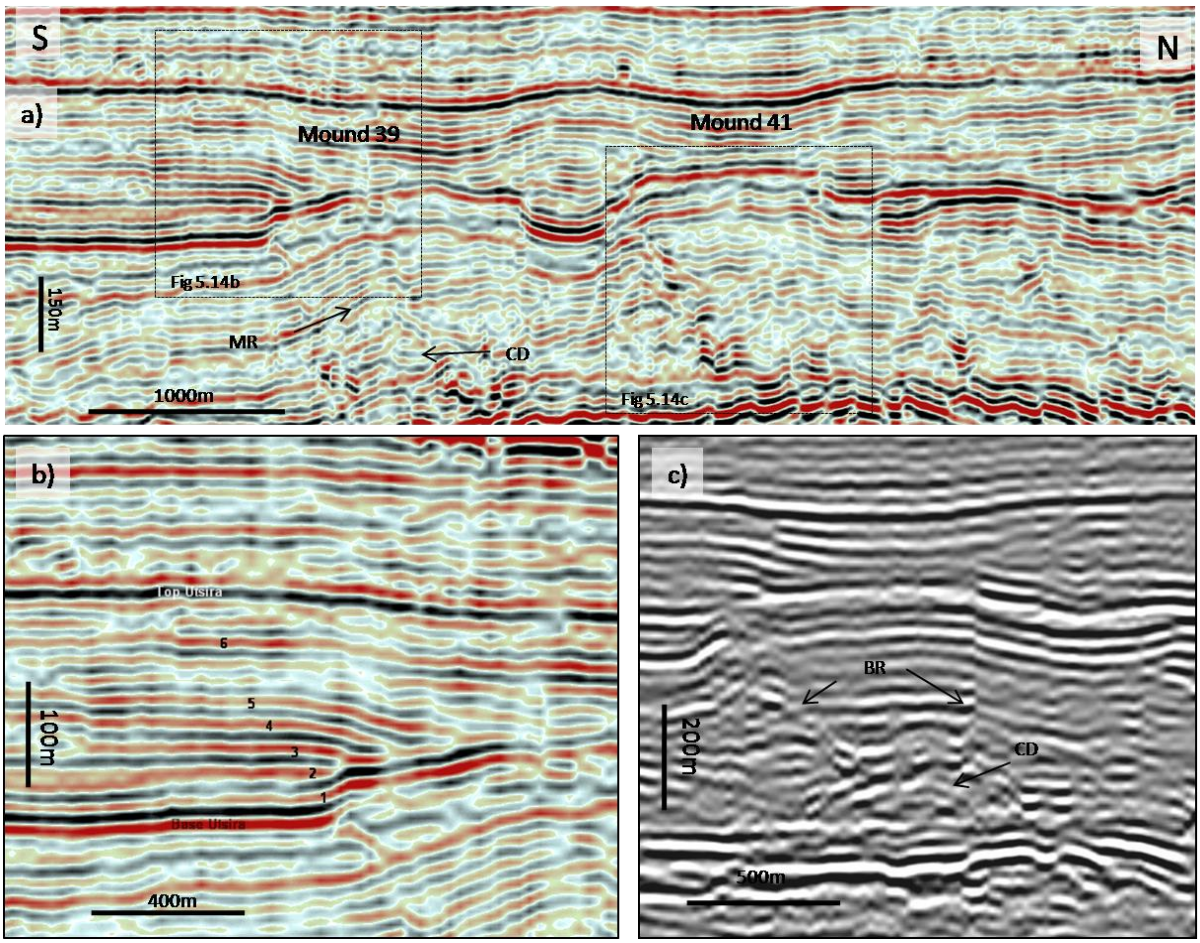

Figure 5.17 a) a seismic section through mounds 39 and 41, mound 39 is underlain by mounded reflections (MR) and a chaotic dome (CD) b) the internal geometry of the Utsira reflections, showing onlap (reflections 1 and 2) and downlap (reflections 3, 4, 5) onto the mound, reflection 6 drapes over the mound c) Mound 41 is also underlain by a chaotic dome (CD) and broken reflections (BR) project upwards from the dome to the Base Utsira Horizon

5.3.4.2. Individual mound

The contoured time-depth outline of an individual mound is rendered over an RMS map of the Lowermost Shale (Fig. 5.18a). The mound covers a total area of over 2km^2, and has a long axis of 2.1km which is orientated north-east south-west. Several areas of high amplitude are contained within the outline contour of the mound, with the majority of the high amplitude features concentrated in the north-east and southern section. An underlying irregular V bright described in section 5.3.2.3, is seen to underlie the mound (Fig. 5.18d).

The north- south profile of the fold is asymmetrical (Fig. 5.18b), with a gradual increase in relief towards the north. The maximum relief of the mound, 60m, is achieved to the north of the mound centre (Point A). The upper reflections of the Lowermost Shale mirror the mound profile, and the lowermost internal UtsiraSand reflections onlap onto the flank of the mound from the north (Point B).

A similar asymmetry is shown across the east-west profile (Fig. 5.18d), with the greater relief located at the western extent of the mound (Point C). Immediately after the point of maximum relief the BUH is broken and detached and the mound relief decreases abruptly. The mound overlies an irregular V bright. Within the central area, bounded by the irregular wings, the reflections appear chaotic, while the first reflection below the BUH mirrors the mound profile.

An arbitrary line (Fig. 5.18c), SE-NW, intercepts two areas of high reflectivity, which are shown to be a pair of opposite dipping discordant high amplitude reflections. An abrupt decrease of mound relief is also seen at the north-west corner of the mound (Point D).

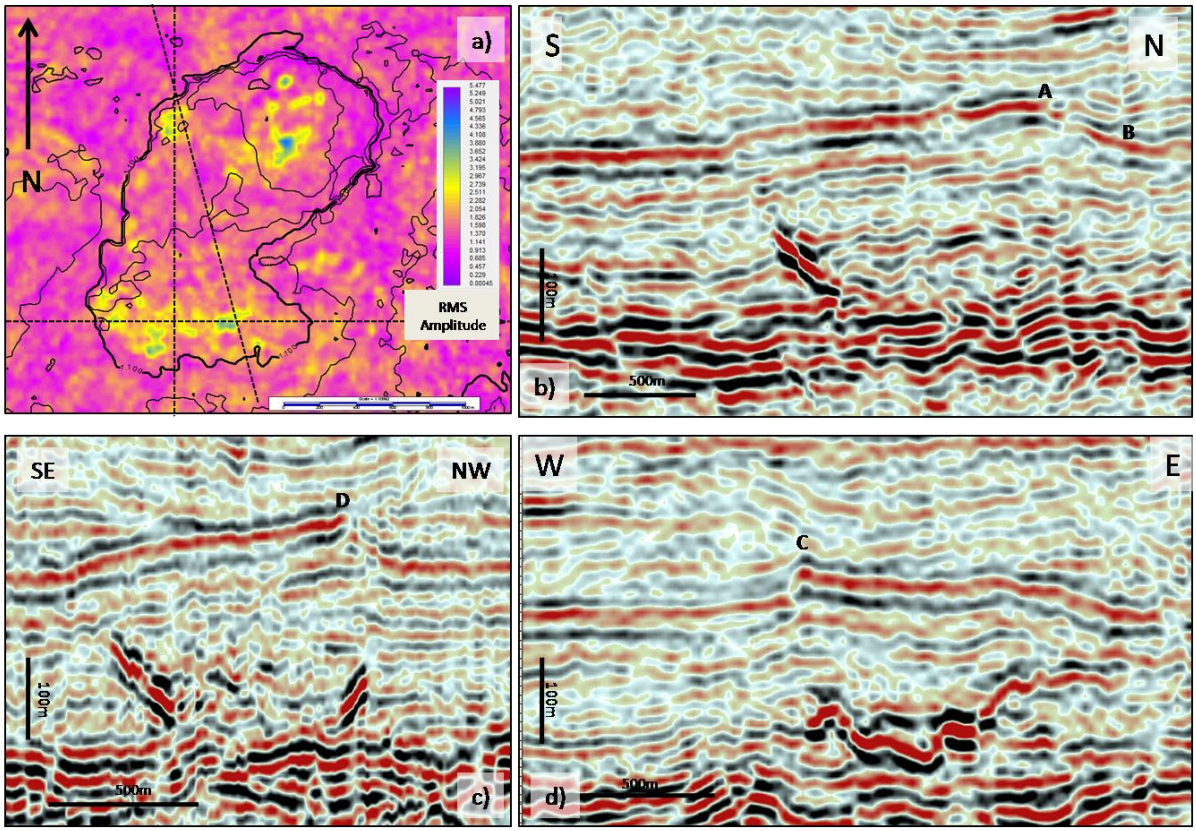

Fig. 5.18 a) time-depth contour of a mound is rendered over a RMS map of the Lowermost Shale b) a S-N seismic section c) a W-E seismic section d) a SE-NW seismic section display the high amplitude reflections underlying the mound

5.3.4.3. Interpretation

5.3.4.3.1. Cause of mounds and mound clustering

The spatial correspondence between the mounds affecting the BUH and underlying amplitude anomalies, interpreted as sand intrusions in section 5.4.2, indicate that a causative relationship exists between the mounds and the sand intrusions, as suggested by Shoulders and Cartwright (2004). The elliptical mounds described in chapter 4 are interpreted as the product of force folding of the paleo-seafloor resulting from the hydraulic ‘jack up' during the emplacement of sand intrusions. The mounds described within this chapter are of similar dimension and geometry as those described in Chapter 4, they also display a similar spatial correspondence with the underlying amplitude anomalies. The mounds described in this chapter are therefore also interpreted as the product of force folding of the paleo-seafloor.

The spatial clustering of sand intrusions is described as 'not uncommon' by Cartwright (2008), and is also noted by Huuse and Michelsen (2004). We suggest that the concentration of the majority of the mounds within the four cluster areas recognised in the study area is therefore due to the spatial clustering of the underlying sand intrusions (Fig. 5.19a). While the presence of individual, outlining mounds, are due to individual sand intrusions (Fig. 5.19c).

5.3.4.3.2. Mound timing

The relationship between the Utsira Sand reflections and the mound can be used as indicators of the timing of mound development. Shoulders and Cartwright (2004) use the presence of onlapping reflections to indirectly date the formation of the mounds. The Utsira Sand has been dated as late Miocene to early Pliocene (Eidvin and Rundberg, 2005), and therefore the mounds must pre-date the lower onlapping reflections of the late-Miocene (Fig. 5.17b). The intrusions which created the mounds are hosted by the mid-Miocene Lowermost Shale unit, and the mounds must post-date this period, therefore mound formation can be inferred to have taken place during the late Miocene.

5.3.4.3.3. Mound dimensions and geometry

Forced folds are defined as 'folds in which the final overall shape and trend are dominated by the shape of some forcing member below,' (Stearns, 1978), and Cartwright et al (2008) suggest that forced fold relief is roughly proportional to sand intrusion aperture. We therefore suggest that the aperture, dimensions, and geometry of the underlying intrusions are the controlling factor on the respective features of the mounds. Changes in mound relief observed along the mound profile are a reflection of changes in the intrusion aperture, while mounds with asymmetrical profiles are the result of asymmetrical intrusions. Broad, low aperture, saucer like intrusions with a greater distance between wing tips would result in wide, low relief mounds. Narrower, wedge shaped, apical cones would result in narrow, high relief mounds.

5.3.4.3.4. Cluster mounds

A north-south section through the North West Cluster area shows three closely spaced mounds (Fig. 5.19a). The profile of the two southernmost mounds are coarse semi-circles in seismic section, and they are underlain by two mound like zones of chaotic reflections (Fig. 5.19a, Points A and B), with

sub-vertical off shoots of broken reflections. A high amplitude V shape is located below the third mound (Point C). We interpret these features as sand intrusions. A and B represent the main body of sand while the sub-vertical zones are the intrusion wings. Sub-vertical disrupted zones emanating from the centre of the sand bodies may be central off-shoots of sand, or even seismic evidence of de-watering features (Fig. 5.19a, Arrows). The V bright at point C is interpreted to be a smaller, apical cone intrusion. The geometry and relief of the mounds overlying features A and B roughly match those of the dome like sandbodies, while the smaller relief mound overlying C reflects the smaller aperture of the interpreted intrusion.

5.3.4.3.5. Individual mound

Three transects through the individual mound are interpreted (Fig.5.19c, d and e). The interpreted aperture of the individual intrusion roughly matches the relief of the mound. The symmetrical profile of the mound may be explained by an asymmetrical sand intrusion, where the greatest aperture is concentrated within north-west section of the aperture, below the greatest relief (Fig. 5.19b). The greatest aperture along the west-east section is located within the west of the intrusion, and this is reflected in the mound profile. A thin finger of sand to the east of the intrusion corresponds with the gradual decrease in mound relief (Fig. 5.19c). Aperture along south-north profile also roughly corresponds with mound relief (Fig. 5.19d).

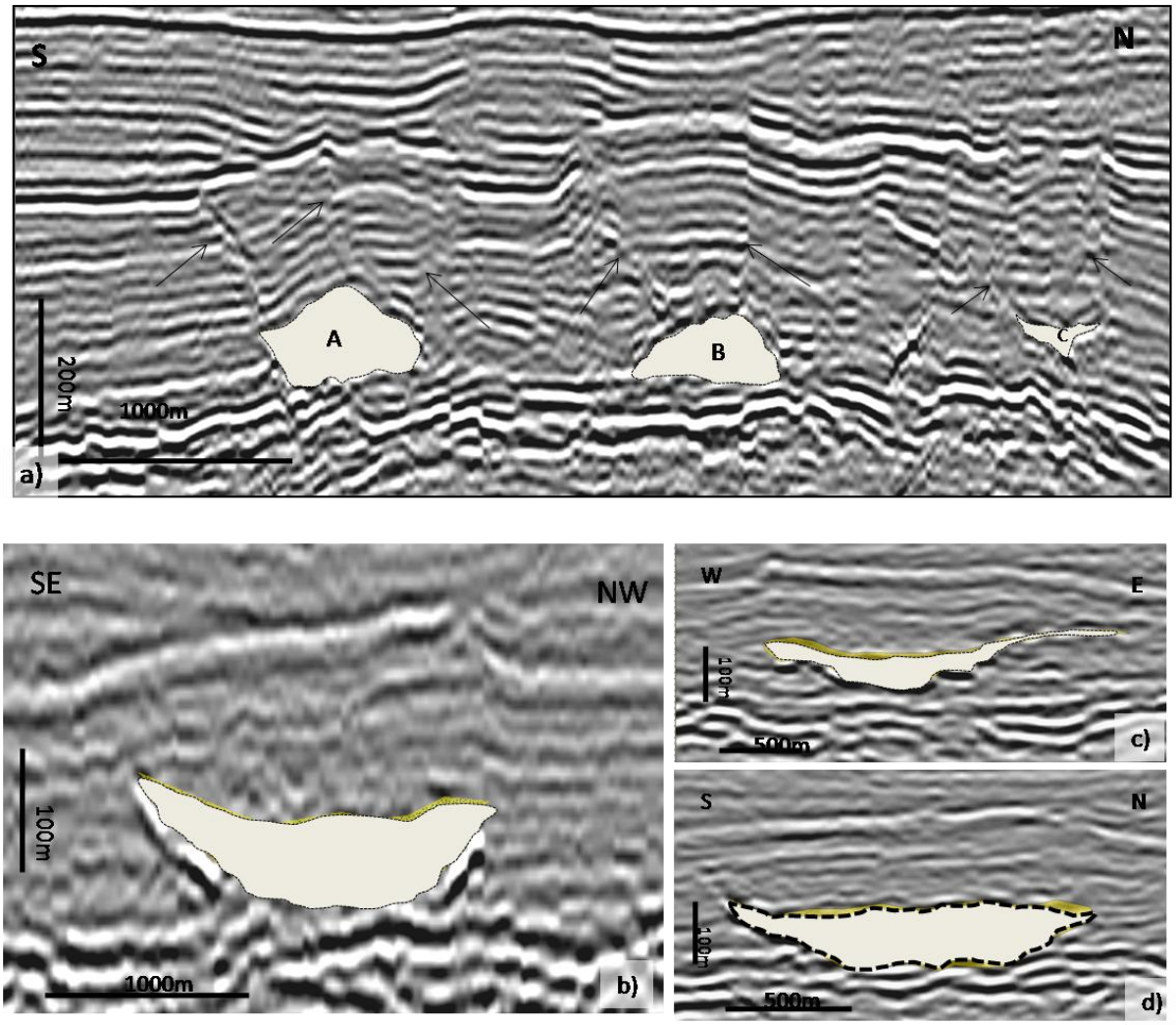

Fig. 5.19 interpreted sand bodies underlying a) Mounds 39 and 41 from Fig. 5.17 b) c) and d) sand body underlying mound from Fig. 5.18

5.3.5. Top Utsira Horizon (TUH)

5.3.5.1. Localised thinning

The undulating nature of the Top Utsira Horizon (TUH) is a clearly observed feature on seismic sections within the study area. A TWT of this horizon shows areas of greatest depth in green (Fig. 5.16b). On an isopach map of the Utsira Sand, areas of considerable thinning can be seen to coincide where the mounds and the low areas of the TUH are located (Fig. 5.20a). The combined effects of the elliptical mounds and the elliptical depressions are significant. The maximum thickness, achieved within the central, undisturbed, area of the data set is around 300m (dark areas). Within the affected area, the areas of mound clusters, this is reduced to just over 50 m (red areas). Individual examples which highlight this relationship between mounds and depressions are presented in section 5.4.4.1

5.3.5.2. Depressions

Where possible, measurements of the area, dimensions, and negative relief of the depressions were taken. The negative relief of the elliptical depressions was measured using a similar method to that used to calculate the positive relief of the mound (Fig. 5.21a). A datum was created using a projected line to connect the points at which the TUH downturns. The maximum vertical distance was then measured perpendicular from this datum line to the lowest point of the reflection.

5.3.5.2.1. Individual depression

Mound 3 is located within the SWCA, it has a relatively symmetrical mound profile, a maximum positive relief of 72 m (Fig. 5.21a)., and covers an area of 1.8 km2. Its long axis is 1.93 km, a short axis of 1.43 m, and has an eccentricity value calculated at 0.67 (Fig. 5.21b). The overlying section of the TUH is depressed and has a maximum vertical displacement of 35 m (Fig. 5.21a). It affects an area of 2.81 km^2, has an eccentricity of 0.64, and a long axis and short axis of 2.21 km and 1.2 km respectively (Fig. 5.21c). The depressed section is larger in both axial distances and in area, the eccentricity is similar, and the negative relief is less than the positive relief of the mound. This is true for all the mounds and their corresponding depressions.

A north to south profile (Fig. 5.21a, inline 11152) across the mound clearly shows the overlying depression and a change affecting the internal geometry of the Utsira Sand. Mound 4 is visible at the left hand side of mound 3 and the low area in between is infilled by reflections which onlap at the flanks of both mounds (Fig. 5.21a, points A and B). Onlapping reflections are also present at the north flank of mound 3 (Fig. 5.21a, point C). Data quality is variable within this section, however the next reflection can be seen to downlap and terminate against the mounds, and the remaining reflections drape downwards and mirror the TUH.

At point D (Fig. 5.21a) the BUH appears broken and a sub-vertical section of disrupted reflections can be seen to extend upwards towards the TUH, and downwards to the BHS. An amplitude anomaly is visible within the Lower Seal, obliquely above the southern flank of Mound 3.

5.3.5.2.2. Conjoined depressions

Mounds 5 and 6 are mapped as individual mounds that are connected by a 'bridge'(Fig. 5.22c). They have areas of 3.24 and 3.09 km^2 respectively, and mound 5 shows a relief of 97 m while Mound 6 is 81 m high. Due to their proximity to each other the hanging effect on the TUH is accentuated and the depressed area is seen as a single elliptical depression on the TWT map (Fig. 5.22c). The total area affected by the depression is 7.82 km^2, and its negative vertical displacement is 35 m. An east-west section across the area is of variable quality (Fig. 5.22a). The BUH is reasonably well imaged along the extent of Mound 6, however it is broken and of low amplitude across Mound 5. The downturn of the TUH can be seen at points A and B.

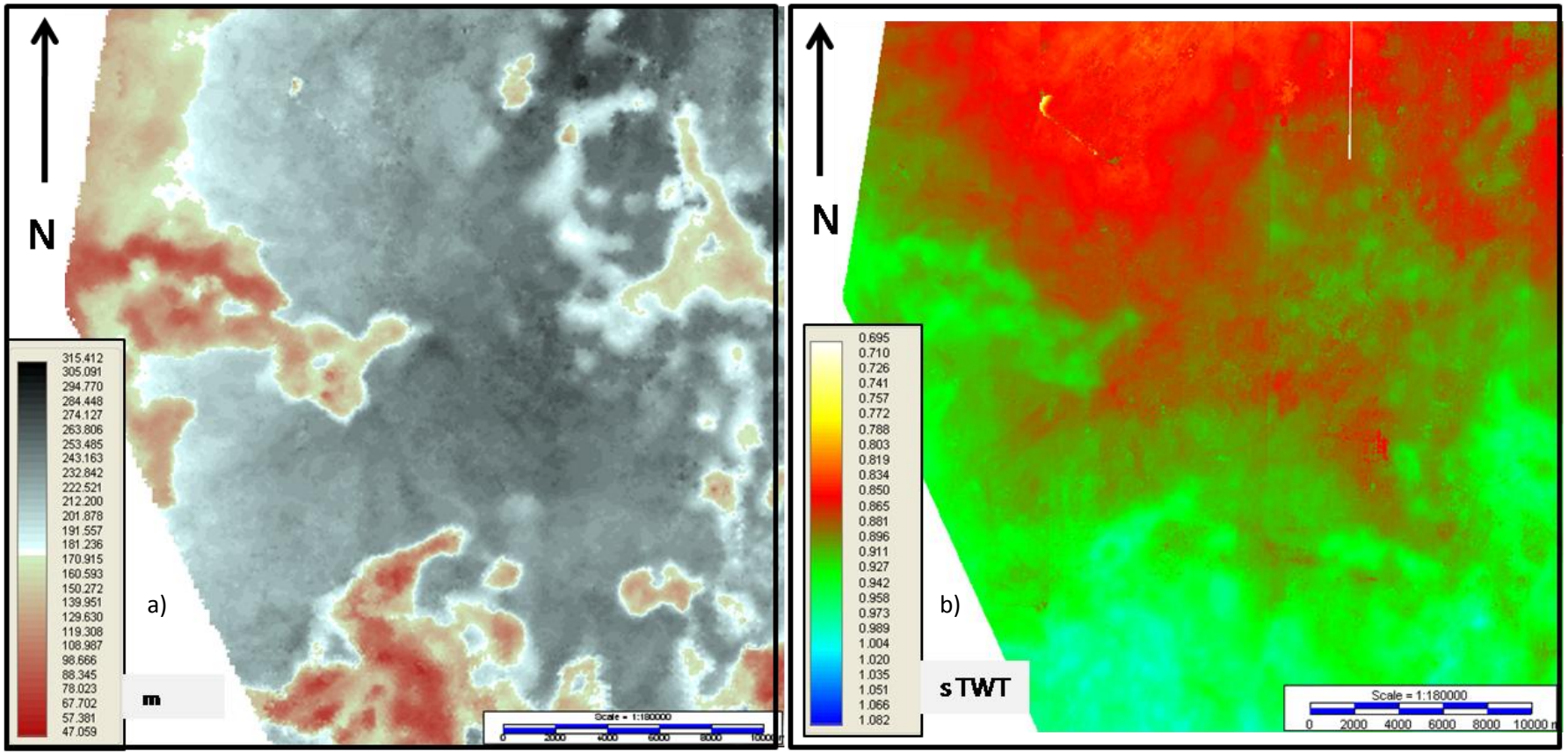

Figure 5.20 a) Isopach map of the Utsira Sand, showing areas of thinning which coincide with mound locations b) TWT map of the Top Utsira Sand demonstrating the subtle changes in topography in comparison with the Base Utsira (Figure 5.1).

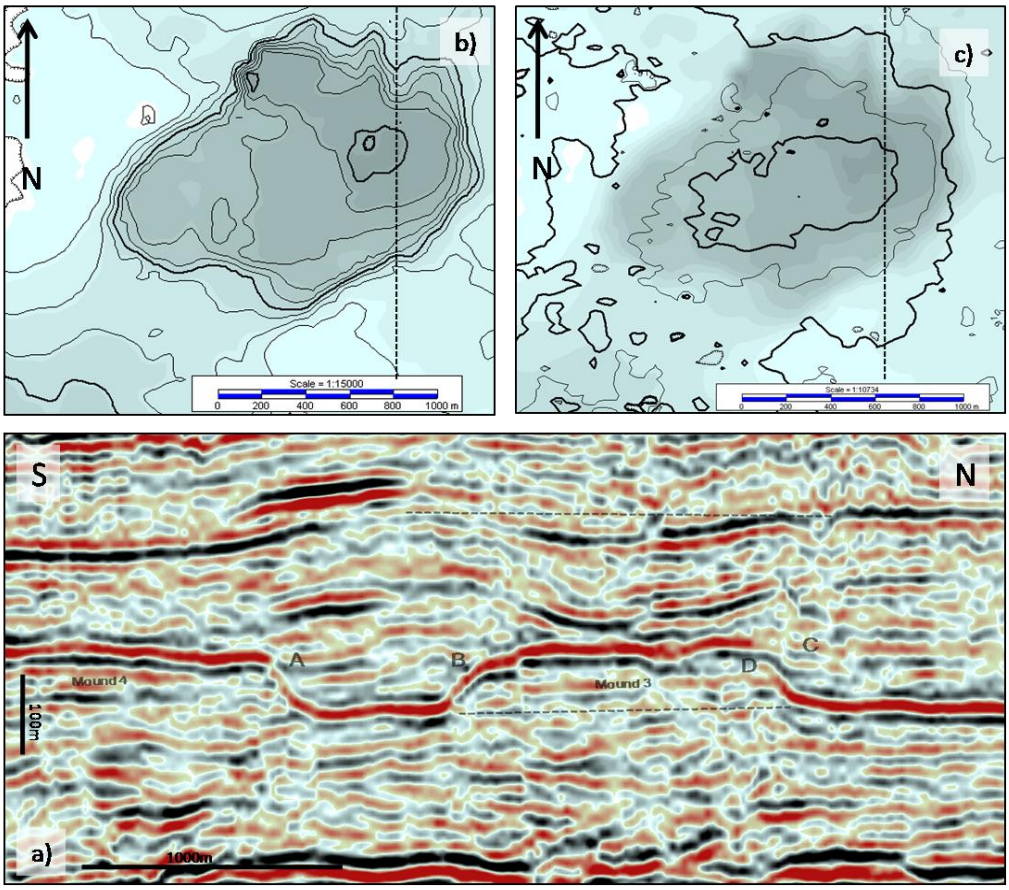

Figure 5.21 a) a S-N seismic section through Mound 3 b) contoured time-depth map of Mound 3 c) time-depth contour of the depression rendered over time-depth map of Mound 3.

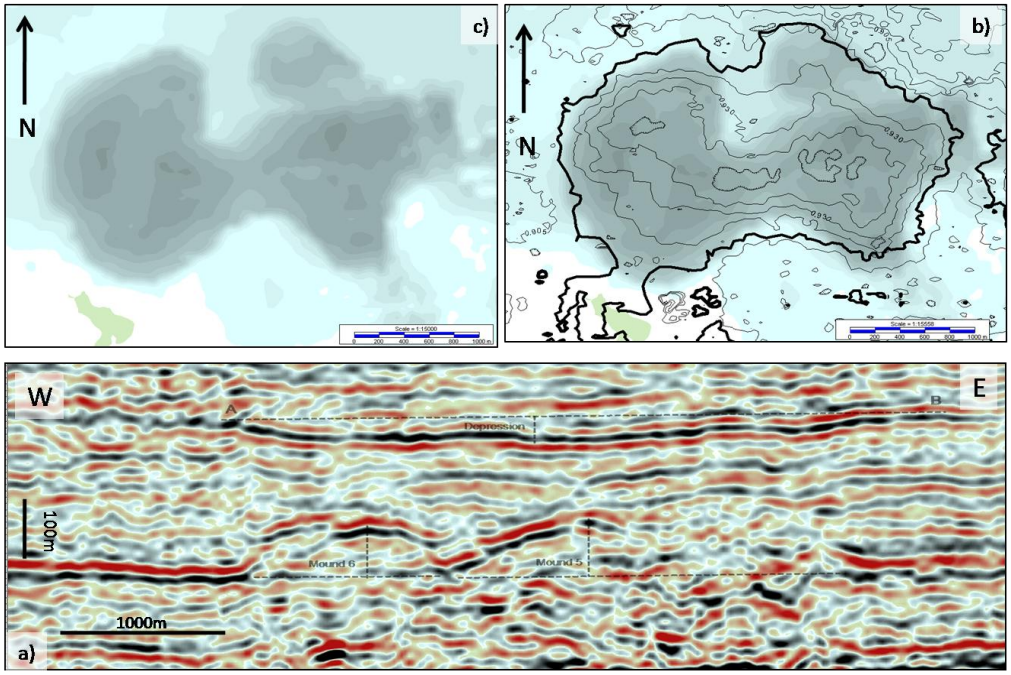

Figure 5.22 a) a W-E seismic section through Mound 6 and 5 b) contoured time-depth map of Mounds 6 and 5 c) time-depth contour of the overlying depression rendered over time-depth map of Mounds 6 and 5.

5.3.5.3. Quantitative comparison of depressions and mounds

Regression analysis was performed to investigate the relationship between subsided and fold area, relief versus area and subsidence versus relief. Best fit regression lines were fitted without transformation. The significance of the relationships was determined by Analysis of Variance (ANOVA) and the adjusted coefficient of determination (R^2). Relationships were deemed significant when $p<0.05$. The P-value is the ''probability of obtaining a test statistic result at least as extreme as the one that was actually observed, assuming that the null hypothesis is true'' (Ott et al.,, 1994).

5.3.5.3.1. Eccentricity v eccentricity

Geometrically the mounds and depressions are similar, and eccentricity values for corresponding mounds and depressions are comparable (Fig. 5.23a). Values for the eccentricity of the mounds and the corresponding depression area are shown on Fig. 5.19, and regression analysis reveals that there is a highly significant relationship ($P<0.005$) between the eccentricity of the mounds and the eccentricity of the depressions.

5.3.5.3.2. Area v area

The regression analysis of the mound area and subsided area values reveal that a highly significant relationship exists between the area of the mound and the area of the depressions (Fig. 5.23b). This relationship has previously been demonstrated by rendering a contour map of a depression over a time depth map of the corresponding mound (section 5.3.4.1).

5.3.5.3.3. Mound relief vs. depression subsidence

A significant relationship is also suggested by plotting the maximum relief of a mound against the maximum subsidence of the depression (Fig. 5.23c). This relationship can be demonstrated further, on a smaller scale, by comparing the amount of vertical movement affecting the Base Utsira Horizon and Top Utsira Horizon along a transect of an individual mound profile. Presented below are 3 representative examples of elliptical mound relief compared to the negative relief of the overlying depressions. Measurements for the vertical movement of internal Utsira Sand reflections are also presented.

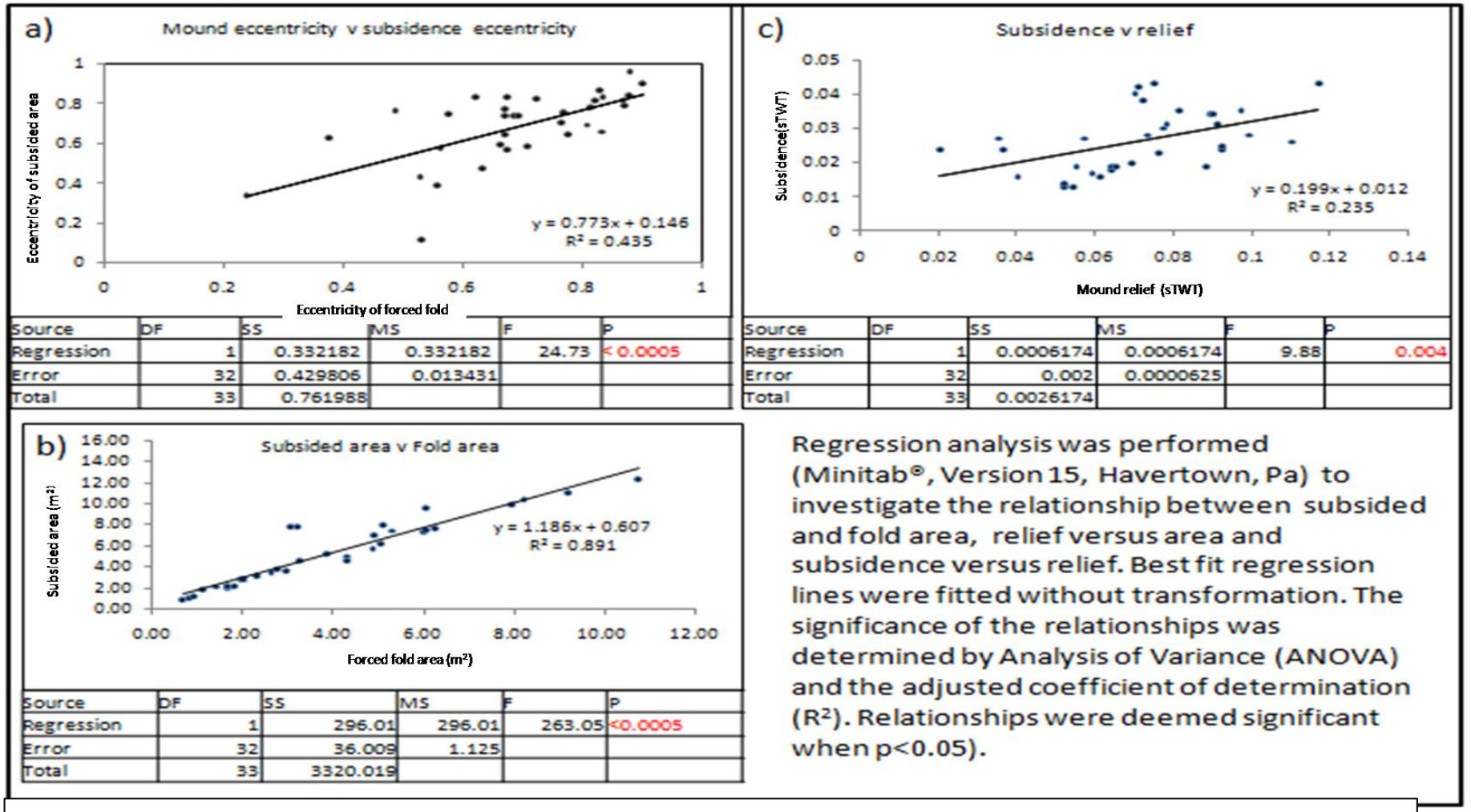

Source	DF	SS	MS	F	P
Regression	1	0.332182	0.332182	24.73	< 0.0005
Error	32	0.429806	0.013431		
Total	33	0.761988			

Source	DF	SS	MS	F	P
Regression	1	0.0006174	0.0006174	9.88	0.004
Error	32	0.002	0.0000625		
Total	33	0.0026174			

Source	DF	SS	MS	F	P
Regression	1	296.01	296.01	263.05	<0.0005
Error	32	36.009	1.125		
Total	33	3320.019			

Fig. 5.23 graphs of a) mound eccentricity v depression eccentricity b)mound area v depression area c)subsidence v relief

Example 1

Measurements were taken from a west to east transect of Mound 12. Measurements of the upwards displacement of the BUH, and the downwards displacement of the TUH and an internal horizon were taken at 200m intervals along the transect (Fig. 5.24a), and then plotted on a graph (Fig. 5.24b). The plot of displacement with distance along transect show the mound to have the greatest vertical movement, these points are located within the central part of the transect, and the displacement tapers off to the edges. The profiles of both the Top Utsira horizon and the intra-Utsira horizon roughly mirror that of the mound, with the greatest displacement concentrated within the centre, and each profile showing maximum displacement at the 1000m point. The displacement of the Top horizon is spread over a greater distance, over 2000m, while the displacement of the Intra-Utsira Horizon and Base Utsira Horizon are limited to between the 200 and 1700m points. As a result the profile of the TUH is flatter and broader than that of the BUH. This reflects the observations made from the seismic data.

Example 2

This example consists of a south to north transect through Mound 9 (Fig. 5.25). As above, the profile of the TUH is shown to be broader with a smaller amount of displacement in comparison to the intra-Utsira Horizon and the BUH. The BUH profile show the greatest vertical displacement at a point 1800m along the transect, and while not at the exact centre of the mound, the greatest area of displacement is concentrated towards the central section. In this example the intra-Utsira profile is broader than the TUH, but narrower than the BUH. The intra-Utsira reflection shows a greatest displacement of 0.035s TWT at a point 1200m along the transect; compared to a greatest displacement of 0.025s TWT at 1500m for the TUH.

Example 3

Data quality along a south to north transect through mound 39 has allowed measurements to be taken from three intra-Utsira horizons in addition to the BUH and TUH (Fig. 5.26). The BUH has the greatest displacement and the narrowest affected area. The greatest displacement of 0.071s TWT is located 1600m along transect and a displacement of 0.064s TWT at 1200m along the transect, a slight loss of relief is located between these points. The profiles of the intra-Utsira horizons and the

TUH roughly replicate the profile of the BUH, with the greatest displacement of each horizon located 1600m along the transect. The TUH profile is again the broadest profile and shows the least amount of vertical displacement. With increasing depth, the intra-Utsira horizons show a decrease in area affected and an increase in their maximum vertical displacement.

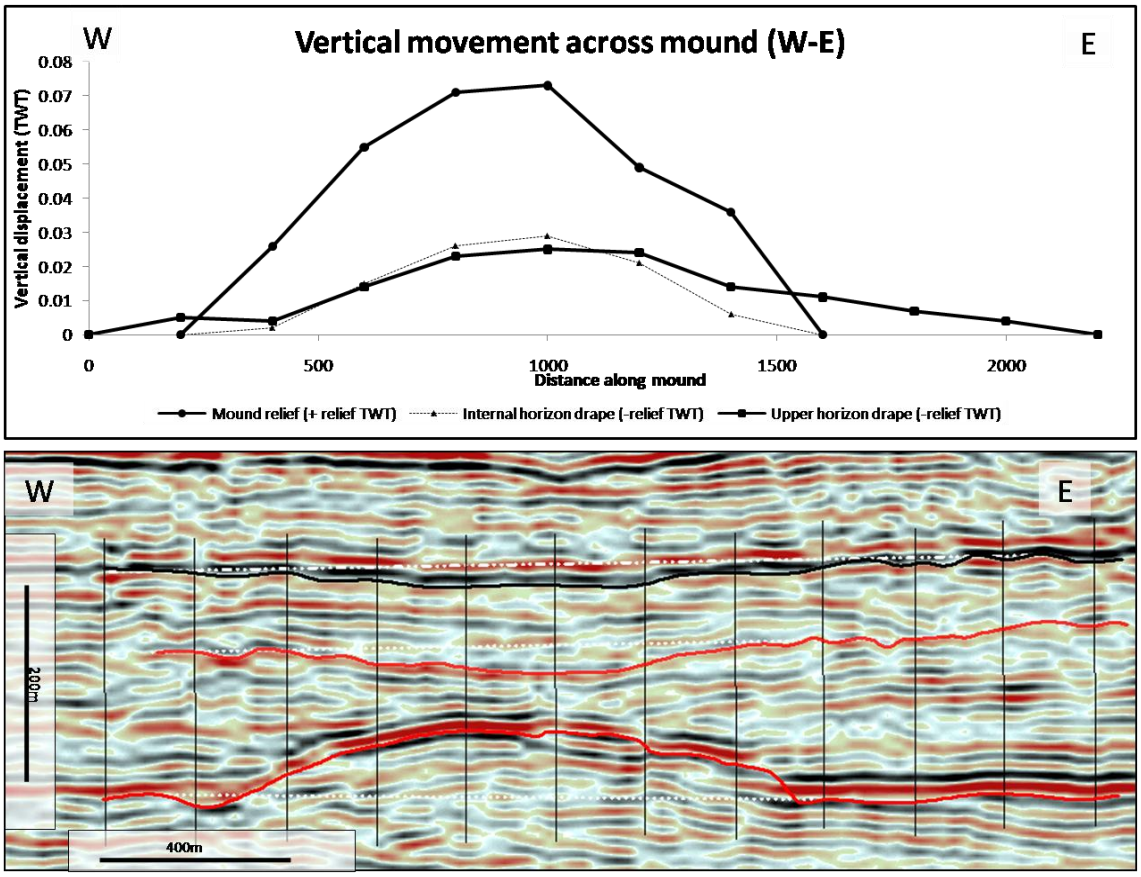

Fig. 5.24, a W-E transect of Mound 12, with the vertical displacement of the Base Utsira Horizon, the Top Utsira Horizon and an internal horizon plotted along mound the profile.

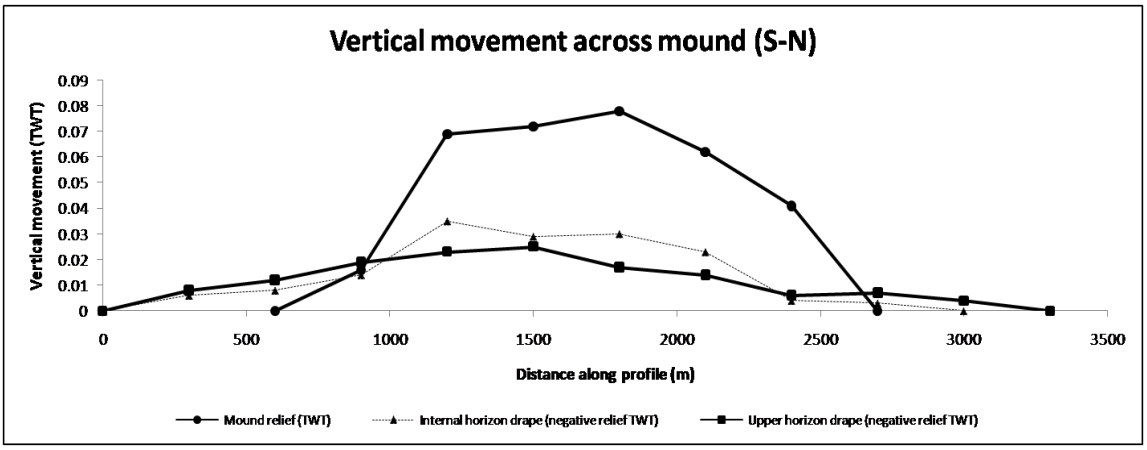

Fig. 5.25 a S-N transect of Mound 9, with the vertical displacement of the Base Utsira Horizon, the Top Utsira Horizon and an internal horizon plotted along the mound profile

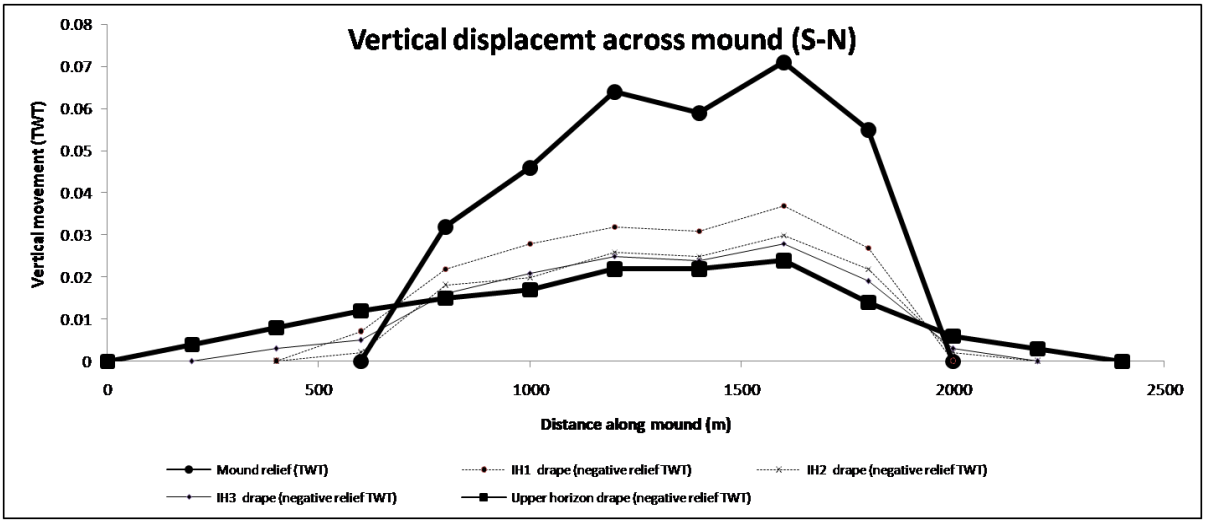

Fig. 5.26 a S-N transect of Mound 39, with the vertical displacement of the Base Utsira Horizon, the Top Utsira Horizon and an three internal horizons plotted along the mound profile.

5.4. Discussion

5.4.1. Partially imaged intrusions

Fully imaged intrusions are rarely seen within the data set. However, the presence of bright spots, high amplitude reflections, and a combination of both, within the Lowermost Shale are indicators of intrusive sand bodies. Observation of force folding of the overburden, sub-vertical disrupted zones, and chaotic packages in association with the high amplitude features are interpretive aids and diagnostic criteria for intrusion recognition. There are many such features which are probably sand intrusions in this area of the North Sea Basin. It seems highly probable that since so few interpretations of intrusions have been made in previous studies, that many reports in well completion logs of depositional sand bodies at this level may be erroneous. At least some reports of Skade Formation sands, for example, may be more likely to be sandstone intrusions.

The location and areal extent of the intrusion indicators are best imaged on an RMS map. However, the detailed nature of the indicators is only revealed through horizontal and vertical seismic sections through these features. Intrusion wings are observed on seismic sections as discordant high amplitude anomalies and are easily distinguished from bright spots, they are also markedly different from bright spots on time slices, and can be seen as linear features of high amplitude, whereas bright spots are rounded to sub-rounded features. It is often the case that indicators of partially imaged wings and central sections of the intrusions are, if not connected, at least in close proximity to each other, and the dimensions of the intrusions can be inferred from the area of high reflectivity.

5.4.2. Mounds and internal reflections

There is a distinguishable change to the internal geometry of the Utsira Sand reflections when in close proximity to the elliptical mounds. Onlapping reflections at the flanks of mounds, created by forced folding of the overburden, have previously been used as indirect indicators of the timing of mound formation. It has previously been suggested that the presence of downlapping reflections at the mound flanks are indicators of vertical movement affecting the mounds (Section 4.3.2.5). Two scenarios of the timing of this movement and effect on intra-Utsira reflections are presented in Figures 5.27a and b.

5.4.2.1. Early movement

The formation of a mound formed at the Base Utsira horizon (T0) and the deposition of onlapping reflections, T1 and T2, are shown diagrammatically in Figure 5.27a. The downward movement of the mound following T2 deposition would result in the downward inflection of reflections T1 and T2 and a decrease in mound relief. If the movement was then to cease, T3 would therefore be expected to infill the space created, and the following deposition of T4 and T5 would result in relatively horizontal reflections overlying the mound (Fig. 5.27a).

5.4.2.2. Late movement

The deposition of T1 to T5 following mound formation at T0 would result in T1 and T2 onlapping the mound flanks, and T3, T4 and T5 to comfortably overlie the mound in the form of horizontal reflections (Fig. 5.27b). Mound settlement following the deposition of T5 would result in the downturn of all the overlying reflections, with the onlapping reflections, T1 and T2, hence appearing as downlapping reflections, and T3 to T5 appearing to drape onto the mounds (Fig. 5.27b).

Neither scenario accounts for the geometrical pattern of the reflections as observed in the data set; it is therefore suggested that rather than viewing the reflections as indicators of the timing of the movement, they should be viewed solely as indicators of the extent of the movement.

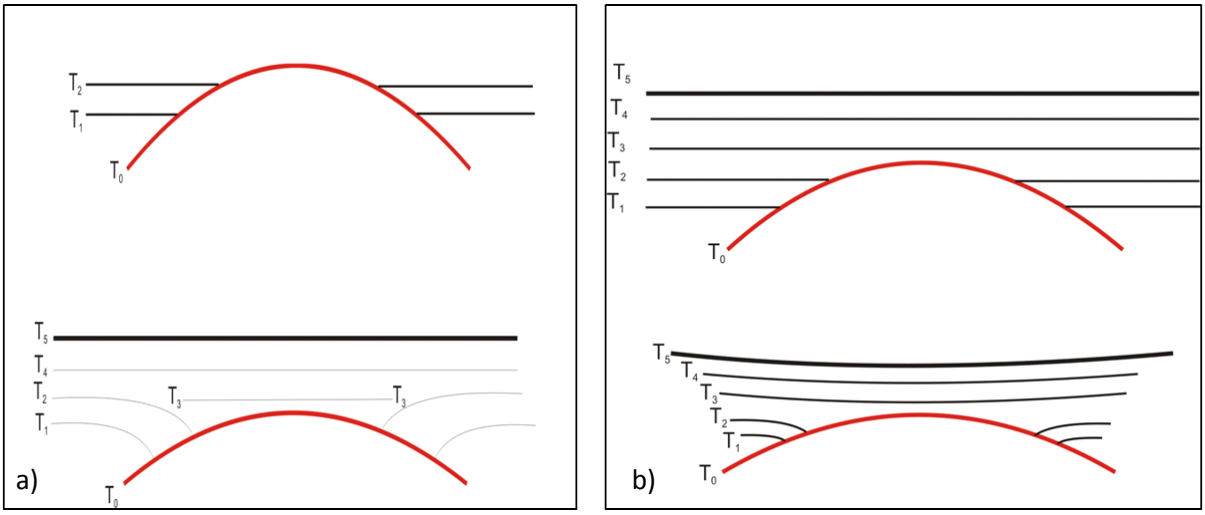

Fig. 5.27 a) demonstrates the expected geometry of the internal reflections at the mound flank if mound subsidence was at T_2 b) demonstrates the expected geometry of the internal reflections at the mound flank if mound subsidence was at T_5

5.4.2.3. Extent of movement

The onlapping reflections are in contact with the mound profile in close proximity to the hinge points, where mound relief is small, while the downlapping reflections are in contact with the mound further along the mound profile, where the mound relief is greater. Mound relief is proportional to intrusion aperture, therefore it follows that the onlapping reflections intercept the mound at points which overlie the thinnest points of the intrusion i.e. the wings, while the downlapping reflections are in contact with the mounds at points which overlie the central, thicker part of the intrusion (Fig. 5.28a).

If it is assumed that post-emplacement loss of aperture is proportional to initial aperture, then the greatest loss of aperture would be within the central parts of the intrusion, while the smaller amounts would be towards the wings. If it is considered that this loss of aperture must facilitate the downward movement of the overlying strata, then this downward movement must be proportional to intrusion aperture, and will therefore be greater at the centre of the mounds and smaller at the flanks (Fig. 5.28b).

This relationship would satisfy the observations made at the mound flanks (Fig. 5.28c and d).

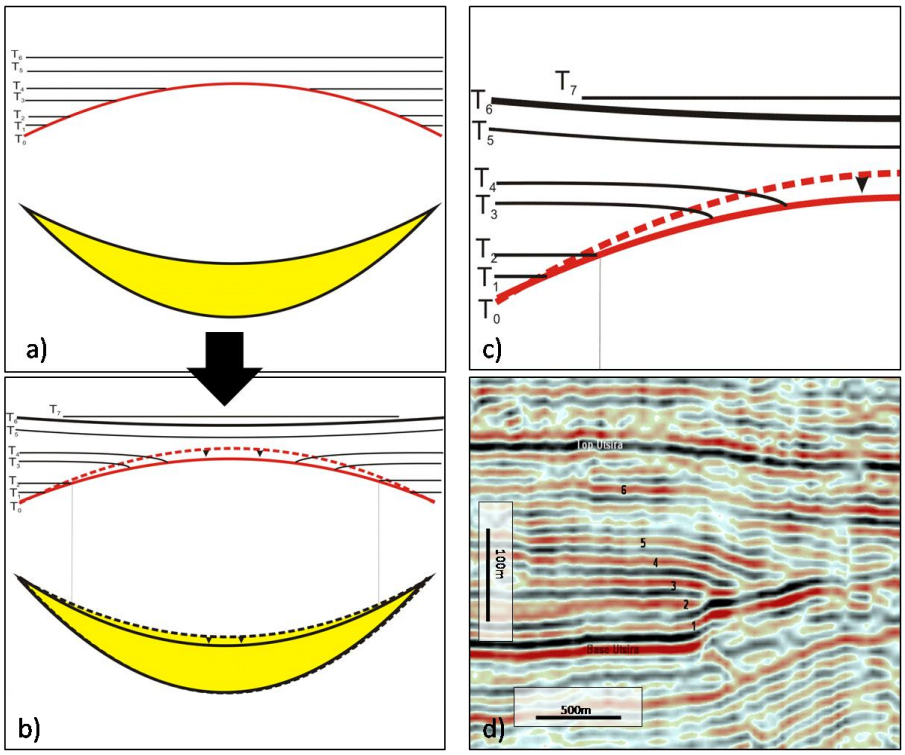

Fig. 5.28 a), b) and c) demonstrate the expected geometry of the reflections at the mound flanks if they are considered to be indicators of the extent of movement along the mound profile

d) is an example of the reflection geometry which fit this hypothesis.

5.4.3. Mound relief ∝ Depression subsidence

This relationship of proportionality between initial intrusion aperture , forced fold relief (i.e. mound relief) and the subsidence related to aperture loss is further emphasised by the measurements of vertical displacement along mound transects in section 5.3.5. It is generally true that the areas of greatest mound relief are overlain by the areas of greatest negative relief of the overlying depressions. As previously suggested this negative relief must be linked to the loss of intrusion aperture, which in turn is linked to initial aperture. The greatest mound relief overlies the greatest aperture, which also corresponds with the area of greatest aperture loss, and therefore the greatest vertical movement overlies the greatest mound relief (Fig. 5.29).

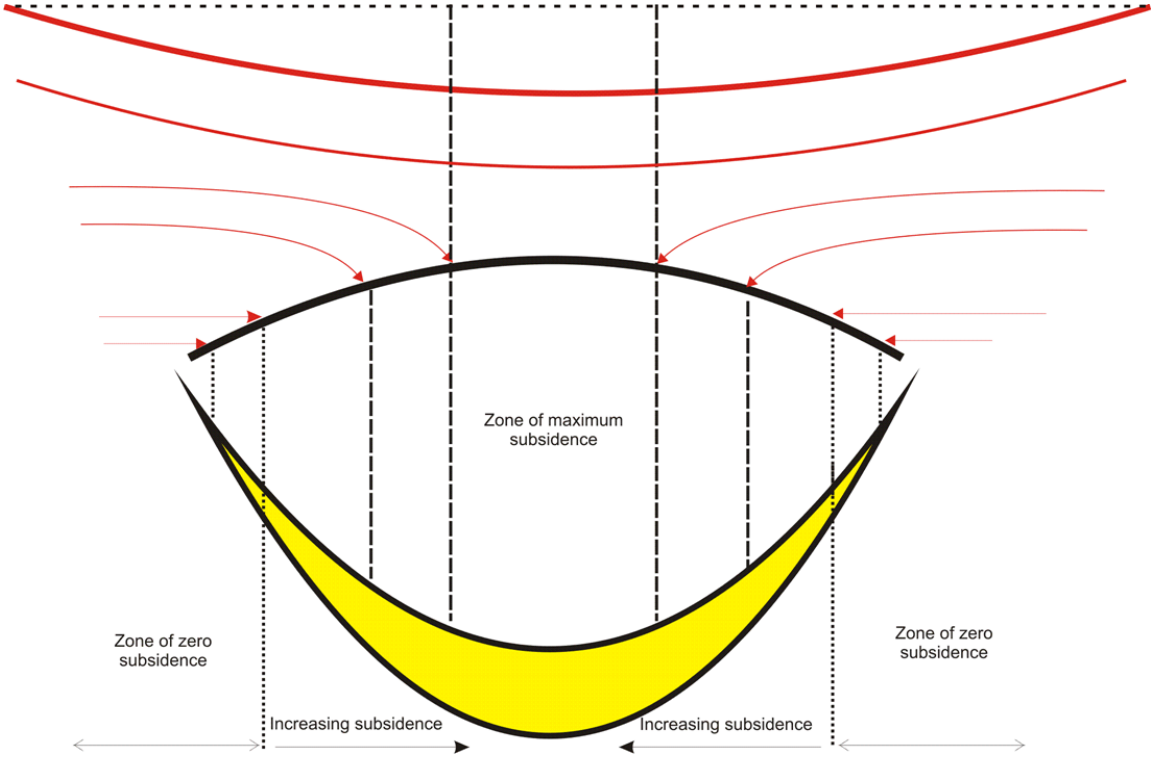

Figure 5.29 demonstrates the discussed relationship between the sand intrusion aperture, and zones of subsidence.

5.5. Conclusion

The observations in this chapter have established the geographic spread of sand intrusion within the Norwegian sector of the study area, and demonstrated further the relationship between the interpreted sand intrusions and the forced folds at the Base Utsira Sand. These folds have been shown to form elliptical-shaped mounds of raised topography, which are mostly contained within 'cluster areas' within this study area.

These mounds are overlain by subtle depressions at the Top Utsira Horizon, and a spatial and geometrical relationship between elliptical mounds and elliptical depressions is identified. The depressions are suggested to be the result of aperture loss within the sand intrusions due to grain reorganisation, compaction, and fluid and sediment loss due to loading or hydraulic pumping. These finding coincide with those from the UK study area (Chapter 4).

The findings from the previous chapter are developed further, and it has been demonstrated that the positive relief of the elliptical mounds is proportional to the negative relief of the elliptical depressions. It is proposed that the subsidence affecting the Top Utsira must also affect the Base Utsira, and the magnitude of the subsidence is proportional to the initial aperture of the intrusion. Therefore the mound relief observed in this study is less than the original relief.

The use of onlapping reflections at the flanks of the mounds to indirectly date the mound formation is an established technique. It is proposed in this study that the geometry of these reflections can be used to indicate vertical movement, and infer the extent of movement, affecting the mounds.

Chapter 6

Amplitude anomalies, fluid flow features and possible seal by-pass above the Utsira Sand

6. Chapter 6

6.1. Introduction

This chapter aims to identify features in the post-Utsira Sand succession that would promote leakage from a CO_2 storage reservoir. It also focuses on the seismic expressions of possible fluid flow which may indicate the paleo-movement of fluid through the Utsira Sand and overlying succession.

Physical trapping is considered the principle means of storing CO_2 (Suekane et al. 2008) and the early dominance of structural and stratigraphic trapping mechanisms following injection determines that the safe storage of CO_2 is reliant on an intact physical barrier to restrict the upward movement of the buoyant CO_2. The trapping mechanisms at work are similar to those which are responsible for oil and gas accumulations. It would therefore follow that any geological features which facilitate leakage of oil and gas would also do so for sequestered CO_2.

Establishing a link between leakage processes and their seismic expression is considered a major challenge in interpreting seismic leakage anomalies (Arntsen et al., 2007), However, significant work in identifying, classifying and understanding geological features and the processes which allow leakage have been presented by Cartwright el al., (2007) and by Andresen (2012), they classify leakage pathways as seal-by-pass systems and fluid flow features respectively. A brief introduction to both sets of features is presented below.

6.1.1. Seal Bypass Systems (SBSs)

Seal by pass systems (SBS's) are defined as 'seismically resolvable geological features embedded within sealing sequences that promote cross-stratal fluid migration and allow fluid to bypass the pore network' (Cartwright et al., 2007). They are described as permeability heterogeneities, and the presence of such features compromise the effectiveness of a sealing lithology to confine CO_2 (or hydrocarbons), as they have been shown to be effective conduits for highly focused fluid flow through sealing sequences (Cartwright et al., 2007). Seal bypass systems are classified into three main groups; fault-related, intrusion-related, and pipe-related. Each group are further sub-divided and associated with different geological settings, dimensions and seismic expression.

6.1.2. Fluid flow features

Some of the seal by-pass systems as defined by Cartwright et al., (2007) are classified as 'fluid flow features' by Andresen (2012) due to their genesis from sub-surface movement of fluid. They are considered to be a 'major but underused tool in basin analysis,' (Andresen, 2012), however, improvements in 3D seismic data quality have increased interest, as has the recognition of their importance on understanding hydrocarbon plumbing systems. Their impact is equally applicable to CO_2 storage reservoirs (Andresen, 2012).

Whereas seal-by-pass systems have been grouped into families based on their geological setting, dimensions, seismic expression, geometry, lithology and impact on the hosting sediment (Cartwright et al., 2007; Loseth et al., 2009; Huuse et al., 2010), Andresen (2012) subdivides fluid flow features into three major groups based on their genesis;

- Subsurface sediment remobilisation – fluid flow due to overpressure build-up causing sediment remobilization. End members include sand intrusions and mud volcanoes.
- Vertically focused fluid flow - highly focused vertical fluid flow resulting in pockmarks, pipes and chimneys.
- Laterally extensive fluid flow - caused when fluid flow is focused at a certain stratigraphic level, creating diagenetic fronts and polygonal faults.

With the exception of polygonal faults, classified as laterally extensive fluid flow features, fault-related seal bypass systems are obviously absent from Andresen's (2012) work due to their tectonic rather than hydrodynamic origin, however there is a clear 'cause and effect' association between pipe-related seal bypasses and vertical focused fluid flow, as there is between intrusion-related seal bypass and subsurface sediment remobilisation.

6.1.3. Seismic expression of leakage

An amplitude anomaly can be defined as a local increase or decrease in the amplitude of a seismic reflection. Loseth et al., (2009) interpret a variety of seismic anomalies associated with hydrocarbon leakage. This study crudely follow a three step workflow for hydrocarbon leakage interpretation as

suggested by their work. Anomalies firstly require observation, description and mapping. They then should be interpreted, followed by a definition of a leakage zone, consisting of a root, the source of the leak, and a top, where the leak terminates.

Leakage zones consist of areas of a seismic section which have undergone various changes to the seismic signal (Loseth et al., 2009.). This study aims to utilise these seismic phenomena, as well as the features described by Cartwright et al., (2007) and Andresen (2012) to identify possible leakage pathways and indicators of fluid movement within the study area.

6.2. Seismic data and methods

A 144 km^2 subarea of the Norway dataset was selected for detailed interpretation of post-Utsira leakage phenomena (evidence of seal bypass). The subarea was selected on the basis of the higher quality and higher resolution data in this area (fig. 6.1a, SA3).

A map of the seafloor of the Norway survey is presented in Fig. 6.1. The junctions between the several individual seismic surveys amalgamated to create the CNS Norway Survey can clearly be seen as linear discontinuities in the amplitude response (arising from polarity shifts and phase shifts between different sets of processing parameters), and abrupt changes of the time values to the seabed. To increase the consistency in interpretation the chosen subarea does not cross any survey boundaries, and has an internally consistent processing sequence.

This selected subarea also coincides with the North-West Cluster Area, as defined in Chapter 5, an area with large number of amplitude anomalies in the Lower Seal. Both these factors give added justification for the site selection for this detailed study.

Data quality

There is no available information regarding the processing history of the data, but observation of the sea bed reflection suggests that the data within this area is presented in the European Convention and is in minimum phase (Fig. 6.2). Within this area the dominant frequency is around 35Hz, and assuming a phase velocity of between 1800 m/s and 200 m/s (synthetic seismogram from well 15/9-11 NPD Fact pages, http://factpages.npd.no/factpages/default.aspx) a vertical resolution of around 13 m has been calculated. Depth conversion was not carried out and deptyhs reported in the study are calculated from a velocity of 2000 m/s.

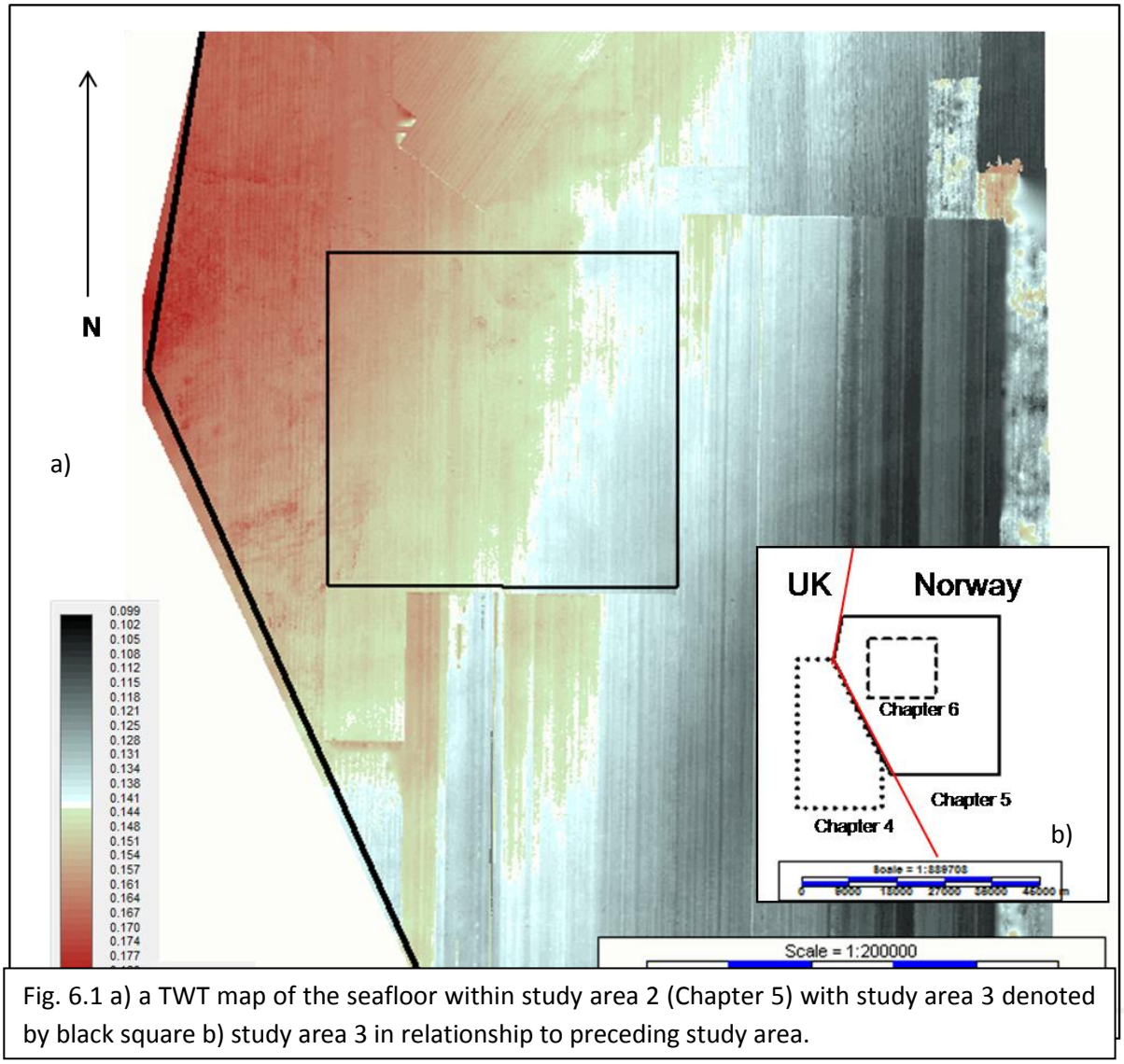

Fig. 6.1 a) a TWT map of the seafloor within study area 2 (Chapter 5) with study area 3 denoted by black square b) study area 3 in relationship to preceding study area.

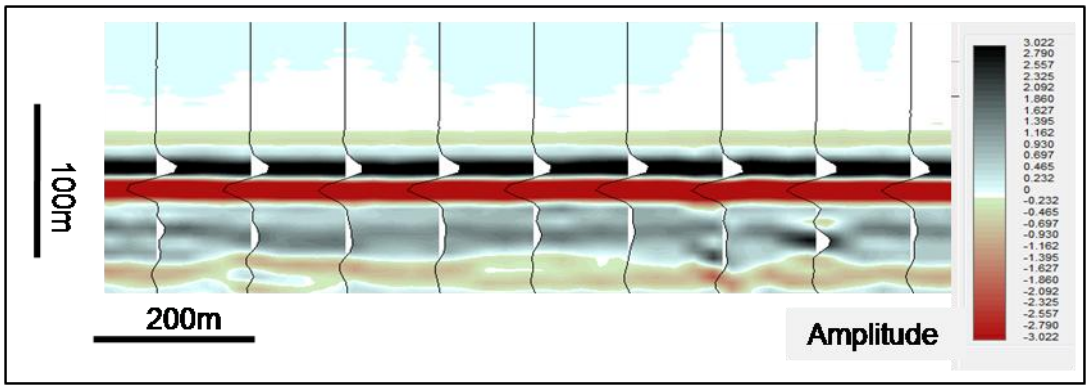

Fig. 6.2 Seafloor reflection where the red (negative) reflection is the dominant amplitude, suggesting that the data is displayed in conformity to the European Convention. Wavelet appears to be in minimum phase.

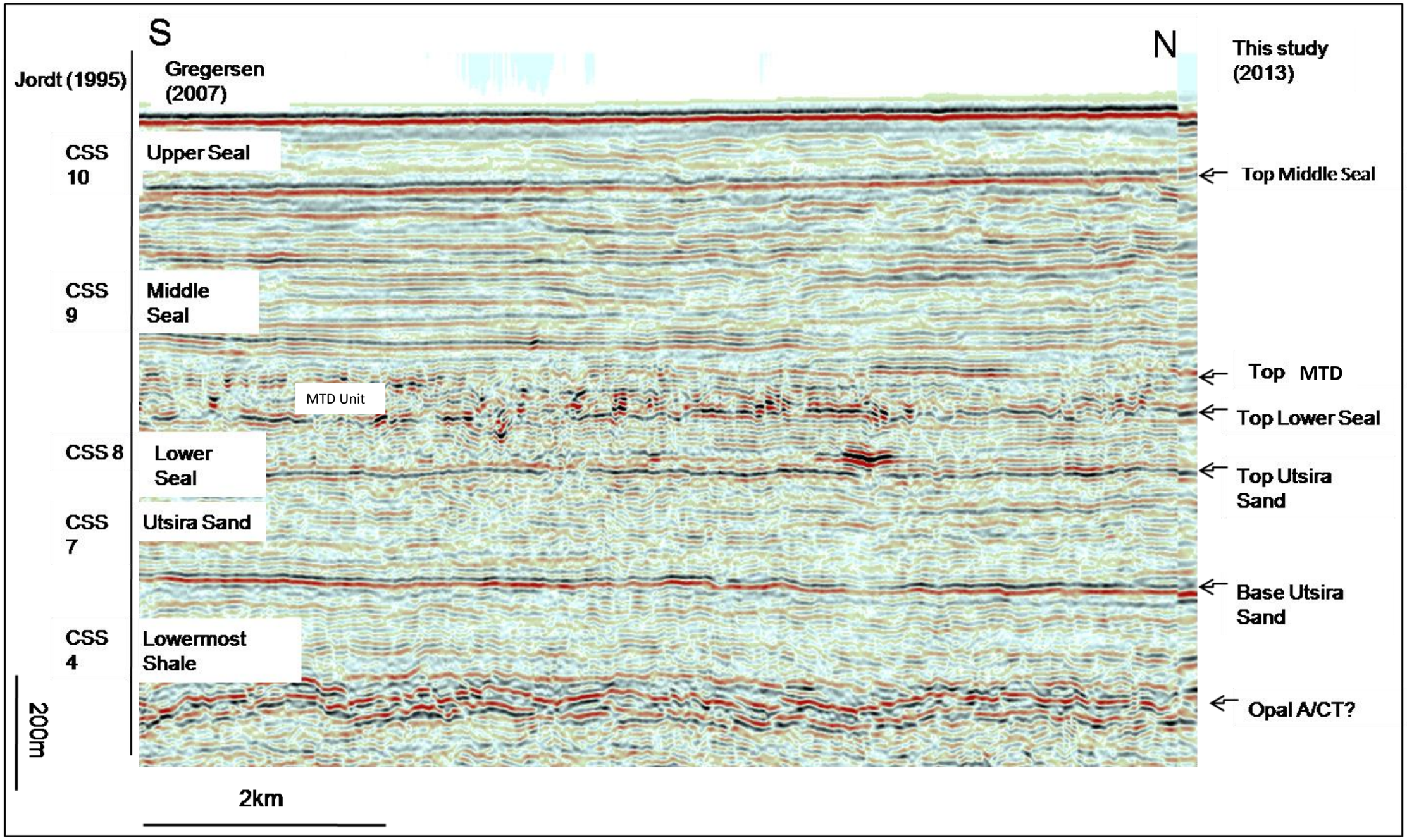

Fig. 6.3 a S-N seismic section presenting the units and horizons discussed in this Chapter.

6.3. Results

6.3.1. Main Units mapped

The main units described in this chapter consist of the Lower Seal, the MTD (Mass Transport Deposit) unit, Middle Seal, and Upper Seal (Fig. 6.3). These informal terms are seismic-stratigraphic units, and were defined by Gregersen et al., (2007). Given the lack of detailed biostratigraphic data in this interval, it was considered prudent to follow the Gregersen et al., (2007) seismic-stratigraphic scheme here. The general characteristics of these 'units' have been described in Chapter 2, Section 2.2.2. A brief overview of their characteristics within this study area is presented below; this is followed by a detailed description of the amplitude anomalies found within each unit. For the discussion for the likely age ranges of these units, see Chapter 2.

6.3.1.1. Lower Seal

The Lower Seal is a tabular unit, consisting of low to medium amplitude reflections which are generally concordant and parallel. Its base is defined by the top of the Utsira Sand, a medium amplitude, continuous, reflection, and its upper limit is an irregular semi-continuous horizon which occasionally incises down into the Lower Seal. This upper horizon is interpreted as the basal shear surface of the overlying mass transport deposit (MTD). Unit thickness is generally between 70m to 120m, it thins where the overlying MTD unit thickens and incises into the Lower Seal.

6.3.1.2. MTD Unit

The MTD unit is a distinct unit of variable internal reflections which can be easily distinguished from the underlying Lower Seal and overlying Middle Seal by virtue of the internal reflection character. As with many MTDs, the internal reflections are variable in amplitude, discontinuous to chaotic, but occasionally better stratified, and variable in frequency (c.f. Frey Martinez et al., 2005; Bull et al. 2009).

The internal reflections are crudely horizontal to sub-horizontal, parallel and concordant, and range between low to medium amplitude within the southeast and northwest sectors of the study area. The unit thickness is on average around 80m within these areas. Unit reflections become more chaotic within a narrow**,** 3.5km wide, central section which is orientated southwest-northeast. This

area coincides with an increase in unit thickness, and shows a greater variability in the nature and amplitude of the reflections, conforming to the more classical seismic facies associated with significant deformation of an MTD (Bull et al., 2009; Moscardelli et al. 2006). Reflections are present as horizontal, concordant sections and discordant, sub-vertical areas which cross-cut the horizontal sections. High amplitude blocks of more intact stratigraphy (Gamboa, et al, 2011) and bright spots (amplitude anomalies significantly higher than the background amplitude values) are present within the unit.

6.3.1.3. Middle Seal

The Middle Seal is the unit of greatest thickness within the study area. It is over 430m thick in the South, and thins to around 300m in the North. It consists of low to medium amplitude, low angle, prograding reflections, which downlap onto the MTD unit with a north-westerly prograding direction. This progradational section is part of a much larger progradational system associated with the onset of glacial conditions in Norway (see Loseth et al. 2012). The base of the unit is defined by the upper limit of the MTD, and a significant difference in reflection continuity and acoustic character exists between the internal reflections of these respective units. The upper boundary is defined by a continuous medium to high amplitude reflection which is recognised as the Basal Pleistocene unconformity (Gregersen, 2007, also Chapter 2, Section 2.2.2.1). Occasional anomalously high amplitude reflections are present within the unit.

6.3.1.4. Upper Seal

The Upper Seal consist of the strata between the Basal Pleistocene unconformity and the seafloor (Gregersen, 2007). The seafloor is defined by a continuous, high amplitude, negative reflection (red), while the Basal Pleistocene unconformity is a medium amplitude, continuous reflection. The unit is around 150m thick, with little variation in thickness, and consists of low amplitude reflections. Internal troughs and incised valleys can be observed as discordant reflections which cross-cut the generally horizontal to sub-horizontal internal reflections. These incisions are also seen to affect the Pleistocene unconformity in places, and are similar to those described from the Pleistocene succession throughout the central North Sea (Graham et al., 2007; Stewart and Loneregran, 2011; Kristensen and Huuse, 2012). Scattered anomalously high amplitude seismic anomalies are also present within the unit.

6.3.2. Amplitude anomalies in the Lower Seal Unit

An RMS amplitude map of the entire Lower Seal Unit reveals several areas of anomalously high amplitude located throughout the study area (Fig. 6.4a). Several anomalies are located within or in close proximity to the outlined contour of the north-west cluster area (NWCA), while others lie within the unaffected area which surrounds the NWCA. The RMS map of the whole of the Lower Seal can be compared to the RMS map of the upper half of the unit (Fig. 6.4b), where there appears to be a scarcity of significant high amplitude features. To illustrate the general features of these amplitude anomalies, two representative seismic sections are described in detail. An east-west and a north-south seismic section through these anomalies (Fig. 6.5a and 6.6a) show that the high amplitude anomalies are horizontal to sub-horizontal, stratal-concordant reflections located within a lower 50m interval of the Lower Seal, and more specifically at a horizon mapped as the Lower Seal High Amplitude Horizon (LSHAH).

6.3.2.1. East-west seismic section

Three high amplitude anomalies are intersected by the east-west seismic section (Fig. 6.5, crossline 10764). Each of these anomalies is remarkable in having irregular outlines and a very sharp amplitude 'cut-off' against the low, and relatively featureless background value.

Amplitude anomaly A (Fig. 6.5c, A) is 0.27 km^2 in area, and is in close proximity, but not connected, to amplitude anomaly B, which is 0.083 km2 (Fig. 6.5c, B). They are visible on a seismic section as three high amplitude reflections, with a central positive (black) reflection which is the dominant amplitude. Anomaly A is in excess of 400 m in length and anomaly B around 300 m in length along this east to west section, the area in between is of low amplitude. Anomaly A has an irregular outline, with fingers (f) of high amplitude protruding at its eastern and north eastern extent. Anomaly B is a sub-rounded feature, with only a slight indication of outward fingering at its eastern extent. Both features have central areas which consist of areas of greatest average amplitude, which in turn are enclosed within outer rings of decreasing amplitude.

Anomaly C is much larger in area and consists of what can be divided into three smaller separate anomalies which are connected by narrow zones of moderate amplitude that are higher than the

background amplitude values. In total they cover an area of 1.79 km^2, and have an irregular outline. Again, the highest amplitude areas are located within the central sections of the anomaly, and a south-easterly orientated finger protrudes from its southern extent (Point F). Irregular outliers (i.o) and circular outliers (c.o) are present to the south and the north of the anomaly respectively. Anomaly C is almost a kilometre in length along the seismic profile, it dims slightly below point C. This point coincides with the connecting zone between the larger central area and the smaller westerly area.

6.3.2.2. North-south seismic section

Two high amplitude areas are located along a north-south section (Fig. 6.6a, inline 11181). Both appear to be stratal-concordant, have a dominant positive amplitude, and are located within a lower 0.4s TWT interval of the Lower Seal. Both also have a considerable lateral extent, exceeding a kilometre in length along this north-south orientation. The Top Utsira horizon appears broken at points below the high amplitude reflections (Fig. 6.6a, Points a and b).

Anomaly D covers an area of 0.79 km^2 and has an irregular outline (Fig. 6.6c, D). In plan, the higher amplitude region is also irregular, with several separate zones of highest amplitude within the outline of the feature. However, all the areas of greater amplitude are located towards the centre of the anomaly and a decrease in amplitude towards the outer edges is still noticeable. Anomaly E exceeds a square kilometer in area, and consists of a central area of high amplitude which is connected to a north-eastern extension (Fig. 6.6c, E). The amplitude is distributed in a more regular fashion within this feature, with a central section of greatest average amplitude which decreases towards the edges, where there is a sharp cut-off in values.

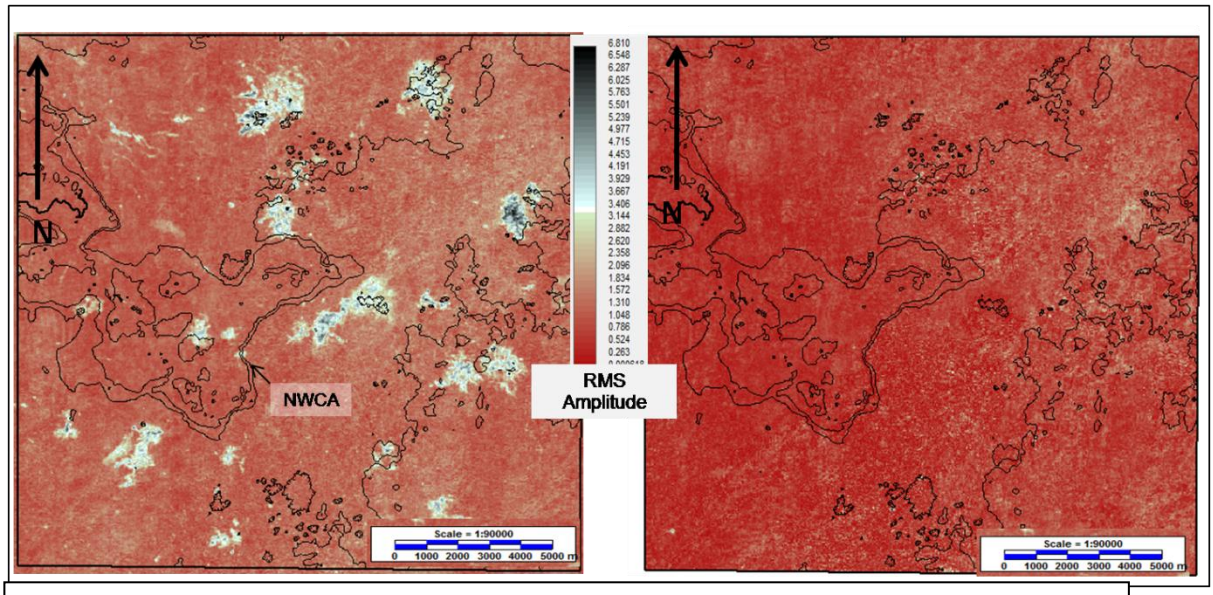

Fig. 6.4 a) an RMS map of the whole Lower Seal b) RMS map of the upper half of the Lower Seal. Both maps are co-rendered with the contour of the NWCA (Chapter 5)

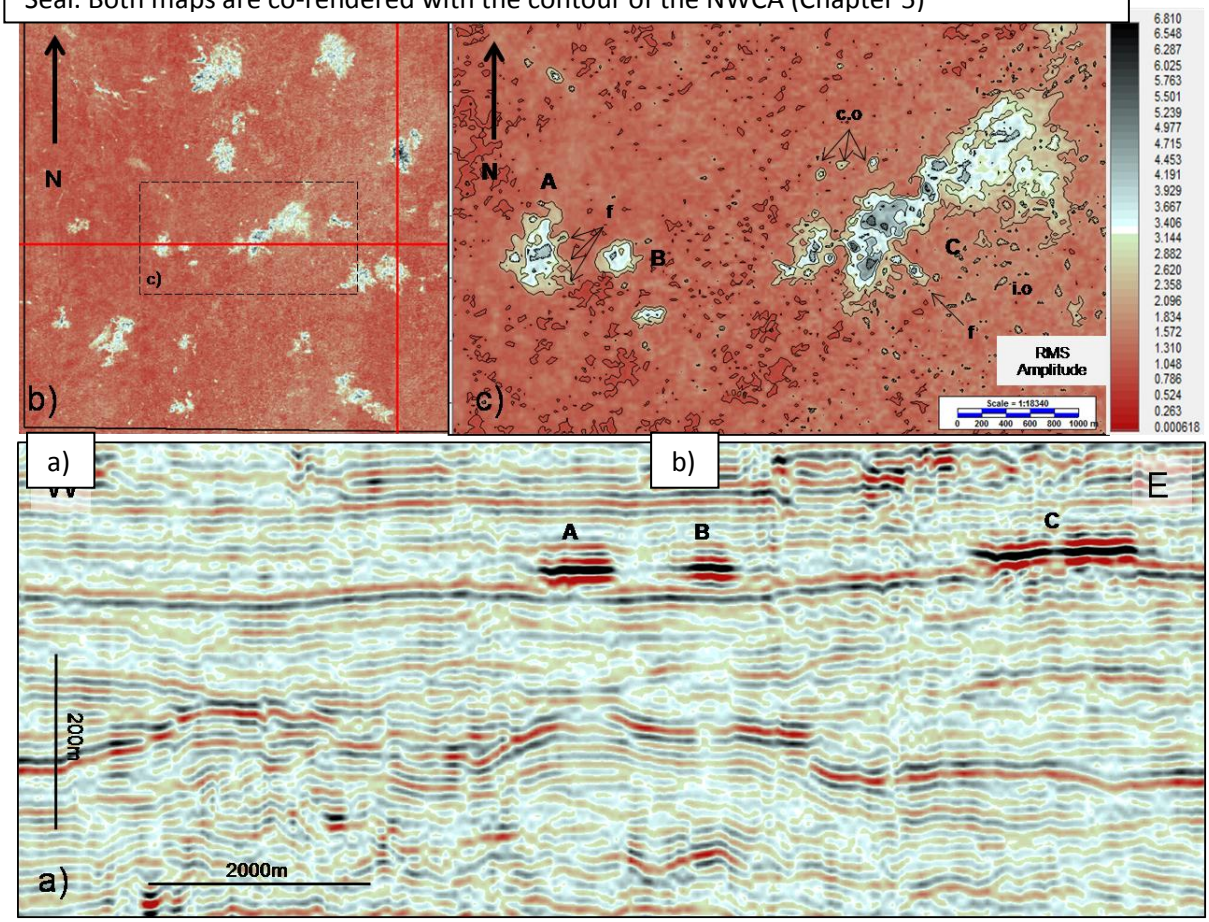

Fig. 6.5 a) a W-E seismic section displaying three high amplitude features within the Lower Seal (A, B and C) b) location map of the W-E line c) contoured RMS map of the three high amplitude areas. The high amplitude areas have associated fingering (f), circular outliers (c.o) and irregular outliers (i.o).

6.3.2.3. Lowers Seal High Amplitude Horizon

As demonstrated in both examples above, the high amplitude areas appear to be located within a specific horizon, LSHAH. This intra-Lower Seal horizon has been mapped, and an amplitude map of the horizon is presented along with the RMS map of the unit (Fig. 6.7 a and 6.7b). It is clear that the location of the high reflectivity areas on the Lower Seal RMS map, and the high amplitude areas of the LSHAH map coincide, and that their geometry and dimensions are also similar. In fact, when the contours of the RMS high reflectivity areas are overlain over the high amplitude areas of LSHAH, they are seen to be identical in area, geometry and extent (Fig. 6.7, c, d and e).

TWT contours of the LSHAH, underlain by the amplitude map of LSHAH, allows the evaluation of whether the amplitude anomalies of LSHAH conform to structure. Initially, an irregular shaped amplitude anomaly (Anomaly F), 2.2km^2 in area, does not appear to exactly match the TWT contours of the LSHAH structure (Fig. 6.8a), however, some areas of the anomaly can be seen to roughly correspond with the geometry of the contours in places (Fig. 6.8b). Since the water depth is approximately constant across this region, and there are unlikely to be large lateral variations in the velocity structure of the post-Utsira interval (observations on completion logs released by Norwegian Petroleum Directorate - see Appendix A), it is considered that the TWT structure contour map is a good proxy for a depth structure map. The lack of strict conformance to structure is therefore an interesting feature (see Discussion).

Two peaks in amplitude are located within an irregular area (Fig. 6.8b), the peaks roughly coincide with two smaller, sub-rounded topographic lows. Away from the peaks, the amplitude decreases outwards mimicking the geometry of the contours. A pair of north-south seismic sections through the peaks reveals they coincide with localised depressions of LSHAH which in turn directly overlie discontinuous segments of the Top Utsira Horizon (Fig. 6.8d and 6.8e, Points D). The spatial association of discontinuities in the Utsira reflections with the depression at LSHAH is highly significant, and discussed below in more detail.

A similar feature is apparent along a second north-south profile (Fig. 6.6a), where an area of low amplitude coincides with a low area, a depression (D) affecting the horizon is also apparent and appears to connect the amplitude anomaly with the Top Utsira Horizon via a vertical zone of discontinuous reflections.

The large anomaly (Anomaly C) shown along the east-west section (Fig.6.8f) is presented as an amplitude map of LSHAH overlain by the time depth contour of the horizon (Fig. 6.9a). In this case, although not exact, the outline of the anomaly appears to be far more coincident with the contours of the LSHAH i.e. it is closely conforming to structure. The irregular shape of the high amplitude feature can generally be seen to comfortably lie within, and conform to, the contours of the horizon. This is particularly noticeable around the western area of high amplitude (Point A), the southern spur of high amplitude (Point B) which protrudes from the central area, and the south-east orientated finger of high amplitude (Point C). Two depressions are located along the north to south profile through the centre of the high amplitude feature (Fig. 6.9b). These are similar features to those observed in conjunction with the high amplitude feature in Fig. 6.8 (d, e, and f). They are located within the central area of the high amplitude feature, and in close proximity to the greatest concentrations of highest amplitude values. As noted in previous examples, a clear decrease in amplitude strength from the centre of the features towards their edges can be observed, again with a very sharp cut-off to the low background values. Indeed, it is this remarkable amplitude cut-off that allows recognition of the strikingly fingered and irregular margins that characterise all these amplitude anomalies.

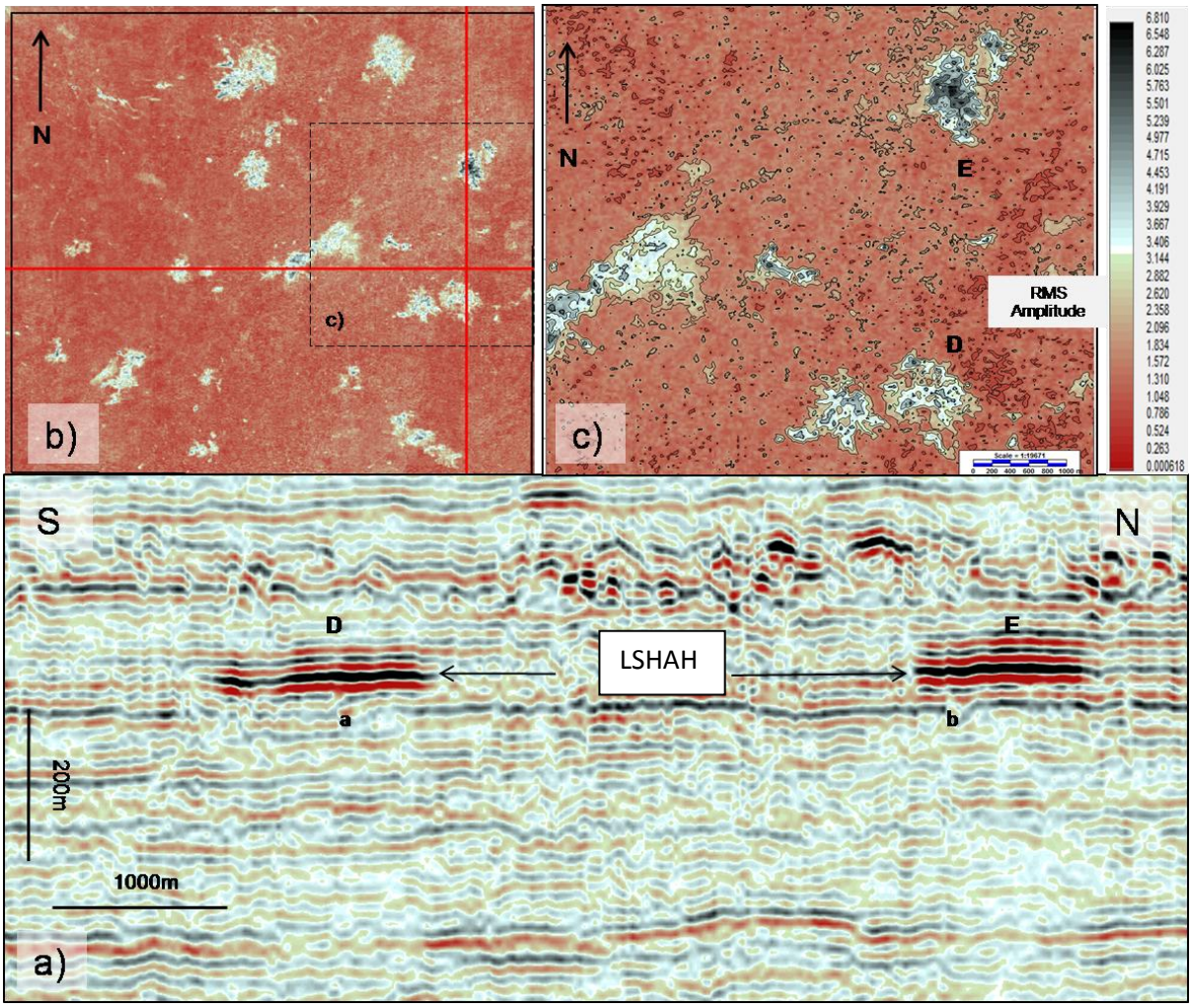

Fig. 6.6 a) a S-N seismic section displaying two high amplitude features within the Lower Seal (D and E) b) location map of the S-N line c) contoured RMS map of the three high amplitude areas. The amplitude anomalies are concentrated within the Lower Seal High Amplitude Horizon (LSHAH).

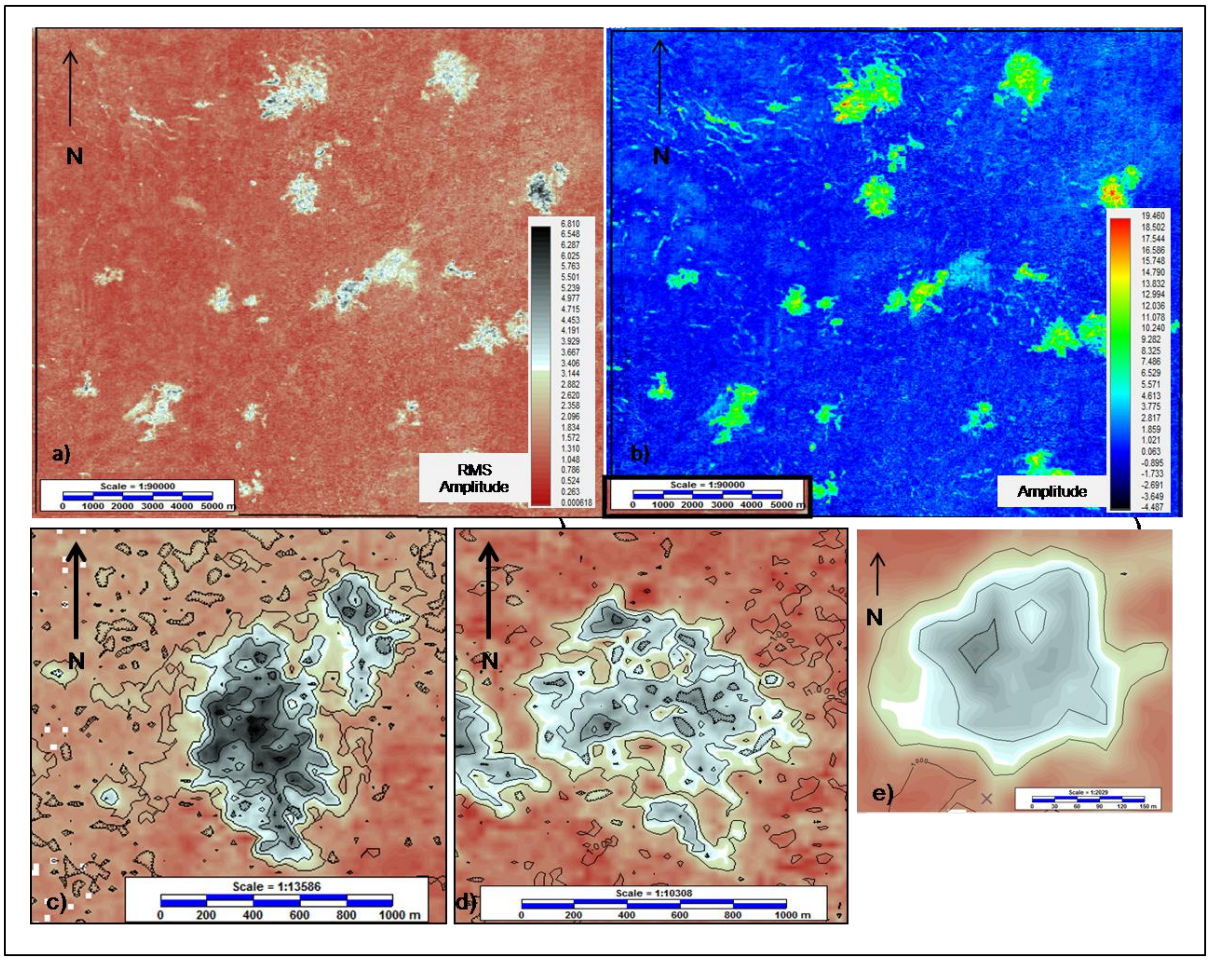

Fig. 6.7 a) RMS map of the Lower Seal in comparison with the b) amplitude map of the LSHAH for more detailed analysis individual examples with the RMS contour co-rendered with the amplitude map of the LSHAH are presented c) d) and e).

Depressions, similar to those presented above, are also identifiable upon time-slices through the areas of high amplitude (Fig. 6.10a). They can be seen as several, small scale (10's m up to a 100m diameter), circular and sub-circular areas of negative polarity reflections (black) enclosed within larger areas of positive polarity. A south-east to north-west seismic section, through two high amplitude areas, intersects several of these depressions (Fig. 6.10b). A single depression is intersected within amplitude anomaly H (AAH). It is located roughly halfway along the 1200m length anomaly, and along this profile it appears to be 100m in width with a vertical offset of around 20m. The time-slice reveals that several other depressions are located within AAH, the largest of which is located just off the centre of the high amplitude feature (Fig. 6.10a, Point D1). A large central depression is also located roughly in the centre of AAI (Fig. 6.10a and 6.10b, Point D2), it is also present along the south-east to north-west seismic section, as are two smaller depressions Fig. 6.10a and 6.10b, Points D3 and D4) . In all cases the depressions appear to terminate in close proximity to the Top Utsira Sand Horizon.

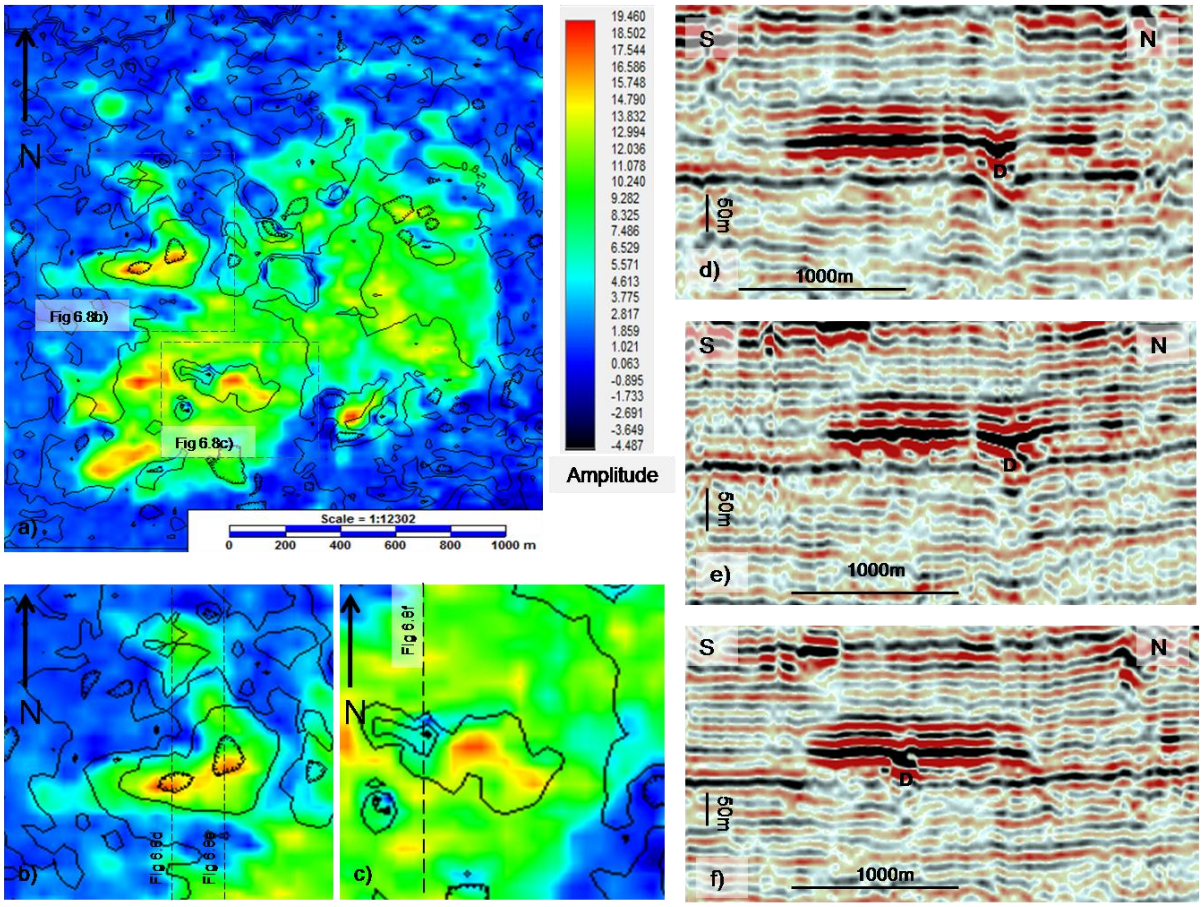

Fig. 6.8 a) the amplitude map of amplitude anomaly F is co-rendered with the contour of the time-depth map of the LSHAH to identify conformity to structure. Only in Fig. b and c is there any indication of conformity in this example. d), e) and f) show the high amplitude features with underlying depressions (D).

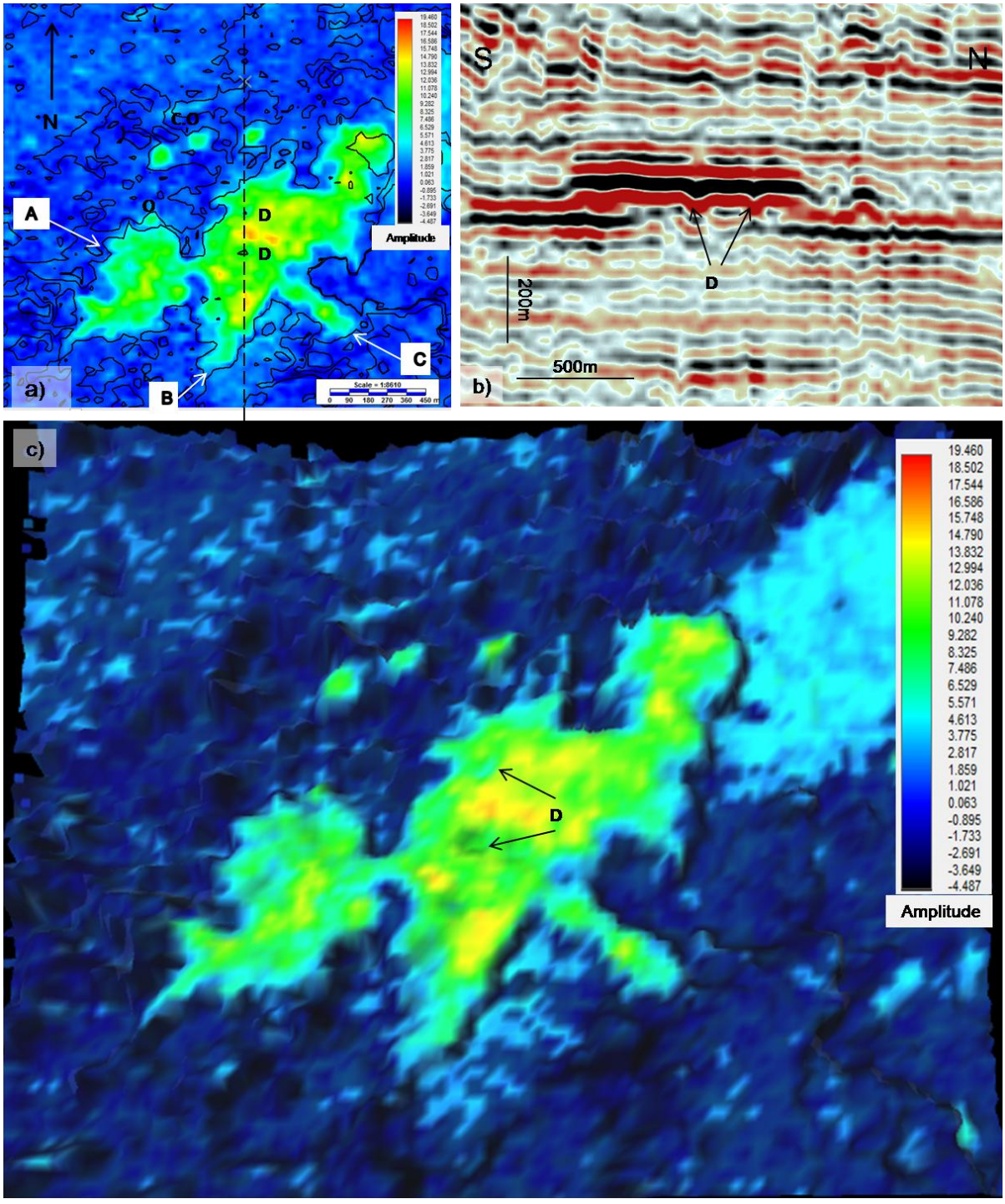

Fig. 6.9 a) amplitude map of the LSHAH is co-rendered with the contour of the time-depth map of the LSHAH to identify conformity to structure. Greater conformity to structure is displayed by this example compared to Fig. 6.8. b) two small scale depressions underlying the high amplitude area c) 3D visualisation of the high amplitude feature.

6.3.2.4. Interpretation and discussion

The high amplitude anomalies shown within the Lower Seal unit are all restricted to a single horizon, the Lower Seal High Amplitude Horizon (LSHAH), and lateral variations along reflections, such as an amplitude increase or decrease along its length or a loss of continuity, are considered the simplest type of leakage-related anomalies (Løseth et al., 2009). The high amplitude features identified within the LSHAH are interpreted as accumulations of shallow gas.

From the completion log of well 15 /8-1, the Lower Seal is shown to consist of clay and is considered an effective sealing lithology (Chadwick, 2000). The featureless background amplitude of the unit also supports a hemipelagic origin. However, even low permeability cap rocks are subject to seal by-pass at the interface of the seal and reservoir and allow intra-seal hydrocarbon accumulation (Cartwright et al. 2007; Jarvie et al., 2007), and geochemical analysis has shown that hydrocarbons are generally more concentrated within their lower sections immediately above the top reservoir (D'Onfro et al., 2000; Leith et al., 1993; Leith and Fallick, 1997). Permeable lenses and layers (e.g. thin silts) are not uncommon in cap rock successions and may host such accumulations, and the distribution of the saturated zones can vary in form from (Løseth et al., 2009)., as can be seen in the examples presented in section 6.3.2.

Several small scale depressions have been shown to be associated with the high amplitude areas, and are generally located within the central sections of the high amplitude areas. These depressions are similar in dimensions (tens of meters in vertical and horizontal scale) to pockmarks as described by Hovland and Judd (1988) and Moss and Cartwright (2010), and may possibly be buried pockmarks. The depressions are also seen to be in spatial correspondence with discontinuities in the Top Utsira Horizon, and in some cases connected to the Utsira Sand by sub-horizontal feeder 'pipes' (Fig 6.8 and 6.9, features D). Loseth et al., (2009) suggest that the vertical movement of hydrocarbons through lithified caprock can occur in three ways; fracture flow, Darcy flow or diffusion, however, in these instances, the proximity of the anomalies to the top Utsira and the apparent presence of pockmarks and connecting pipes, suggest that it is these features that facilitated the movement of gas into the permeable layers. It is suggested here, therefore, that these features represent an interconnected caprock bypass system similar to those illustrated by Cartwright et al. (2007) and andresen (2012).

An important general observation in this study is that most of the high amplitude anomalies overlying the Top Utsira have sharp lateral amplitude cutoffs and a 'fingered' perimeter. The irregular shape of most of the high amplitude areas and the evidence of fingering suggests that these are probably dynamically migrating batches of gas. It is interesting to draw a possible analogy between the fingered or 'stellate' anomaly shapes and the patterns obtained experimentally for fingered invasion by percolation of one fluid displacing another in a granular host medium (c.f. Meakin, 1998, Meakin et al., 2000).

The question of conformance to structure is critical when considering dynamic migration effects and gas accumulations (see for example Løseth et al., 2009).In the case of Anomaly F (Figure 6.8), it is difficult to determine a relationship between the contours of the Lower Seal High Amplitude Horizon and the high amplitude areas because the horizon is relatively flat lying, and the topography is very subtle. However, there are suggestions that the gas is moving away from the low topography of the feeder pipes and is trying to conform to the contours. This would be expected in a dynamically filling plumbing system. Although velocity variations in the overburden may be the cause of the non-conformity to contour, synthetic seismograms from the NPD fact pages suggest a relatively constant velocity in the overburden (http://factpages.npd.no/factpages/default.aspx).

A general pattern is observed where the areas of greatest amplitude are located within the central sections of the high amplitude features with decreasing amplitudes towards the edges and away from peaks (Anomalies A, B, C, D, E, Figures 6.5, 6.6 6.7 and 6.9). It is possible that this amplitude variation is an indication to saturation gradients. There also appears to be a relationship between the feeder depressions and areas of high amplitude (Fig. 6.8). In the cases where a strong positive amplitude (soft event) coincides with a depression it is suggested that the feeder pipe is still gas filled (Fig. 6.8b), and the gas is migrating buoyantly away from the low points. Conversely, in Fig. 6.8c, the depression coincides with an area of relatively low amplitude, a proximal area (<100 m) to the south-east is of a higher amplitude suggests that in this case the gas has fully migrated away from the feeder pipe. It is also worth considering that there are multiple feeders underlying Anomaly F, which may also help explain the irregular distribution of amplitude.

Anomaly C (Fig. 6.5 and 6.9) shows a greater conformity to the contours of the LSHAH. Two feeders underlie the feature and are located within the central area of the anomaly (D), and the greatest area of amplitude is also concentrated in the middle, inbetween the feeders. The contrast between the amplitude of the feeders and the main areas of high amplitude is also less noticeable than in the

case of Anomaly F, indicating that there is no noticeably greater concentration of gas in either feature. This would suggest that it a more 'mature' accumulation which has time to equilibrate with the contours of the 'reservoir' horizon. The reduced number of feeders may also contribute to the greater conformity and more even distribution of gas.

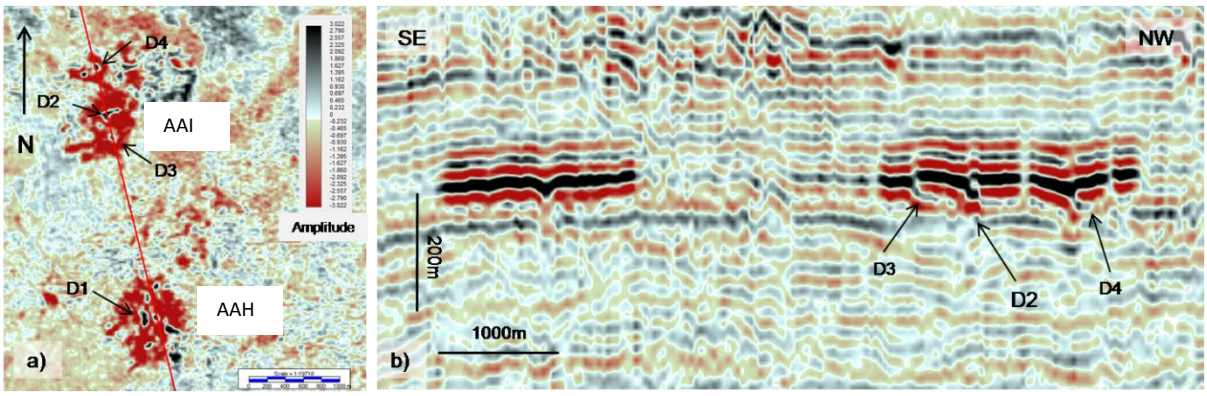

Fig. 6.10 a) a time-slice shows the outline of the negative, lower, reflection of amplitude anomalies H and I, sub-circular features of black reflections are seen within their outline b) these are visible as small scale depressions along a SE-NW seismic section. The black, positive, reflection has the dominant amplitude of these features, and they are considered 'soft' events.

6.3.3. Features of MTD unit

A TWT structure contour map of the top MTD horizon reveals the unit to be shallower in the north east of the study area, at around 600 m bsl, and deeper towards the south west to around 720 m bsl. However, this deepening is not uniform, and a promontory of shallower topography is located within the south central section of the study area (Fig. 6.11). This promontory consists of a shallow (650 m bsl) central section, between 500 to 800 m wide and around 4 km long, which is surrounded by a slightly deeper (680 m bsl) larger area, which is around 5.5 km wide and 6.5 km in length.

With the exception of a western section of the study area, the lower surface of the MTD unit has an irregular base, and a time-depth map of the basal horizon reveals several north-east to south-west orientated features that are located within the central and south western sectors of the study area (Fig. 6.11a). The most prominent of these features is an irregular, linear depression which is interpreted as a pronounced erosional feature or 'scour' (Fig. 6.11b, Point S). Linear erosional features of this scale and geometry have been interpreted at the bases of MTDs in several previous studies (see Bull et al. 2009, and references therein), and have been termed slots or grooves. They form by preferential erosion at the base of the MTD and give the transport direction of the slope failure. The width of the scour in the study area varies between 300 and 700m, with an occasional shallower central section present along its length. At its north-eastern extent this raised central section divides the scour into two separate features.

To the south-east, another raised section of topography separates the scour from a larger, irregular shaped, deeper area, which is also orientated north-east to south west. An arbitrary seismic section perpendicular to the scour orientation shows the scours as two small scale depressions which cut down into the underlying reflection (Fig. 6.12a). The scours are separated by a flatter, slightly raised, area which can be seen on the TWT map. Above the scours the reflections of the MTD unit are discontinuous and chaotic, with a large variation in amplitude. The edge of the deeper area located to the south-east of the scours is also visible along this section (Fig. 6.12a). To the north-west of the scours the basal horizon of the unit is relatively continuous and no down-cutting scours are observed.

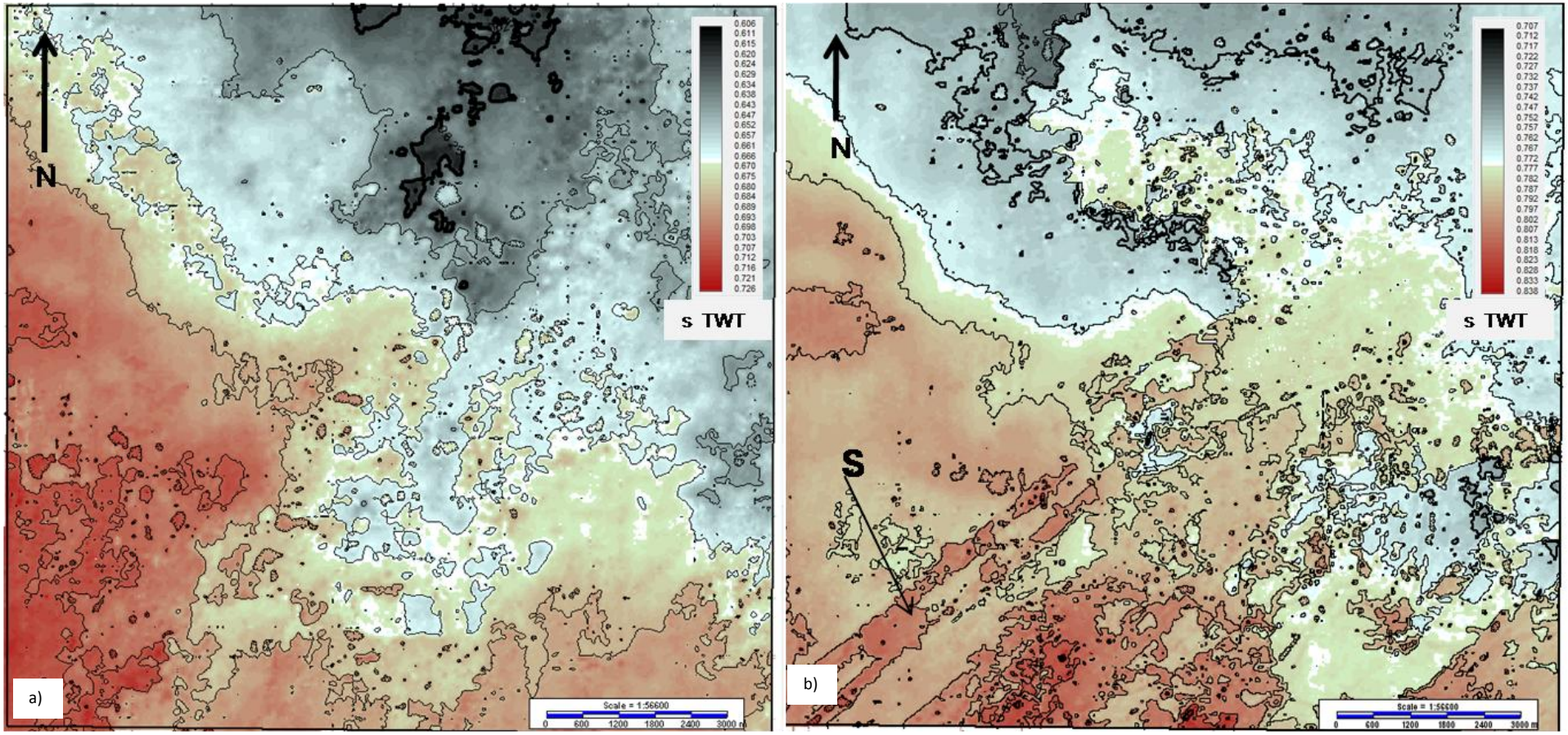

Fig. 6.11 a) TWT structure contour map of the top of the MTD unit with the protruding promontory of shallower topography (Grey area) b) a TWT structure contour map of the base of the MTD unit, showing large scour feature (S).

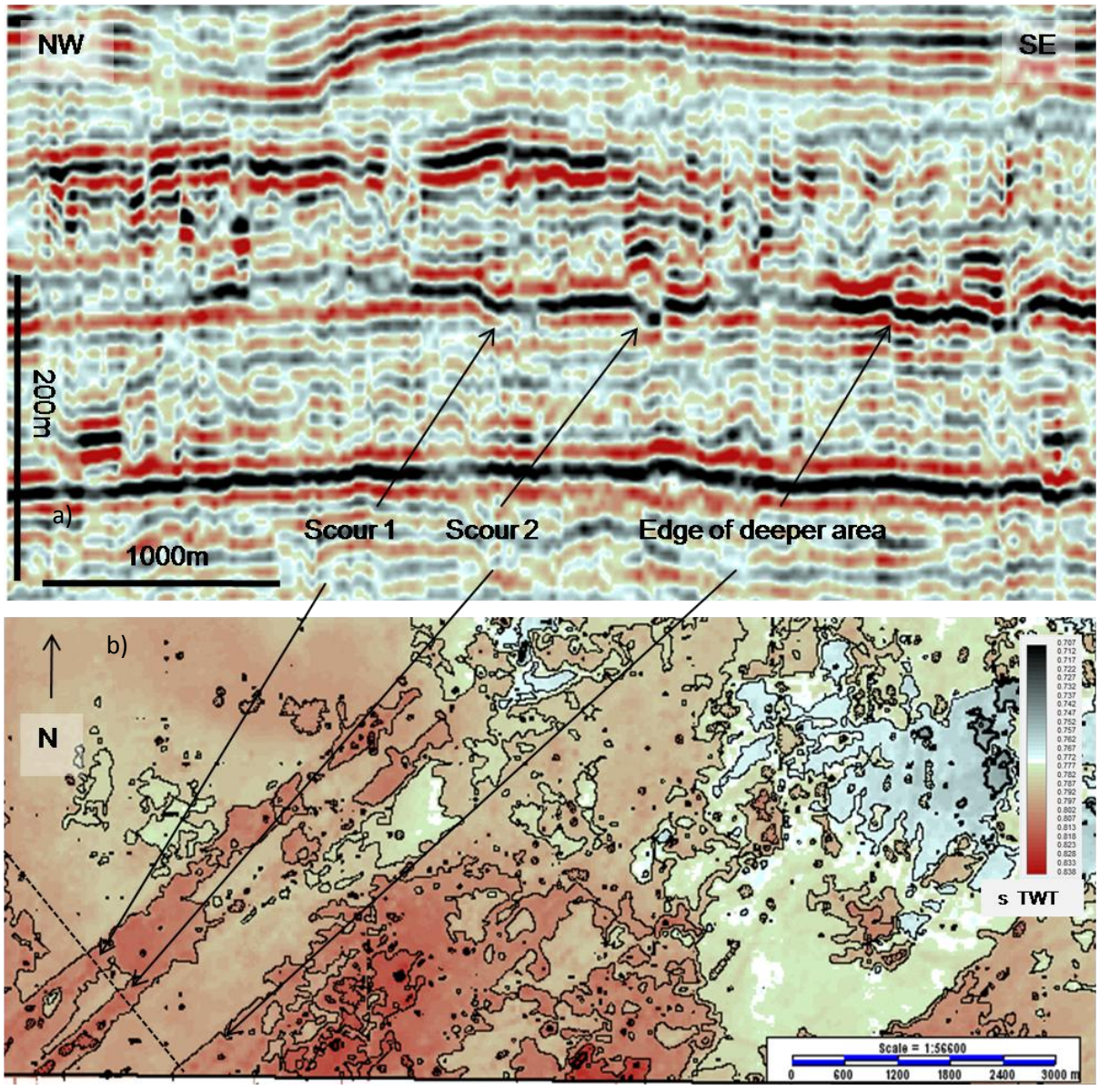

Fig. 6.12 a) NW-SE seismic section intersecting the scour feature shown in Fig. 6.11b.

Two time-slices which dissect the MTD unit at 0.756s TWT and 0.776sTWT (approx 756m bsl and 776m bsl respectively) also highlight the prominence of north-east to south-west orientated features. Both slices also show two areas that are noticeably different in their seismic appearance. The shallower time-slice, T756 (Fig. 6.13a), shows an area (Area A), covering the central west, north-western and northern sections of the study area, which is significantly different to that in the rest of the study area. Area A has alternating bands of opposite polarity which is consistent with the relatively uniform dip of the unit deepening towards the south-west within this area. To the south-east of this area the seismic response becomes chaotic, with irregular changes in polarity.

Concentrated in the central and eastern areas are several south-westerly and west south-westerly orientated features. Three of the most evident of these are shown in greater detail in Fig. 6.13b, and a section across their profile in Fig. 6.13.c (Points 1.2 and 3). As with the examples in Fig. 6.12, these scours are visible as small scale depressions which down cut into the underlying reflections. Separating the scours is a flat lying, slightly elevated reflector, which corresponds with the areas of red polarity seen on the time-slice which cover a greater areal extent than the scours themselves.

The deeper time-slice, T776 (Fig. 6.14), shows that the south-westerly and west south-westerly orientated features are mostly concentrated in the south west and south central areas at this deeper level. Area A has increased in extent, while the more chaotic area is reduced. The large scour, as seen in Fig. 6.12(Point S), is also visible upon this time slice (Fig. 6.14, Point S). Located within the south-eastern corner is a relatively large area of red polarity with occasional linear features of black polarity (Point 6.14, Point R), similar features are seen in Fig. 6.13b, and would suggest further scours separated by a flat lying reflection.

It is noticeable that the internal reflection character of the MTD is more blocky in character where there are basal scours on the base of the MTD surface. This perhaps suggests that the scours were formed by the translation and erosive action of more intact blocks of stratigraphy that were entrained in the MTD (c.f. Moscardelli et al. 2009; Bull et al. 2009). This point is developed below.

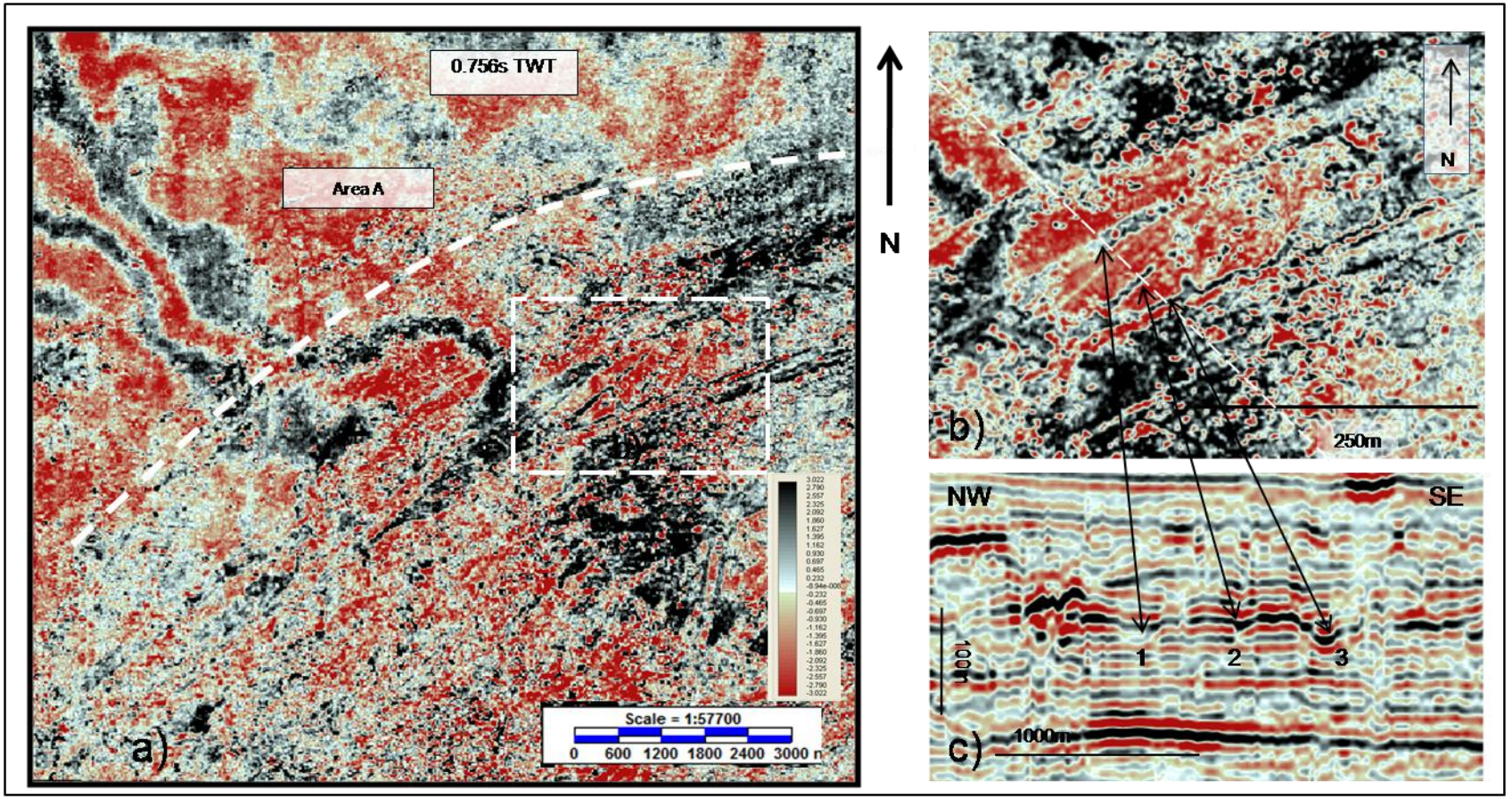

Fig. 6.13 a) a time-slice dissecting the MTD unit, with two distinctly different areas of reflections,b) a smaller scale section of the time-slice displaying linear features c) a seismic section intersecting these linear features, interpreted as basal scours.

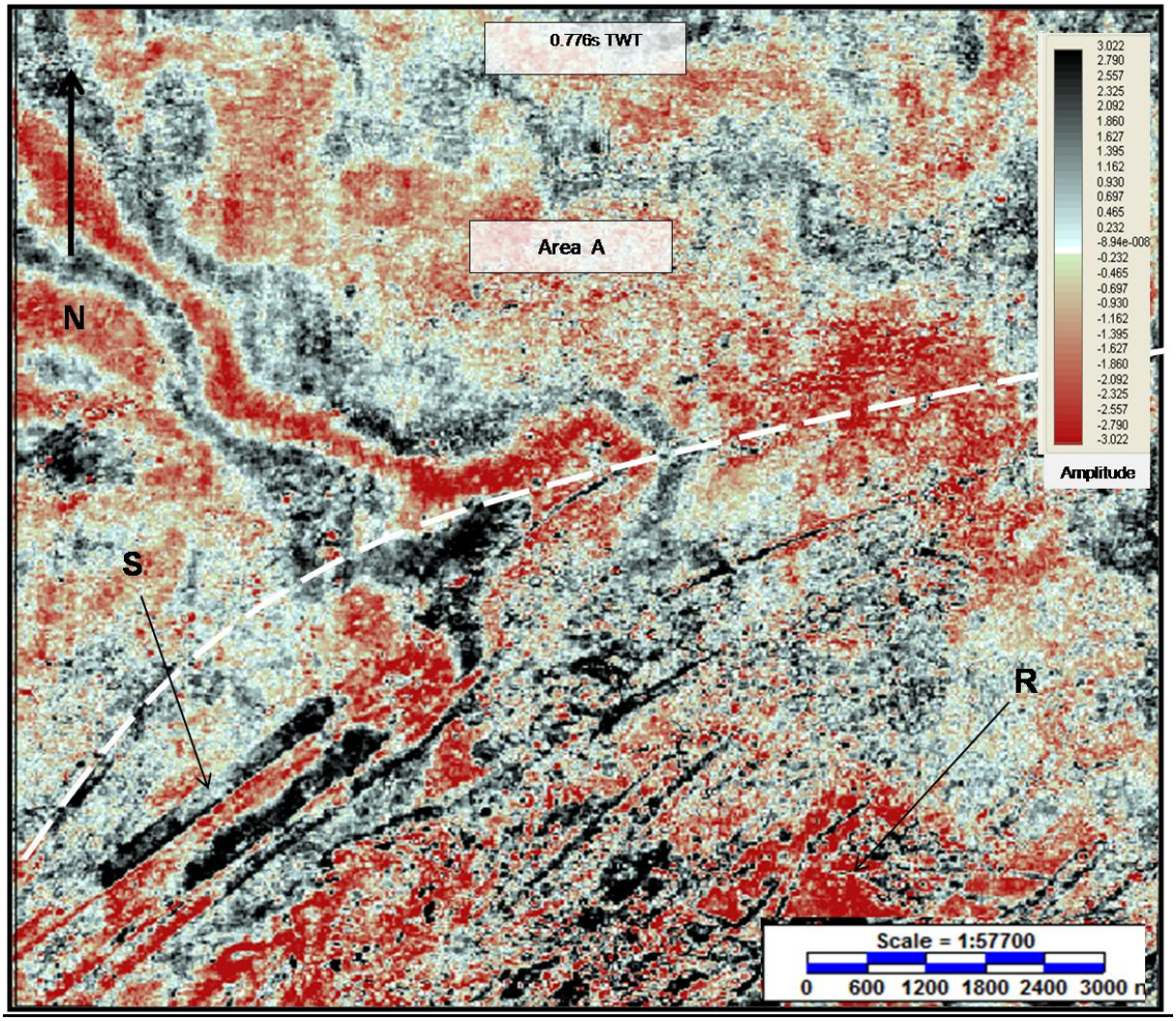

Fig. 6.14 a deeper time-slice dissecting the MTD unit, the chaotic area has progressed more to the southeast, a large area of a red reflection is located at point R

6.3.3.1. MTD Isopach

The combined effect of the features present on the top and bottom surfaces clearly has a pronounced effect on the unit thickness and is reflected by an isopach map of the unit (Fig. 6.15). The unit is of significant thickness (>100m) within the north-east, central and south-west sections of the study area (denoted by the contour). Several areas exceeding 130m (darker colours) are also located within this section. A markedly south-west to north-east orientated area of increased thickness is located within the southern section, and the effect of the large scour is visible in the south-western corner (Fig. 6.15, Point S).

An arbitrary seismic line perpendicular to the narrow south-west to north-east trending ridge of greater thickness is presented in Fig. 6.16a. Along this profile the thicker area is around 3750m wide and exceeds 135m in thickness (Fig. 6.16b) and is delimited at both edges by areas of less than 100m in thickness. A time-slice of this area at the depth of the basal horizon of the unit is shown in Fig. 6.16c. There are several south-west orientated features present within this area at this depth, however they are absent within the north-west corner. The boundary of this area, shown as Area A in Fig. 6.14, roughly coincides with the MTD unit 100m contour. To the south-east is another area less than a 100m thick, and this area can be seen to coincide with the relatively large section of red polarity upon the time-slice and the flat lying reflection on the seismic section.

The thicker area is clearly visible within the centre of the seismic section (Fig. 6.16a), while the thinner areas at the periphery coincide with a relatively horizontal, high amplitude and continuous basal horizon. The basal horizon within the central section of the profile is disrupted, of varying amplitude, and at several points cuts down into the underlying unit (Points 1,2,3,4 and 5). The overlying reflections are chaotic in nature, consisting of discontinuous and discordant reflectors which range from low to high amplitude. Above the chaotic area the upper horizon of the unit becomes semi-continuous and is slightly displaced when associated with sections or spots of high amplitude. There are no traceable horizons through the chaotic package, although semi-continuous and concordant reflections are present at its periphery.

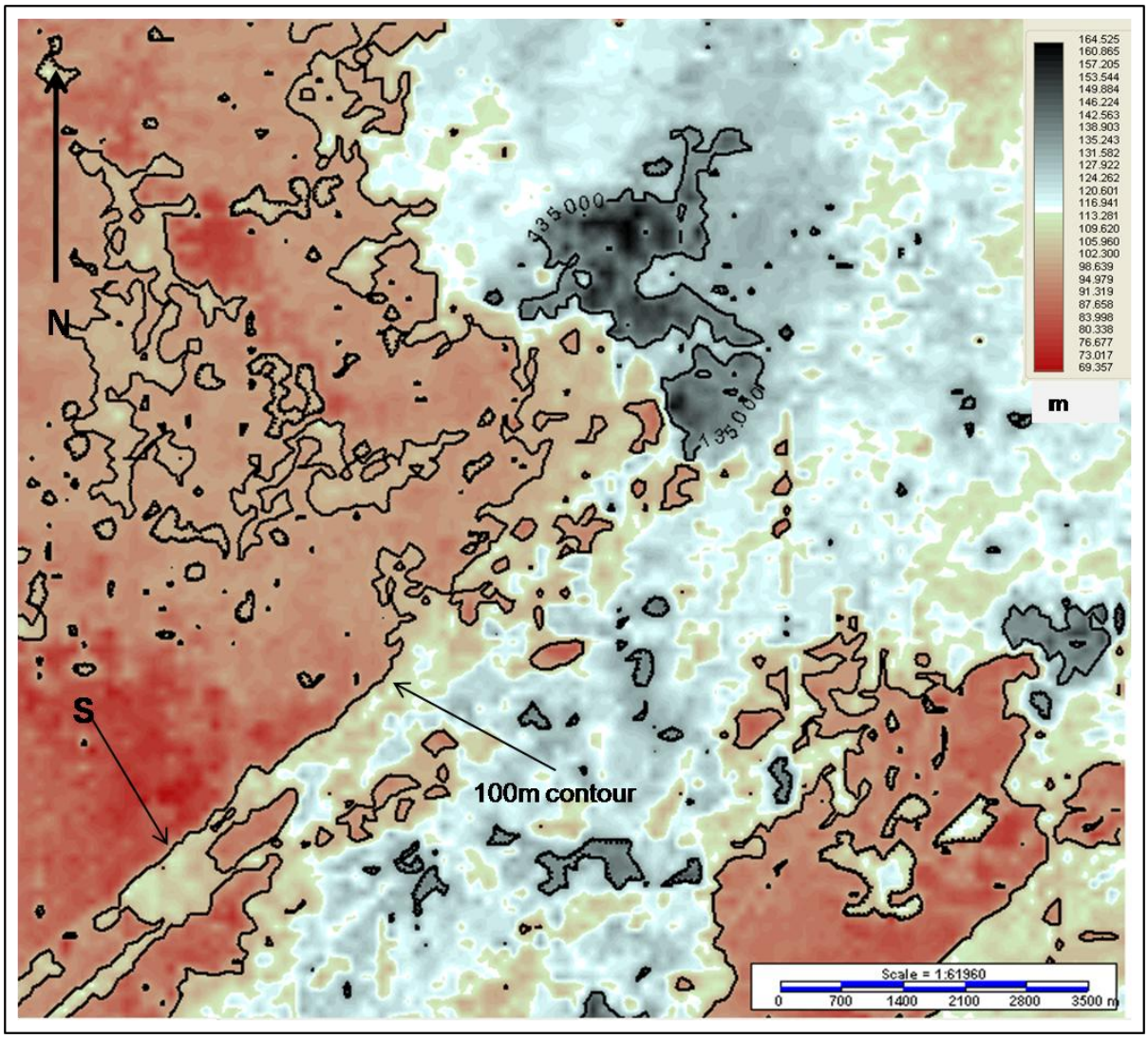

Fig. 6.15 an isopach map of the MTD unit with a 100m thickness contour.

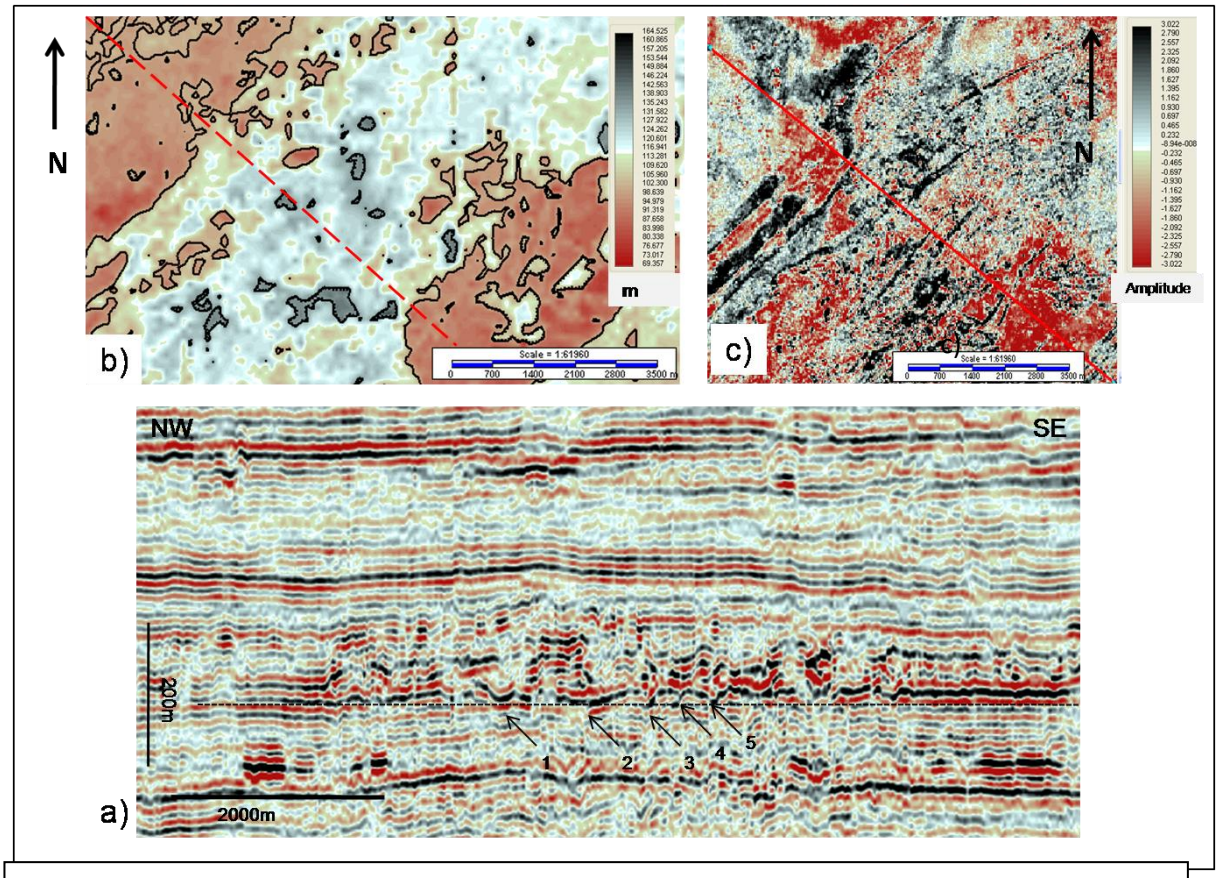

Fig. 6.16 a) a NW-SE orientated seismic section transecting the b) area of greatest thickness. Scours at the base of the unit coincide with the black linear features evident on the c) time-slice which dissects the basal section of the MTD unit.

6.3.3.2. MTD amplitude variations

An RMS map of the unit co-rendered with the isopach contours is presented in Fig. 6.17. Although not exclusive to, the majority of incidents of high amplitude (blue) are contained within the section of the unit which exceeds 100 m in thickness. Examples of the high amplitude features which lie within and outside this section of greatest thickness are presented below.

6.3.3.3. Amplitude anomalies within the area of greater thickness

Two intersecting arbitrary lines, orientated roughly perpendicular to each other are presented in Fig. 6.18. A north-west to south-east orientated line which transects the protruding head of raised topography and area of greater thickness is presented in Fig.6.18b. This seismic section intercepts several high amplitude areas, the most prominent of which is visible on the RMS slice as an irregular shaped area of high amplitude (Fig. 6.18a, point A). Along the seismic section it consists of a high

amplitude reflection, around 200 m in length, located within a chaotic package of reflections, and adjacent to an area of low amplitude (point D). In close proximity are several other high amplitude features, while the chaotic package affects a total section close to 4km in length. The base of the unit is irregular and difficult to trace, and there are incisions into the underlying unit present (point E), which have been shown to be associated with scours in Fig.s 6.13, 6.14 and 6.16. At the edges of the chaotic package there are relatively horizontal and continuous reflections, these closely coincide with the areas of low amplitude and the edges of the 100m MTD contour (Fig. 6.19a and b, points B and C).

The second arbitrary line runs along the length of the raised area of topography, roughly south-west to north-east, and intercepts several high amplitude areas (Fig. 6.18c). The MTD unit can be seen to consist of chaotic reflections which are generally discontinuous and discordant, with regular high amplitude features along the length of the section. The basal horizon can be traced along some of the section with relative ease, with the exception of where it underlies the most chaotic area (Point F), while scours are not obviously evident in this area. There are some horizontal, semi-continuous reflections present (Points G and H), while the orientation of other reflections suggest a slight imbrication of the internal reflections in some parts of the MTD unit (Points I and J).

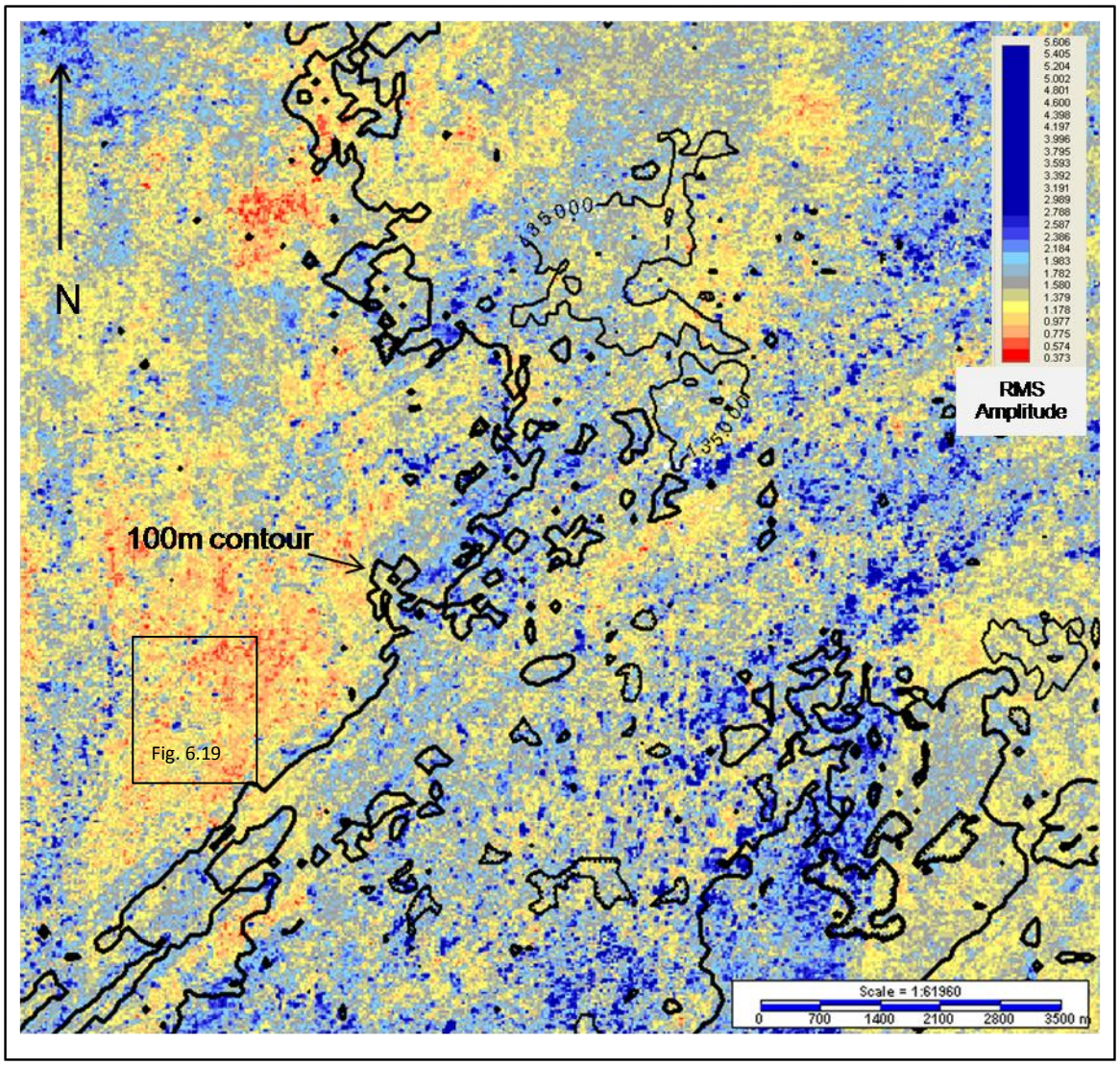

Fig. 6.17 the 100m contour co-rendered with the RMS map of the MTD unit. A large proportion of the high amplitude areas are located within the boundaries of the 100m contour.

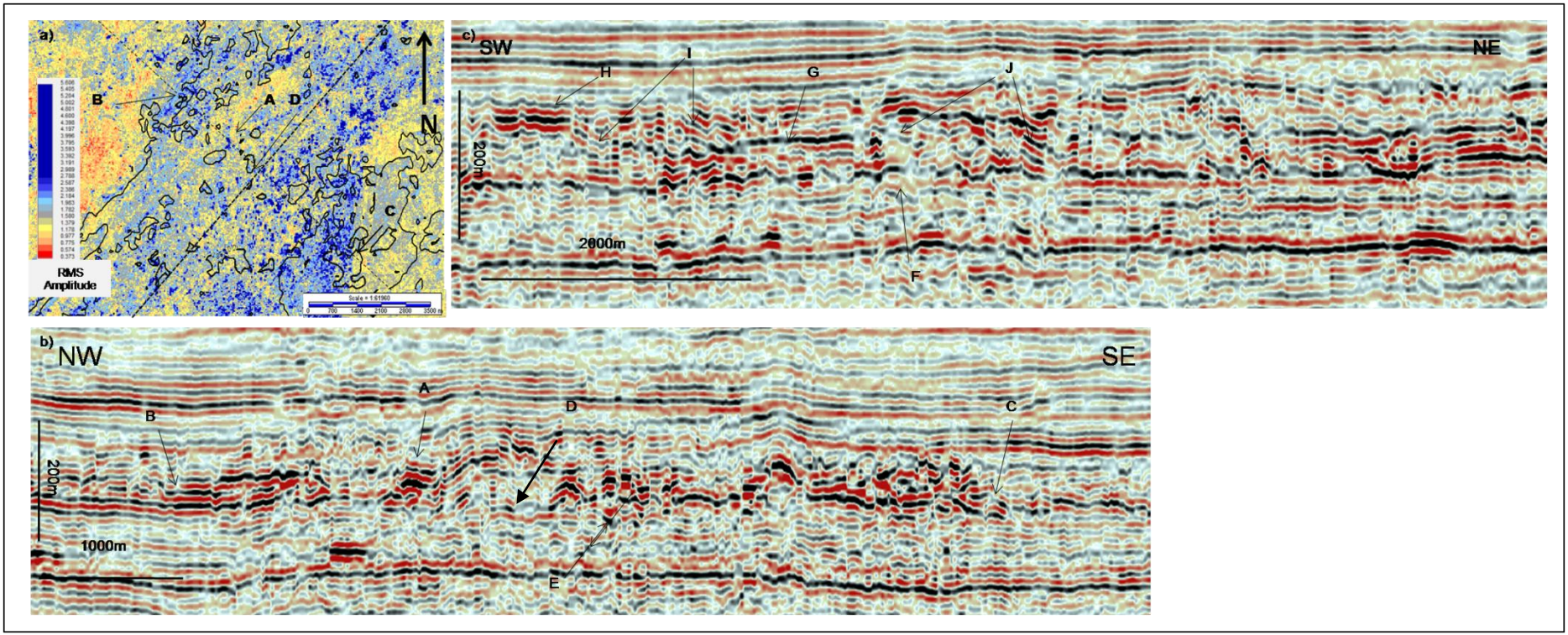

Fig. 6.18 a) a small scale section of the RMS map with locations of seismic sections b) NW-SE section along the demonstrating the variable nature of the MTD unit within the thicker area, features include; **A** high amplitude bright spot, **B** stratified reflections ,**C** low amplitude reflections, **D** areas of low amplitude and **E** downward incisions. c) SW-NE section across the area of greatest thickness includes the following features; F chaotic area, **G and H** horizontal semi-continuous reflections, **I and J**. imbrication of the internal reflections

6.3.3.4. Amplitude anomalies outside the area of greater thickness

Although the majority of the high amplitude features lie within the thicker section of the unit, there are several occurrences outside this area. Representative examples of these are presented below.

6.3.3.4.1. Bright spots

Bright spots 1 and 2 are both located over a kilometre to the north-west of the 100 m thickness contour of the MTD unit (Fig. 6.19a). Both are noticeable sub-circular areas of high amplitude in an area characterised by relatively low amplitude (Fig. 6.19b). An arbitrary seismic line orientated south-south-west intercepts both features (Fig. 6.19c). Both features are hosted within the unit identified as an MTD unit; however the nature of the internal reflections here, outside the area of greatest thickness, is markedly different to that of the reflections inside the area of greatest thickness. The bright spots consist of three high amplitude stacked reflections less than a 100 m wide. The unit reflections are generally stratified, concordant and sub-horizontal, although there appears to be a loss of resolution proximal to the bright spots. Bright spot 1 displays a possible polarity reversal, although the lack of resolution gives a degree of uncertainty (Fig. 6.19d, Point PR?).

There are other, less prominent amplitude anomalies along the profile, (Fig. 6.19c, Point BS3, BS4 and BS5), and they appear to affect the same reflection as anomalies BS1 and BS2. Both BS1 and BS2 have underlying features of interest. Anomaly BS1 is directly underlain by a discordant high amplitude feature (Fig. 6.19d , Point A), while around 100 m below BS2 is a stacked concordant anomaly, which is less than 50 m wide, and appears to be affecting the top horizon of the Utsira Sand (Fig. 6.19c , Point B). The whole group of bright spots are underlain by an elliptical mound affecting the Base Utsira horizon, which is in turn underlain by high amplitude reflections interpreted as cemented sections of a sand intrusion (Chapter 5, Section 5.3.2) At locations directly underlying the amplitude anomalies the Base Utsira horizon reflection dims and appears broken (Fig. 6.19c, arrowed).

A further example of a bright spot with an associated zone of disrupted reflections is presented below.

6.3.3.4.2. Bright spot with vertical disruption

Another example of an outlying amplitude anomaly is shown in Fig. 6.20a. It is located over 2km away from the 100 m contour, and around 3km to the north-east of Bright spots 1 and 2 shown in Figure 6.19. On the RMS map it is seen as a sub-circular, elongated feature less than 100 m in long axial length (Figure 6.20b). It is present on the south to north seismic section (Fig. 6.20c) and appears as a pair of high amplitude sub-vertical reflections of opposite polarity. As in the previous example the anomaly is seen to overlie an ellipsoidal mound present at the Base Utsira horizon, and there is a suggestion of vertical zone disruption between the anomaly and the Base Utsira horizon (Fig. 6.20c, Point VZ). This zone appears to emanate from the hinge point of Base Utsira forced fold, proximal to where the reflection appears to be broken and displaced (Fig. 6.20c, Point HP). From this point the zone, between 200 and 300 m wide, penetrates upwards through the Utsira Sand towards the Top Utsira horizon.

Within the Utsira Sand the internal reflections of the zone are dimmed and chaotic, and the zone itself is bounded on both sides by the stratified and continuous internal reflections of the Utsira Sand. Within the Utsira Sand interval, the vertical zone of disruption coincides with a point where the internal reflectors of the Utsira transform from horizontal to downwards dipping. The zone continues upwards through the Top Utsira horizon, which is broken with a slight brightening of the underlying reflector at the point of intersection (Fig. 6.20c, Point B). The zone persists for a further 130m, and appears to terminate at BS6 within the MTD unit. A second vertically disrupted zone of reflections appears adjacent to BS6, it appears to begin at the top MTD level and penetrate upwards through the Middle Seal (Fig. 6.20c, Point VZ2). Another feature of note is a high amplitude feature affecting the Top Utsira horizon, located at a crestal high, adjacent and up dip from the vertical zone (Fig. 6.20c, Point A).

6.3.3.4.3. Anomaly at flank of mound

A group of several small scale elongated anomalies are located over 1 km to the west from the 100 m contour (Fig. 6.21a, Point G). A north-south seismic line intercepts one of the high amplitude features (Fig. 6.21b, Point G), and it can be observed as an area of the MTD unit where the sub-horizontal and stratified reflections appear to be effectively ‘pushed up’ to form an asymmetrical pyramidal geometry. The anomaly is underlain by a vertical zone of disrupted reflections (Point VZ),

and seems to emanate from a point where the Base Utsira horizon is broken (Point BU), and at a point where the angle of the sand intrusion wing would penetrate the Utsira Sand (W). This zone of disrupted reflections appears to cover a vertical distance of over 300m upwards from the Base Utsira, breaching the Top Utsira Horizon (Point TU), and terminating in the MTD unit (Point G).

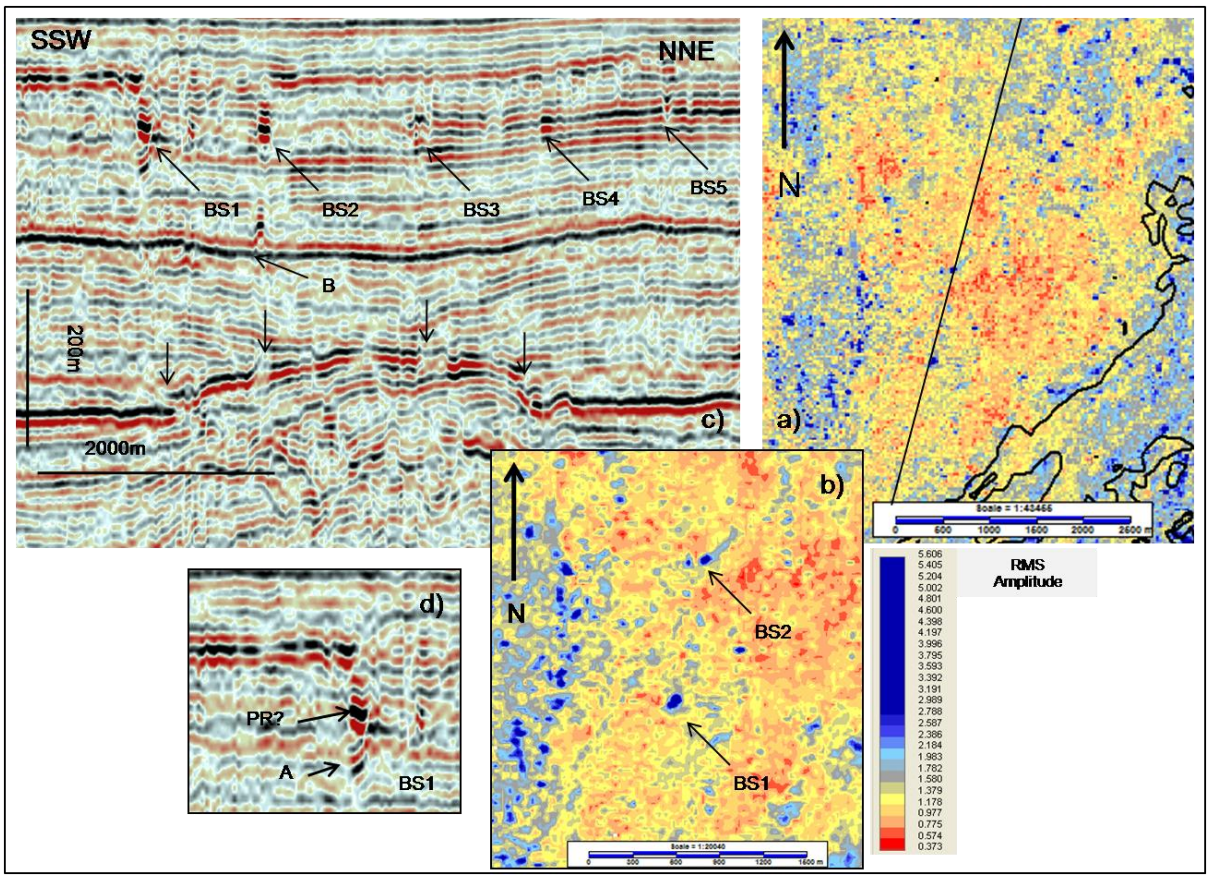

Fig. 6.19 a) location of the seismic section b) BS1 and BS2 are circular areas of high energy c) SSW-NNE seismic section showing five bright spots above a Base Utsira forced fold, discontinuous sections of the Base Utsira Horizon are arrowed, with a possible pockmark at the Top Utsira (B) d) possible polarity reversal (PR?) with a underlying discordant bright spot.

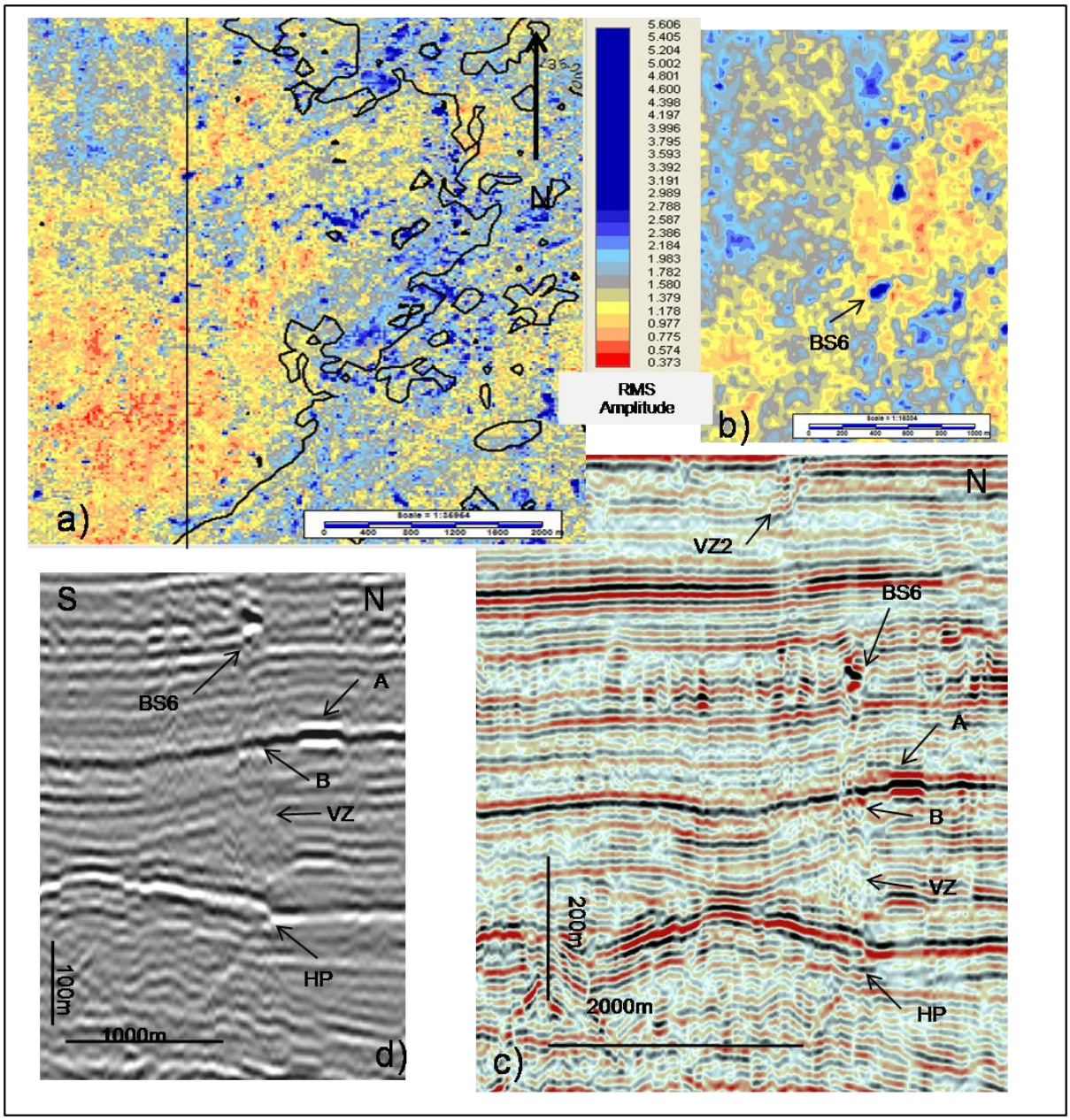

Fig. 6.20 a) RMS map of MTD horizon with location of seismic section b) BS6 is sub-circular feature, c and d) S-N section with BS6. The hinge point of the Base Utsira Horizon is broken (HP), and is associated with a vertical disruption zone (VZ) which extends to the Top Utsira Horizon (B), proximal to a high amplitude section of the Top Utsira Horizon (A), a secondary vertical disruption zone (VZ2) extends upwards from the MTD unit.

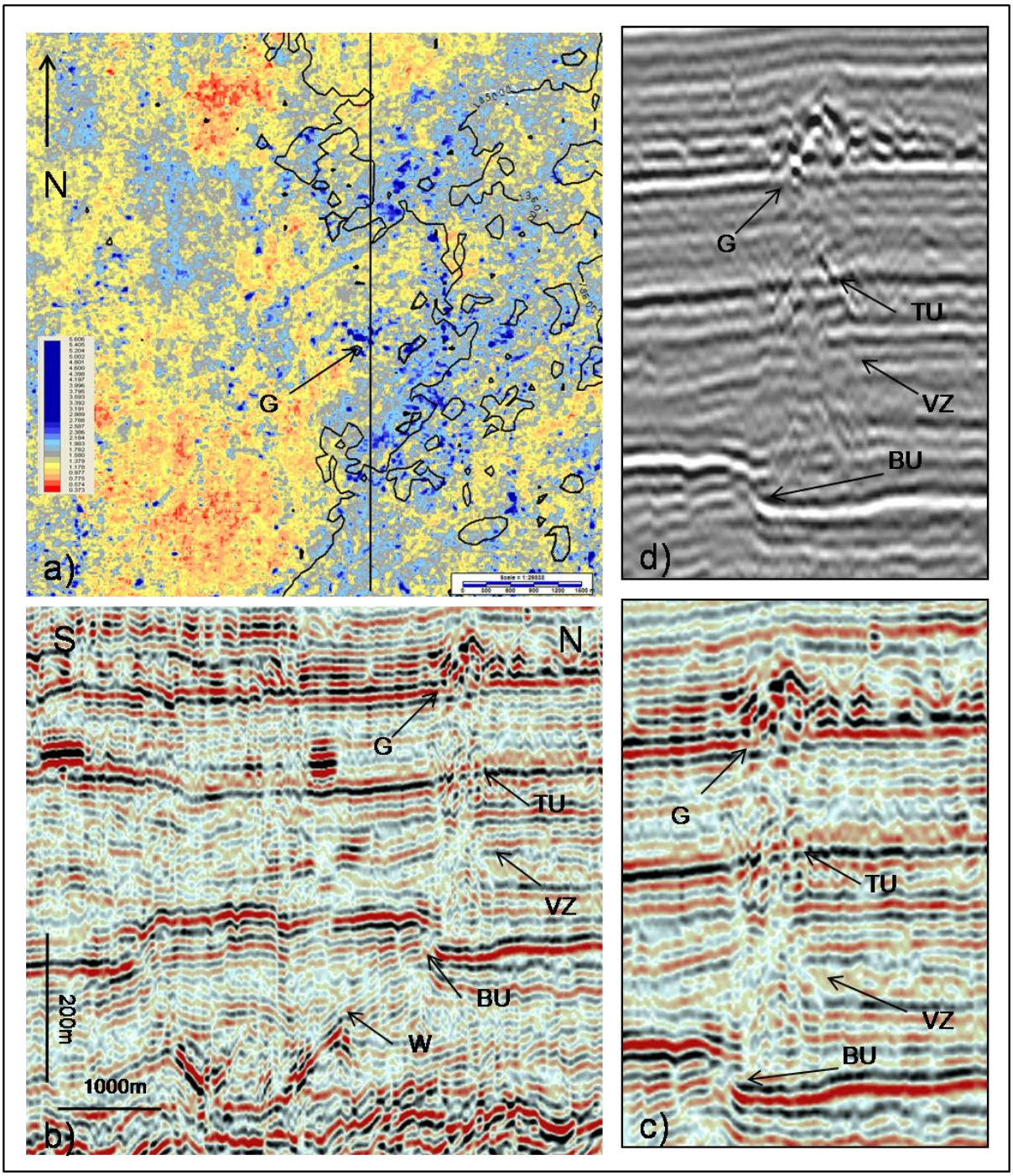

Fig. 6.21 a) RMS map of MTD horizon with location of seismic section and the group of high amplitude areas b) c) and d) S-N section with high amplitude section within the MTD unit (G). The hinge point of the Base Utsira Horizon is broken (BU), and is associated with a vertical disruption zone (VZ) which extends to the Top Utsira Horizon (TU). Sand intrusion wings are evident in the Lowermost Shale unit (W).

6.3.3.5. Interpretation and discussion

Maps, time-slices and seismic sections of this unit demonstrate its highly variable nature through the study area. It is proposed that the unit may in fact be split in two, consisting of an unaffected 'host' unit and a separate Mass Transport Deposit. The boundary between the unit components can roughly be equated to the 100 m thickness contour, which has been shown to crudely correspond with the change in reflection character seen in the presented time-slices and seismic sections.

6.3.3.5.1. Directional indicator of MTD

Several examples of 'scours' which affect the basal surface of the MTD unit have been presented. They are seen on time-slices proximal to the base of the unit as linear striations, generally orientated south-west to north-east. Similar small scale 'V' shaped cross sectional features have been presented by Bull et al. (2009) as kinematic indicators that are located in the translational (central) domain of mass transport complexes. Flat-based, wider, features are also presented by these authors who term them striations; these are similar to the features presented in Fig. 6.12. Both types of features indicate a direction of movement parallel to their orientation.

We also present a seismic section along the length of the north-east to south-west orientated raised area (Figure 6.17), this seismic profile displays sections of reflections which appear to be imbricated; tilted from their base to tip towards the south-west. These features display a similarity to thrusts related to MTC pressure ridges presented by Bull et al. (2009). These are also considered to be directional indicators, which are orientated perpendicular to flow (Frey Martinez et el., 2006 and Moscardelli et al., 2006). This would also suggest a north-east to south-west direction of movement for the MTD in the study area. This direction of movement is further supported by Figures 6.13 and 6.14, where the movement of the scour features and chaotic reflections from the north-west to south-east is evident in deeper time-slices.

6.3.3.5.2. Amplitude variations within MTD

There is a large variation in amplitude across the MTD unit, the majority of the higher amplitude features are located within the area on the thicker side of the 100 m isopach, considered to consist of the mass transported component. It is proposed that these high amplitude areas and the variations seen within the 100 m contour are a result of changes in the internal constituents of the

MTD. MTD units have been shown to consist of stratified and concordant, medium and high amplitude reflections and zones of chaotic high amplitude reflections which are surrounded by low amplitude zones, termed 'debritites' (Gamboa et al., 2010, 2011).

The stratified and concordant sections of the MTD are termed blocks, and are classified as remnant or rafted. Remnant blocks are in-situ and generally unaffected by the MTD, while rafted blocks have been 'plucked' from their original position and transported by the MTD. They are often rotated, and show an imbrication of their internal strata. Although the basal shear surface is considered to act as a permeability barrier (Allan et al., 2006). The blocks themselves retain some of their original cohesion and may represent permeable pathways through the MTD unit. (Gamboa et al., 2011).

The higher amplitude areas seen within the 100m contour in this study area coincide with chaotic high amplitude reflections, the more moderate areas appear to be remnant blocks which display clear stratification, while the lower amplitude areas correspond with chaotic low amplitude zones which resemble the 'debritites' of Gamboa et al. (2010).

6.3.3.5.3. Bright spots above elliptical mounds

The bright spots located outside the 100m contour all overlie elliptical mounds which affect the Base Utsira Horizon (Figure 6.19, 6.20, 6.21). Each one also overlies points where the BUH is discontinuous. In some cases indistinct and narrow vertical zones of disrupted reflections appear to connect the breaks in the BUH with the bright spots within the overlying strata. These zones consist of narrow sections (<100m) of the seismic profile where the reflections dim and appear broken in places.

Below BS2 (Fig. 6.19) there is a small, positive bulge of the Top Utsira reflection, it protrudes upwards into the horizon defined as the LSHAH (Section 6.4.2). It is possible that this is a pockmark, as seen to underlie the amplitude anomalies of the LSHAH level (Fig. 6.9). In this instance it appears that this feature has developed vertically rather than laterally; forming a pipe which terminated at BS2 instead of creating a lateral amplitude anomaly as seen in the other examples. It is suggested that these bright spots and vertical disrupted zones are linked to fluid flow from depth, possibly focused through the highly permeable sand intrusion wings and parasitic intrusive sand 'off-shoots.' These 'offshoots' are envisaged to be the equivalent of a localised halo of small intrusions clustered around large wings as described by Huuse et al (2005).

6.3.3.5.4. Bright spots above flanks of elliptical mounds

The vertical disruption zones presented in Figures 6.20 and 6.21 are more prominent than in Figure 6.19. They are wider (>100 m) and display a greater disruption to the internal reflections of the Utsira Sand. BS6 (Fig. 6.20) appears to be the terminal point of a vertical disruption zone which extends upwards from the hinge point of the Base Utsira ellipsoid mound past the Top Utsira and into the MTD unit. An adjacent high amplitude section of the Top Utsira Horizon suggests that a portion or 'batch' of the migrating fluid or gas may have been diverted to fill this structural high while the remainder has progressed vertically.

A similar example is presented in Figure 6.21, however the vertical disruption zone is slightly wider (>250 m) and the amplitude anomaly within the MTD unit affects a greater area. The vertical disruption zone consists of chaotic and dimmed reflections, emanating from the hinge point and continuing past the Top Utsira Horizon.

6.3.3.5.5. Fluid pathways associated with sand intrusion

We consider that the small scale vertical zones underlying the bright spots in Figure 6.19 are the result of small scale fluid flow features caused by fluid flow focused through the sub-seismic wings and parasitic sand off shoots of the highly permeable sand intrusion. The vertical zones related to the amplitude anomalies in Figures 6.20 and 6.21 are larger and have a more pronounced effect on the internal reflections of the Utsira Sand. Both these examples are located at the hinge points of ellipsoid mounds, where the sand intrusion wings are interpreted to intersect the Base Utsira Horizon. It is possible that at these points the greater volume of the wings, compared to smaller parasitic off shoots; allow a greater flux of fluid, thus causing a wider zone of disruption. However, it is worth considering that these vertical zones coincide with the hinge points at both the Base Utsira and Top Utsira levels, a zone, which has been demonstrated in Chapter 5 to have undergone a significant level of vertical movement related to sand intrusion emplacement and post-emplacement compaction.

We have shown that following the formation of the ellipsoid mound due to sand intrusion emplacement, the mounds experience a loss of relief and the overlying strata form broad ellipsoid shaped depressions as the sand intrusion lose aperture due to compaction and grain reorganisation (Sections 4.3.2.5.1 and 5.4.4.1). The central zones of the depressions, which overlie the crest of the

mounds experience the greatest amount of subsidence and should be considered a compressive zone. The flanks of the depressions must therefore experience a degree of extension to compensate for this movement, creating a zone which would be prone to faulting (Fig. 6.22a). In plan view this zone would form an outer rim of disrupted reflections (Fig. 22b). Ring faults are commonly observed elsewhere to define the perimeter of collapse-type structures, as for example in the case of karst collapse (Bertoni and Cartwright, 2006). We therefore propose that the vertical zones of disruption shown in Fig.s 6.20 and 6.21 have exploited these extensional features as permeable fluid pathways. Similar arguments have recently been advanced in the case of carbonate dissolution collapse pipes, as regards their role in engendering vertical bypass of gas across thick sealing sequences in the South China Sea (Sun, et al., 2012). It is therefore proposed that the vertical zones of disruption shown in Fig.s 6.20 and 6.21 have exploited these extensional features as permeable fluid pathways.

Fig. 6.22 a) a schematic diagram of extensional and compression zones associated with sand intrusion compaction. The extensional zones represent possible permeability pathways obliquely upwards from edges of the elliptical mounds b) a contour of a base Utsira mound is co-rendered with a time-slice dissecting the Utsira Sand around a 100m from the mound hinge point. An outer rim of disrupted reflections is seen to encompass the mound contour, suggesting the presence of ring faults.

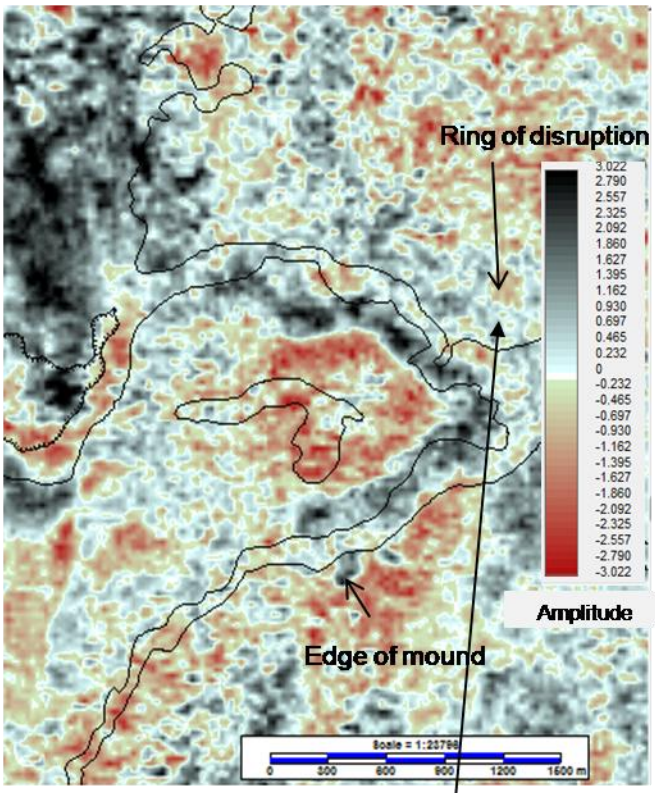

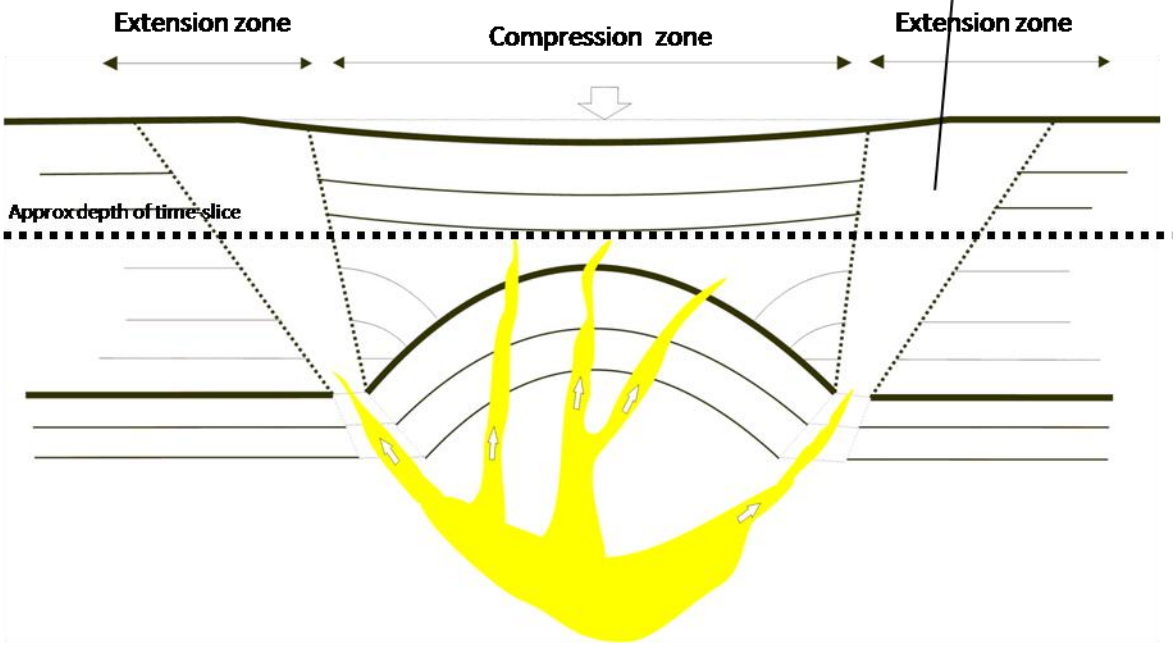

6.3.4. Middle Seal

6.3.4.1. Branch network

A time slice at the depth of the relatively flat-lying Middle Seal horizon reveals a series of channel-like branches which appear to splay outwards from an area within the south central part of the study area (Fig. 6.23, Point CA). The feature consists of four main branches (Fig. 6.23, dashed arrows), with several other minor offshoot branches. There does not appear to be a preferential orientation, with the main branches orientated to the south-west, south-east and the east-south-east respectively.

A south to north seismic line intersects the two western branches (Fig. 6.24b). The south-west orientated branch is seen to affect a significantly larger area than the east south-eastern branch along this profile. It appears as a lenticular shaped disruption which affects the Top Middle Seal Horizon (TMSH), the Middle Seal itself and the overlying Quaternary unit (6.24b, Point A). It affects a section around 1.8km in length, cutting around 60m downwards into the Middle Seal, and mounded upwards around 20m into the Quaternary unit. The down-cutting horizon truncates the upper reflections of the Middle Seal, which in turn onlap at the sides of the lower half of the lens (Points B and C). The reflections of the lens area are of noticeably higher amplitude than those of the underlying and overlying units.

The second of the western branches, orientated to the west-north-west, is not such a noticeable feature on this seismic section. It consists of a short length horizontal high amplitude reflection which deflects downwards into the Middle Seal (Point D). The length of the high amplitude reflection does not exceed 300 m. However, a lower amplitude continuation of this reflection appears to cut downward into the middle seal forming a broad and shallow but faint 'U' shaped feature.

An arbitrary line, orientated SW-NE, intercepts the two eastern branches (Fig. 6.24c), the southern one of which is indistinctly imaged in seismic section. TMSH is seen to be slightly disrupted, while a discordant low amplitude reflection appears to cut down though the Upper Seal/Quaternary Unit (Fig. 6.24, point F), and continues below the TMSH as a short length (100m) high amplitude discordant reflection (Point G). Along the section to the north-west the second branch is a more prominent feature. A high amplitude discordant reflection is clearly seen in the Upper Seal, continuing down to the TMSH, and proceeding into the Middle Seal (Point H). The reflection becomes dimmed and semi-continuous and sub-horizontal, before deflecting upwards towards the

TMSH and brightening slightly before they intersect (Point I). A medium amplitude discordant reflection within the Upper Seal (Point J) is of a similar dip to the reflection at point I.

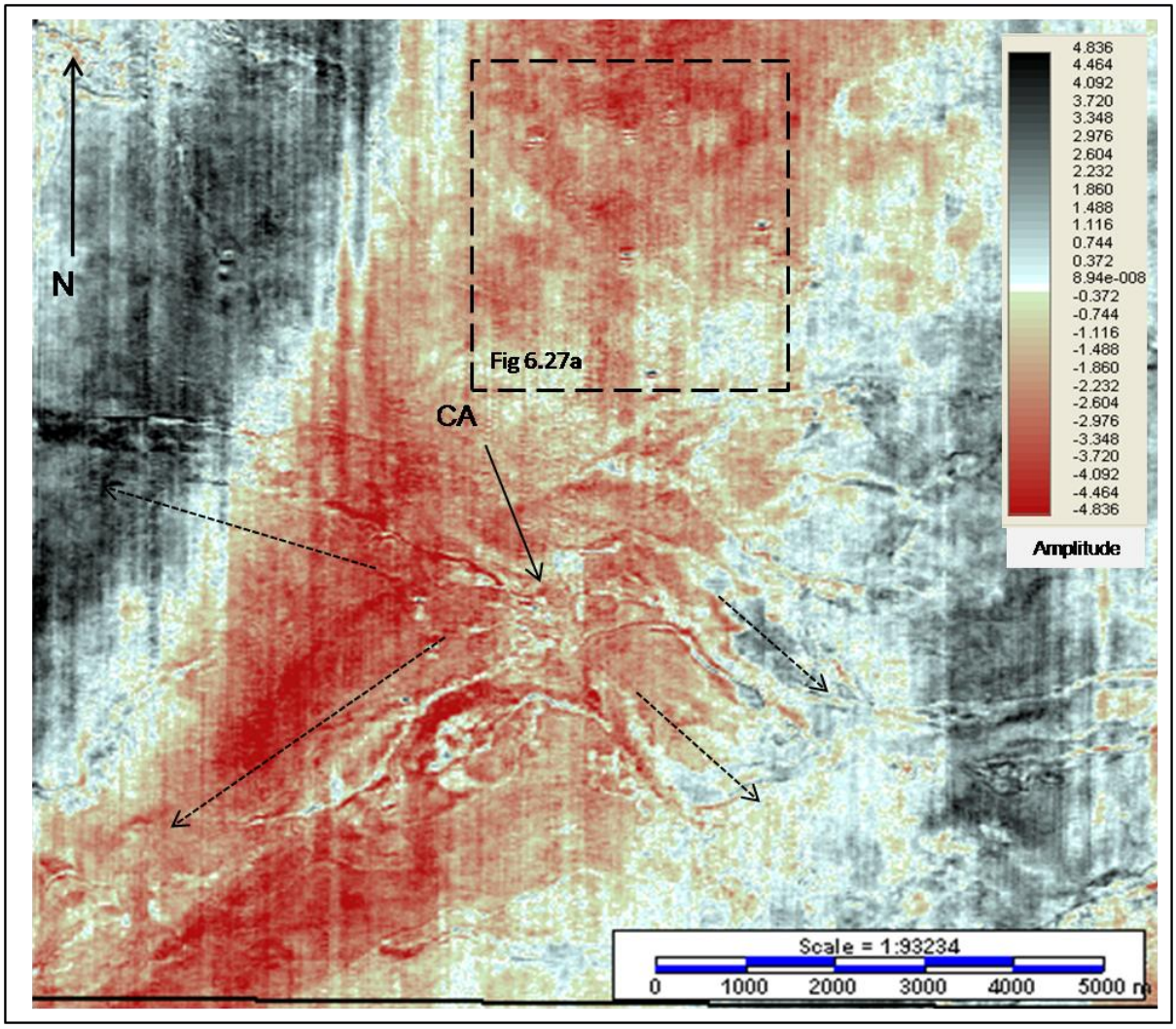

Fig. 6.23 a time-slice dissecting the Middle Seal upper boundary horizon displays branch like system (arrows) emanating from a central area (CA).

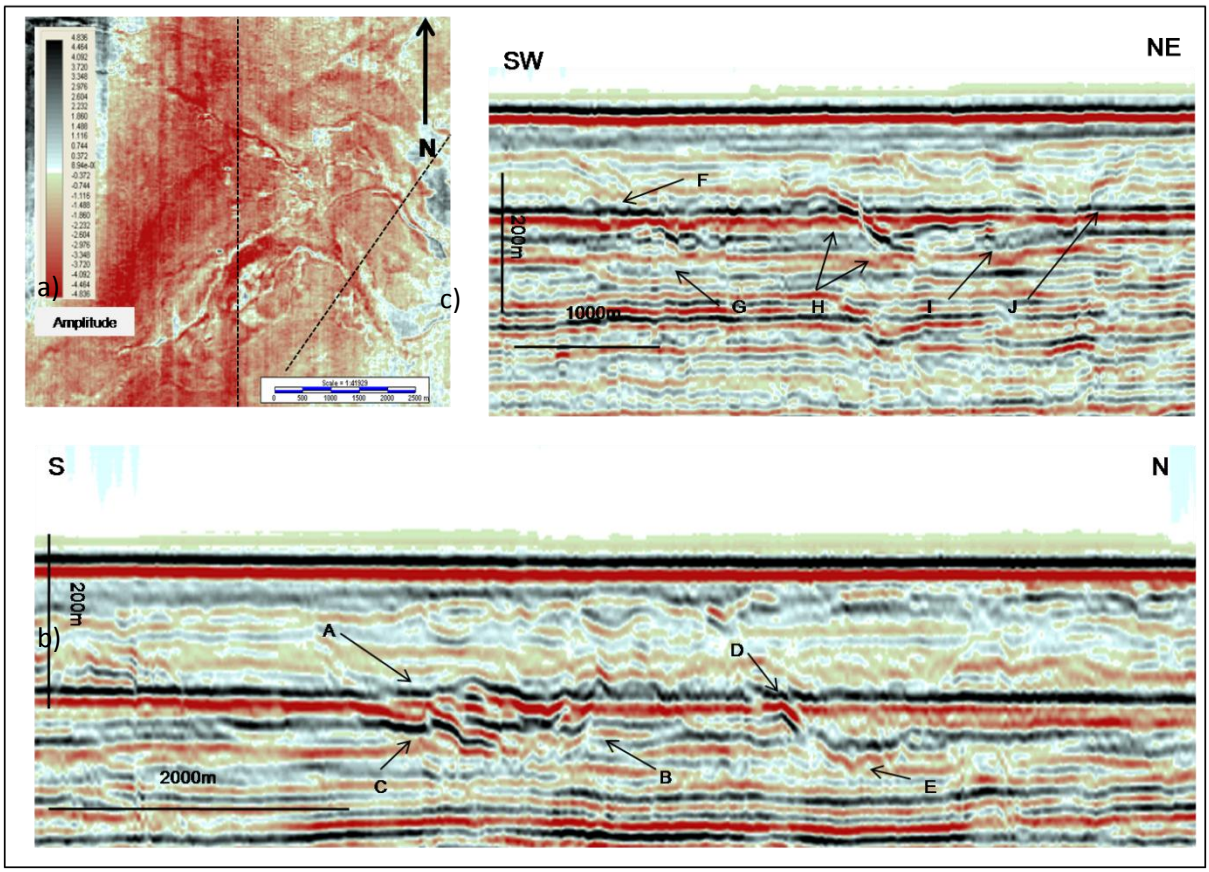

Fig. 6.24 a) locations of seismic section on the time-slice of the Middle Seal upper boundary b) S-N section highlighting the features of the two western branches c) arbitrary line intersecting the two main eastern branches.

Further time-slices of the branch system, at increasing depths, are presented in Fig. 6.25. There is a noticeable change in prominence of the channel branch system from the NW at shallow depth to the SE at deeper levels. The widening of the features, with depth, from the NW to SE suggests an increase in erosion in this direction, and a possible orientation of movement.

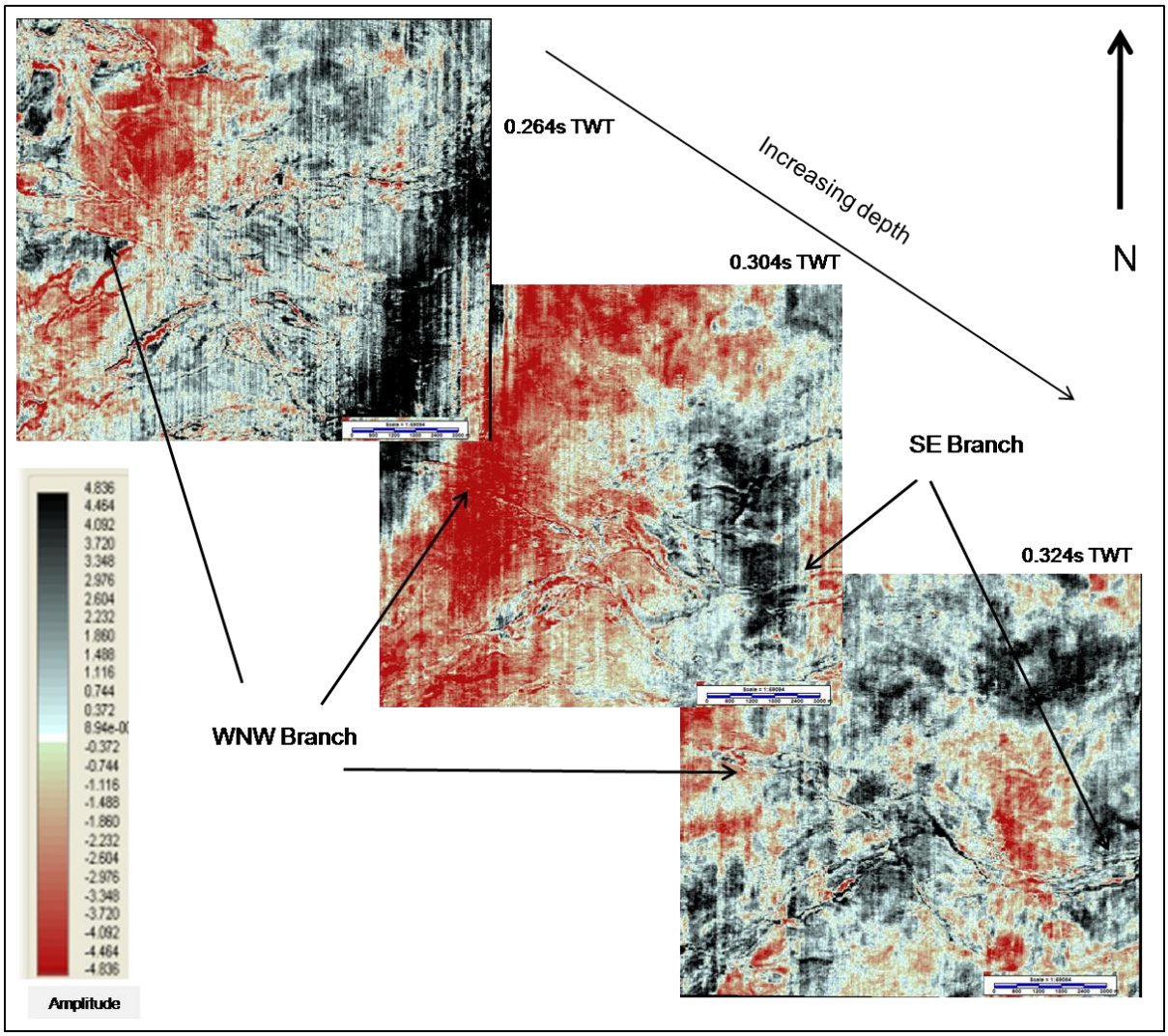

Figure 6.25 a series of progressively deepening time slices indicating the progression of the branch features from the NW to the SE.

6.3.4.2. High amplitude lobes

A set of interesting features located in the north-east of the study area are revealed by an RMS map of the Middle Seal unit (Fig 6.26a). They consist of lobe shaped bodies of high amplitude which are orientated towards the south south-east. An arbitrary line intersecting three of these bodies is presented in Figure 6.26b. They can be seen on the seismic section as high amplitude, concave upwards sections of a reflection within the lower 50m of the Middle Seal.

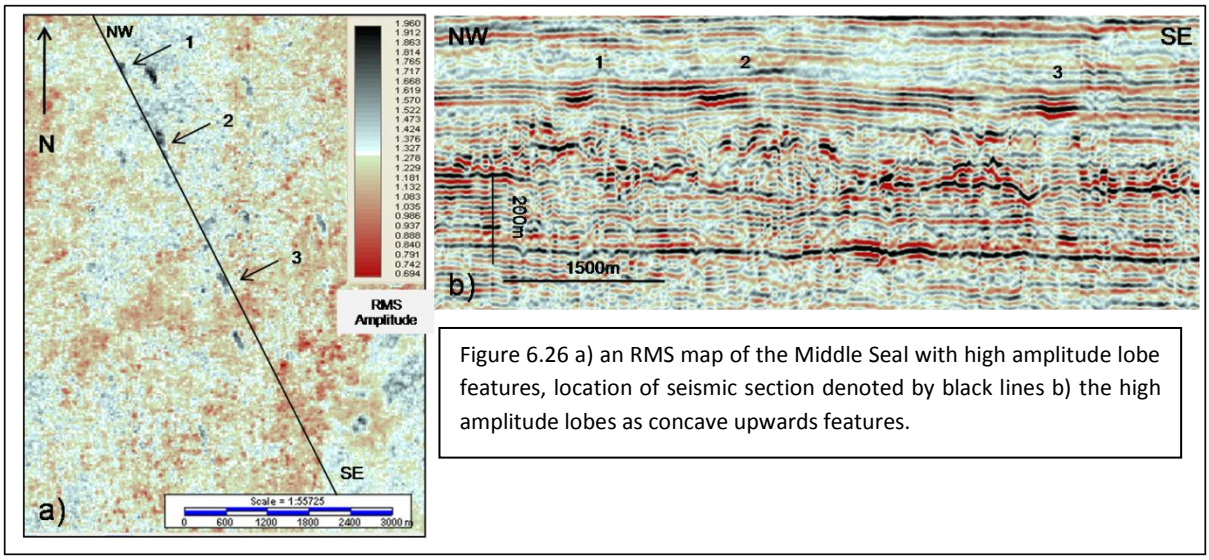

Figure 6.26 a) an RMS map of the Middle Seal with high amplitude lobe features, location of seismic section denoted by black lines b) the high amplitude lobes as concave upwards features.

6.3.4.3. Middle Seal 'breach'

Somewhat overshadowed by the large scale branches seen on the time-slice at the Top Middle Seal Horizon are a smaller scale set of features which also affect this horizon. A smaller scale map of the time-slice, which shows several of these features, is presented in Fig. 6.27a. They appear as sudden changes in polarity on the time-slice, either as sub-rounded or more linear features. They are generally less than 100 m in long axial length and less than 50 m in short axis.

A seismic section through one of the linear features is presented in Fig. 6.27b. It is evident as a break in the Top Middle Seal horizon (TMS) with a discordant high amplitude reflection situated within the break (Point DR1). Further discordant reflections are present below DR1 (Points DR2 and DR3) as is a bright spot (Point BS). These features are contained in what appears to be a vertical zone of disrupted reflections (Point VZ), which directly underlies DR1. The disrupted zone appears to continue downwards, is traceable around 40 0m below DR1, and appears to reach an amplitude anomaly affecting LSHAH (Point AA) in the Lower Seal unit (ref to section 6.4.2).

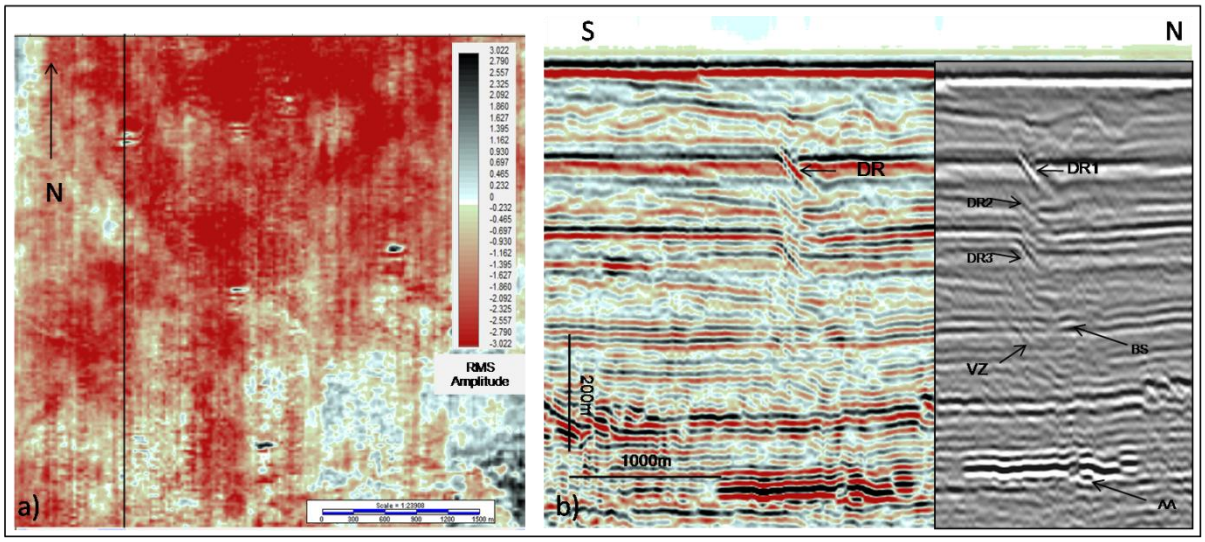

Fig. 6.27 a) locations of seismic section on the time-slice of the Middle Seal upper boundary b) an apparent vertical chimney crosscutting the Middle Seal reflections, apparent as a discordant reflection at the Middle Seal upper boundary (DR) c) bright spots (BR) located within the chimney, also discordant reflection (DR). The chimney appears to be in connection with a high amplitude area within the LSHAH.

6.3.4.4. Interpretation and discussion

6.3.4.4.1. Channel Branches

The cross sectional appearance of these features resemble buried glacial tunnel valleys and glacial valleys as described by Huuse et al., (2000), Praeg (2003), Jorgensen (2006), and Lonergan (2006). It is difficult to determine a direction of flow for these features, and they appear to be randomly orientated, however the time slices in Fig. 6.25 suggest a greater prominence of the north-western features at shallower depth, with an increase in prominence of the south-eastern and eastern branches at deeper levels. This suggests a north-west to south-east progression of the valley channels.

6.3.4.4.2. Amplitude anomalies

Seismic amplitude anomalies, seen as bright spots, are evident in the caprock succession above the Utsira Sand. These are suggested to indicate localised occurrences of sandy strata, probably gas filled, and perhaps indicative of conduits for gas migration (Chadwick et al., 2004). They have also been correlated to sandy intervals in wells, and are considered to be 'bottom set sands' by Gregersen (2007).

6.3.4.4.3. Middle Seal breach

Possible example of vertically focused fluid flow similar are presented by andresen (2012), present further examples and discuss their origin in the following section.

6.3.5. Upper Seal breaches

An example of a breach feature affecting the Top Middle Seal (TMS) horizon is presented in Section 6.4.4. In the example given in Fig. 6.27, this breach is a vertical feature affecting a vertical section of around 500 m which appears to terminate at the TMS. However, a TWT and amplitude map of the sea floor reveals that similar features are present at this higher stratigraphic level (Fig. 6.28). They appear as sub-circular to circular features which range between 70 and 250 m in diameter. On the time-depth map they are small scale depressions with a negative relief of tens of meters while they can be seen on the amplitude map as changes in polarity (Fig. 6.28a and b).

Detailed examples of these depression features are presented below. It is important to emphasise that although these features like artefacts at first sight, they do not correspond to any surface infrastructure, and hence may not be due to gaps in the data coverage (a common cause of shallow artefacts in data from the North Sea).

6.3.5.1. Pair of depressions from within the MTD 100m contour

Two of these features are presented along a south to north seismic section (Fig. 6.29c). They consist of a slight break in the seafloor horizon, with an associated small scale (tens of meters) downwards convex depression, there also appears to be a loss of seismic signal in the centre of the depression. Around 150 m directly beneath the seafloor they can also be seen to affect the TMS horizon. The southern feature (D1) consists of an upward disruption to the TMS horizon. There is a break in the reflection and a discordant high amplitude reflection which obliquely crosscuts the horizon. There are three instances of bright spots in the vertical column which underlies D1. This depression is also seen to overlie a section of increased thickness and a mound shaped area of chaotic reflection within the MTD unit (Fig. 6.29a). A zone of disrupted reflections is seen to emanate upwards from a MTD crestal high, this zone is initially around 500 m wide and tapers off towards the top of the Middle Seal and the sea floor (Fig. 6.29d). Indeed this observation that the depression directly overlies the crest of a distinct seismic body within the underlying MTD, raises the possibility of a causal link, and also reduces the likelihood that these features above the MTD are entirely seismic artefacts.

The second depression is also underlain by a disrupted section at the TMS horizon, however there does not appear to be a break in the reflection in this instance. There is a slight deflection upwards in the horizon and there is a discordant, sub-vertical, high amplitude reflection which splays from the horizontal reflection (Point DR). The depression is located above and to the north of the north flank of the chaotic mound of the MTD unit. Bright spots are also present in the narrow (less than 100 m wide) underlying vertical column of disrupted reflections.

6.3.5.2. Depression overlying the North-West cluster area

Three of the depression features are located above the area classified as the North-West Cluster area (this chapter, section 6.3, and chapter 5, section 5.3.2). They are visible on the amplitude map of the seafloor as sub-circular polarity changes, are relatively closely spaced (less than 800 m apart) and range between 100 and 140 m in diameter (Figure 6.30a). An arbitrary seismic line intercepting all three depressions is shown in Figure 6.31b.

As in the previous examples the depressions constitute a section where the seafloor reflection is displaced and is accompanied by a loss of seismic signal in the centre of the depression. Each depression has an associated underlying vertical column of disrupted reflections and bright spots, although each vertical column appears to attain different depths. The deepest point of each column is better highlighted by displaying the seismic section using a colour bar emphasising high values of negative and positive amplitude (Figure 6.30c). The middle column (VDC3) appears to penetrate a mid amplitude continuous couplet at a discontinuity in the reflection around 450m below the seafloor (Figure 6.30c, Point 1), suggesting a termination around the top level of the MTD. A second break in this couplet suggests that VDC4 also continues past this level, possibly to the upper MTD level (Figure 6.30c, Point2), however a stack of four high amplitude bright spots within the MTD unit suggests that the column may even penetrate the MTD unit itself (Figure 6.30c, Point 2?). The third column, VDC5, underlying the north-west depression, appears to extend the deepest, passing the base of the MTD (Figure 6.30c, Point3), while a washed out zone past the large amplitude anomaly, down to the Base Utsira, may even suggest a deeper root (Figure 6.30c, Point3?).

6.3.5.3. Controls on depression location

In Figure 6.31, the location of the seafloor depressions are shown as white specks, and are overlain by the MTD 100 m contour (Fig. 6.31a) and the Base Utsira contour (Fig. 6.31b). All the depressions are encompassed within the MTD 100m contour. However, only three depressions, given in the example above, directly overlie the ellipsoid mounds located within the North West Cluster Area, while the remainder are located outside the mound cluster.

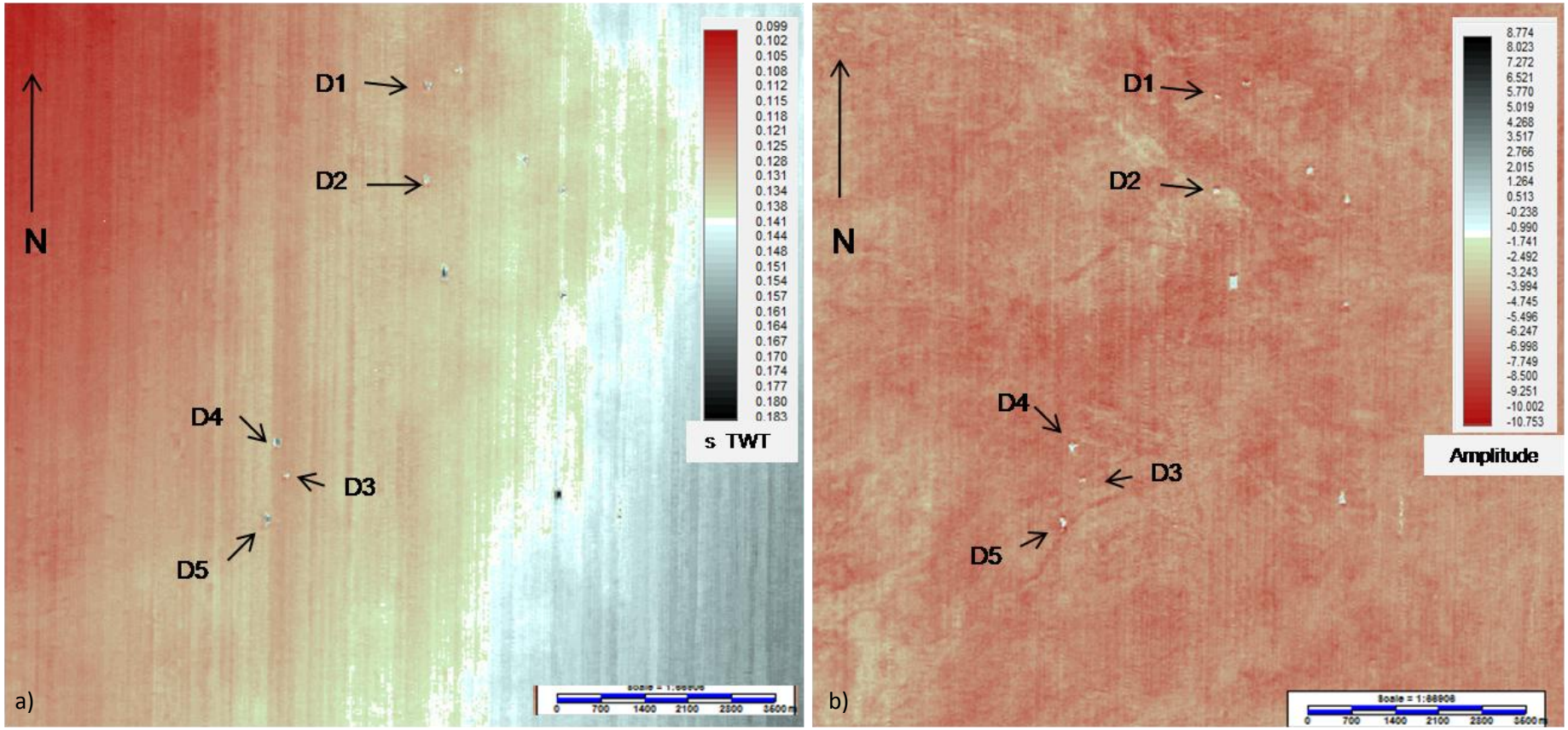

Fig. 6.28 a) a TWT and b) amplitude map of the Seafloor horizon. Small scale depressions and reversals in amplitude are present at this horizon. The labelled depressions are presented in more detail within this section.

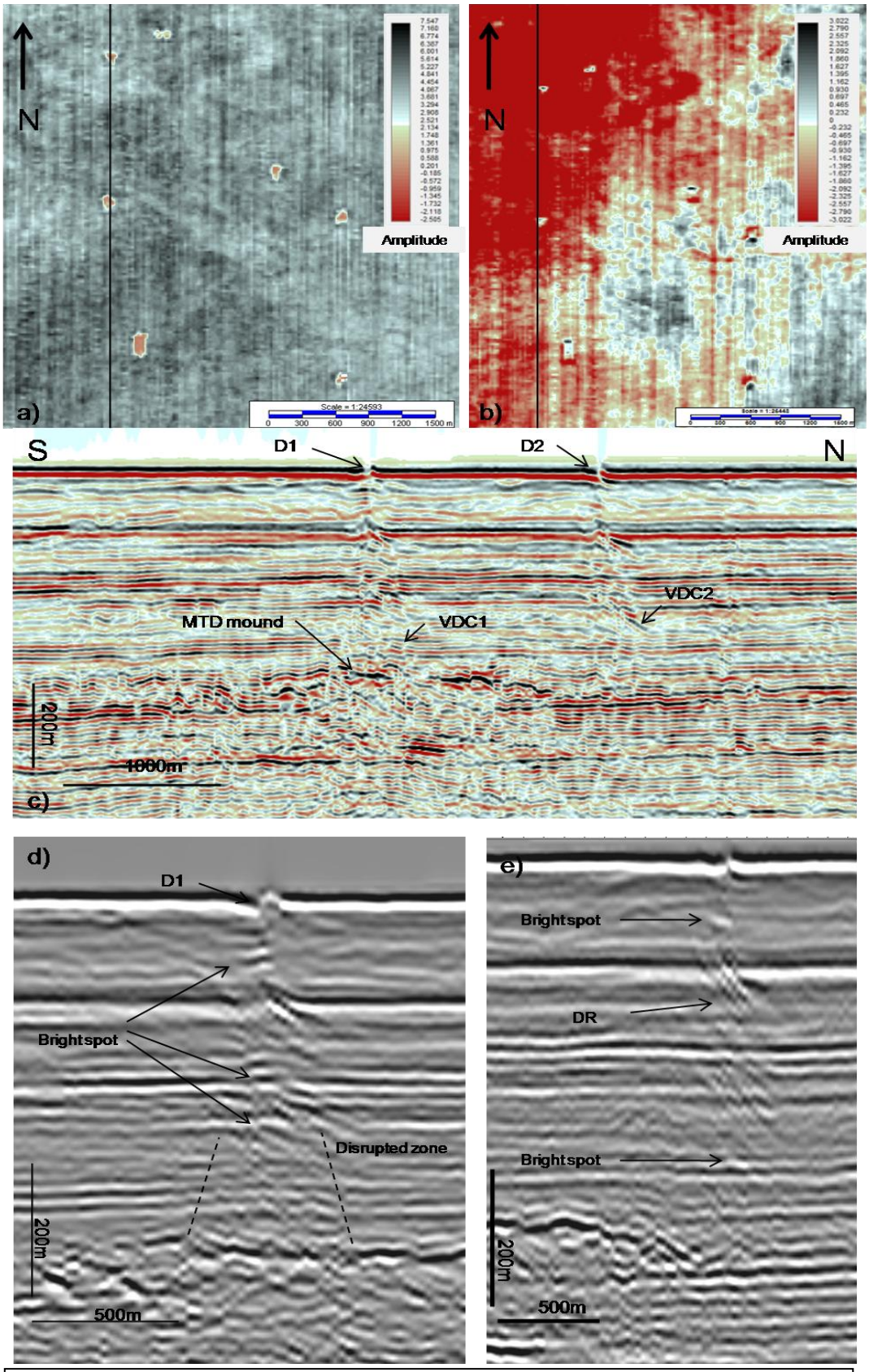

Fig. 6.29 seafloor features D1 and D2 on a) amplitude map b) seafloor time slice with seismic line location c) a S-N seismic section of the seafloor features, apparent as breaks in the seismic signal, they are underlain by vertical disruption chimneys (VDC1 and VDC2) and are proximal to a mounded area of disrupted MTC reflections, d) and e) the VDC's include bright spots and dim or weak zones of reflections.

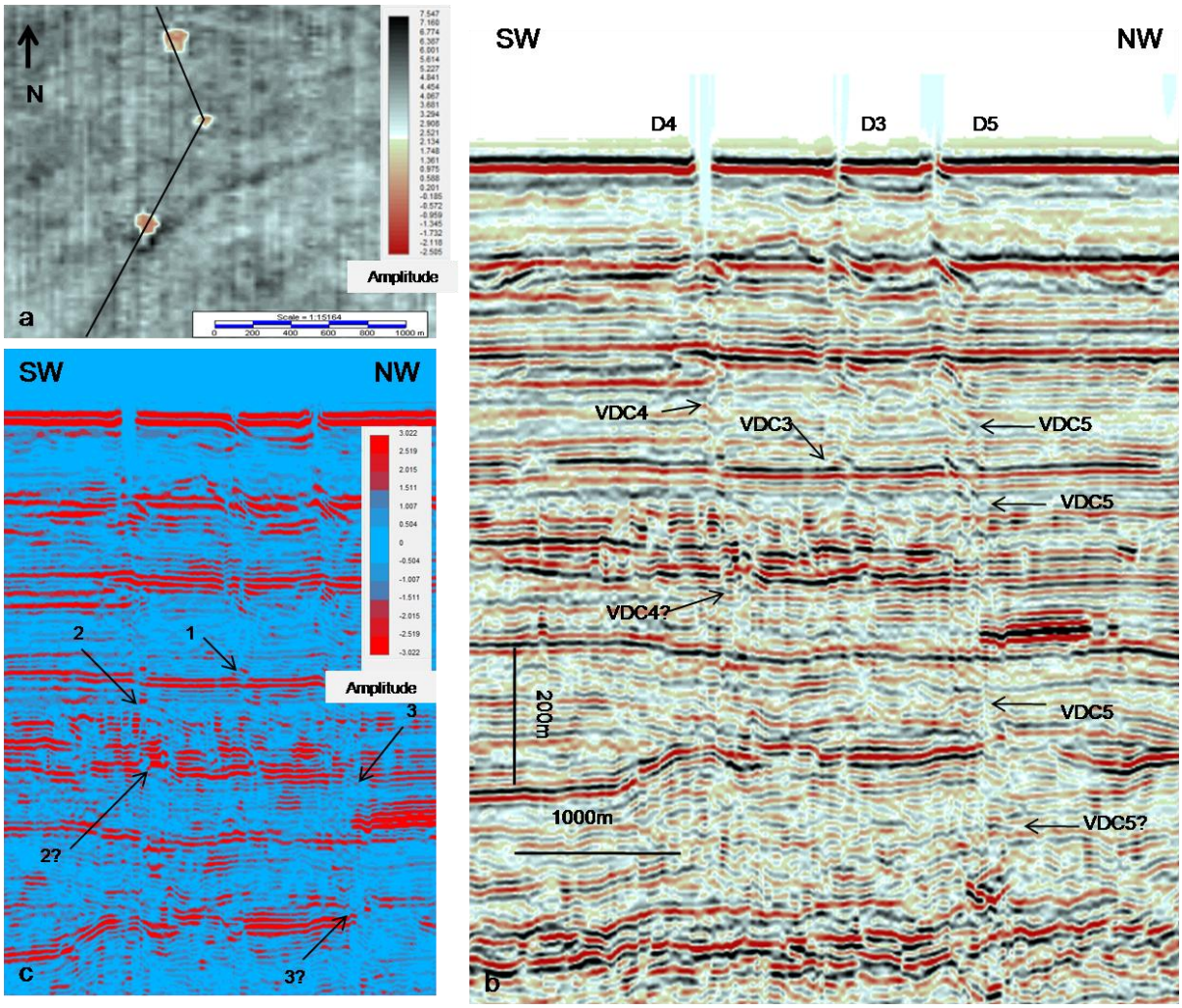

Fig. 6.30 seafloor features D3, D4 and D5 on a) amplitude map with seismic section location b) a SW-NW arbitrary seismic section of the seafloor features, apparent as breaks in the seismic signal, they are underlain by vertical disruption chimneys (VDC3, VDC4 and VDC5) and overlie an area where the Base Utsira Horizon is displaced c)VDC's include bright spots and dim or weak zones of reflections, while their deepest extent is difficult to determine.

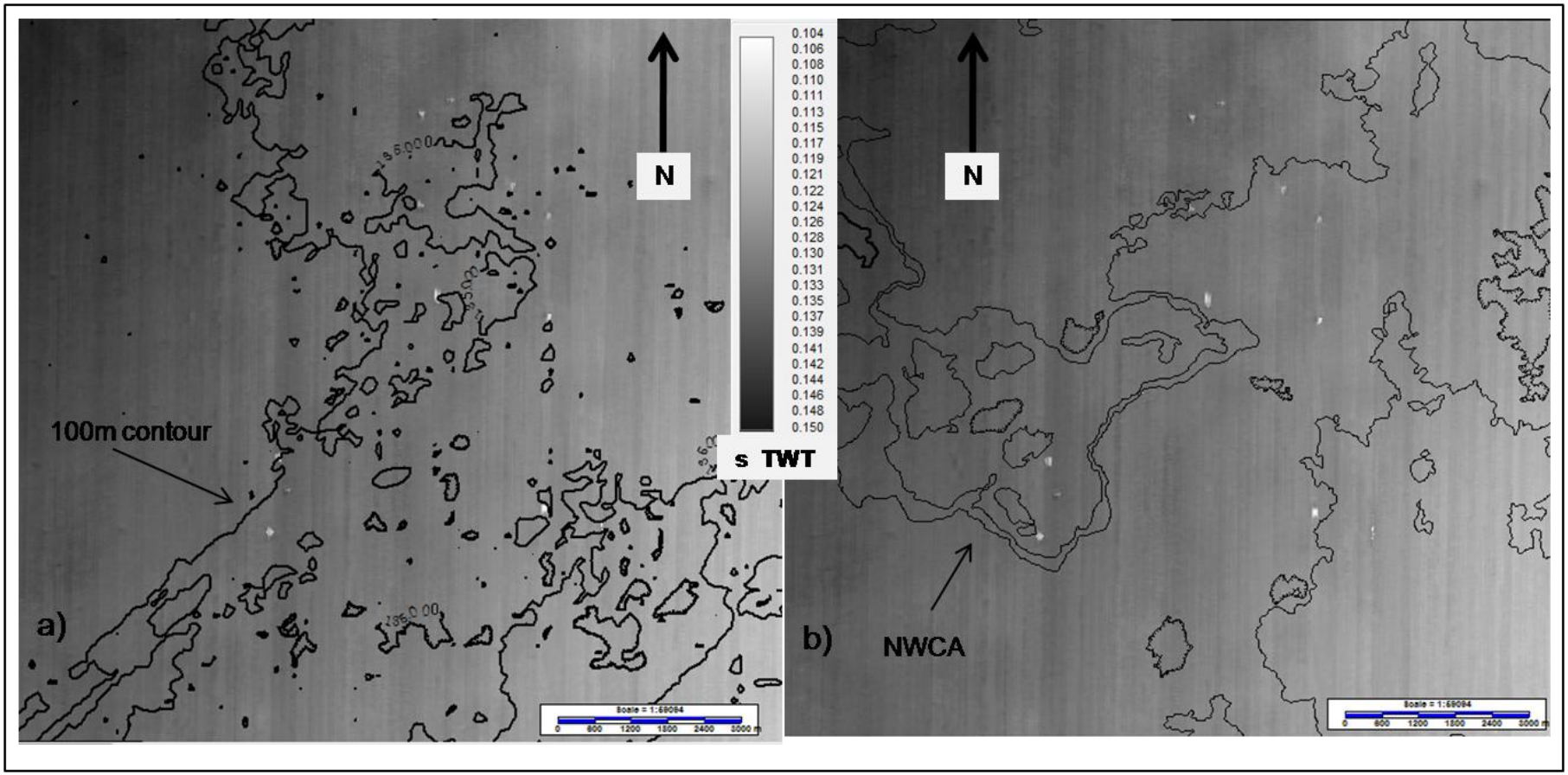

Fig. 6.31 a TWT map of the seafloor co-rendered with a) 100m MTD contour and b) the Base Utsira Horizon with the NWCA labelled. The entire seafloor features lie within the 100m contour, while there is no apparent relationship with the contour of the Base Utsira Mounds.

6.3.5.4. Interpretation and discussion

A point of contention is the origin of the modern seafloor depressions and their underlying disrupted zone of reflections. Loss of data due to surface infrastructure would support the artefactual nature of these features; however, comparison between the coordinates of these features and those of surface infrastructure and wells does not reveal a correlation between locations. This lack of correlation with infrastructure is important, but it is also worth considering that the imaging is perhaps not all it should be in this shallow section and some uncertainty remains as to whether they are real or artefactual.

The loss of signal within the central section of the depressions hinders interpretation; however these features bear some resemblance to pockmarks presented by Moss and Cartwright (2010), especially when viewed on seismic profiles slightly offset from the central area. They are also underlain by 'wipeout zones', which are areas of a seismic section where reflections from stratigraphic layers are degenerated to the point that they are either absent or weak (Loseth et al., 2009 (Fig. 6.32a). These zones are considered to be anomalous seismic patterns resulting from mobilisation of fluids through strata, and may also suggests zones of gas-fluid migration (Hovland and Judd, 1988; Loseth et al., 2001; Gay et al., 2007; Huuse et al., 2010). Examples of wipeout zones are seen to underlie seafloor craters and pockmarks (Macelloni et al., 2012).

Several observations support a 'real' origin for these features. The widening of the vertical disruption zone below D1 with depth (Fig. 6.29), contradicts the excepted narrowing with depth of zones associated with loss of signal at the surface, while the presence of bright spots (Fig. 6.29d and e) lends credence to a real origin. We also demonstrate that the three depressions observed in Fig. 6.30 appear to have vertical zones of disrupted reflections with roots at different depths. If these were top-down features, caused by loss of signal at surface, then their areal extent (Fig. 6.30a) and the width of loss of signal on seismic section should reflect their terminal depth. D3 has the smallest areal coverage and narrowest loss of signal; it terminates at the shallowest depth at around 550 bsl. D4 has a slightly larger areal extent than D5, and appears to display a significantly larger loss of seismic signal (Fig. 6.30b and c), however the vertical disrupted column, VDC4, which underlies D4 appears to terminate at the base of the MTD unit, at around 650m bsl, while VDC5 continues to an apparent root point past the Base of the Utsira Sand at a depth of a kilometre below sea level.

Also worth consideration is the vertical disruption column presented in Fig. 6.27, which is similar in its seismic expression to the other vertical column, except that it is observed to terminate at the top Middle Seal Horizon.

If these features are genuine, these are interpreted them to probably be either fluid escape pipes or elongated pipes, derived from fluid focused in the MTD and ascending from the local crests in the top MTD surface. While determining their correct origin is problematic, if these features are genuine their significance is considerable is that they may link the leakage at depth to the seabed, and they suggest that leakage is dynamic.

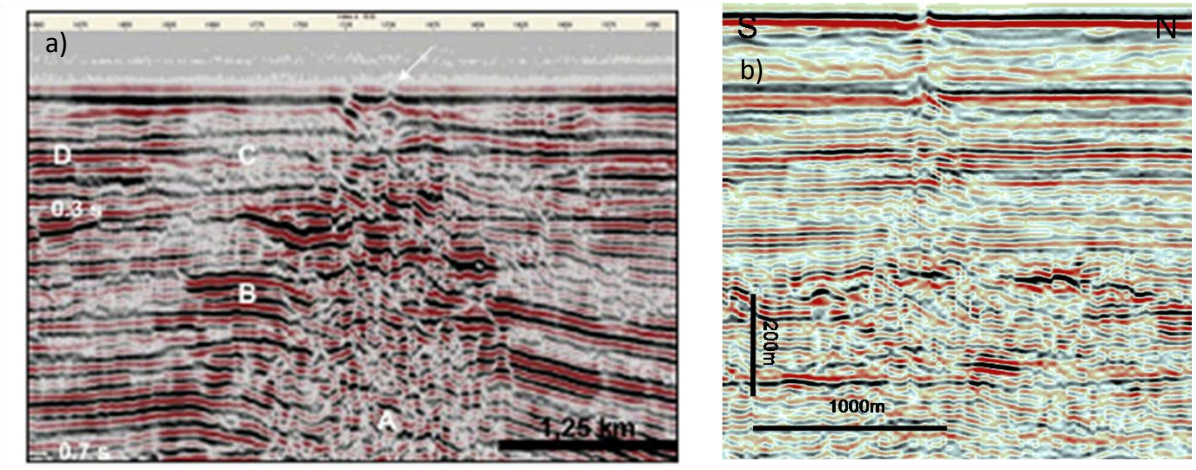

Fig. 6.32 a) an example of a 'wipe out zone' (A) interpreted by Løseth et al.,(2009) as a gas chimney b) example of a 'wipe out zone' from within the MTD unit from this study area. A vertical disrupted zone of reflections emanates from the crest of the 'wipe out zone', and may be linked to pressure build up due to gas accumulating within the MTD.

6.4. Discussion

The recognition of sand intrusions and their effect on the hosting and overlying strata are a significant part of this study. Their seismic expression within this study area does not strictly conform to the classic 'V' or 'U' brights described in other work (Løseth et al., 2003, Cartwright et al., 2008). Alternatively, the recognition of their presence within this study area has been deduced from intrusion diagnostic aids and 'indicators' such as discordant high amplitude anomalies, bright spots, chaotic zones of reflections, and the forced folding of overlying strata.

At progressively shallower levels, from sand intrusion 'break through' points at the Lowermost Shale, to ellipsoid mounds at the Base Utsira, and the ellipsoid depressions at Top Utsira, the area affected by the sand intrusion increases to form a 'cone of disruption'(Fig. 6.33. It is proposed that several leakage pathways, to varying stratigraphic levels, are associated with the sand intrusions. These will be discussed further in Chapter 7.

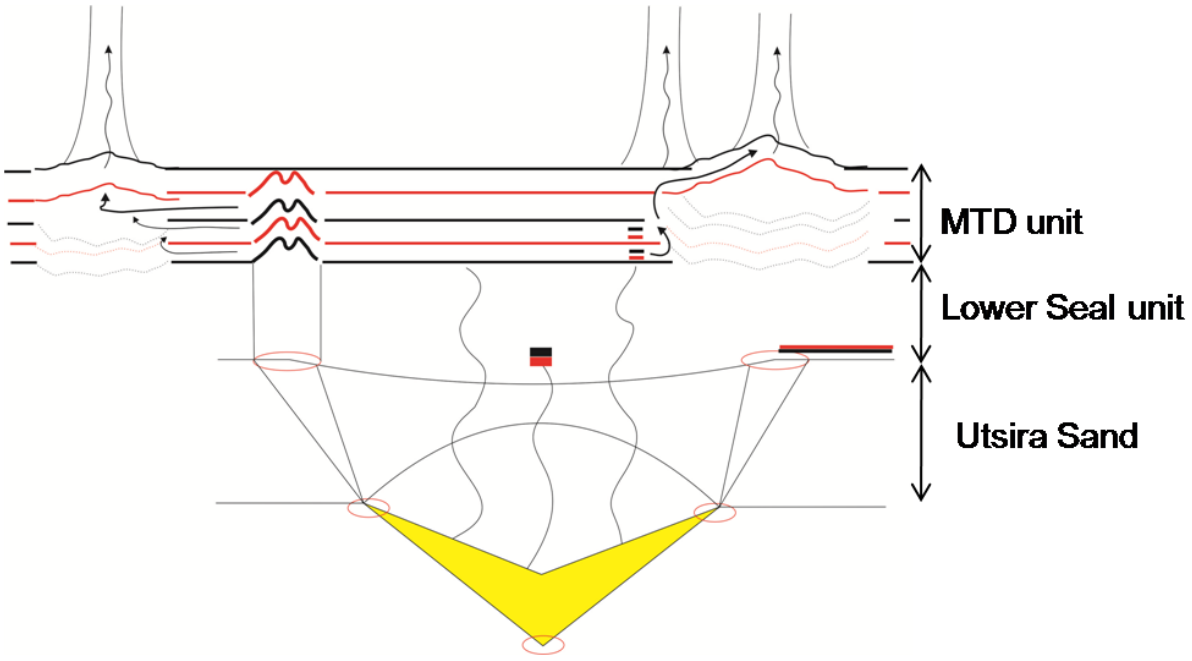

Fig. 6.33 a schematic diagram representing the interpreted effect and increasing magnitude of the high permeability 'cone of disruption' associated with the sand intrusions.

6.5. Conclusion

Indicators of leakage and leakage pathways are present at several levels in the strata which overlie the Utsira Sand.

- The Lower Seal High Amplitude Horizon hosted within the Lower Seal displays several examples of lateral amplitude variations. These features are consider to be soft events (when compared with the polarity of the seafloor), and are interpreted as accumulations of gas within a permeable layer of the Lower Seal. It is suggested that fluid flow to these features was achieved through buried pockmarks connected to the Utsira Sand by what appear to be short sub-vertical feeder pipes. The irregular outline and fingering features of these high amplitude areas forms the basis of their interpretation as dynamically migrating batches of gas.

- The overlying unit, termed the Mass Transport unit, is shown in effect to consist of two components; the Mass Transport Deposit, and areas remaining of the original unit. Directional indicators have been described which suggest a north-east to south-west transport direction. Variations in amplitude within the section defined as the MTD area are attributed to changes in the internal components of the unit. Amplitude anomalies located outside this area are shown to have roots in association with ellipsoid mounds at the Base Utsira and underlying sand intrusions. It is suggested that small scale vertical disruption zones located above the ellipsoid mounds are linked to fluid flow through the intrusion wing tips and through parasitic sand offshoots from the main body of the intrusion. Larger vertical disruption zones, located at the flanks of the mounds are thought to exploit fracture zones formed by post-emplacement compaction of the sand intrusions. In some cases, fluid movement along both sets of suggested pathways appear to terminate within the Mass Transport unit. However, leakage past and beyond this stratigraphic level cannot be discounted.

- Seafloor depressions of uncertain origin are seen to overlie vertical disruption zones with varying root depths. The majority of these are associated with the mass transport component of the Mass Transport Unit, although rare examples are seen to extend deeper. They are interpreted as either fluid escape pipes or elongated pipes, derived from fluid focused in the MTD. While their origin is unclear, if genuine, their significance is enormous, as they may allow or have allowed leakage from depth to seafloor.

In the following chapter a detailed discussion regarding a proposed plumbing system is presented. This system is based upon, and incorporates, the features seen in this chapter and in Chapters 4 and 5.

Chapter 7

Discussion

7. Discussion

In chapters 4, 5 and 6 the geographic and stratigraphic distribution of amplitude anomalies and related features within the study area has been demonstrated. From these observations it can be attempted, at least in part, to determine the 'plumbing system' in place within the post-Mid Miocene succession. In this chapter the discussions from Chapters 4, 5 and 6 are summarised, and the implications of the features observed and their effect on the plumbing system are discussed. Also discussed is the acceptability of leakage and suggest possible leakage scenarios of CO_2 from the Utsira Sand.

7.1. Plumbing system

Evidence of fluid flow and seal breaches in addition to examples of seismic expressions of leakage has been presented based on observations in the preceding chapters (Chapters 4, 5 and 6).

7.1.1. Sub-Utsira Sand

Sand intrusions are classified as members of the intrusion-related seal bypass family (Cartwright et al., 2007) and as a subsurface sediment remobilisation fluid flow feature (andresen, 2012). Their emplacement results in the forced folding of the overburden (Cartwright et al., 2008), and despite post-emplacement settlement and compaction resulting in some loss of porosity, intrusions are considered to retain porosity values that are high in comparison with the hosting stratigraphy (Hurst et al., 2003).

From examples presented in Chapter 4, Section 4.3.2.1, and Chapter 5, Sections 5.3.2.1, 5.3.2.2 and 5.3.2.3, it is observed that their interpreted bases are in close proximity to the polygonally faulted basal horizon of the Lowermost Shale unit, and in some cases they appear to 'break through' from this horizon (Chapter 5, Fig. 5.6d). Polygonal faults, members of the fault-related seal bypass family (Cartwright el al., 2007), are also considered as laterally extensive fluid flow features (andresen, 2012).

Intrusions are rarely seen to be fully imaged in this study, but are represented by a range of seismic features from 'bright spots' to high amplitude discordant or concordant reflections (Section 4, Fig. 4.5), which are accompanied by the diagnostic forced folding of the overburden. The high amplitude

sections are associated with sub-vertical zones of disturbed reflections which project from the visible (high amplitude) intrusion sections towards discontinuous points of the Base Utsira Horizon, and especially the hinge points of the forced folds.

The hydraulic pumping of sediment from, and through, the highly permeable sand intrusions to the contemporary sea floor to form extrusive deposits is considered plausible (cf. Huuse et al., 2004). Observed high amplitude 'bridges' or 'infill' at the flanks of the sand intrusion-induced forced folds supports this theory (Fig. 4.17), and reinforces the likelihood of a permeable pathway from the sand intrusion main body, through the intrusion wings, to the seafloor (Fig. 7.1a). Furthermore, the proximity of the polygonal fault seal bypass system to the intrusion bypass system, suggest possible links to deeper fluid flow networks, and hydraulic connection to underlying sand bodies such as the Skade Formation.

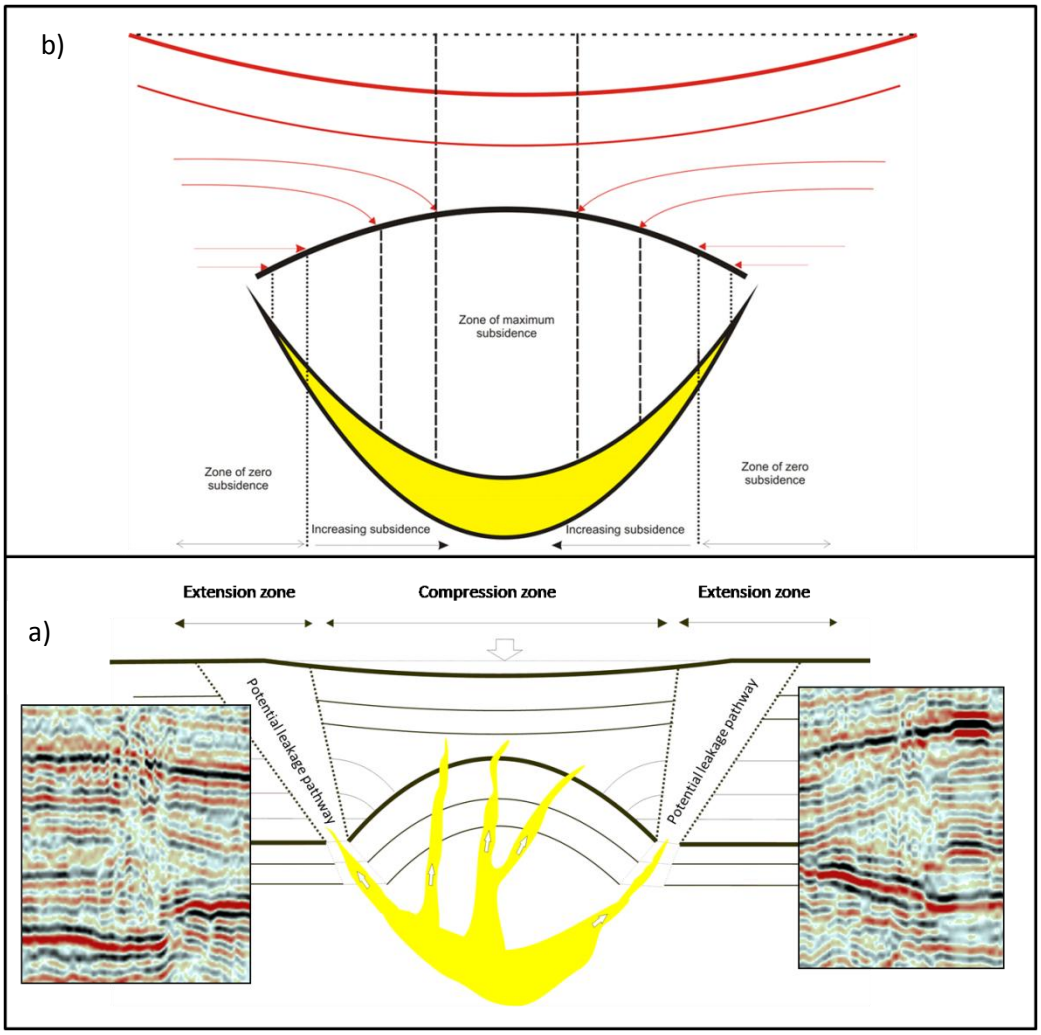

Fig. 7.1a) schematic diagram demonstrating the formation of permeability pathways following post emplacement compaction of sand intrusions with representative examples from the study area b) diagram demonstrating the subsidence differential along the mound profile

7.1.2. Utsira Sand

The forced folding of the Base Utsira, due to the hydraulic 'jack up' of the overburden associated with sand intrusion emplacement, is accompanied by the overlying sagging of the Top Utsira Horizon. It is suggested that the subsidence affecting this horizon is the result of post-emplacement compaction and grain reorganisation within the sand intrusion (Sections 4.3.2.5.1 and 5.4.4.1). It has been shown that the magnitude of the subsidence is proportional to the relief of the overlying mound, which in turn suggests that the subsidence is proportional to the initial, pre-compaction aperture of the intrusion (Section 5.5.4). The greatest amount of subsidence therefore overlies the crest of the underlying mound and the central area of the intrusion, where the greatest aperture is located (Fig. 7. 2a). This central area of greatest subsidence is defined as a compressive zone, either side of which are sections defined as extensional zones (Fig. 7. 2b). It is suggested that these extensional zones are most likely to be prone to faulting and fracturing.

Observations from the study area support the presence of these zones (Fig. from Chapter 6, Chapter 7, Geosketch 2c and d). They are imaged as vertical to sub-vertical zones where the reflections of the host unit appear displaced, discontinuous and of noticeably lower amplitude, with occasional bright spots. These characteristics have previously been noted by Løseth et al., (2009) as internal features of 'leakage zones'. The zones affecting the internal reflections of the Utsira Sand, when associated with forced folds, are generally located at the hinge points of the forced folds. At these points the Base Utsira reflection is discontinuous, and the zones project upwards through the Utsira Sand towards the points where the Top Utsira reflection deflects downwards (Chapter 6).

The location and vertical extent of these 'leakage zones' raises the possibility that the post-emplacement compaction of the sand intrusions and the subsequent subsidence of the overlying strata may have resulted result in the formation of permeable pathways from the base of the Utsira Sand to its top. These permeable pathways may extend deeper; the termination of the highly permeable intrusion wings at the forced fold hinge points and the connection between the intrusion itself and the underlying polygonal faults suggests the presence of an interconnected permeable network between the fault bypass system, the intrusion bypass system, and the sub-vertical expression of a leakage zone.

There is further potential for fluid movement from the Base Utsira through the parasitic sand offshoots from the central body of the intrusion. This will be discussed in section 7.2.3.2.

7.1.3. Supra-Utsira Sand

A possible permeable pathway from the polygonally faulted horizon, through the Lowermost Shale and Utsira Sand, up to the top Utsira Sand level has been established in the preceding sections. A discussion of further extension of this network, upwards from the top Utsira level, is presented below.

Lower Seal High Amplitude Horizon

Several examples of high amplitude areas contained within a single horizon of the Lower Seal are presented in Section 6.4.2. Lateral amplitude variations along a reflection, such as those presented, are considered the simplest type of leakage-related anomalies (Loseth et al., 2009). It is proposed that these anomalies represent direct leakage from the Utsira Sand.

The individual anomalies are shown to overlie one or more small-scale depressions, often with a connecting pipe feature (Fig. 7.2). These depressions are considered to represent buried pockmarks, subsequently re-established by migrating gas focused through the underlying pipes. The irregular 'stellate' geometry, protruding fingers and general non-conformity with the structures contours of the horizon suggests that the gas is dynamically migrating away from the feeder pipes.

These anomalies may be hosted by a permeable layer or permeable lenses within the Lower Seal. Accumulation in permeable lenses would suggest that further migration, once the lens is filled, would be limited unless fracturing facilitated by overpressure was induced. Accommodation of the gas in a laterally extensive layer would limit vertical migration unless it encounters vertical or a sub-vertical bypass within the Lower Seal.

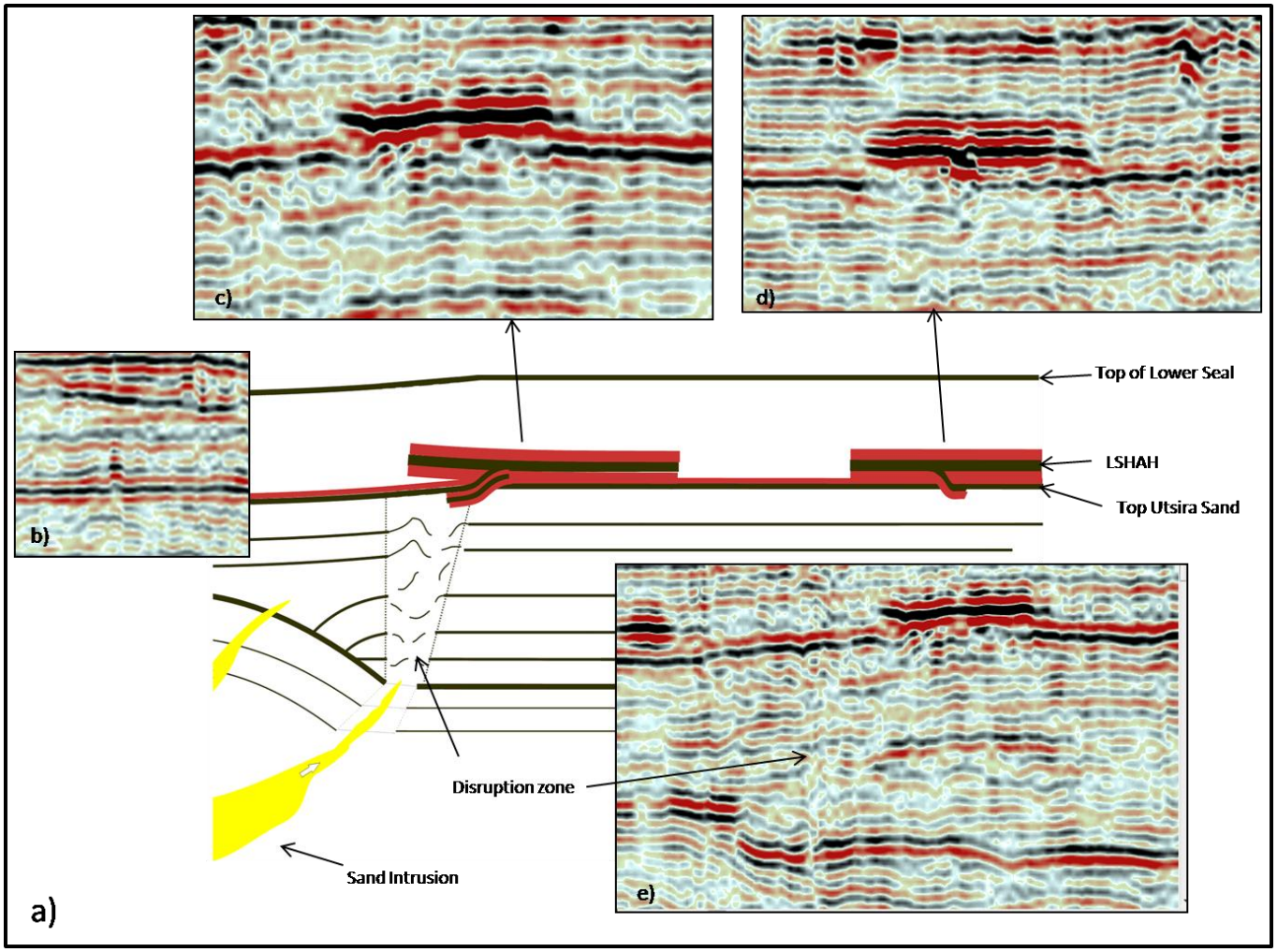

Fig. 7.2a) schematic diagram demonstrating the exploitation of the permeability pathways at the forced fold flank by migrating gas. Representative examples from the study area of; b) pockmark at the Top Utsira Horizon c) and d) gas accumulation within the Lower Seal High Amplitude Horizon e) sub-vertical disruption zone leading to a high amplitude area.

7.1.3.1. MTD

This unit has been shown to consist of two very different components, a Mass Transport Deposit and remnant sections of the original unit. The MTD component is of greater thickness with large variations in its internal reflections and amplitude, while the remnant component of the original lithology is notable for its stratification. Based on the differing internal structures of the separate components it can be assumed that each plumbing system must differ, and therefore they will be discussed in separate sections.

7.1.3.2. Remnant unit

High amplitude features within the Remnant Unit are more prominent due to the relatively undisturbed nature of this part of amplitude of the unit compared to that of the mass transport section. Examples of bright spots within this section are presented in Section 6.4.3 and they appear to have vertical connectivity to discontinuous points located along the Base Utsira Horizon (Fig. 6.20). While bright spots overlying mound flanks may be attributed to fluid flow through the sub-vertical leakage zones caused by extension, as discussed in section 7.2.2, the zones of vertical disruption in some cases are narrower, and also present along the mound profile, and within the compression zone (Fig. 7. 3). It is most likely that these narrower vertical disruption zones leading to the bright spots are the result of focused fluid flow through parasitic sand offshoots from the main sand intrusion body, and represent a direct vertical permeability pathway from the sand intrusion, through the Utsira Sand and Lower Seal, to the Remnant Unit of the mass transport complex.

Wider vertical disruption zones are also related to high amplitude areas within the remnant section of the MTD unit (Chapter 6 Fig.s 6.21 and 6.22, 7, Chapter Fig. 7.3). They are located at the flanks of forced folds, as described in 7.2.2, and project upwards from a root at the hinge point of the fold to a terminal point of high amplitude within the remnant section (Fig. 7.3).

The remnant section is defined by a well developed stratification and lateral continuity of reflections, lateral migration from the terminal point of the vertical leakage zones is therefore a possibility.

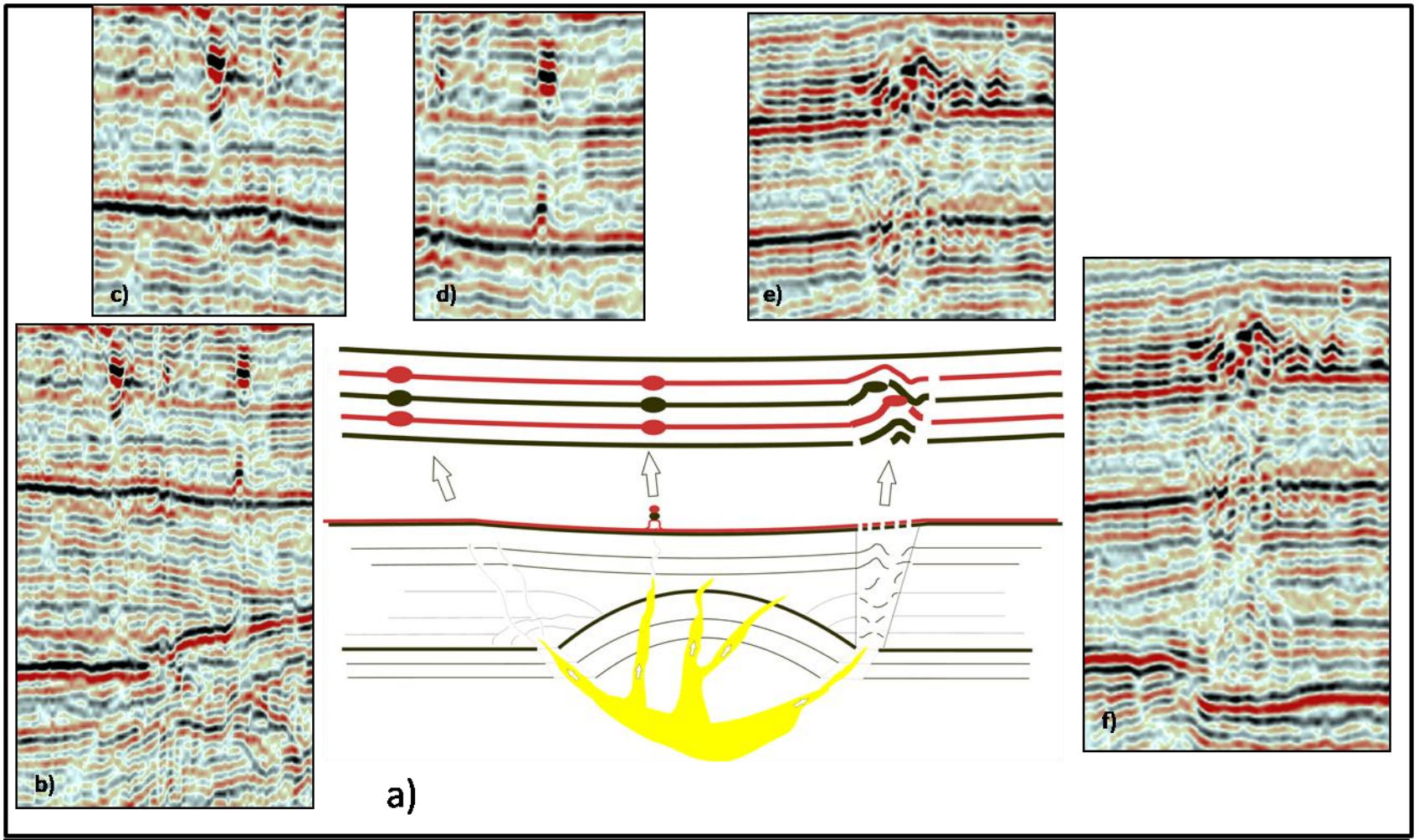

Fig. 7.3a) Schematic diagram demonstrating the presence of permeability pathways from the Utsira Sand to the MTD unit. Representative examples from the study area of; b) narrow vertical zones leading to bright spots c) and d) bright spots within MTD unit e) high amplitude areas of greater extent within the MTD unit f) wider vertical zone leading to high amplitude area.

7.1.3.3. Mass transport section

MTD are predominantly mud-rich units which are considered competent sealing units (Moscardelli et al., 2006; Moscardelli and Wood, 2008; Prather, 2003). However, examples of MTD's consisting permeable strata have been recognised within the North Sea Basin (Shanmugan et al., 1996; Davison, 2004).

The basal shear surface is considered to act as a permeability barrier (Allan et al., 2006). However, the basal surface is often indistinct or discontinuous within the study area, and disruption to the surface is associated with the 'debrites' sections of the MTD (Gamboa et al., 2009, this study Chapter 6, Section 6.4.3).

The variation of internal components of the mass transport component of this is recognised by the range of high amplitude features within this unit. Rafted blocks of the remnant unit retain some of their original cohesion and may represent permeable pathways through the MTD unit, especially so when retained stratification in tilted blocks form sub-horizontal ramps from the base of the unit to its top.

Blocks which retain their stratification and remain horizontal to sub-horizontal within the mass transit section of the unit, would allow lateral migration along their length. The stratified rafted and remnant blocks are regularly observed to uncomfortably lie adjacent to lower amplitude more chaotic zones. The interface between these lower amplitude 'debritite' zones and the stratified blocks may be potential fluid pathways that allow bypass of the MTD unit and promote upwards migration (Fig. 7.4).

It is also possible that these low amplitude chaotic zones are 'wipe out' zones as described and interpreted as gas chimneys by Løseth et al., (2009). Heggland (1997) has previously interpreted the presence of gas within this unit. These concentrations of gas or fluid may be the result of lateral migration along the stratified section of the Remnant Unit, or possibly from direct vertical 'feeders' from the Utsira Sand (Fig. 7.4). The presence of vertical disruption zones emanating vertically from local crests in the top MTD surface to the seafloor further suggests that there are permeable networks through the MTD (Chapter 6, Section 6.4.5, this Chapter, Fig. 7.4).

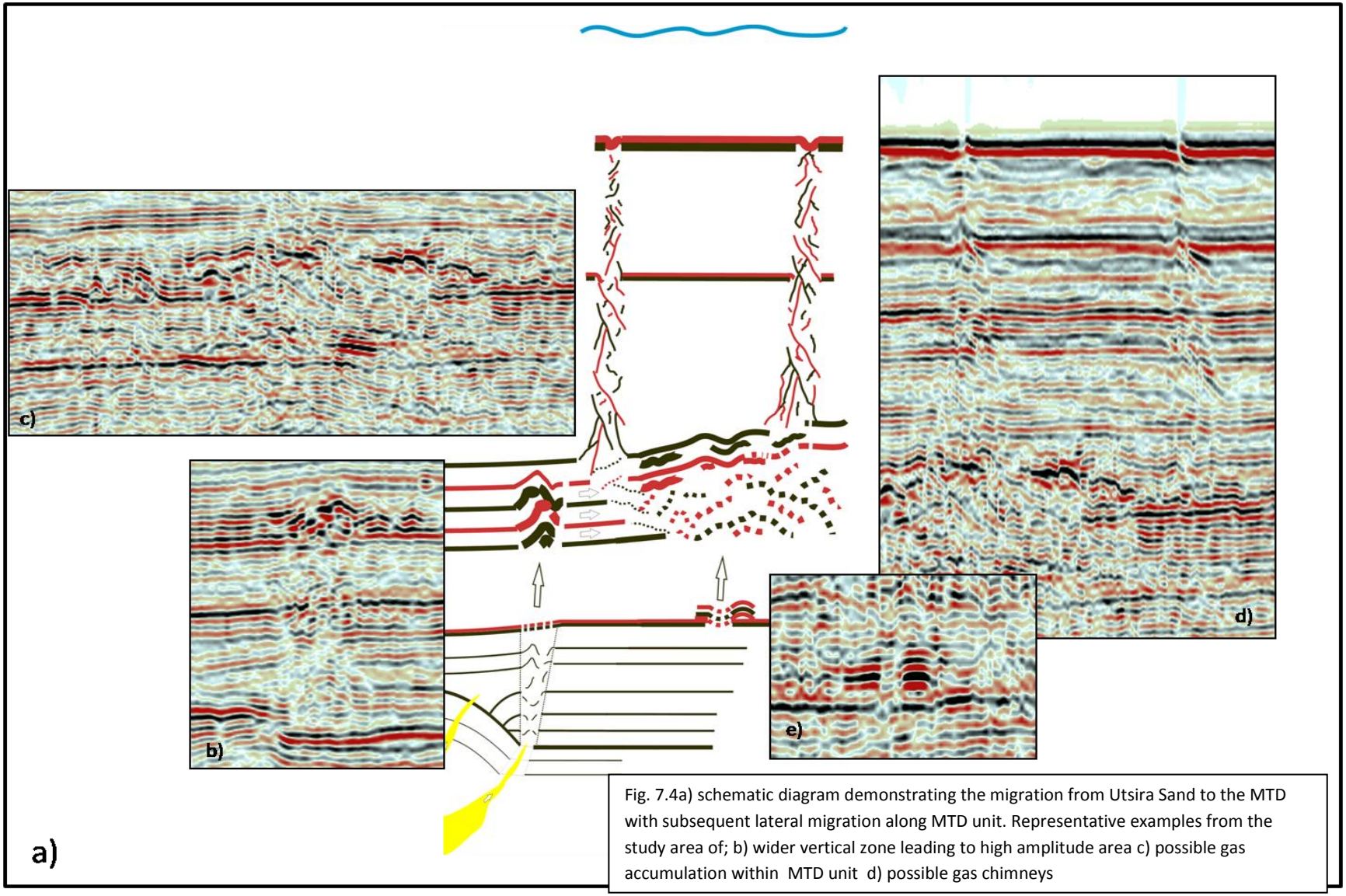

Fig. 7.4a) schematic diagram demonstrating the migration from Utsira Sand to the MTD with subsequent lateral migration along MTD unit. Representative examples from the study area of; b) wider vertical zone leading to high amplitude area c) possible gas accumulation within MTD unit d) possible gas chimneys

7.1.3.4. Seafloor breaches

The origin of the seafloor 'breaches' or pockmarks presented in Section 6.4.5 is contentious. If real, they pose a significant risk to sequestered CO_2, as in some cases they represent potential leakage pathways from the Utsira Sand to the seafloor. Their origin is discussed in Section 6.4.5.1, and for the purpose of this discussion a geological origin is assumed.

Examples of these vertical disrupted zones are presented in Chapter 6 (Sections 6.4.4 and 6.4.5). They are defined by internal reflections which are discontinuous and displaced, of lower amplitude, and often very weak or absent. Such vertical discontinuities are believed to indicate gas flow in fine-grained sediments (Løseth, 2009), such as the sealing lithologies overlying the Utsira Sand, and are therefore considered to be 'gas chimneys' (Arntsen et al., 2007).

With the exception of one example (Chapter 6, Fig. 6.27), all these vertical columns terminate at the modern seafloor. The seismic expression of a leakage zone is unlikely to match that of the real leakage zone (Løseth, 2009), and while the upper extent of these chimneys can be determined by their disruption of the seafloor reflection, there is greater ambiguity in defining a leakage 'root'.

Several of the chimneys are linked to chaotic low amplitude areas of the MTD (Chapter 6, Fig. 6.29), either at crestal highs or at sections where the chaotic zones are in contact with stratified reflections (Fig. 7.4). Chimneys above the crestal highs are possibly due to heterogeneities in permeability within the MTD unit allowing migration in some parts and causing pressure build up in others, resulting in localised 'blow outs' which form the vertical chimneys to the seafloor. Chimneys at the flanks of these chaotic zones may be the result of gas migration exploiting the low angle contact with the stratified sections and the chaotic zones. A permeable pathway from the MTD to the seafloor can therefore be established.

Examples of vertical disruption zones from the base of the Utsira which terminate as high amplitude features within the Remnant Unit have been presented (Chapter 6 Fig.s 6.21 and 6.22, 7, Chapter 7.3), and discussed in Section 7.2.3.2. Considering that there is possible lateral connectivity between the Remnant Unit and the MTD Unit, it is possible to infer an indirect permeable network from the base of the Utsira, via lateral migration within the MTD unit, to the seafloor (Fig. 7.4).

Two examples of chimneys which suggest a direct link between the sub-MTD strata and the seafloor are presented in Chapter 6 (6.30) and Fig. 7.5. They have indication of roots to at least the depth of the base of the MTD unit (Fig. 7.5, Chimney 1) or even as deep as a sand intrusion within the Lowermost Shale (Fig. 7.5, Chimney 2). Within the Quaternary and Middle Seal unit Chimney 1 is

expressed as a ‘dim zone’. Several stacked bright spots within the MTD unit underlie the ‘dim zone’ and suggest the continuation of the chimney. A secondary ‘dim zone’ exists within the Lower Seal, which in turn is underlain by bright spots at the top of and within the Utsira Sand. The ‘dim zone’ of Chimney 2 contains disrupted reflections and can be traced from the seafloor to a sand intrusion within the Lowermost Shale unit. It appears to break through the Base Utsira Horizon at the crest of a forced fold and advances passed a high amplitude anomaly affecting the Lower Seal High Amplitude Horizon. Both features present evidence to suggest historic migration of fluid or gas from below the Utsira Sand to the modern day seafloor, and represent a possible current permeability pathway.

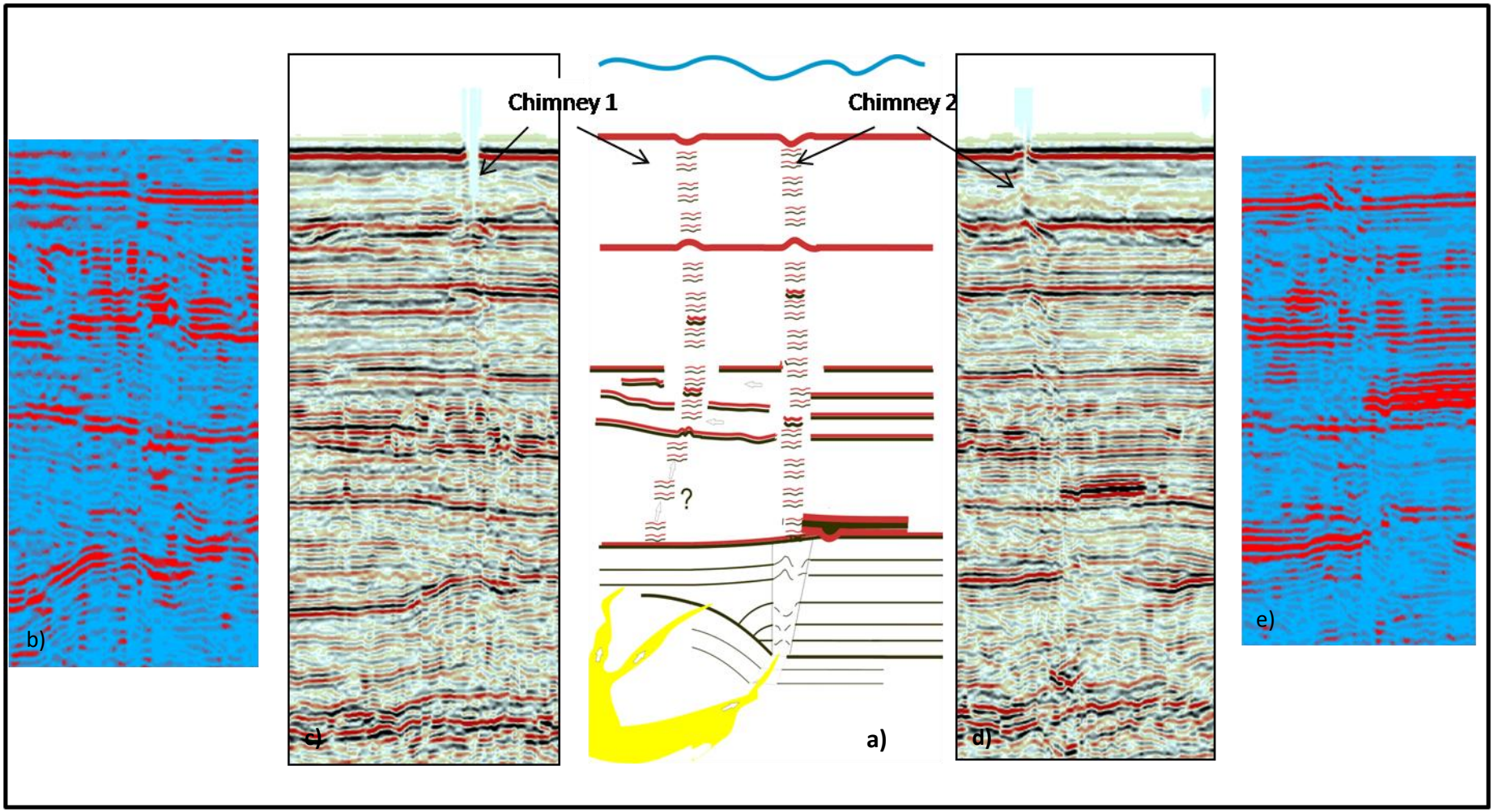

Fig. 7.4a) schematic diagram demonstrating gas chimneys from Utsira Sand through the MTD unit to seafloor. Representative examples from the study area indicating roots of chimneys b) c) chimney 1 d) and e) chimney 2.

7.2. Implications for injected CO_2

Significant natural leakage routes through the major top seal of the Utsira Sand have been identified; CO_2 sequestered in the vicinity of the plumbing systems described above would be likely exploit the same leakage zones. CO_2 leakage is considered unavoidable (Humez et al., 2011), while the amount has been a matter of considerable discussion according to Bøe et al., (2005), with the authors suggesting a minimum requirement is that leakage should not have a worse effect on climate change than its direct venting to atmosphere.

The EU Directive (2009/31/EC) requires very tight monitoring of CO_2 movement in the subsurface. Operators are required to demonstrate that the CO_2 is behaving as predicted and that it is totally contained in the storage complex. Failure to do so could result in financial penalties. The EU directive defines leakage as 'any release of CO_2 from the **storage complex.**' A CCS **storage site** is 'a defined volume area within the geological formation used for geological storage of CO_2 and associated surface and injection facilities.' However, the **storage complex** includes 'the storage site and surrounding geological domain which can have an effect on overall storage integrity and security.' This definition of the storage complex would appear to give provision for secondary accumulations of CO_2 at shallower depths. Storage efficacy at shallower depth is decreased as the CO_2 is not in a supercritical state; however, these shallower accumulations are preferable to seafloor venting.

A further definition by Det Norske Veritas (2012) describes the storage complex as a 'subsurface volume delineated by the operator and approved by the regulator for the purpose of environmentally safe long-term containment of injected CO_2 streams.' The authors stipulate that the volume must contain vertical boundaries which should be defined 'such that the storage complex includes, **at least**, the injection zone and the primary seal.' This also suggests that there is scope to define vertical boundaries for the storage complex which are at shallower levels than the primary sealing lithology, providing the operator and regulator are in agreement.

It is also worth considering that storage permits are granted for storage of CO_2 within the storage site, not within the storage complex. Any leakage from the site would require an increase in monitoring activity. However, corrective measures need to be taken only in case of leakage from the storage complex (ROAD, 2013).

The stratigraphic extent of the leakage in this study area is dependent on the terminal points of the individual and interconnected leakage zones described. The severity of the leakage, under the EU

Directive, would depend on the definition of the storage complex and specifically on the vertical boundaries of the complex, as would be agreed upon between the operator and regulator.

It is suggested that risk assessments for CCS storage sites must evaluate potential leakage scenarios (Pruess, 2008); presented below are four potential leakage scenarios based on the plumbing system described in section 7.2.

7.2.1. Utsira Sand to Lower Seal

Leakage pathways directly from the Utsira Sand to a permeable horizon within the Lower Seal have been established. Injected CO_2 would rise to the top of the Utsira and exploit the feeder pipes at the Top Utsira Horizon which are connected to overlying pockmarks (Fig. 7.2a).

Pockmark location or high amplitude areas within the Lower Seal High Amplitude Horizon (LSHAH) do not appear to have a direct link to the sand intrusions or forced folds, although CO_2 migration to the top of the reservoir would be accelerated through the sub-vertical disrupted zones associated with the extensional zones at the mound flanks (Fig. 7.2e).

The extent of the permeable layer or lenses within Lower Seal High Amplitude Horizon (LSHAH) is unknown. If the layer was laterally extensive, CO_2 could still remain contained within the horizon if sequestered in areas distal to vertical breaches of the Lower Seal. Evidence of pockmarks that haven't extended laterally is present in the study area (Fig. 7.2b), suggesting that the permeable layer is not continuous, and that small pockets of CO_2 could be contained in the Lower Seal.

In this scenario, the CO_2 would have migrated from the storage site, and would require an escalation in monitoring. However, it could still be considered to be contained within the 'surrounding geological domain' and that leakage from the storage complex had not taken place.

7.2.2. Utsira to MTD

Vertical and sub-vertical zones of disrupted reflections from the Base Utsira Horizon to the MTD unit are suggested to represent evidence of fluid flow between these units. Wider zones of disruption are generally located at the flanks of forced folds which affect the Base Utsira Horizon while narrower

zones mostly emanate from the crests of the folds (Fig. 7.3a). Sequestered CO_2 could exploit these features and leak directly from the Utsira Sand to the MTD unit.

If the injected CO_2 were to flow from the Utsira Sand to the MTD unit it would be considered to have migrated from the storage site and leaked from the storage complex; if the vertical boundary of the complex was limited to the top of the Lower Seal. If the sealing capacity of the MTD could be determined, a case could be put forward to include the MTD unit within the storage complex, thus redefining the CO_2 movement as migration within the complex rather than a leakage. However, due to the expected large variability in the permeability of this unit, a site-by-site case for its sealing capacity would be required.

As mentioned in the previous section, not all the pockmark features have developed into laterally extensive high amplitude areas. Some have remained as small scale stacked bright spots at the level of, and directly above, the Top Utsira Horizon (Fig. 7.2b). However, there is evidence of their vertical development (Fig. 7.3d and 7.4e), which would constitute a further pathway from the Utsira Sand to the MTD unit.

7.2.3. MTD upwards

Vertical chimneys which emanate from chaotic sections of the MTD unit are present within the study area. They are interpreted as possible gas or fluid 'blow outs' to the seafloor, and represent permeable pathways. These 'blow outs', from top of the MTD, do not extend deeper than the MTD unit, and therefore do not pose a direct link to sequestered CO_2. However, permeable pathways from the Utsira Sand to the remnant section of MTD unit have been established, and continuous and stratified reflections within the remnant section suggest that lateral migration of CO_2 once it has reached the MTD is possible.

The sealing capacity of the MTD can be considered variable, so can its the internal permeability. In many cases the leakage zones from the Utsira Sand terminate at the point where they reach MTD unit. If they terminate within low permeability sections of the MTD, then the CO_2 would be contained at that level. In cases where the vertical boundary of the storage complex can be defined as the top of the MTD, then migration of CO_2 to this level would not constitute a leakage, and would not require any further action other than an increased in monitoring.

If there was sufficient lateral permeability within the relevant areas, migration of CO_2 within the MTD unit would be possible. Leakage to the seafloor would therefore be a possibility via the vertical chimneys located at crestal highs and at the boundary areas between the MTD chaotic sections and stratified reflections (Fig. 7.4a). Except for one example, where a vertical chimney is seen to emanate from a high amplitude area in LSHAH and terminates at the top of the Middle Seal (Fig. 6.27), all other gas chimneys within the study area terminate at the seafloor. Adjusting the vertical boundary of the storage section in these cases would be irrelevant, as venting of CO_2 to the seafloor would have taken place provide that the interpreted pathways are still permeable.

7.2.4. Direct to seafloor

As with the scenario in 7.3.3, direct venting of CO_2 cannot be classified as anything but a leakage, even by redefining the vertical boundary of the storage complex. This would be the worst case scenario. However, unlike the leakage scenario in section 7.3.3, this direct venting to the seafloor does not have the benefit of the possible safety 'buffer' of the MTD unit as a possible restriction on the leakage process.

Two vertical chimneys which penetrate and advance passed the MTD unit are presented in Fig. 7.5a. They represent a direct permeability link from the Utsira Sand to the seafloor, and would pose the most significant risk to sequestered CO_2 within the study area.

7.3. Summary

The observations from Chapters 4, 5 and 6 are compiled and a plumbing system based on these observations is proposed. Permeability pathways within the Lowermost Shale, Utsira Sand and the overburden are recognised.

These permeability pathways are intrinsically linked with fluid flow features as defined by andresen (2012). Polygonal faults at the base of the Lowermost Shale are classified as laterally extensive fluid flow features; sand intrusions, hosted by Lowermost Shale, are recognised as subsurface sediment remobilisation features; and gas chimneys, features within the Utsira Sand and the sealing sequence, are classified as vertically focused fluid flow features.

In many cases, individual permeability pathways are linked to form networks which represent cross-stratal migration routes. Within this study area, there is significant evidence to suggest that the formation of each sub-class of fluid flow feature is dependent on the presence of a stratigraphically deeper fluid flow feature. This sequential development also suggests a permeability connection; whereas if one feature is the result of fluid flow focused through an earlier feature then a remnant of this hydraulic connection must remain.

Polygonal faults, sand intrusions and gas chimneys/blow out pipes are members of the fault-related, intrusion-related, and pipe-related seal bypass systems respectively (Cartwright et al., 2007). It is therefore suggested that the plumbing system in place within the study area consist of a linked network of seal bypass systems and fluid flow features.

CO_2, if injected in close proximity to the permeability pathways, is likely to migrate out of the storage site. The extent of the migration depends on the extent of the permeability pathway or leakage zone it exploits. Examples of leakage zones from the Utsira Sand which appear to terminate within the Lower Seal and the MTD unit are presented. However, other examples demonstrate that leakage from the Utsira to the seafloor is also a possibility.

What constitutes a leakage as defined in the EU Directive (2009/31/EC) is the migration of CO_2 from the 'storage complex'. The storage complex is defined as the storage site itself (the storage reservoir) and the 'surrounding geological domain'. The extent storage complex is limited by 'vertical boundaries', and may be set at the level of immediate seal, or even at shallow depths.

This study recognises twelve vertical chimneys which extend from the MTD to the seafloor. Their origin is contentious, but they are assumed to be real geological features. It is proposed that in the areas unaffected by these chimneys that the shallowest vertical limit of the geological storage complex, with careful investigation, may be set at the MTD level.

It is also worth bearing in mind that the Sleipner injection project, located around 10km to the south-west of the features identified, does not appear to be leaking, and that the storage structure being utilised may be the result of sand intrusion related subsidence at the Top Utsira Sand horizon. The presence of sand intrusions, therefore, does not necessarily compromise the sealing lithology.

Chapter 8

Conclusion

8. Conclusion

Evidence of paleo-fluid flow and leakage from the Utsira Sand to the overburden, indirectly and directly, to various levels of the overlying strata is presented in this study. Any operator injecting CO_2 into the Utsira Sand, needs to appreciate the risk element of these plumbing systems. Seal analysis has previously been considered limited by the analysis of core-scale properties (Cartwright et al, 2007). This study further highlights the need to analyse the seal as a whole for seismic expressions of leakage, seal bypass systems and fluid flow features, before risking of the top seal takes place.

The Utsira Sand is one of the likeliest storage reservoirs that could be used by the Carbon Capture and Storage industry. The total pore volume of the Utsira Sand has been estimated at $6x10^{11}$ m^3. This is reduced to a calculated effective storage capacity of $6.6x10^8$ m^3 by Chadwick et al. (2004), based on available volume below structural traps. The features recognised within this study, if present within the rest of the Utsira Sand area, significantly compromises the storage capacity of the Utsira Sand, and would reduce this effective capacity further.

From the features observed and interpreted it is vital to develop a conceptual understanding of the plumbing system, and analyse resultant leakage scenarios. It is also apparent that fluid flow features and seal bypass systems hosted below the storage reservoir are instrumental in the development of shallower fluid flow features. This highlights the need to fully understand the storage reservoir and the adjacent units to allow a complete evaluation of not only the risk of storage, but also the short and medium term behaviour of the CO_2 plume.

Good practice for CO_2 sequestration is vital, and regulations in place ensure that operators select storage sites which limit leakage, while also ensuring that they monitor the migration of the CO_2 and can demonstrate that the plume is behaving as predicted. The determination of the vertical limit of the storage complex is a key parameter in defining whether the migration of CO_2 to the 'surrounding geological domain' is classified as leakage or not. While there seems to be some ambiguity regarding what defines a 'storage complex', the extent of the complex must be determined on a case-by-case basis.

It can be concluded that the viability and development of carbon sequestration technology as a climate change mitigation option requires that it represents an attractive proposition for those that operate the technology. In addition carbon sequestration requires a finely measured balance between strict regulation and appropriate penalties for poor practice that are coupled with flexibility in what constitutes the 'storage complex' and 'leakage.'

8.1. Recommendations for further future work

The areas analysed in this study are relatively small cubes of data from a larger 3D seismic volume. The extension of this study to investigate and determine the geographic spread and effects of the features observed throughout the area where the Utsira Sand is present would be priority if its CO_2 storage capacity is to be fully investigated.

A more detailed analysis of the lithology of the individual sealing units is also suggested, especially the MTD unit, with special focus on the sealing ability and the internal permeability and connectivity of the MTD. The use of well data to better validate the interpretation given in this study is also highly recommended.

References

Aandresen, K. J. (2012). Fluid flow features in hydrocarbon plumbing systems: What do they tell us about the basin evolution? *Marine Geology*, *332*, 89-108.

Anell, I., Thybo, H., and Rasmussen, E. (2012). A synthesis of Cenozoic sedimentation in the North Sea. *Basin Research*, *24*(2), 154-179.

Arts, R. J., Zweigel, P., and Lothe, A. E. (2000). Reservoir geology of the Utsira Sand in the Southern Viking Graben area–a site for potential CO2 storage. In *62nd EAGE meeting, Glasgow, paper B-20*.

Arts, R., Eiken, O., Chadwick, A., Zweigel, P., Van der Meer, L., and Zinszner, B. (2004). Monitoring of CO2 injected at Sleipner using time-lapse seismic data. *Energy*, *29*(9), 1383-1392.

Arts, R., Chadwick, A and Eiken, O. (2004). "Recent time-lapse seismic data show no indication of leakage at the Sleipner CO2-injection site." *Proceedings of the 7th International Conference on Greenhouse Gas Technologies (GHGT-7)*..

Avseth, Per, TapanMukerji, and Gary Mavko.(2005). "Quantitative seismic interpretation." *Quantitative Seismic Interpretation, by Per Avseth and TapanMukerji and Gary Mavko, pp. 376. ISBN 0521816017. Cambridge, UK: Cambridge University Press, March 2005.* 1

Bachu, Stefan, W. D. Gunter, and E. H. Perkins(1994). "Aquifer disposal of CO< sub> 2</sub>: Hydrodynamic and mineral trapping." *Energy Conversion and Management* 35.4: 269-279.

Bachu, S. (2000). Sequestration of CO2 in geological media: criteria and approach for site selection in response to climate change. *Energy Conversion and Management*, *41*(9), 953-970.

Bachu, S., and Adams, J. J. (2003). Sequestration of CO2 in geological media in response to climate change: capacity of deep saline aquifers to sequester CO2 in solution. *Energy Conversion and Management*, *44*(20), 3151-3175.

Bachu, S., Bonijoly, D., Bradshaw, J., Burruss, R., Holloway, S., Christensen, N. P., andMathiassen, O. M. (2007). CO2 storage capacity estimation: Methodology and gaps. *International Journal of Greenhouse Gas Control*, *1*(4), 430-443.

Bachu, S. (2008). CO2 storage in geological media: Role, means, status and barriers to deployment. *Progress in Energy and Combustion Science*, *34*(2), 254-273.

Bachu, S., and McEwen, T. (2011). Geological media and factors for the long-term emplacement and isolation of carbon dioxide and radioactive waste. In *Geological Disposal of Carbon Dioxide and Radioactive Waste: A Comparative Assessment* (pp. 23-79). Springer Netherlands.

Bacon, M., Simm, R. and Redshaw, T. (2003). 3-D Seismic Interpretation. Cambridge Uinv Pr, 209pp.

Benson, S. M., and Cole, D. R. (2008). CO2 sequestration in deep sedimentary formations. *Elements*, *4*(5), 325-331.

Bentham, M., and M Kirby. (2005). "CO2 storage in saline aquifers." *Oil and gas science and technology* 60.3 (2005): 559-567.

Berg, Robert R.(1975). "Capillary pressures in stratigraphic traps." *AAPG bulletin* 59.6 (1975): 939-956.

Bertoni, Claudia, and Joe A. Cartwright. (2006). "Controls on the basinwide architecture of late Miocene (Messinian) evaporites on the Levant margin (Eastern Mediterranean)." *Sedimentary Geology* 188 (2006): 93-114.

Brown, A.R., (2004). Interpretation of Three-Dimensional Seismic Data, sixth Ed. AAPG Memoir, 42. American Association of Petroleum Geologists, Tulsa.

Buchardt, B. (1978). Oxygen isotope palaeotemperatures from the Tertiary period in the North Sea area.*Nature.com.*

Bull, S., Cartwright, J, and Huuse, M. (2009). "A review of kinematic indicators from mass-transport complexes using 3D seismic data." *Marine and Petroleum Geology* 26.7 (2009): 1132-1151.

Cartwright, J., Huuse, M., and Aplin, A. (2007). "Seal bypass systems." *AAPG bulletin* 91.8 (2007): 1141-1166.

Cartwright, J., James, D., Huuse, M., Vetel, W., and Hurst, A. (2008). The geometry and emplacement of conical sandstone intrusions. *Journal of Structural Geology*, *30*(7), 854-867.

Cartwright, J. (2010). "Regionally extensive emplacement of sandstone intrusions: a brief review." *Basin Research* 22.4 (2010): 502-516.

Celia, Michael A., Nordbotten, J. M., Bachu, S., Dobossy, M., and Court, B. (2009). "Risk of leakage versus depth of injection in geological storage." *Energy Procedia* 1.1 (2009): 2573-2580.

Chadwick, R. A., Zweigel, P., Gregersen, U., Kirby, G. A., Holloway, S., and Johannessen, P. N. (2004). Geological reservoir characterization of a CO2 storage site: The Utsira Sand, Sleipner, northern North Sea. *Energy*, *29*(9), 1371-1381

Chadwick, A., Arts, R., Eiken, O., Williamson, P., and Williams, G. (2006). *Geophysical monitoring of the CO2 plume at Sleipner, North Sea* (pp. 303-314). Springer Netherlands.

Chadwick, A., Noy, D., Arts, R and Eiken, O. (2009). "Latest time-lapse seismic data from Sleipner yield new insights into CO2 plume development." Energy Procedia1(1): 2103-2110.

Chadwick, A., Williams, G., Delepine, N., Clochard, V., Labat, K., Sturton, S., Buddensiek, M., Dillen, M., Nickel, M., Lima, A., Williams, G., Neele, F., Arts, R and Rossi, G. (2010). Quantitative analysis of time-lapse seismic monitoring data at the Sleipner CO 2 storage operation. *The Leading Edge*, *29*(2), 170-177.

Chadwick, R. A., Williams, G. A., Williams, J. D. O., andNoy, D. J. (2012). Measuring pressure performance of a large saline aquifer during industrial-scale CO< sub> 2</sub> injection: The Utsira Sand, Norwegian North Sea. *International Journal of Greenhouse Gas Control*, *10*, 374-388.

Coward, M P., Dewey, J F., Hempton, M., Holroyd, J and Mange, M A. (2003). Tectonic evolution. 17-33 in *The Millennium Atlas:petroleum geology of the central and northern North Sea.* Evans, D.,

Curtis, M. L., and Riley, T. R. (2003). Mobilization of fluidized sediment during sill emplacement, western Dronning Maud Land, East Antarctica. *Antarctic Science*, *15*(03), 393-398.

Gaus, I., Azaroual, M., andCzernichowski-Lauriol, I. (2005). Reactive transport modelling of the impact of CO< sub> 2</sub> injection on the clayey cap rock at Sleipner (North Sea). *Chemical Geology*, *217*(3), 319-337.

Daniel, R. F., and Kaldi, J. G. (2008). Evaluating seal capacity of caprocks and intraformational barriers for the geosequestration of CO2. In *Eastern Australasian Basins Symposium (3rd: 2008: Sydney, Australia) EABS III*.

Davies, R. J., and Cartwright, J. (2002). A fossilized Opal A to Opal C/T transformation on the northeast Atlantic margin: support for a significantly elevated Palaeogeothermal gradient during the Neogene. *Basin Research*, *14*(4), 467-486.

Davies, R. J., Huuse, M., Hirst, P., Cartwright, J., and Yang, Y. (2006). Giant clastic intrusions primed by silica diagenesis. *Geology*, *34*(11), 917-920.

Davies, R. J., and Cartwright, J. A. (2007). Kilometer-scale chemical reaction boundary patterns and deformation in sedimentary rocks. *Earth and Planetary Science Letters*, *262*(1), 125-137.

Deegan,C.E and Scull,B.J, (1977).*A standard lithostratigraphic nomenclature for the Central and Northern North Sea*. Vol. 1. HMSO, 1977.

Eidvin, T., Jansen, E., Rundberg, Y., Brekke, H., and Grogan, P. (2000). The upper Cainozoic of the Norwegian continental shelf correlated with the deep sea record of the Norwegian Sea and the North Atlantic. *Marine and Petroleum Geology*, *17*(5), 579-600.

Eidvin, T., andRundberg, Y. (2007). Post-Eocene strata of the southern Viking Graben, northern North Sea; integrated biostratigraphic, strontium isotopic and lithostratigraphic study. *NorskGeologiskTidsskrift*, *87*(4), 391.

Eiken, O., Ringrose, P., Hermanrud, C., Nazarian, B., Torp, T. A., and Høier, L. (2011). Lessons learned from 14 years of CCS operations: Sleipner, In Salah and Snøhvit. *Energy Procedia*, *4*, 5541-5548.

Ennis-King, J., and Paterson, L. (2007). Coupling of geochemical reactions and convective mixing in the long-term geological storage of carbon dioxide. *International Journal of Greenhouse Gas Control*, *1*(1), 86-93.

Faleide, J. I., Kyrkjebo, R., Kjennerud, T., Gabrielsen, R. H., Jordt, H., Fanavoll, S., and Bjerke, M. D. (2002). Tectonic impact on sedimentary processes during Cenozoic evolution of the northern North Sea and surrounding areas. *SPECIAL PUBLICATION-GEOLOGICAL SOCIETY OF LONDON*, *196*, 235-270.

Frey-Martinez, J., Cartwright, J. A., Burgess, P. M., and Bravo, J. V. (2004). 3D seismic interpretation of the Messinian Unconformity in the Valencia Basin, Spain. *Geological Society, London, Memoirs*, *29*(1), 91-100.

Frey-Martínez, J. (2010). "3D Seismic Interpretation of Mass Transport Deposits: Implications for Basin Analysis and Geohazard Evaluation." *Submarine Mass Movements and Their Consequences*. Springer Netherlands, 2010. 553-568.

Gamboa, D., Alves, T., Cartwright, J., andTerrinha, P. (2010). MTD distribution on a 'passive'continental margin: The Espírito Santo Basin (SE Brazil) during the Palaeogene. *Marine and Petroleum Geology*, *27*(7), 1311-1324.

Gamboa, D., Alves, T., and Cartwright, J. (2011). Distribution and characterization of failed (mega) blocks along salt ridges, southeast Brazil: Implications for vertical fluid flow on continental margins. *Journal of Geophysical Research: Solid Earth (1978–2012)*, *116*(B8).

Gallo, F., and Woods, A. W. (2004). On steady homogeneous sand–water flows in a vertical conduit. *Sedimentology*, *51*(2), 195-210.

Galloway, W. E., Garber, J. L., Liu, X., and Sloan, B. J. (1993). Sequence stratigraphic and depositional framework of the Cenozoic fill, Central and Northern North Sea Basin. In *Geological Society, London, Petroleum Geology Conference series* (Vol. 4, pp. 33-43). Geological Society of London.

Galloway, W. E. (2001). Seismic expressions of deep-shelf depositional and erosional morphologies, Miocene Utsira Formation, North Sea Basin. *Marine Geophysical Researches*, *22*(5-6), 309-321.

Galloway, W. E. (2002). Paleogeographic setting and depositional architecture of a sand-dominated shelf depositional system, Miocene Utsira Formation, North Sea Basin. *Journal of Sedimentary Research*, *72*(4), 476-490.

Gaus, I., Azaroual, M., andCzernichowski-Lauriol, I. (2005). Reactive transport modelling of the impact of CO2 injection on the clayey cap rock at Sleipner (North Sea). *Chemical Geology*, *217*(3), 319-337.

Gay, A., Lopez, M., Berndt, C., Seranne, M., (2007). Geological controls on focused fluid flow associated with seafloor seeps in the Lower Congo Basin. Mar. Geol. 244, 68–92

Gill, W. D., and Kuenen, P. H. (1957). Sand volcanoes on slumps in the Carboniferous of County Clare, Ireland. *Quarterly Journal of the Geological Society*, *113*(1-4), 441-460.

Gras, R., Cartwright, J.A., 2002. 3D seismic analysis of sandstone intrusions. European Association of Petroleum Geologists Annual Meeting, Florence. Extended Abstracts, H020.

Graham, A. G. C., Lonergan, L., and Stoker, M. S. (2007). Evidence for Late Pleistocene ice stream activity in the Witch Ground Basin, central North Sea, from 3D seismic reflection data. *Quaternary Science Reviews*, *26*(5), 627-643.

Gregersen, U. (1998). Upper Cenozoic channels and fans on 3D seismic data in the northern Norwegian North Sea. *Petroleum Geoscience*, *4*(1), 67-80.

Gregersen, U., and Johannessen, P. N. (2007). Distribution of the NeogeneUtsira Sand and the succeeding deposits in the Viking Graben area, North Sea. *Marine and Petroleum Geology*, *24*(10), 591-606.

Gunter, W. D., Wiwehar, B., and Perkins, E. H. (1997). Aquifer disposal of CO2-rich greenhouse gases: extension of the time scale of experiment for CO2-sequestering reactions by geochemical modelling. *Mineralogy and Petrology*, *59*(1-2), 121-140..

Hansen, D. M., and Cartwright, J. (2006). The three-dimensional geometry and growth of forced folds above saucer-shaped igneous sills. *Journal of Structural Geology*, *28*(8), 1520-1535.

Hart, B., (2008). Stratigraphically significant attributes. The Leading Edge, 27: 320-324.

.

Head, M.J., Riding, J.B, Eidvin, T. and Chadwick, R.A., (2004). Palynological and foraminaferal biostratigraphy of (Upper Pliocene) Nordland Group mudstones at Sleipner, northern North Sea. Marine and PetroleumGeology, 21, pp. 277-297.

Heggland, Roar. (1997). "Detection of gas migration from a deep source by the use of exploration 3D seismic data." *Marine Geology* 137.1 (1997): 41-47.

Heggland, R. (1998). Gas seepage as an indicator of deeper prospective reservoirs. A study based on exploration 3D seismic data. *Marine and Petroleum Geology*, *15*(1), 1-9.

Henriksen, Sverre, and Tore O. Vorren.(1996). “Late Cenozoic sedimentation and uplift history on the mid-Norwegian continental shelf." *Global and Planetary Change* 12.1 (1996): 171-199.

Hepple, Robert P., and Sally M. Benson.(2002). "Implications of surface seepage on the effectiveness of geologic storage of carbon dioxide as a climate change mitigation strategy." (2002).

Hermanrud, C., andresen, T., Eiken, O., Hansen, H., Janbu, A., Lippard, J., and Østmo, S. (2009). Storage of CO2 in saline aquifers–Lessons learned from 10 years of injection into the Utsira Formation in the Sleipner area. *Energy Procedia*, *1*(1), 1997-2004.

Holloway, S. (2005). "Underground sequestration of carbon dioxide—a viable greenhouse gas mitigation option." *Energy* 30.11 (2005): 2318-2333.

Holloway, S., Vincent, C. J., and Kirk, K. (2006). Industrial carbon dioxide emissions and carbon dioxide storage potential in the UK. Report No. COAL R308 DTI/Pub URN 06/2027, October 2006

Hosa, A., Esentia, M., Stewart, J., andHaszeldine, S. (2011). Injection of CO2 into saline formations: Benchmarking worldwide projects. *Chemical Engineering Research and Design*, *89*(9), 1855-1864.

Hovland, M., and Judd, A. (1988). *Seabed pockmarks and seepages: impact on geology, biology, and the marine environment*. Springer.

Humez, P., Audigane, P., Lions, J., Chiaberge, C., andBellenfant, G. (2011). Modeling of CO2 leakage up through an abandoned well from deep saline aquifer to shallow fresh groundwaters. *Transport in porous media*, *90*(1), 153-181.

Hurst, A., Cartwright, J., Huuse, M., Jonk, R., Schwab, A., Duranti, D., and Cronin, B. (2003). Significance of large-scale sand injectites as long-term fluid conduits: evidence from seismic data. *Geofluids*, *3*(4), 263-274.

Hurst, A., Cartwright, J. A., Huuse, M., andDuranti, D. (2006). Extrusive sandstones (extrudites): a new class of stratigraphic trap?.*Geological Society, London, Special Publications*, *254*(1), 289-300.

Hurst, A., Scott, A., andVigorito, M. (2011). Physical characteristics of sand injectites. *Earth-Science Reviews*, *106*(3), 215-246.

Huuse, M., and Clausen, O. R. (2001). Morphology and origin of major Cenozoic sequence boundaries in the eastern North Sea Basin: top Eocene, near-top Oligocene and the mid-Miocene unconformity. *Basin Research*, *13*(1), 17-41.

Huuse, M., and Mickelson, M. (2004). Eocene sandstone intrusions in the Tampen Spur area (Norwegian North Sea Quad 34) imaged by 3D seismic data. *Marine and Petroleum Geology*, *21*(2), 141-155.

Huuse, M., Cartwright, J. A., Gras, R., and Hurst, A. (2005). Kilometre-scale sandstone intrusions in the Eocene of the Outer Moray Firth (UK North Sea): migration paths, reservoirs and potential drilling hazards. In *Geological Society, London, Petroleum Geology Conference series* (Vol. 6, pp. 1577-1594). Geological Society of London.

Huuse, M., Jackson, C. A. L., Van Rensbergen, P., Davies, R. J., Flemings, P. B., and Dixon, R. J. (2010). Subsurface sediment remobilization and fluid flow in sedimentary basins: an overview. *Basin Research*, *22*(4), 342-360.

Isaksen, D., and KeTonstad, eds. *A revised Cretaceous and Tertiary lithostratigraphic nomenclature for the Norwegian North Sea*. Norwegian Petroleum Directorate, 1989.

Jager, D. D. H., Giles, M. R., and Griffiths, G. R. (1993, January). Evolution of Paleogene submarine fans of the North Sea in space and time. In *Geological Society, London, Petroleum Geology Conference series* (Vol. 4, pp. 59-71). Geological Society of London.

Jarvie, D. M., Hill, R. J., Ruble, T. E., andPollastro, R. M. (2007). Unconventional shale-gas systems: The Mississippian Barnett Shale of north-central Texas as one model for thermogenic shale-gas assessment. *AAPG bulletin*, *91*(4), 475-499.

Jenkins, C. R., Cook, P. J., Ennis-King, J., Undershultz, J., Boreham, C., Dance, T., Caritat, P., Etheridge, D., Freifeld, B., Hortle, A., Kirste, D., Paterson, L., Pevzner, R., Schacht, U., Sharma, S., Stalker, L and Urosevic, M. (2012). Safe storage and effective monitoring of CO2 in depleted gas fields. *Proceedings of the National Academy of Sciences*, *109*(2), E35-E41.

Jolly, R. J., and Lonergan, L. (2002). Mechanisms and controls on the formation of sand intrusions. *Journal of the Geological Society*, *159*(5), 605-617.

Jonk, R. (2010). Sand-rich injectites in the context of short-lived and long-lived fluid flow. *Basin Research*, *22*(4), 603-621.

Jordt, H., Faleide, J. I., Bjørlykke, K., and Ibrahim, M. T. (1995). Cenozoic sequence stratigraphy of the central and northern North Sea Basin: tectonic development, sediment distribution and provenance areas. *Marine and Petroleum Geology*, *12*(8), 845-879.

Jørgensen, F., and Sandersen, P. B. (2006). Buried and open tunnel valleys in Denmark—erosion beneath multiple ice sheets. *Quaternary Science Reviews*, *25*(11), 1339-1363.

Jørgensen, F., and Sandersen, P. B. (2008). Mapping of buried tunnel valleys in Denmark: new perspectives for the interpretation of the Quaternary succession. *Geological Survey of Denmark and Greenland Bulletin*, *15*, 33-36.

Juanes, R., Spiteri, E. J., Orr, F. M., and Blunt, M. J. (2006). Impact of relative permeability hysteresis on geological CO2 storage. *Water Resources Research*, *42*(12).

Kearey, P., Brooks, M. and Hill, I., (2002). An introduction to geophysical exploration. Wiley-Blackwell, 268 pp.

Kristensen, T. B., and Huuse, M. (2012). Multistage erosion and infill of buried Pleistocene tunnel valleys and associated seismic velocity effects. *Geological Society, London, Special Publications*, *368*(1), 159-172.

Kane, I. A. (2010). Development and flow structures of sand injectites: The Hind Sandstone Member injectite complex, Carboniferous, UK. *Marine and Petroleum Geology*, *27*(6), 1200-1215.

Kårstad, O. (2002). Geological storage, including costs and risks, in saline aquifers. In *Proceedings of the Workshop on Carbon Dioxide Capture and Storage* (pp. 53-60).

Kongsjorden, H., Kårstad, O., and Torp, T. A. (1998). Saline aquifer storage of carbon dioxide in the Sleipner project. *Waste management*, *17*(5), 303-308.

Larsen, J. W. (2004). The effects of dissolved CO< sub> 2</sub> on coal structure and properties. *International Journal of Coal Geology*, *57*(1), 63-70.

Leith, T. L., andFallick, A. E. (1997). AAPG Memoir 67: Seals, Traps, and the Petroleum System. Chapter 8: Organic Geochemistry of Cap-Rock Hydrocarbons, Snorre Field, Norwegian North Sea.

Li, S., Dong, M., Li, Z., Huang, S., Qing, H., and Nickel, E. (2005). Gas breakthrough pressure for hydrocarbon reservoir seal rocks: implications for the security of long-term CO2 storage in the Weyburn field. *Geofluids*, *5*(4), 326-334.

Lindeberg, E., Vuillaume, J. F., and Ghaderi, A. (2009). Determination of the CO2 storage capacity of the Utsira formation. *Energy Procedia*, *1*(1), 2777-2784.

Lokhorst, A., andWildenborg, T. (2005). Introduction on CO2 Geological storage-classification of storage options. *Oil and gas science and technology*, *60*(3), 513-515.

Lonergan, L., Lee, N., Johnson, H. D., Cartwright, J. A., andJolly, R. J. (2000). Remobilization and injection in deepwater depositional systems: Implications for reservoir architecture and prediction. In *Deep-water reservoirs of the world: Gulf Coast Section SEPM Foundation, 20th Annual Conference, Houston* (pp. 515-532).

Lonergan, L., Maidment, S. C., and Collier, J. S. (2006). Pleistocene subglacial tunnel valleys in the central North Sea basin: 3-D morphology and evolution. *Journal of Quaternary Science*, *21*(8), 891-903.

Løseth, H., Wensaas, L., Arntsen, B., and Hovland, M. (2003). Gas and fluid injection triggering shallow mud mobilization in the Hordaland Group, North Sea. *Geological Society, London, Special Publications*, *216*(1), 139-157.

Løseth, H., Gading, M., andWensaas, L. (2009). Hydrocarbon leakage interpreted on seismic data. *Marine and Petroleum Geology*, *26*(7), 1304-1319.

Løseth, H., Rodrigues, N., and Cobbold, P. R. (2012). World's largest extrusive body of sand?.*Geology*, *40*(5), 467-470.

Macelloni, L., Simonetti, A., Knapp, J. H., Knapp, C. C., Lutken, C. B., andLapham, L. L. (2012). Multiple resolution seismic imaging of a shallow hydrocarbon plumbing system, Woolsey Mound, Northern Gulf of Mexico. *Marine and Petroleum Geology*, *38*(1), 128-142.

Martinsen, O. J., Lien, T., and Jackson, C. (2005, January). Cretaceous and Palaeogene turbidite systems in the North Sea and Norwegian Sea Basins: source, staging area and basin physiography controls on reservoir development. In *Geological Society, London, Petroleum Geology Conference series* (Vol. 6, pp. 1147-1164). Geological Society of London.

McKerrow, W. S., Mac Niocaill, C., Ahlberg, P. E., Clayton, G., Cleal, C. J., and Eagar, R. M. C. (2000). The late Palaeozoic relations between Gondwana and Laurussia. *Geological Society, London, Special Publications*, *179*(1), 9-20.

McGrail, B. P., Schaef, H. T., Ho, A. M., Chien, Y. J., Dooley, J. J., and Davidson, C. L. (2006). Potential for carbon dioxide sequestration in flood basalts. *Journal of Geophysical Research: Solid Earth (1978–2012)*, *111*(B12).

Meakin, P. (1998). *Fractals, scaling and growth far from equilibrium* (Vol. 5). Cambridge university press.

Meakin, P., Wagner, G., Vedvik, A., Amundsen, H., Feder, J., and Jøssang, T. (2000). Invasion percolation and secondary migration: experiments and simulations. *Marine and Petroleum Geology*, *17*(7), 777-795.

Michael, K., Golab, A., Shulakova, V., Ennis-King, J., Allinson, G., Sharma, S., and Aiken, T. (2010). Geological storage of CO2 saline aquifers—A review of the experience from existing storage operations. *International Journal of Greenhouse Gas Control*, *4*(4), 659-667.

Michael, K., Golab, A., Shulakova, V., Ennis-King, J., Allinson, G., Sharma, S., and Aiken, T. (2010). Geological storage of CO< sub> 2</sub> in saline aquifers—A review of the experience from existing storage operations. *International Journal of Greenhouse Gas Control*, *4*(4), 659-667.

Molyneux, S., Sandstone remobilisation in the Eocene to Miocene of the central and northern North Sea. PhD thesis, University of London.

Molyneux, S., Cartwright, J., andLonergan, L. (2002). Conical sandstone injection structures imaged by 3D seismic in the central North Sea, UK. *First Break*, *20*(6).

Moscardelli, L., Wood, L., and Mann, P. (2006). Mass-transport complexes and associated processes in the offshore area of Trinidad and Venezuela. *AAPG bulletin*, *90*(7), 1059-1088.

Moss, J. L., and Cartwright, J. (2010). 3D seismic expression of km-scale fluid escape pipes from offshore Namibia. *Basin Research*, *22*(4), 481-501.

Nordgård Bolås, H. M., Hermanrud, C., and Teige, G. M. (2005). Seal capacity estimation from subsurface pore pressures. *Basin Research*, *17*(4), 583-599.

Ott, L., Mendenhall, W., Ott, R. L., &Ott, L. (1994). *Understanding statistics*. Duxbury Press.

Piasecki, S. T. E. F. A. N. (1984). Dinoflagellate cyst stratigraphy of the Lower Cretaceous Jydegård Formation, Bornholm, Denmark. *Bulletin of the Geological Society of Denmark*, *32*, 145-161.

Praeg, D. (2003). Seismic imaging of mid-Pleistocene tunnel-valleys in the North Sea Basin—high resolution from low frequencies. *Journal of Applied Geophysics*, *53*(4), 273-298.

Price, P. N., and Oldenburg, C. M. (2009). The consequences of failure should be considered in siting geologic carbon sequestration projects. *International Journal of Greenhouse Gas Control*, *3*(5), 658-663.

Pruess, K. (2008). Leakage of CO 2 from geologic storage: Role of secondary accumulation at shallow depth. *International Journal of Greenhouse Gas Control*, *2*(1), 37-46.

Rodrigues, N., Cobbold, P. R., and Løseth, H. (2009). Physical modelling of sand injectites. *Tectonophysics*, *474*(3), 610-632.

Rundberg, Y., and Smalley, P. C. (1989). High-resolution dating of Cenozoic sediments from northern North Sea using 87Sr/86Sr stratigraphy. *AAPG Bulletin*, *73*(3), 298-308.

Rundberg, Y., andEidvin, T. (2005). Controls on depositional history and architecture of the Oligocene-Miocene succession, northern North Sea Basin. *Norwegian Petroleum Society Special Publications*, *12*, 207-239.

Saadatpoor, E., Bryant, S. L., andSepehrnoori, K. (2010). New trapping mechanism in carbon sequestration. *Transport in porous media*, *82*(1), 3-17.

Sheriff, R.E. and Geldart, L.P., (1995). Exploration Seismology. Cambridge University Press, second edition, 628 pp.

Shi, J. Q., andDurucan, S. (2005). CO2 storage in deep unminable coal seams. *Oil and gas science and technology*, *60*(3), 547-558.

Shoulders, S. J. and J. Cartwright (2004). "Constraining the depth and timing of large-scale conical sandstone intrusions." Geology32(8): 661-664.

Shoulders, S. J., Cartwright, J., andHuuse, M. (2007). Large-scale conical sandstone intrusions and polygonal fault systems in Tranche 6, Faroe-Shetland Basin. *Marine and petroleum geology*, *24*(3), 173-188

Stearns, D. W. (1978). Faulting and forced folding in the Rocky Mountains foreland. *Laramide folding associated with basement block faulting in the western United States: Geological Society of America Memoir*, *151*, 1-37.

Stewart, M. A., andLonergan, L. (2011). Seven glacial cycles in the middle-late Pleistocene of northwest Europe: Geomorphic evidence from buried tunnel valleys. *Geology*, *39*(3), 283-286.

Sturkell, E.F.F. andOrmö, J., (1997). Impact-related clastic injections in the marine Ordovician Lockne impact structure, central Sweden. Sedimentology 44, 793-804.

Suekane, T., Nobuso, T., Hirai, S., andKiyota, M. (2008). Geological storage of carbon dioxide by residual gas and solubility trapping. *International Journal of Greenhouse Gas Control*, *2*(1), 58-64.

Sun, Q., Wu, S., Cartwright, J., and Dong, D. (2012). Shallow gas and focused fluid flow systems in the Pearl River Mouth Basin, northern South China Sea. *Marine Geology*, *315*, 1-14.

Szarawarska, E., Huuse, M., Hurst, A., De Boer, W., Lu, L., Molyneux, S., and Rawlinson, P. (2010). Three-dimensional seismic characterisation of large-scale sandstone intrusions in the lower Palaeogene of the North Sea: completely injected vs. in situ remobilised sandbodies. *Basin Research*, *22*(4), 517-532.

Taku Ide, S., Jessen, K., and Orr Jr, F. M. (2007). Storage of CO< sub> 2</sub> in saline aquifers: Effects of gravity, viscous, and capillary forces on amount and timing of trapping. *International Journal of Greenhouse Gas Control*, *1*(4), 481-491.

Torp, T. A., and Gale, J. (2004). Demonstrating storage of CO2 in geological reservoirs: The Sleipner and SACS projects. *Energy*, *29*(9), 1361-1369.

Trude, J., Cartwright, J., Davies, R. J., and Smallwood, J. (2003). New technique for dating igneous sills. *Geology*, *31*(9), 813-816.

Ujiie, K., Yamaguchi, A., Kimura, G., andToh, S. (2007). Fluidization of granular material in a subduction thrust at seismogenic depths. *Earth and Planetary Science Letters*, *259*(3), 307-318.

Wang, S., and Jaffe, P. R. (2004). Dissolution of a mineral phase in potable aquifers due to CO< sub> 2</sub> releases from deep formations; effect of dissolution kinetics. *Energy conversion and management*, *45*(18), 2833-2848.

White, D. (2009). Monitoring CO 2 storage during EOR at the Weyburn-Midale Field. *The Leading Edge*, *28*(7), 838-842.

Wild, J., andBriedis, N. (2010). Structural and stratigraphic relationships of the Palaeocene mounds of the Utsira High. *Basin Research*, *22*(4), 533-547.

Xu, T., Apps, J. A., andPruess, K. (2004). Numerical simulation of CO< sub> 2</sub> disposal by mineral trapping in deep aquifers. *Applied geochemistry*, *19*(6), 917-936.

Yilmaz, Ö.,and Doherty, S. M. (1987). *Seismic data processing* (Vol. 2). Tulsa: Society of Exploration Geophysicists..

Zachos, J. C., Shackleton, N. J., Revenaugh, J. S., Pälike, H., and Flower, B. P. (2001). Climate response to orbital forcing across the Oligocene-Miocene boundary. *Science*, *292*(5515), 274-278.

Zanella, E., and M. P. Coward. (2003). "Structural framework." *The Millennium Atlas: Petroleum Geology of the Central and Northern North Sea* (2003): 45-59.

Ziegler, P. A. (1975). Geologic evolution of North Sea and its tectonic framework. *AAPG Bulletin*, *59*(7), 1073-1097.

Ziegler, P.A., Von Hoorn, B. (1989). Evolution of the North Sea rift system. In: Tankard A.J., Balkwill H.R., (Eds.), Extensional Tectonics and Stratigraphy of the North Atlantic Margins, American Association of Petroleum Geologists , 46, pp. 471-500

Ziegler, Peter A. *Geological Atlas of Western and Central Europe 1990*. 1990 (2nd Edition). (Bath: Geological Society for Shell Internationale Petroleum Maatschappij B.V., The Hague.)
Ziegler, P.A., (1992). North Sea rift system. Tectonophysics 208(1), 55 -75

Zweigel, P., Hamborg, M., Arts, R., Lothe, A., Sylta, Ø.,andTømmerås, A. (2000, August). Prediction of migration of CO2 injected into an underground depository: reservoir geology and migration modelling in the Sleipner case (North Sea). In *5th International Conference on Greenhouse Gas Control Technologies, Cairns (Australia)*.

Appendix A

NPD WELL DATA

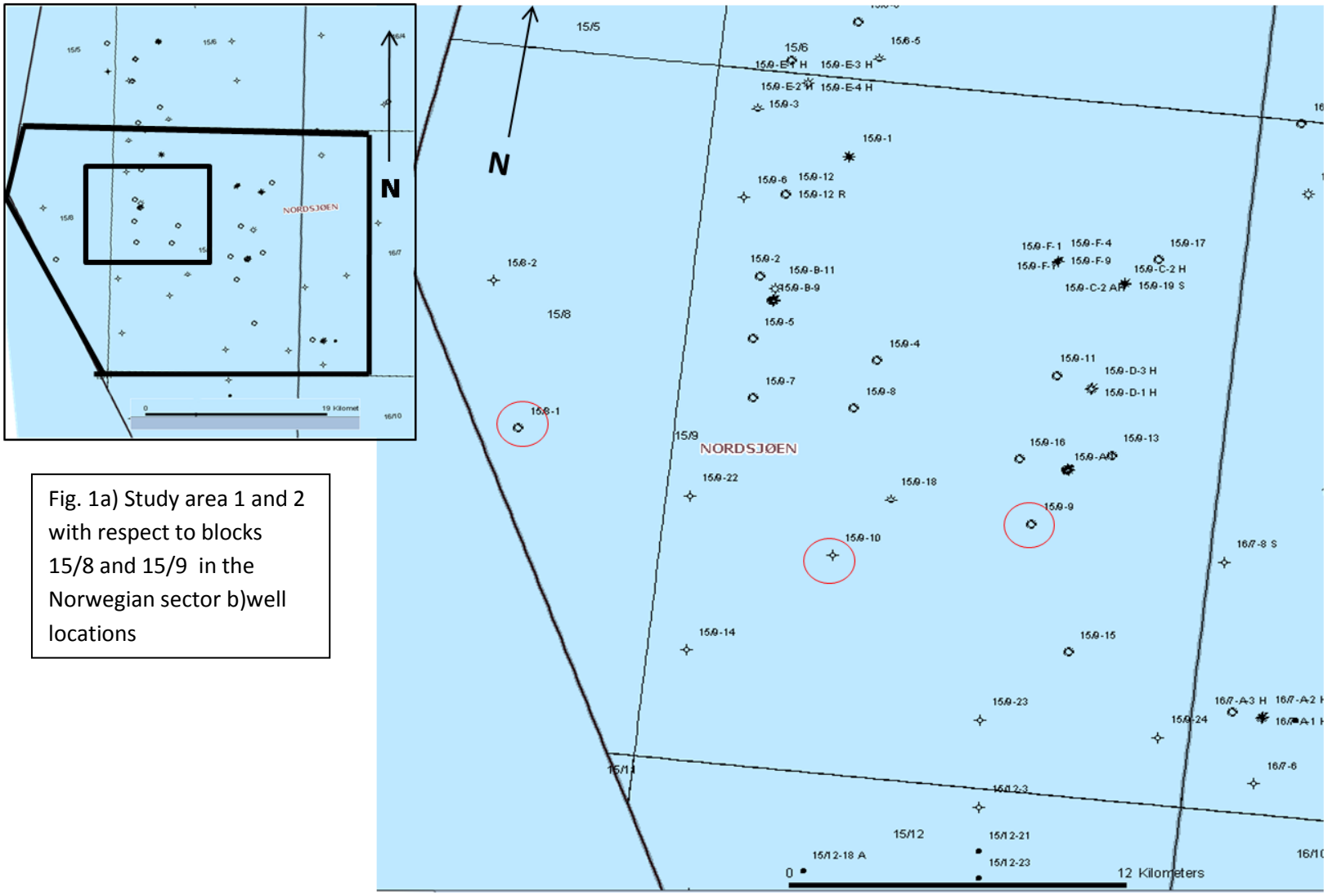

Fig. 1a) Study area 1 and 2 with respect to blocks 15/8 and 15/9 in the Norwegian sector b)well locations

Completion log for 15/8-1

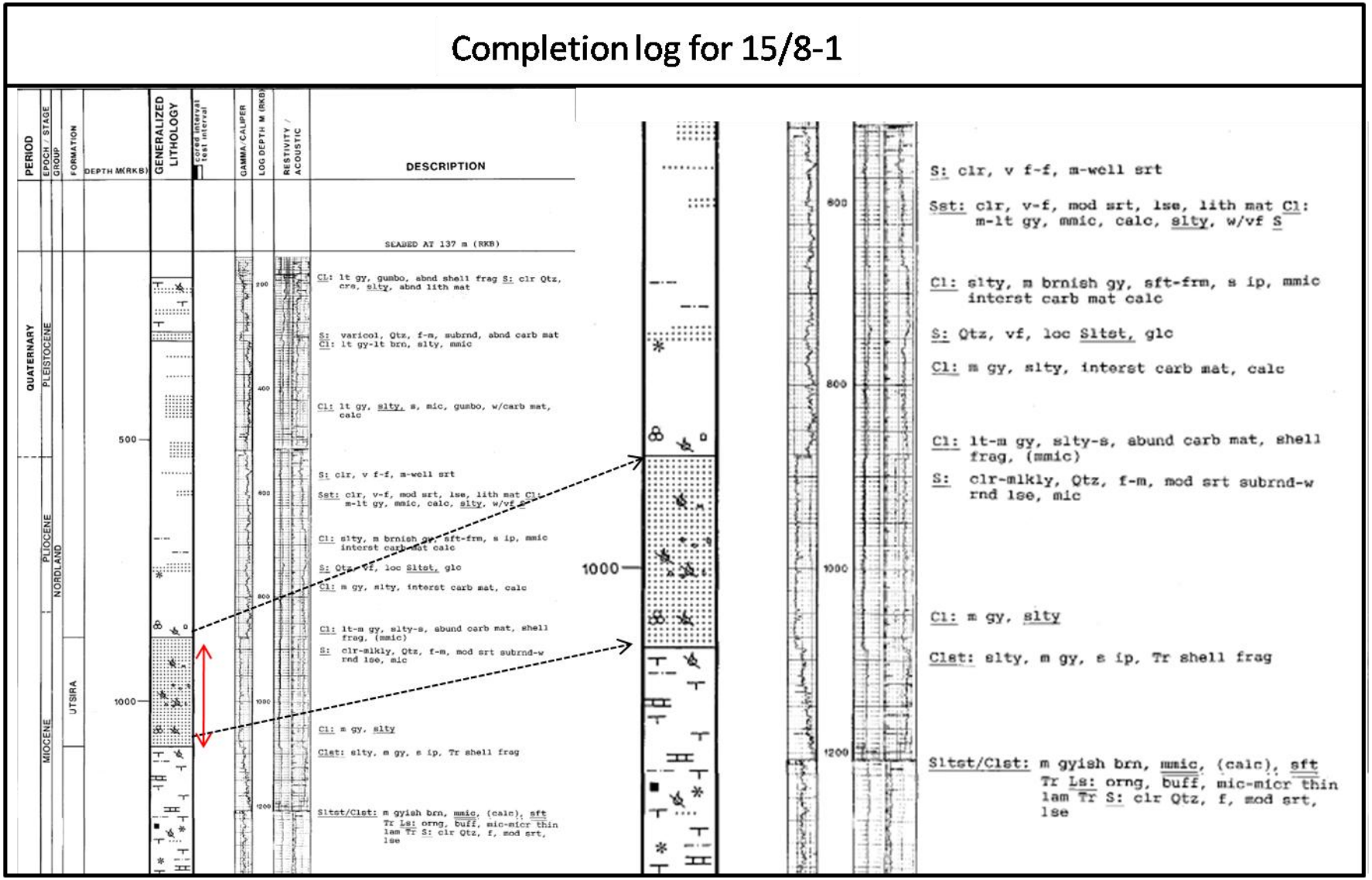

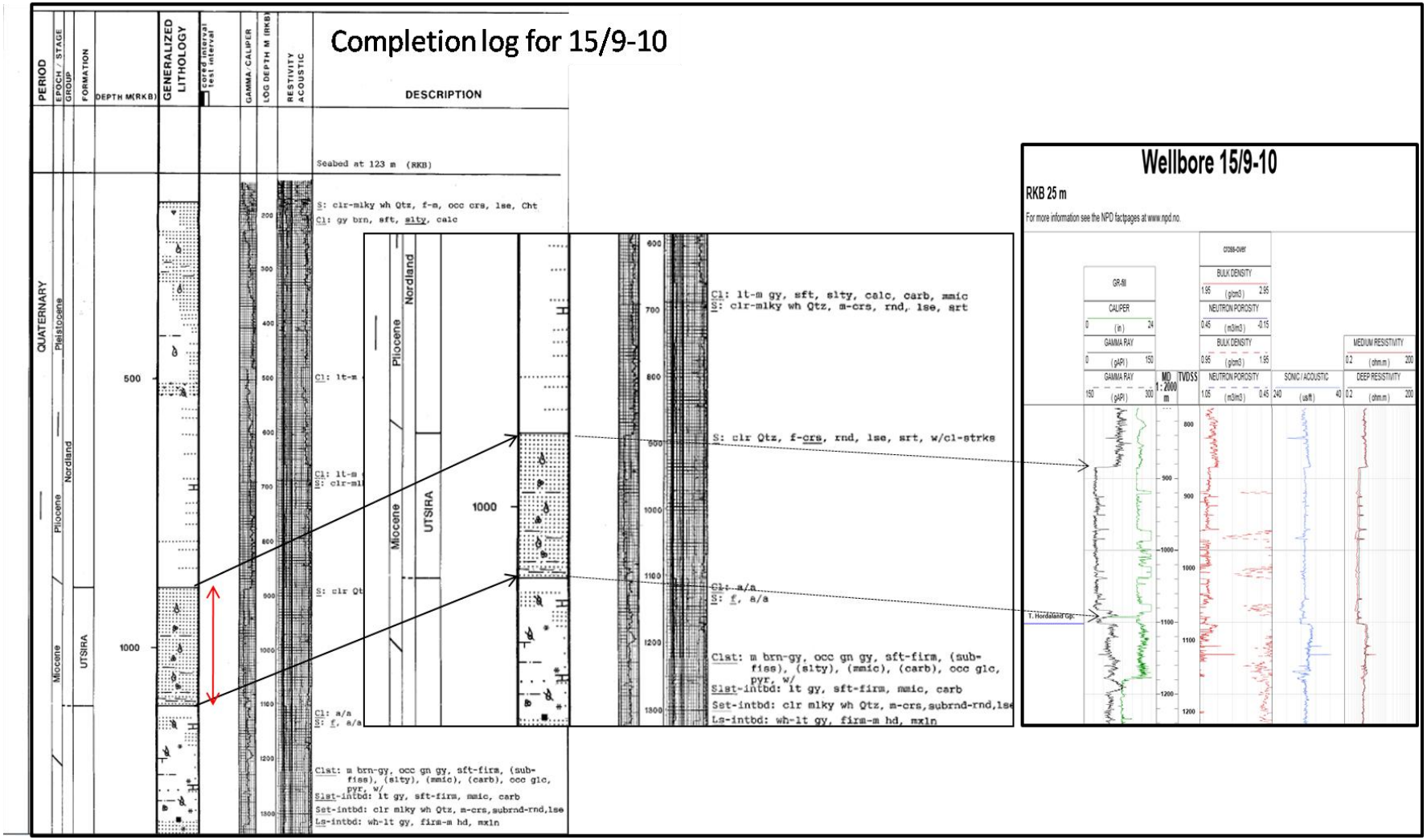
Completion log for 15/9-10
PERIOD
EPOCH / STAGE
GROUP
FORMATION
DEPTH M(RKB)
GENERALIZED LITHOLOGY
core& interval test interval
GAMMA CALIPER
LOG DEPTH M (RKB)
RESTIVITY ACOUSTIC
DESCRIPTION
QUATERNARY
Pleistocene
Pliocene
Miocene
Nordland
UTSIRA
Seabed at 123 m (RKB)
S: clr-mlky wh Qtz, f-m, occ crs, lse, Cht
Cl: gy brn, sft, slty, calc
Cl: lt-m
S: clr Qt
Cl: a/a
S: f, a/a
Clst: m brn-gy, occ gn gy, sft-firm, (sub-fiss), (slty), (mmic), (carb), occ glc, pyr, w/
Slst-intbd: lt gy, sft-firm, mmic, carb
Set-intbd: clr mlky wh Qtz, m-crs,subrnd-rnd,lse
Ls-intbd: wh-lt gy, firm-m hd, mxln
Cl: lt-m gy, sft, slty, calc, carb, mmic
S: clr-mlky wh Qtz, m-crs, rnd, lse, srt
S: clr Qtz, f-crs, rnd, lse, srt, w/cl-strks
Cl: a/a
S: f, a/a
Clst: m brn-gy, occ gn gy, sft-firm, (sub-fiss), (slty), (mmic), (carb), occ glc, pyr, w/
Slst-intbd: lt gy, sft-firm, mmic, carb
Set-intbd: clr mlky wh Qtz, m-crs,subrnd-rnd,lse
Ls-intbd: wh-lt gy, firm-m hd, mxln
Wellbore 15/9-10
RKB 25 m
For more information see the NPD factpages at www.npd.no.
GR-RI
CALIPER
GAMMA RAY
MD 1 : 2000 m
TVDSS
cross-over
BULK DENSITY
NEUTRON POROSITY
SONIC / ACOUSTIC
DEEP RESISTIVITY
MEDIUM RESISTIVITY
T. Hordaland Grp.

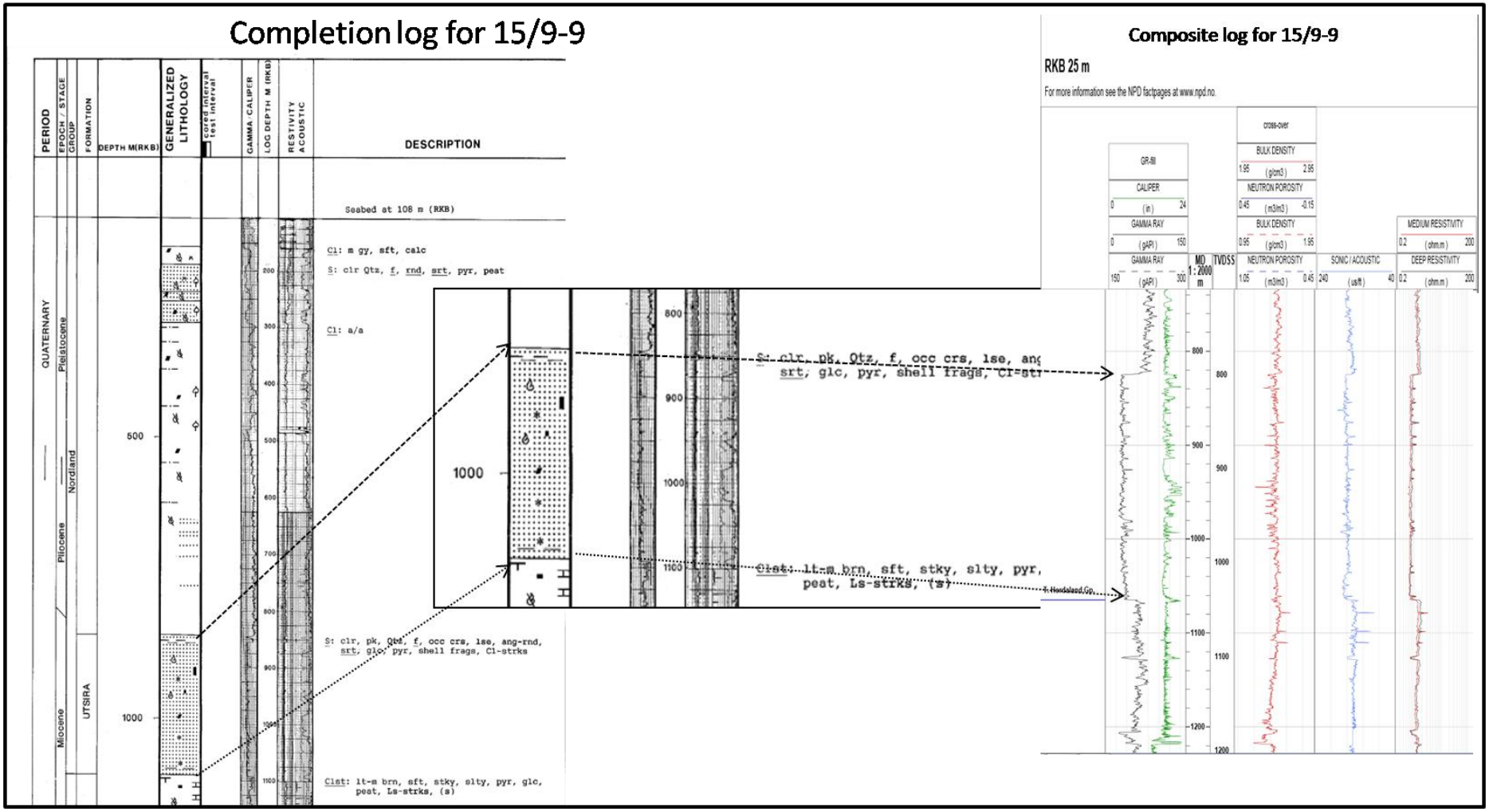
Completion log for 15/9-9
PERIOD
EPOCH / STAGE
GROUP
FORMATION
DEPTH M(RKB)
GENERALIZED LITHOLOGY
cored interval
test interval
GAMMA CALIPER
LOG DEPTH M (RKB)
RESTIVITY ACOUSTIC
DESCRIPTION
QUATERNARY
Pleistocene
Pliocene
Miocene
Nordland
UTSIRA
500
1000
Seabed at 108 m (RKB)
Cl: m gy, sft, calc
S: clr Qtz, f, rnd, srt, pyr, peat
Cl: a/a
S: clr, pk, Qtz, f, occ crs, lse, ang-rnd, srt, glc, pyr, shell frags, Cl-strks
Clst: lt-m brn, sft, stky, slty, pyr, glc, peat, Ls-strks, (s)
1000
800
900
1000
1100
S: clr, pk, Qtz, f, occ crs, lse, ang
srt, glc, pyr, shell frags, Cl-str
Clst: lt-m brn, sft, stky, slty, pyr,
peat, Ls-strks, (s)
Composite log for 15/9-9
RKB 25 m
For more information see the NPD factpages at www.npd.no.
cross-over
GR-fill
CALIPER
GAMMA RAY
BULK DENSITY
NEUTRON POROSITY
MEDIUM RESISTIVITY
SONIC / ACOUSTIC
DEEP RESISTIVITY
MD
TVDSS
1 : 2000 m

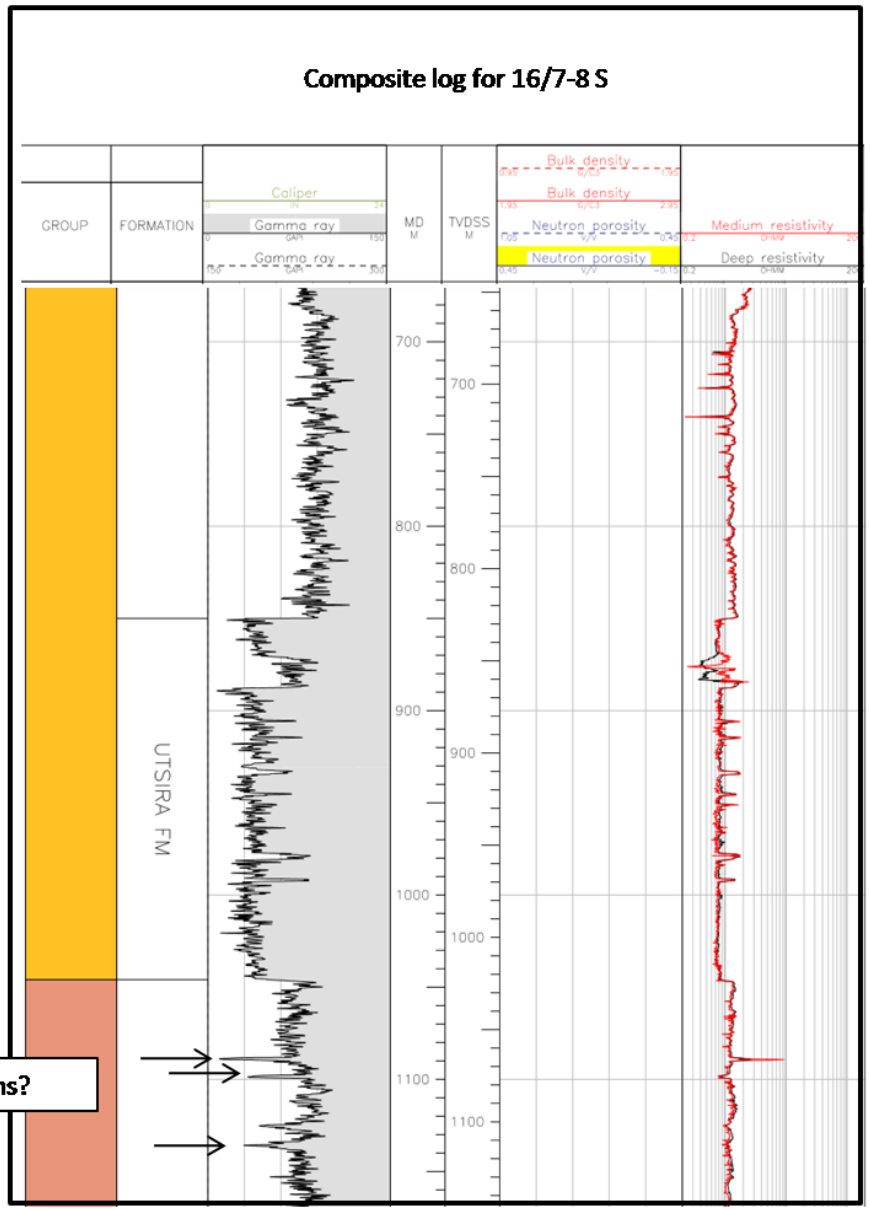
Composite log for 16/7-8 S
GROUP
FORMATION
Caliper
Gamma ray
Gamma ray
MD
M
TVDSS
M
Bulk density
Bulk density
Neutron porosity
Neutron porosity
Medium resistivity
Deep resistivity
UTSIRA FM
700
800
900
1000
1100
Sand intrusions?

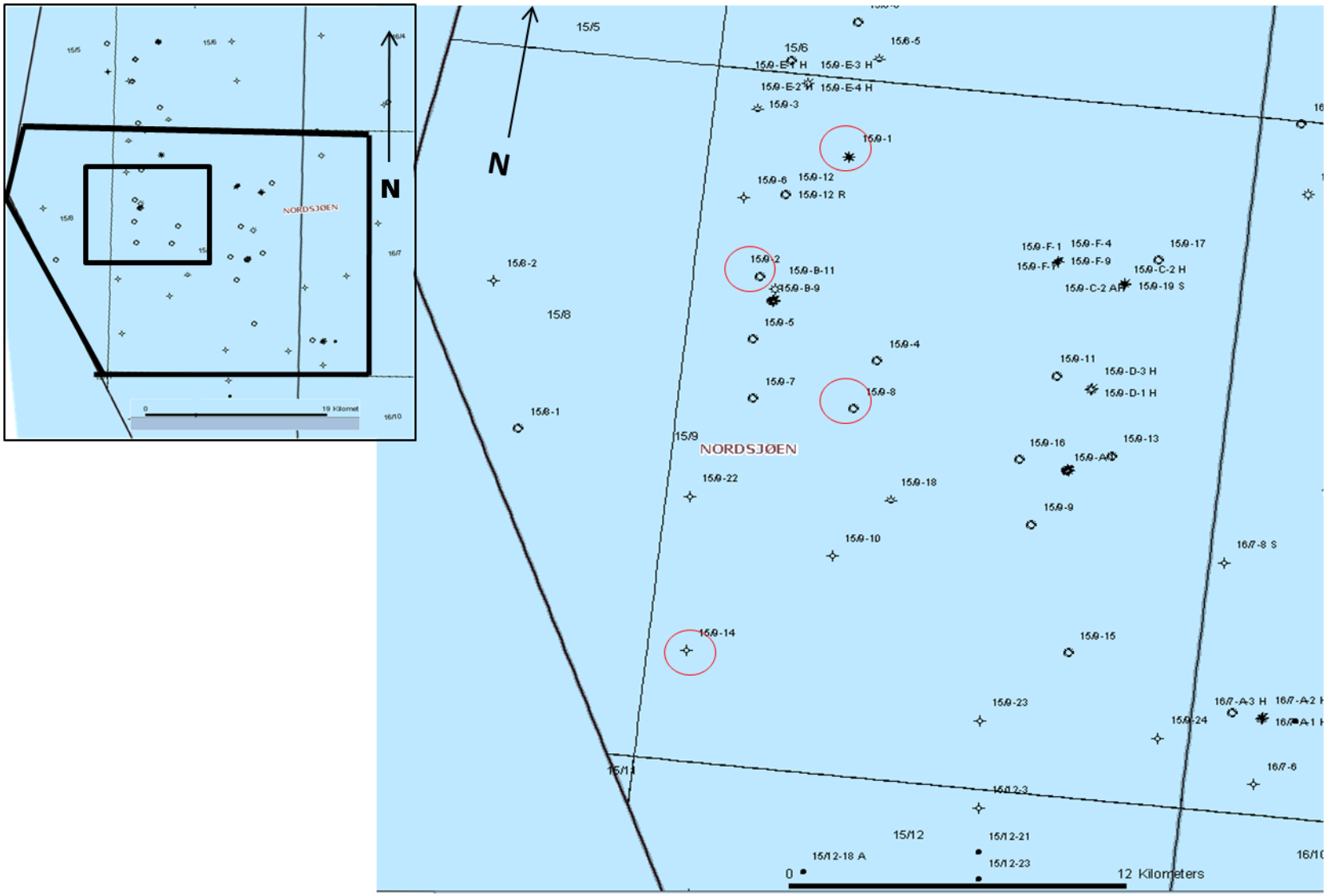
N
NORDSJØEN
15/5
15/6
15/8
15/9
15/12
15/6-5
15/6-E-1 H
15/6-E-3 H
15/6-E-2 H
15/6-E-4 H
15/6-3
15/6-1
15/6-6
15/6-12
15/6-12 R
15/8-2
15/6-2
15/6-B-11
15/6-B-9
15/6-5
15/8-1
15/6-4
15/6-7
15/6-8
15/6-F-1
15/6-F-4
15/6-17
15/6-F-7
15/6-F-9
15/6-C-2 H
15/6-C-2 AH
15/6-19 S
15/6-11
15/6-D-3 H
15/6-D-1 H
15/6-16
15/6-13
15/6-A
15/6-22
15/6-18
15/6-9
15/6-10
16/7-8 S
15/6-14
15/6-15
15/6-23
16/7-A-3 H
16/7-A-2 H
15/6-24
16/7-A-1 H
16/7-6
15/12-3
15/12-21
15/12-18 A
15/12-23
0
12 Kilometers

Completion log for 15/9-14

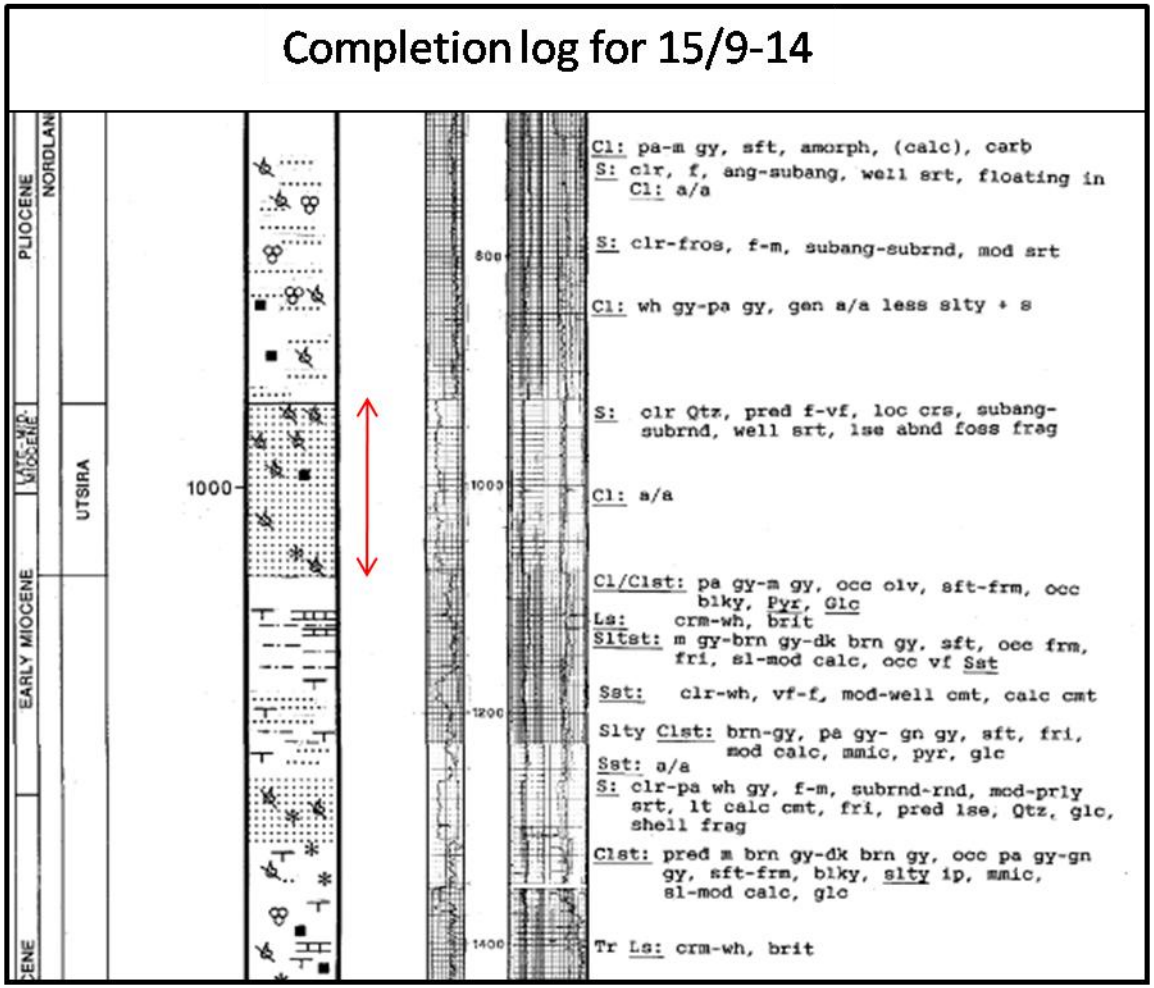

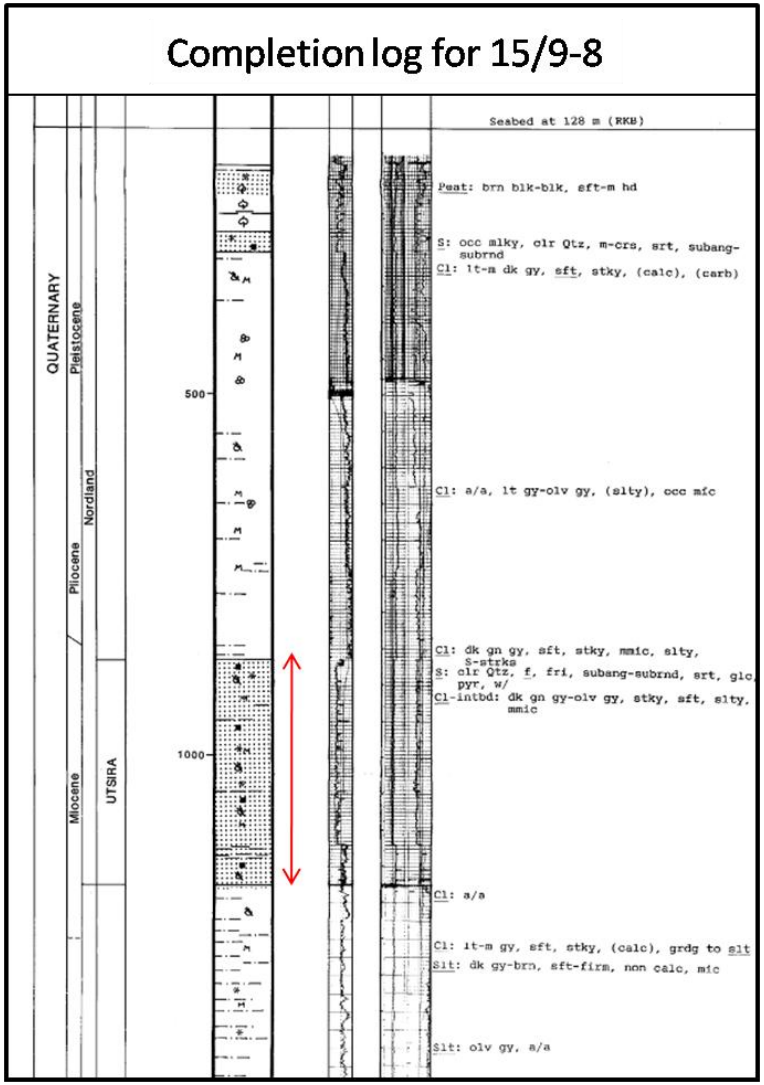
Completion log for 15/9-8
QUATERNARY
Pleistocene
Pliocene
Miocene
Nordland
UTSIRA
500
1000
Seabed at 128 m (RKB)
Peat: brn blk-blk, sft-m hd
S: occ mlky, clr Qtz, m-crs, srt, subang-subrnd
Cl: lt-m dk gy, sft, stky, (calc), (carb)
Cl: a/a, lt gy-olv gy, (slty), occ mic
Cl: dk gn gy, sft, stky, mmic, slty, S-strks
S: clr Qtz, f, fri, subang-subrnd, srt, glc pyr, w/
Cl-intbd: dk gn gy-olv gy, stky, sft, slty, mmic
Cl: a/a
Cl: lt-m gy, sft, stky, (calc), grdg to slt
Slt: dk gy-brn, sft-firm, non calc, mic
Slt: olv gy, a/a

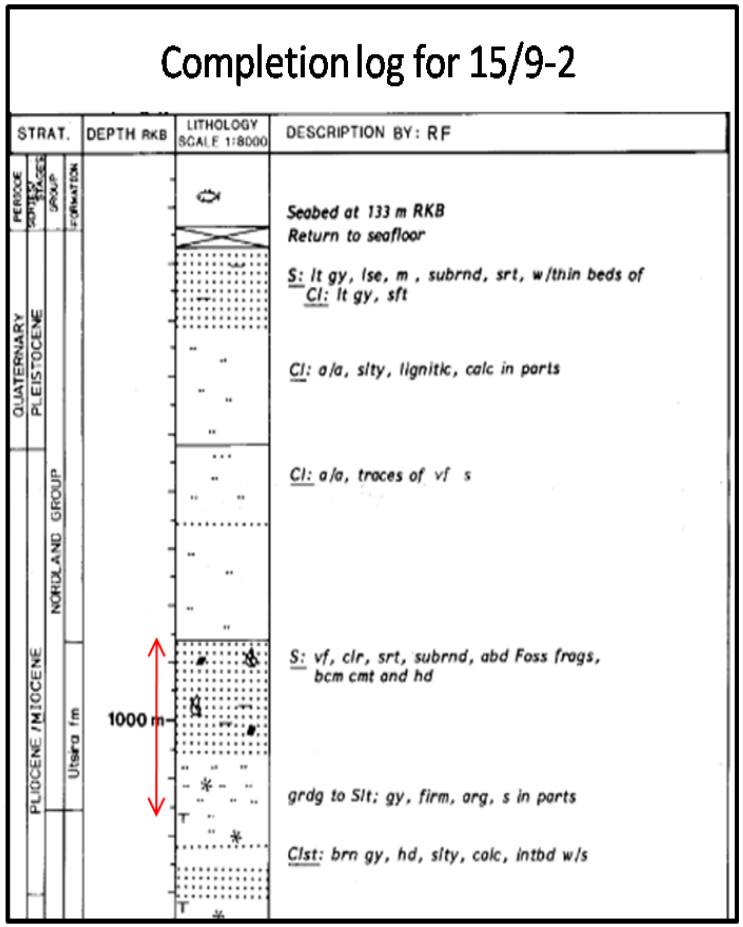
Completion log for 15/9-2
STRAT.
DEPTH RKB
LITHOLOGY SCALE 1:8000
DESCRIPTION BY: RF
QUATERNARY
PLEISTOCENE
PLIOCENE / MIOCENE
NORDLAND GROUP
Utsira fm
1000 m
Seabed at 133 m RKB
Return to seafloor
S: lt gy, lse, m , subrnd, srt, w/thin beds of Cl: lt gy, sft
Cl: a/a, slty, lignitic, calc in parts
Cl: a/a, traces of vf s
S: vf, clr, srt, subrnd, abd Foss frags, bcm cmt and hd
grdg to Slt; gy, firm, arg, s in parts
Clst: brn gy, hd, slty, calc, intbd w/s

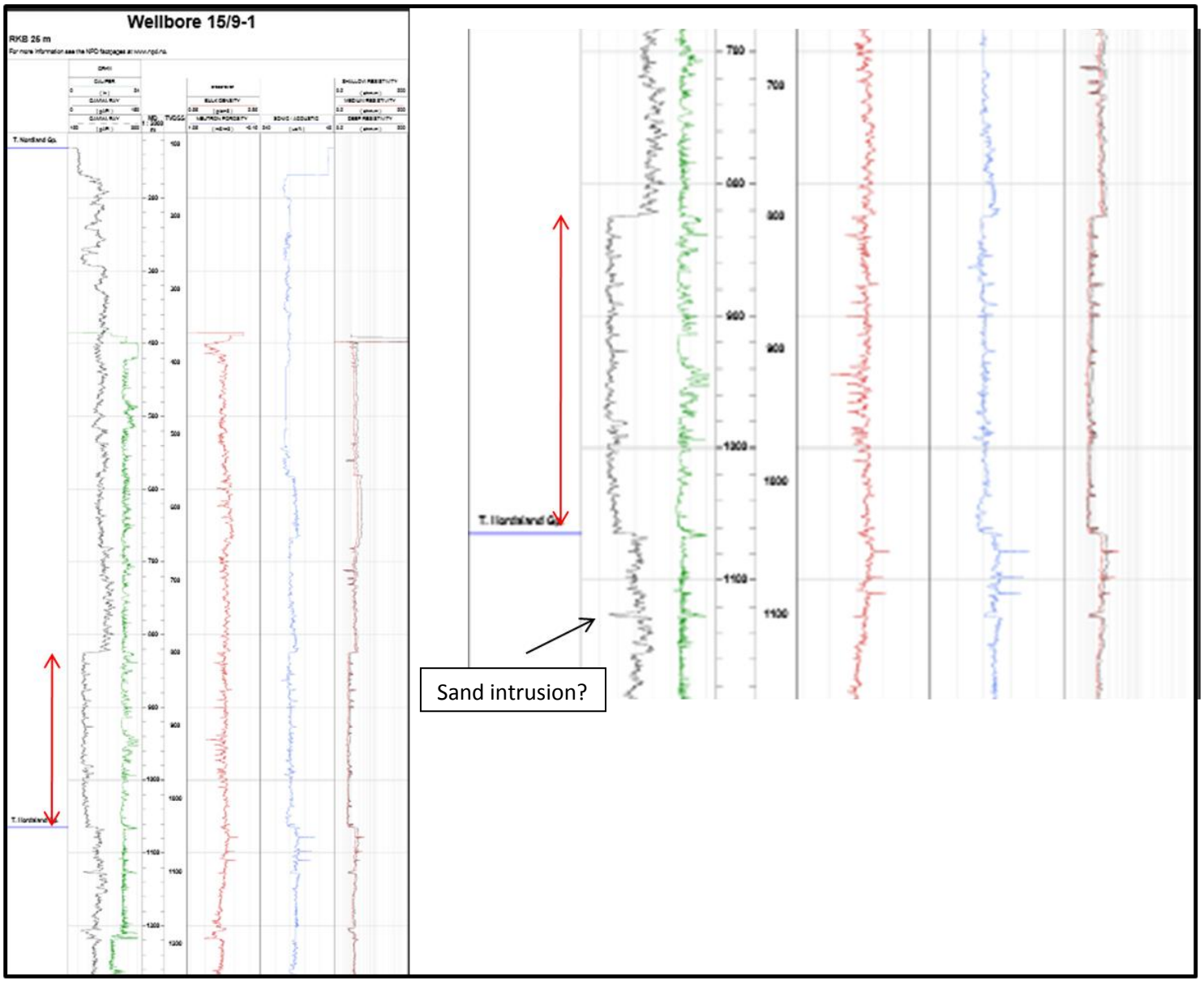
Wellbore 15/9-1
RKB 25 m
T. Nordland Gp.
T. Nordland Gp.
Sand intrusion?

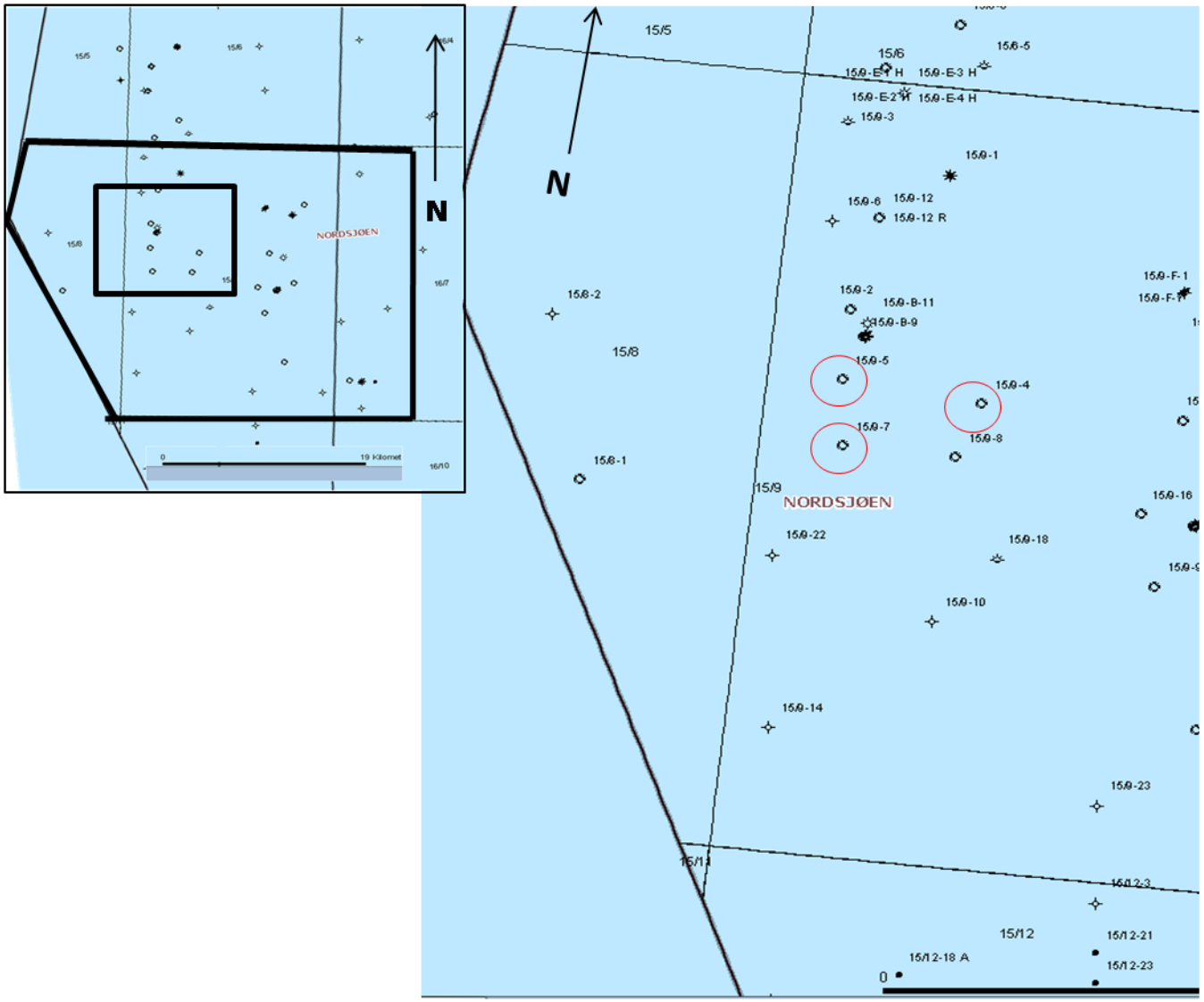
N
NORDSJØEN
15/5
15/6
15/6-5
15/6-E-1 H
15/6-E-3 H
15/6-E-2 H
15/6-E-4 H
15/6-3
15/6-1
15/6-6
15/6-12
15/6-12 R
15/8-2
15/6-2
15/6-B-11
15/6-B-9
15/8
15/6-5
15/6-4
15/6-7
15/6-8
15/8-1
15/9
NORDSJØEN
15/6-16
15/6-22
15/6-18
15/6-10
15/6-14
15/6-23
15/11
15/12-3
15/12
15/12-21
15/12-18 A
15/12-23
0

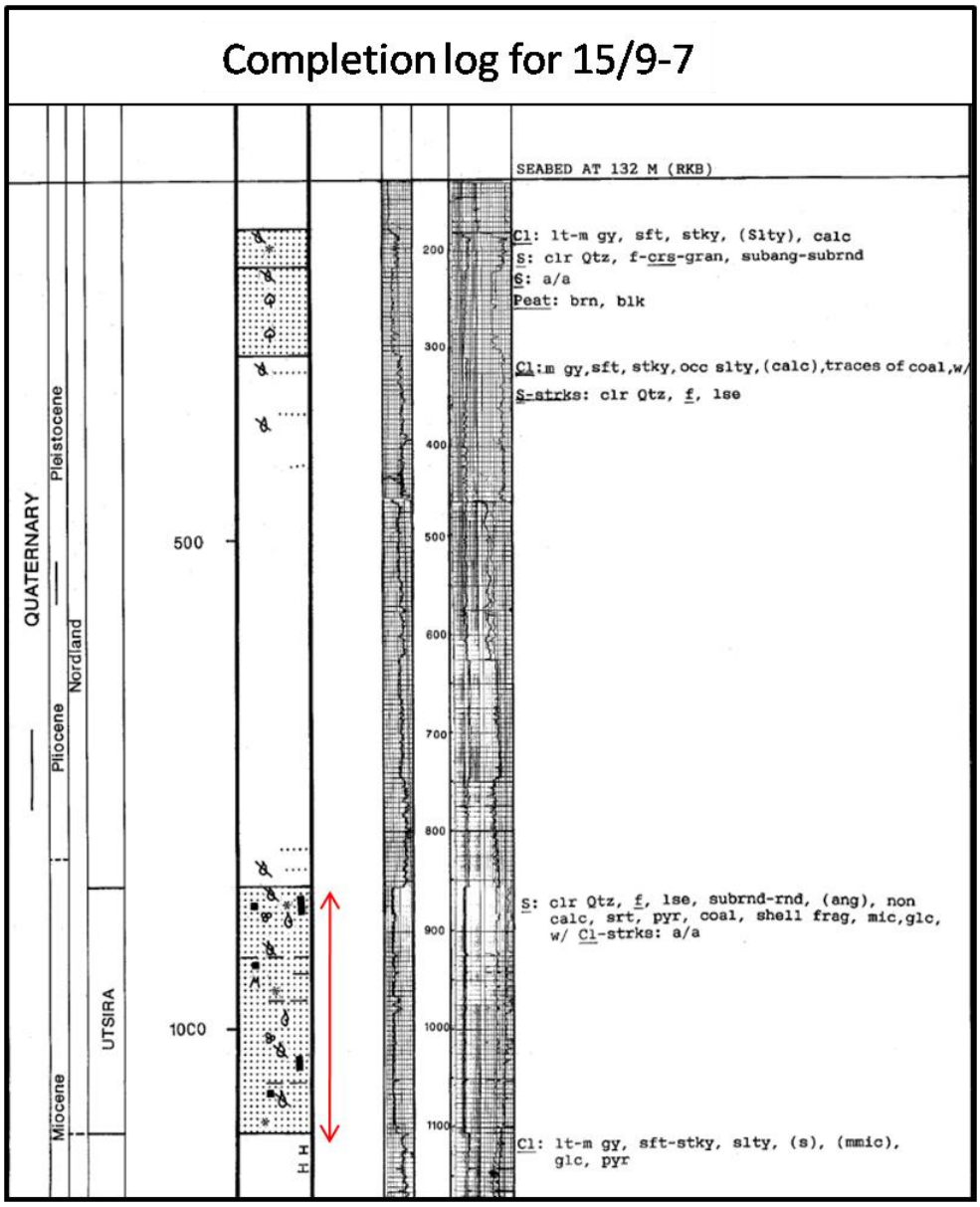
Completion log for 15/9-7
SEABED AT 132 M (RKB)
QUATERNARY
Pleistocene
Pliocene
Miocene
Nordland
UTSIRA
500
1000
200
300
400
500
600
700
800
900
1000
1100
Cl: lt-m gy, sft, stky, (Slty), calc
S: clr Qtz, f-crs-gran, subang-subrnd
G: a/a
Peat: brn, blk
Cl:m gy,sft, stky,occ slty,(calc),traces of coal,w/
S-strks: clr Qtz, f, lse
S: clr Qtz, f, lse, subrnd-rnd, (ang), non calc, srt, pyr, coal, shell frag, mic,glc, w/ Cl-strks: a/a
Cl: lt-m gy, sft-stky, slty, (s), (mmic), glc, pyr

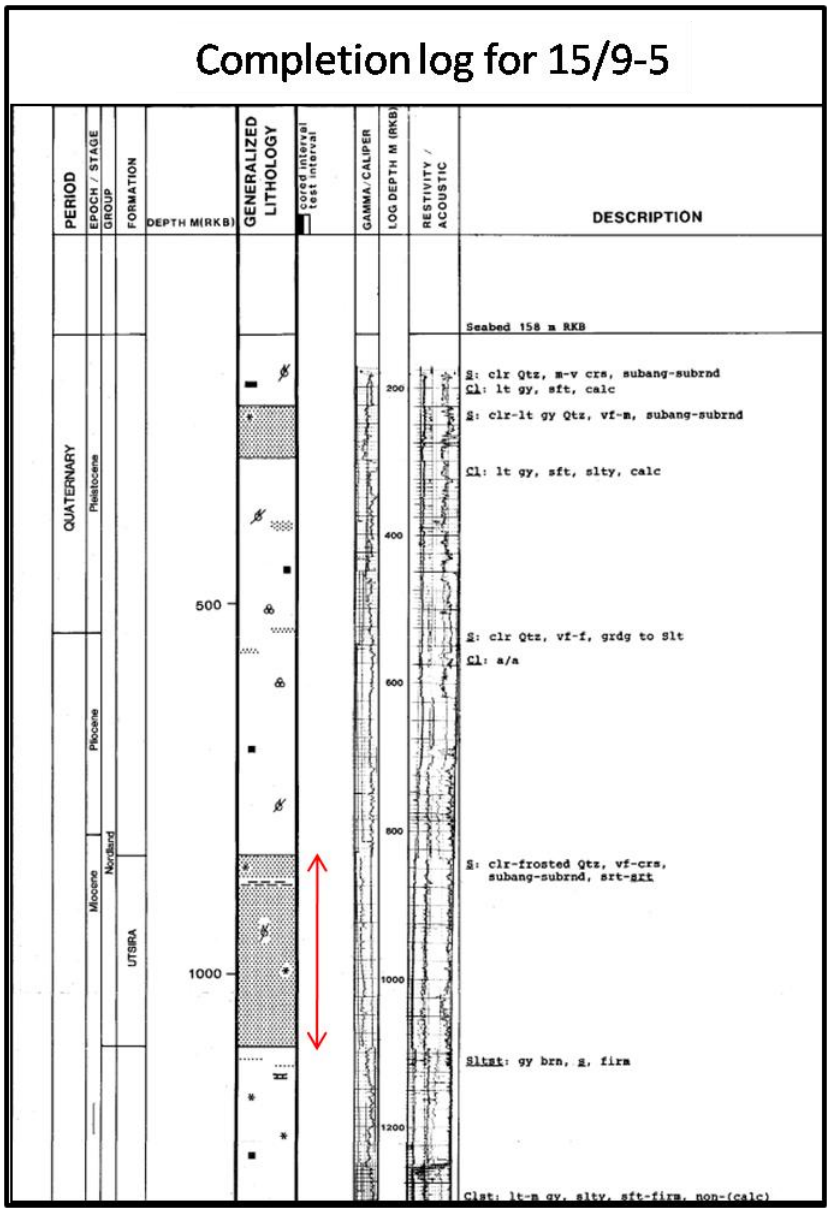
Completion log for 15/9-5
PERIOD
EPOCH / STAGE
GROUP
FORMATION
DEPTH M(RKB)
GENERALIZED LITHOLOGY
cored interval
test interval
GAMMA/CALIPER
LOG DEPTH M (RKB)
RESTIVITY / ACOUSTIC
DESCRIPTION
QUATERNARY
Pleistocene
Pliocene
Miocene
Nordland
UTSIRA
500
1000
200
400
600
800
1000
1200
Seabed 158 m RKB
S: clr Qtz, m-v crs, subang-subrnd
Cl: lt gy, sft, calc
S: clr-lt gy Qtz, vf-m, subang-subrnd
Cl: lt gy, sft, slty, calc
S: clr Qtz, vf-f, grdg to Slt
Cl: a/a
S: clr-frosted Qtz, vf-crs, subang-subrnd, srt-grt
Siltst: gy brn, s, firm
Clst: lt-m gy, slty, sft-firm, non-(calc)

Completion log for 15/9-4

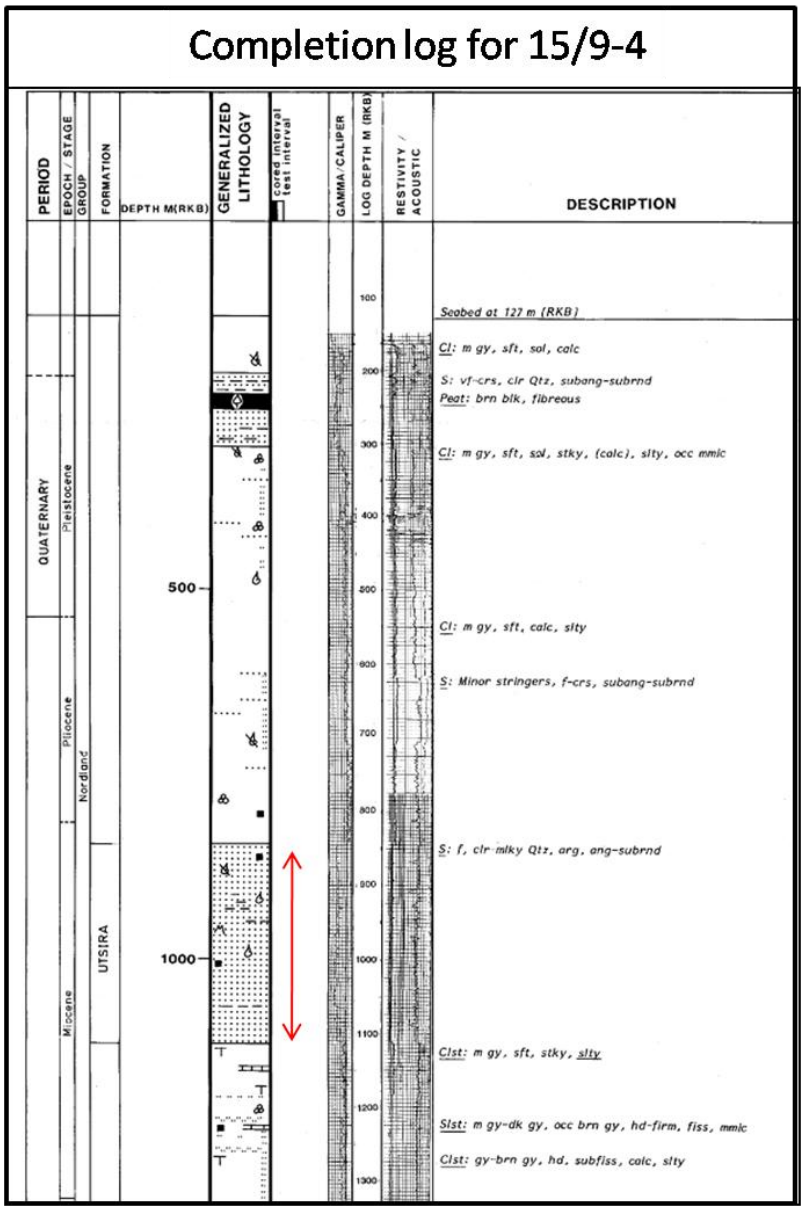

Appendix B

Pockmark, wellbore and surface facility coordinates

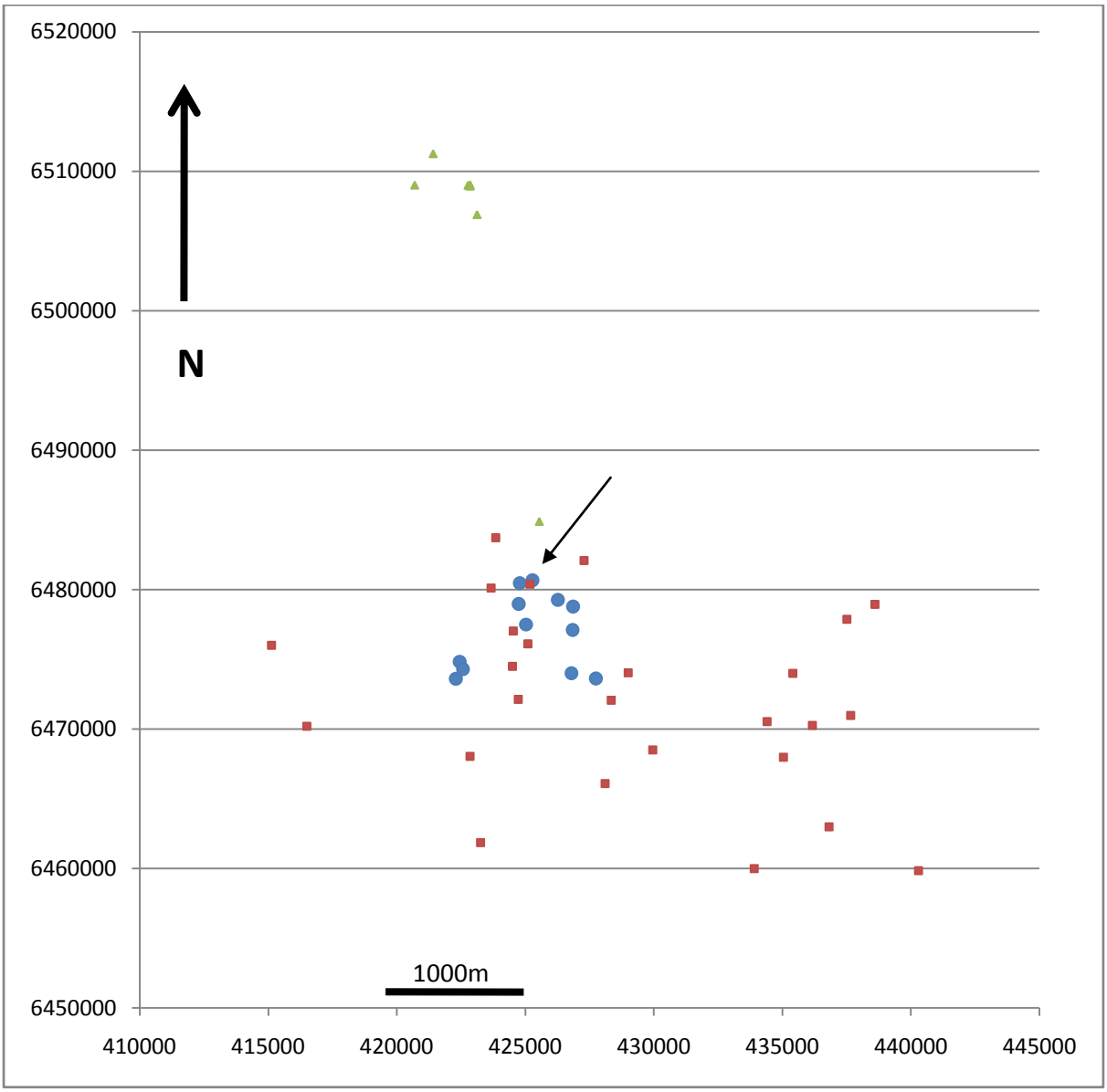

Location of pockmarks (circles) well locations (squares) and surface facilities (triangles) with respect to each other. Although some are in close proximity to each other (arrow), the majority of pockmarks are at least a 100m away from possible interruptions to seismic signal. Coordinates for each set of features are presented on the following pages.

Well bore		
15/9-24	440297.52	6459848.56
15/9-23	433900.09	6459999.91
15/9-14	423258.77	6461865.65
15/9-15	436817.55	6462991.44
15/9-10	428101.86	6466097.13
15/9-9	435038.52	6467984.08
15/9-22	422842.96	6468037
15/9-18	429961.76	6468508.49
15/8-1	416499.09	6470198.7
15/9-20 S	436165.07	6470257.29
15/9-16	434400.89	6470536.25
15/9-13	437653.7	6470978.02
15/9-8	428335.92	6472060.11
15/9-7	424724.77	6472135.59
15/9-11	435410.76	6474001.57
15/9-4	428999.05	6474041.91
15/9-5	424497.43	6474503.53
15/8-2	415122.23	6476013.73
15/9-21 S	425102.97	6476104.07
15/9-2	424529.68	6477027.07
15/9-19 A	437510.03	6477882.41
15/9-19 B	437510.03	6477882.41
15/9-19 S	437510.03	6477882.41
15/9-19 SR	437510.03	6477882.41
15/9-19 SR2	437510.03	6477882.41
15/9-17	438602.65	6478951.28
15/9-17 R	438602.65	6478951.28
15/9-6	423668.06	6480120.13
15/9-12	425174.97	6480390.26
15/9-12 R	425174.97	6480390.26
15/9-1	427277.67	6482077.91
15/9-3	423852.54	6483722

Facility	x	y
15/5-A-7 H	420694	6509004.77
15/5-B-1 H	421412	6511255.57
15/6-A-5 H	422770	6508993.25
15/6-A-1 H	422844	6509014.07
15/6-A-3 H	422847	6509005.03
15/6-A-4 H	422850	6508933.5
15/6-A-2 H	422853	6508995.32
15/6-A-6 H	423123	6506895
15/9-E H	425548	6484899.06

Pockmark	X	y
3	422298.55	6473595.5
1	422449.28	6474828
2	422577.57	6474290.76
4	424745.84	6478958.76
5	424785.84	6480453.97
6	425027.74	6477489.26
7	425280.36	6480666.06
8	426267.6	6479255.49
11	426798.22	6473995.74
10	426845.75	6477097.49
9	426863.92	6478775.64
12	427750.9	6473621.15